Sede Amministrativa: Università degli Studi di Padova

Dipartimento di Biologia

SCUOLA DI DOTTORATO DI RICERCA IN BIOSCIENZE E BIOTECNOLOGIE

INDIRIZZO: BIOTECNOLOGIE

CICLO XXVIII

NOVEL LRRK2 SUBSTRATES AT THE PRESYNAPTIC SITE IN VESICLE RECYCLING PATHWAYS IN PARKINSON'S DISEASE

Direttore della Scuola : Ch.mo Prof. Paolo Bernardi

Coordinatore d'indirizzo: Ch.mo Prof. Fiorella Lo Schiavo

Supervisore: Ch.mo Prof. Luigi Bubacco

Co-Supervisore: Prof. Elisa Greggio

Dottorando: Adriano Gonnelli

Index

Abstract

Parkinson's disease (PD) is the second most common neurodegenerative disorder after Alzheimer's disease (AD) affecting about 1-2% of the population over 65 years of age (Farrer, 2006). The pathological hallmarks of PD are the loss of dopaminergic neurons in the *substantia nigra pars compacta* (SNpc) and the presence of intracellular proteinaceous inclusions called "Lewy bodies" (LB) in surviving neurons (Damier et al., 1999; Frank et al., 2007). The etiology of PD is unknown, with a complex relationship between environmental and genetic factors, and aging being a required factor. The majority of cases, about 90-95%, is sporadic, while the remaining 5-10% can be explained by mutations in single genes (Van Den Eeden et al., 2003). The discovery of PD-related genes holds the potential to shed light into disease treatments, since the sporadic and familial forms are likely to share common pathogenic mechanisms and compromised pathways (Lesage and Brice, 2012). To date, five genes have been conclusively associated to familial PD, with both autosomal-dominant and autosomal-recessive modes of inheritance (Valente et al., 2004; Lakshminarasimhan et al., 2008; Nemani et al., 2013; Singleton et al., 2013; Kuang et al., 2013). Accordingly, several studies focused on the physiological role of PD-related proteins and on how pathogenic mutations cause the pathology. In 2004, two studies found that mutations in *Lrrk2* (*PARK8*) are responsible for a familial form of PD (Paisan-Ruiz et al., 2004; Zimprich et al., 2004) and, currently, mutations in this gene represent the most common genetic cause of PD (10%). *Lrrk2* encodes leucine-rich repeat kinase 2 (LRRK2), a large multi-domain protein with both GTPase and kinase activities (Marín et al., 2008). The majority of LRRK2 pathological mutations are located within the enzymatic core of the protein, and they can affect LRRK2 activity causing impaired cellular functions and cytotoxicity. Among all, the G2019S mutation is the most frequent (Gilks et al. 2005), thus the most studied. This mutation lies in the kinase domain and increases LRRK2 kinase activity (Greggio and Cookson, 2009). Several studies support a role for LRRK2 in synaptic vesicle trafficking, although the exact mechanism is unclear. Thus, understanding which pathways are compromised in pathological conditions is fundamental to develop efficient strategies against synaptic impairment in PD. While LRRK2 pharmacological

inhibition may block the PD-related LRRK2 phenotypes, the use of LRRK2 inhibitors has been shown to cause severe side-effects on peripheral organs (Baptista et al., 2013; Luerman et al., 2014). Thus, alternative therapeutic strategies may be directed toward other proteins that take part in LRRK2 pathways. In this scenario, identifying putative LRRK2 substrates at the presynaptic site, among the plethora of possible interactors, is fundamental to understand the downstream effects related to LRRK2 pathological mutations. Previous studies showed that LRRK2 can modulate synaptic vesicle trafficking through phosphorylation of components of the exo- endocytic machinery (Heo et al., 2010; Matta et al., 2012; Yun et al., 2013). For this reason, an outstanding question is to identify physiologically relevant, substrates of LRRK2 kinase activity and the effects of LRRK2 PD-related mutations on substrate phosphorylation. In this thesis, we focused on N-ethylmaleimide Sensitive Fusion protein (NSF) and Rab7L1. These two proteins have been previously indicated as LRRK2 interactors in neurons (Piccoli et al., 2011; MacLeod et al., 2013, Beilina et al., 2014). Here, our aim was to test whether they are also substrates of LRRK2 kinase activity.

NSF is an AAA+ (ATPases Associated with various cellular Activities) and its function is pivotal at the presynaptic site for proper synaptic vesicle recycling. More in detail, NSF uses the energy produced from ATP hydrolysis to disassemble SNARE proteins (Soluble N-ethylmaleimide Attachment protein REceptors), together with its adaptor protein alpha-SNAP (Soluble NSF Associated Protein), allowing them to another fusion cycle (Zhao and Brunger, 2015). NSF displays a homo-hexameric structure, where each monomer is composed by three different domains: the N-terminal domain (N-ter) required for alpha-SNAP:SNARE complex interaction, the D1 domain with an ATP-binding site necessary for the ATPase activity and a D2 domain with another ATP-binding site required for oligomerization (Zhao et al., 2015). Since NSF has been largely studied using non-human orthologous proteins (Chang et al., 2012; Cipriano et al., 2013; Vivona et al., 2013; Zhao et al., 2015), we set up a protocol to purify human Flag-tagged NSF from HEK293T mammalian cells. Firstly, we investigated the biochemical properties of NSF and subsequently its interaction with LRRK2. We demonstrated that the purified protein is an active ATPase and is able to interact with LRRK2. In particular, data obtained from pull-down assays revealed an interaction between NSF D2 domain and LRRK2.

Moreover, we demonstrated that NSF is also a substrate of LRRK2 kinase activity and this phosphorylation preferentially occurs at Thr-645 in the D2 domain. We confirmed this result by measuring the ^{33}P incorporation with kinase assays incubating NSF non-phosphorylatable mutants (NSF-T645A, T646A and S647A) together with LRRK2 G2019S. Kinetic studies of NSF ATPase activity revealed that NSF is 2-fold more active upon LRRK2 G2019S phosphorylation. Noteworthy, NSF-T645A, which resulted in a 50% reduction of ^{33}P incorporation compared to wild-type, abolishes LRRK2-mediated increased ATPase activity. In addition, we demonstrated that NSF disassembles the SNARE complex at a higher rate after phosphorylation by LRRK2 G2019S. Taken together, these results highlight a possible regulatory mechanism in which LRRK2 is involved in synaptic vesicle recycling through phosphorylation of NSF. Importantly, NSF ATPase activity could be compromised by excessive phosphorylation due to LRRK2 G2019S pathological mutation.

As mentioned, an important aspect in the development of PD may be linked to impaired synaptic vesicle trafficking, which may trigger neurodegeneration at early stages. A major class of proteins orchestrating vesicle sorting inside the cell are Rab proteins. Rabs constitute a large family of monomeric small GTPases associated with all cellular compartments (Grosshans et al., 2006). There are more than 60 different Rab proteins in humans (Schwartz et al., 2007; Pereira-Leal et al., 2001) and a switch between the GTP- (active) and GDP- (inactive) bound form regulates the interactions with their effectors. To date, several studies highlight a possible interaction between LRRK2 and a number of Rabs (MacLeod et al., 2013; Gomez-Suaga et al., 2014; Dodson et al., 2014; Waschbusch et al., 2014). Here, we tested whether different Rab proteins are also substrates of LRRK2 kinase activity. We performed kinase experiments on Rab7, Rab7L1, Rab9, Rab11 and Rab32. Kinase assays revealed that, among them, only Rab7L1 is a substrate of both LRRK2 wild-type and G2019S kinase activity. *Rab7L1* is located within the *PARK16* locus, a non-familial PD risk-associated *locus*, and Rab7L1 has been found to associate with LRRK2 to regulate the degradation of trans-Golgi derived vesicles (Beilina 2014). Mass spectrometry analysis revealed that phosphorylation by LRRK2 G2019S preferentially occurs on Rab7L1-T21, a residue localized in the highly conserved region responsible for GTP binding (P-loop region). In addition, we detected Rab7L1-S22 as a less probable

phosphorylation site. To test which residue was phosphorylated, we generated Rab7L1-T21A and S22A mutants. Kinase assays indicate that Rab7L1 likely possesses additional sites, other than T21 or S22, able to be phosphorylated by LRRK2 G2019S.

In summary, this work identified two novel substrates of LRRK2 kinase activity *in vitro* with potential relevance for disease. Our studies revealed an increased NSF ATPase activity upon LRRK2 G2019S phosphorylation and highlighted a novel regulatory mechanism that might be compromised in PD. In addition, we found that Rab7L1 is another substrate of LRRK2 kinase activity. Future studies should uncover whether NSF and Rab7L1 are substrates of LRRK2 also in the cellular context and whether pathological phosphorylation is relevant for PD.

Riassunto

La malattia di Parkinson (PD) è la seconda malattia neurodegenerative più comune dopo la malattia di Alzheimer (AD) e colpisce circa l'1-2% della popolazione oltre I 65 anni (Farrer, 2006). Gli elementi caratteristici del morbo di Parkinson sono la perdita dei neuroni nella *sustantia nigra pars compacta* (SNpc), e la presenza di aggregati proteici intracellulari denominati corpi di Lewy (LB) nei neuroni che sopravvivono (Damier et al., 1999; Frank et al., 2007). L'eziologia della malattia di Parkinson è sconosciuta, con una complessa correlazione tra fattori ambientali e genetici, e fattori legati all'invecchiamento. La maggior parte dei casi, circa 95%, è di origina sporadica, mentre il rimanente 5-10% può essere collegato a mutazioni in singoli geni (Van Den Eeden et al., 2003). La scoperta di geni collegati al morbo di Parkinson ha messo in luce possibili trattamenti terapeutici, dato che la forma sporadica e quella familiare hanno in comune molti meccanismi patologici e pathway compromessi (Lesage and Brice, 2012). Ad oggi, cinque geni sono stati associati alla forma familiare del morbo di Parkinson, sia ad una forma genetica autosomica dominante che recessiva (Valente et al., 2004; Lakshminarasimhan et al., 2008; Nemani et al., 2013; Singleton et al., 2013; Kuang et al., 2013). Per questo motivo, numerosi studi si sono focalizzati sul ruolo fisiologico delle proteine collegate alla malattia di Parkinson e come le mutazioni patologiche causino la patologia. Nel 2004, due studi hanno identificato come mutazioni nel gene *Lrrk2* (*PARK8*) siano causa della forma familiare di morbo di Parkinson (Paisan-Ruiz et al., 2004; Zimprich et al., 2004) e, ad oggi, mutazioni all'interno di questo gene rappresentano la più comune causa genetica di malattia di Parkinson (10%). *Lrrk2* Questo gene codifica per la proteina leucine-rich repeat kinase 2 (LRRK2), una grande proteina composta da vari domini con attività GTPasica e chinasica (Marín et al., 2008). La maggior parte delle mutazioni sono localizzate all'interno del core enzimatico della proteina, e possono colpire l'attività di LRRK2 causando un danno alle funzioni cellulari e citotossicità. Tra tutte, la mutazione G2019S è la più frequente (Gilks et al. 2005), quindi la più studiata. Questa mutazione avviene all'interno del dominio chinasico e aumenta l'attività chinasica di LRRK2 (Greggio and Cookson, 2009). Numerosi studi sostengono un ruolo di LRRK2 a livello del traffico delle vescicole sinaptiche, anche se il meccanismo esatto non

è ancora chiaro. Perciò, capire quali pathway sono compromessi in condizioni patologiche è fondamentale per sviluppare strategie efficienti contro i danni provocati dalla malattia di Parkinson. Mentre l'inibizione farmacologica di LRRK2 potrebbe bloccare il fenotipo patologico, l'uso di inibitori di LRRK2 ha mostrato effetti secondari gravi a livello degli organi periferici (Baptista et al., 2013; Luerman et al., 2014). Per questo motivo, strategie terapeutiche alternative potrebbero essere dirette verso altre proteine che sono coinvolte all'interno dei pathway di LRRK2. In questo scenario, l'identificazione di substrati di LRRK2 a livello presinaptico, tra tutti i possibili interattori, è fondamentale per capire gli effetti a valle relativi a mutazioni patologiche di LRRK2. Studi precedenti hanno dimostrato che LRRK2 può modulare il traffico delle vescicole sinaptiche attraverso la fosforilazione di componenti facenti parte dei processi di eso- ed endocitosi (Heo et al., 2010; Matta et al., 2012; Yun et al., 2013). Per questa ragione, una domanda ancora senza risposta è quella di identificare possibili substrati dell'attività chinasica di LRRK2, rilevanti a livello fisiologico, e gli effetti che le mutazioni di LRRK2 associate al morbo di Parkinson hanno sulla fosforilazione. In questa tesi, ci siamo focalizzati sulla proteina N-ethylmaleimide Sensitive Fusion (NSF) protein e Rab7L1. Queste due proteine sono state precedentemente indicate come interattori di LRRK2 nei neuroni (Piccoli et al., 2011; MacLeod et al., 2013, Beilina et al., 2014). In questo lavoro, il nostro scopo era quello di testare se queste due proteine siano anche substrati dell'attività chinasica di LRRK2.

NSF è classificata come proteina AAA+ (ATPases Associated with various cellular Activities) e la sua funzione è fondamentale a libello presinaptico per un corretto riciclo delle vescicole sinaptiche. In dettaglio, NSF usa l'energia prodotta dall'idrolisi dell'ATP per disassemblare le proteine del complesso SNARE (Soluble N-ethylmaleimide Attachment protein REceptors), insieme alla sua proteina adattatrice alpha-SNAP (Soluble NSF Associated Protein), consentendo un nuovo ciclo di fusione (Zhao and Brunger, 2015). NSF mostra una struttura omo-esamerica, dove ogni monomero è composto da tre differenti domini: l'N-terminale (N-ter) necessario all'interazione con alpha-SNAP ed il complesso SNARE, il dominio D1 con un sito di legame dell'ATP necessaria per l'attività ATPasica, ed un dominio D2 con un altro dito di legame per l'ATP richiesta all'oligomerizzazione (Zhao et al., 2015). Dato che NSF è stato largamente

studiato usando una proteina ortologa non umana, abbiamo messo a punto un protocollo per purificare NSF umano con un Flag-tag da cellule di mammifero HEK293T. Per prima cosa, abbiamo deciso di studiare la biochimica di NSF e successivamente la sua interazione con LRRK2. Abbiamo dimostrato che la proteina purificata è attiva ed è in grado di interagire con LRRK2. In particolare, i risultati ottenuti attraverso esperimenti di pull-down rivelano una interazione tra il dominio D2 di NSF e LRRK2. Inoltre, abbiamo dimostrato che NSF è anche un substrato dell'attività chinsica di LRRK2 e questa fosforilazione avviene preferenzialmente nella treonina-645 all'interno del dominio D2. Abbiamo confermato questo risultato misurando l'incorporazione di ^{33}P con saggi chinasici incubando dei mutanti non-fosforilabili di NSF (NSF-T645A, T646A and S647A) insieme a LRRK2 G2019S, Studi cinetici sull'attività ATPasica di NSF hanno rivelato che NSF è due volte più attivo dopo la fosforilazione da parte di LRRK2 G2019S. E' importante notare che il mutante NSF-T645A, dove l'incorporazione di ^{33}P risulta essere il 50% in meno rispetto al wild-type, non presenta un aumento dell'attività ATPasoca dovuto alla fosforilazione ad opera di LRRK2 G2019S. Inoltre, abbiamo dimostrato che NSF dopo essere stato fosforilato da LRRK2 G2019S disassembla il complesso SNARE più velocemente. Tutti questi risultati evidenziano un possibile meccanismo regolatorio in cui LRRK2 è implicato all'interno del riciclo delle vescicole sinaptiche attraverso la fosforilazione di NSF. L'attività ATPasica di NSF potrebbe quindi essere compromessa da una sua aumentata fosforilazione ad opera del mutante patologico G2019S.

Come illustrato precedentemente, un aspetto importante nello sviluppo della malattia di Parkinson potrebbere essere collegato ad un danno nel traffico delle vescicole, che potrebbe far scaturire la neurodegenerazione a stadi precoci (Fernandez-Chacon et al., 2004; Burre et al., 2010). La principale classe di proteine che governa l'organizzazione delle vescicole all'interno della cellula, è composta dalle proteine Rab. Esse costituiscono una vasta famiglia di piccole GTPasi monomeriche associate a tutti i compartimenti cellulari (Grosshans et al., 2006). Nell'uomo ci sono più di 60 tipi di Rab ((Schwartz et al., 2007; Pereira-Leal et al., 2001)) che passando da una forma attiva, legata al GTP, ad una forma inattiva, legata al GDP, regolando la loro interazione con proteine effettrici. Ad oggi, numerosi studi hanno evidenziato una possibile interazione tra LRRK2 e varie proteine Rab (MacLeod et al., 2013; Gomez-Suaga et al., 2014; Dodson et al., 2014;

Waschbusch et al., 2014). Nel nostro lavoro, abbiamo testato se alcune proteine Rab siano anche substrati dell'attività chinasica di LRRK2. Abbiamo eseguito saggi chinasici con varie Rab, su Rab7, Rab7L1, Rab9, Rab11 e Rab32. I saggi chinasici hanno rivelato che, tra tutte, solamente Rab7L1 è un substrato di LRRK2, sia wild-type che G2019S. Il gene *Rab7L1* è localizzato all'interno del locus *PARK16*, un locus associato al richio di insorgenza della forma di malattia di Parkinson non-familiare, Rab7L1 è stato trovato associato a LRRK2 nella regolazione della degradazione delle vescicole a livello dell'apparato del Golgi (Beilina 2014). Analisi di spettrometria di massa hano rivelato comee la fosforilazione ad opera di LRRK2 G2019S avvenga preferenzialmente sulla treonina-21 di Rab7L1, un residuo localizzato nella regione altamente conservata responsabile del legame col GTP (P-loop). In aggiunta, abbiamo individuato come meno probabile sito di fosforilazione la serina-22. Per testare quale residuo fosse quello fosforilato, abbiamo generato i mutati non fosforilabili Rab7L1-T21A ed S22A. I saggi chinasici ci hanno indicato che Rab7L1 possiede verosimilmente siti di fosforilazione aggiuntivi, oltre la T21 e la S22, che possono essere fosforilati da LRRK2 G2019S.

Riassumendo, questo lavoro ha identificato due nuovi substrati dell'attività chinasica di LRRK2 *in vitro* con una potenziale rilevanza a livello della malattia. I nostri studi hanno rivelato un aumento dell'attività ATPasica di NSF successivamente alla fosforilazione da parte di LRRK2 G2019S ed hanno evidenziato un nuovo meccanismo regolatorio che potrebbe essere compromesso nella malattia di Parkinson. In aggiunta, abbiamo trovato che Rab7L1 è un altro substrato dell'attività chinasica di LRRK2. Studi futuri sono necessari per scoprire se NSF e Rab7L1 siano substrati di LRRK2 anche in un contesto cellulare, e se la fosforilazione in condizioni patologiche è rilevante nel morbo di Parkinson.

Chapter I
Introduction

1. Parkinson's Disease

Parkinson's disease (PD) is the second most common neurodegenerative disorder after Alzheimer's disease (AD) and affects about 1-2% of the population over 65 years old (Farrer, 2006). This percentage increases to 4% over the age of 85 (Fahn, 2003). The mean age of onset is 60, but 4% of the patients show an early-onset before 50 years old. Being that the development of the disorder is strongly associated with aging (de Lau and Breteler, 2006), the fraction of population affected is expected to increase parallel with the increasing life expectancy. The etiology of PD has unknown causes, with a complex relationship between environmental and genetic factors. The environmental hypothesis is based on toxins able to mimic clinical and pathological characteristics of PD. The sporadic form of the disease has been linked to herbicide (paraquat) and insecticide (rotenone) largely used in agriculture, and chemical compounds toxic to mitochondria (such as, MPTP), as discussed below. Although this is the most common form of the disease, 10-15% of PD cases are linked to pathogenic mutations in single genes (Sherer et al., 2002). The discovery of PD-related genes holds the potential to shed a light into disease treatments since the sporadic and familial forms are likely to share common pathogenic mechanisms and compromised pathways. Several studies are focused on the physiological role of PD-related proteins and how mutations cause the development of the pathology. Of interest, besides genetic and environmental causes, there are additional predisposing factors that lead to an increased risk of PD. For example, estrogens seem to have a beneficial effect on dopaminergic neurotransmission and protect neurons via antioxidant effects (Behl et al., 1997). For this feature, men and women without hormone replacement have an increased risk of 25% to incur in this pathology (Popat et al., 2005; Lees et al., 2009).

1.1 Clinical Features

Clinical characteristics can be summarized with the acronym *TRAP*: Tremor at rest, Rigidity, Akinesia (or bradykinesia) and Postural instability. These motor dysfunctions contribute to diagnose the disease. Symptoms derive from loss of dopaminergic neurons

in the substatia nigra pars compacta (SNpc) of the midbrain (Damier et al., 1999). These neurons are part of the circuitry of the basal ganglia which controls motor functions. The depletion in the dopamine (DA) level is considered the starting point of motor impairment in PD and the onset of symptoms is caused by a progressive worsening of neuronal dysfunction that ends with cell death. The main problem is that a definitive diagnosis of this disease can only be made with a post-mortem detection of neuronal loss in patient brains with resulting in the depigmentation of the substantia nigra and the presence of intracellular proteinaceous inclusions called “Lewy Bodies” (LBs) in surviving neurons (Fig.1.1.1). Several proteins have been described in aggregates and α-synuclein (aSyn) is the major component (Spillantini et al., 1998). Although LBs are a typical feature of PD, they are not specific for this disease and they can be also found in AD and “dementia with LB” (Gibb and Lees, 1988). The mechanism underlying PD remain an open question, but one hypothesis is that intracellular protein aggregates may represent the starting point of toxicity. Aggregates, or misfolded proteins, could cause directly injury interfering with intracellular pathways or recruit proteins that are important for cellular mechanisms: this leads to the hypothesis of a strong correlation between inclusion formation and neurodegeneration.

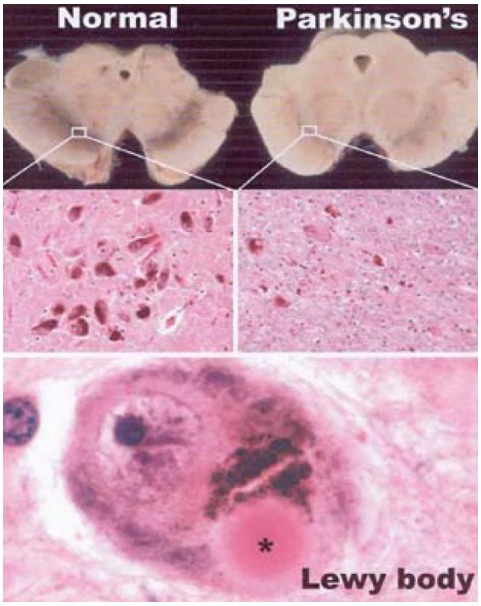

Fig.1.1.1 | Hallmarks of Parkinson's disease (PD). Images of the SNpc in the midbrain that highlight its depigmentation due to the loss of the dopaminergic neurons and the presence of Lewy bodies (LB) as pathological hallmarks of the disease (Frank et al., 2006).

1.2 Etiology Of PD

To date, the etiopathogenesis of PD is unclear. About 90-95% of PD cases are classified as sporadic and only 5-10% of the patients present a familial form of the disease. The sporadic form of the disease is likely caused by a complex interaction between genese and environment, with aging being a required factor. An early evidence that exposure to environmental toxins may cause parkinsonism came in 1980s. MPTP (1-methyl-4-phenyl-1,2,3,6-tetrahydropyridine), an additive in the heroin preparation, was identified to be the cause of an irreversible motor disorder with symptoms of PD among heroin users (Langston et al., 1983). The most important feature is that MPTP is able to cross the blood-brain barrier (BBB) and in glial cells it can be oxidized and deprotonated to MPP+, which is the active toxic species (Kopin, 1987). In addition, epidemiological studies identified how compounds used in agriculture, such as paraquat (herbicide) and rotenone (insecticide), can induce mitochondrial dysfunction at complex I (Betarbet et al., 2000), and, a long term exposure, the typical PD phenotype. Another hypothesis is that the preferential loss of dopaminergic neurons in the *substantia nigra pars compacta* could be ascribed to the chemical properties of DA. An impairment in the storage of this neurotransmitter could cause cytotoxicity and this could be one of the aspects that

explain why DA neurons are preferentially involved in this pathology (Bisaglia et al., 2013). DA is normally stored within large dense core synaptic vesicles where the low pH stabilizes the neurotransmitter. However, if the concentration of cytosolic DA arises, DA can undergo autoxidation. The oxidized forms of DA, the quinones (DAQs), are highly reactive species that can react with and damage several cellular components, such as lipids, proteins and DNA, and generate DA adducts (Berman and Hastings, 1999; Bisaglia et al., 2010; Girotto et al., 2012). For this reasons, cytosolic accumulation of DA may promote dopaminergic neuron degeneration. As discussed, even though the majority of PD cases have an unknown etiology (idiopathic PD), about 5-10% of cases are caused by mutations in single genes. The discovery of PD-related genes has been crucial for understanding the intracellular pathways compromised in PD, since sporadic and familial forms of the disease share most of the clinical aspects (Lesage and Brice, 2012). Among them, five genes have been associated to familial PD both autosomal-dominant (*SNCA* coding for α-synuclein and *Lrrk2* coding for leucine-rich repeat kinase 2, LRRK2) and autosomal-recessive (*PARKIN*, *PINK1* and *DJ-1*). PD is rarely the result of mutations in single genes and the PD onset is influenced by polymorphic genetic variations shared between PD and AD, as highlighted through genome wide association studies (GWAS).

1.3 Dominant Form Of PD

Mutations in genes that cause autosomal-dominant forms of PD can have different effects on protein function. Neurotoxicity could derive from a “gain of existing function” where the activity of the PD protein is abnormally high (this is thought to underlie the pathogenic mechanism of mutant LRRK2) or it can originate from a “gain of a novel function”. This last mechanism has been proposed for aSyn, that, when mutated, is prone to form neurotoxic oligomers and aggregates typical of PD.

1.3.1 Alpha-Synuclein (PARK1/4)

α-Synuclein (aSyn) is a natively unfolded protein of 140 amino acids with a molecular weight of 14,5 kDa. Duplication and triplication of the aSyn gene (*SNCA*) cause autosomal dominant form of PD. aSyn is abundantly expressed in mammalian brain in nerve terminals (Fortin et al., 2004) and it is the major component of the LBs and Lewy Neurites (LNs) (Spillantini et al., 1998), the hallmark of PD and other neurodegenerative disorders called "synucleinopathies". Even if the precise function of aSyn is still under investigation, its presynaptic localization argues for a role in neurotransmitter release and synaptic plasticity (Burré et al., 2010; Diao et al., 2013). Given that, impairment in the physiological role of aSyn due to aggregates formation, might be one of the starting point of neurodegeneration (Nemani et al., 2010). Several studies showed that this protein can bind lipid bilayers through its N-terminal region and acquire an alpha-helix conformation (Davidson et al., 1998; Ulmer and Bax, 2005; Burré et al., 2013) which has been proposed to stabilize the curvature of synaptic vesicles (Nuscher et al., 2004). Interestingly, aSyn knockout mice show defects in neurotransmission, confirming that this protein is important for synaptic function (Greten-Harrison et al., 2010). aSyn is the major component of Lewy bodies and multiple lines of evidence indicate that the protein can aggregate in vitro and in cells. In the oligomerization process, that ends with the formation of toxic fibrils, aggregates are organized in β-sheets (el-Agnaf and Irvine, 2002). Additional studies identified point mutations that increase the propensity of aSyn to aggregate (Hardy et al., 2009) and post-translational modification of aSyn result in increased oligomerization or alteration in lipid binding. To date, A53T (Polimeropoulos et al., 1997), A30P (Krüger et al., 1998), E46K (Zarranz et al., 2004), H50Q (Proukakis et al., 2013) and G51D (Lesage et al., 2013) point mutations have been associated to familial PD. Even though the exact mechanism of aggregation process and how these aggregates are harmful to neurons is unclear, several studies observed that aSyn aggregates can induce neuroinflammation and oxidative stress to neurons resulting in neurodegeneration (Béraud et al., 2011).

1.3.2 LRRK2 (PARK8)

The *Lrrk2* gene encodes a protein of 286 kDa, which, in 2004, was identified as the gene responsible for PARK8-linked PD (Zimprich et al., 2004; Paisan-Ruiz et al., 2004). Autosomal dominant mutation in LRRK2 are the most common genetic cause of late-onset PD, since LRRK2 mutations affect approximately 10% of patients with familial PD (Singleton et al., 2013). Despite more than ten years after this discovery and the impressive amount of research conducted on LRRK2, it is still unclear how mutation cause neurodegeneration. Several studies have been focused on understanding LRRK2 pathobiology, because LRRK2-linked PD and sporadic are clinically and pathologically very similar. Therefore, understanding the pathways altered by LRRK2 could shed light into the pathogenic mechanisms of the more common idiopathic disease and disclose novel therapeutic strategies. Among all the mutations, the G2019S is the most diffuse in North American and European populations where it may account for 30-40% of all PD cases (Gilks et al., 2005), but other pathogenic mutations (R1441C, R1441G, Y1699C, and I2020T) have been identified in a number of families (Nichols et al., 2005). As discussed in the next paragraph, depending on their position these mutations can affect LRRK2 kinase and/or GTPase activities, which may cause an impairment of the downstream signaling pathways and, in turn, induce neurodegeneration. Of interest, LRRK2 has been shown to physically and/or functionally interact with the products of *MAPT* (microtubule associated protein tau gene) (Golub et al., 2009) and *Rab7L1* (MacLeod et al., 2013; Beilina et al., 2014), two risk factor for PD.

1.4 Recessive Forms Of PD

Mutations in *Parkin*, *PINK1* and *DJ-1* cause a recessive form of PD, characterized by an early onset of the disease and a slow progression. Of interest, all these three proteins are involved in common pathways protecting mitochondria and cells against reactive oxygen species and oxidative stress.

1.4.1 PARKIN (PARK2)

Parkin is a cytosolic E3 ubiquitin-protein ligase (Shimura et al., 2000) of about 51 kDa containing an N-terminal ubiquitin-like domain followed by four zinc fingers domains. Mutations in this gene account for 50% of all recessive PD forms. This protein is involved in the protein ubiquitination pathway and impairments in mitochondrial activity and loss of mitochondrial membrane potential cause Parkin recruitment on the outer mitochondrial membrane to initiate mitophagy (Narendra et al., 2008). The involvement of Parkin in the maintenance of healthy mitochondria and other cellular processes (Winklhofer, 2014) suggests that a "loss-of-function" mutation of this protein may cause accumulation of toxic substrates (including mitochondria) with consequent dopaminergic degeneration (Kuang et al., 2013).

1.4.2 PINK1 (PARK6)

Mutations in *PINK1* gene are the second most common cause of autosomal-recessive form of PD (Valente et al., 2004). PINK1 is a serine-threonine protein kinase of about 63 kDa that act as a neuroprotective agent against oxidative stress (Wang et al., 2006). PINK1 is localized on the inner mitochondrial membrane and is normally subjected to protease degradation under normal conditions. When the mitochondrial potential is lost, these proteases are inactivated and PINK1 accumulates on the mitochondrial surface where it phosphorylates Ubiquitin, which then acts as a receptor for Parkin. Upon additional phosphorylation events, Parkin is activated and can attach ubiquitin to key proteins on the mitochondrial outer membrane to initiate mitophagy, a process of elimination of damaged mitochondria through autophagy (Beilina and Cookson, 2015). Thus PINK1 and Parkin cooperate to maintain mitochondrial homeostasis and mutations in both genes are thought to compromise this process, with consequent accumulation of damaged mitochondria, and, in turn, neurodegeneration.

1.4.3 DJ-1 (PARK7)

DJ-1 encodes for a protein of 189 aa which is active in a dimeric conformation The exact biological function of DJ-1 is still unclear. At present, the most corroborated function of DJ-1 is its neuronal protective role against oxidative stress (Cookson, 2012). Overexpression of DJ-1 has a neuronal cytoprotective effect against oxidative damages (Taira et al., 2004; Martinat et al., 2004), whereas DJ-1 deficiency leads to increased oxidative stress-induced cell death (Kim et al., 2005; Meulener et al., 2005; Lavara-Culebras and Paricio, 2007). Nevertheless, how exactly this function is exerted is not clear. As for other proteins involved in recessive forms of PD, pathogenic DJ-1 mutations have been described to cause a loss of protein function. As many mutations induce a loss of protein thermal stability, a possible explanation for the loss of the protective function relies on structural perturbations induced by the mutations (Lakshminarasimhan et al., 2008; Malgieri and Eliezer, 2008). This is clearly the case of the L166P mutant which is highly and globally unfolded (Malgieri and Eliezer, 2008). Nevertheless, as some mutant retains biophysical properties that make these proteins structurally indistinguishable from wild-type DJ-1 (Lakshminarasimhan et al., 2008; Malgieri and Eliezer, 2008; Ramsey and Giasson, 2008), some other mechanism should exist.

1.5 Therapeutic Strategies

To date, no therapeutic treatments can block the cell loss and the development of the pathology. The current therapeutic strategies are only symptomatic and whilst they can improve the quality of life, they cannot halt or slow disease progression. Since the DA depletion is the main cause of motor symptoms, this deficit can be attenuated by a DA replacement therapy. The most effective compound levodopa (L-DOPA), the precursor of dopamine, which is able to cross the BBB while the neurotransmitter itself is not. Restoring the physiological level of DA by L-DOPA administration attenuates the motor symptoms of the disease and this was considered the perfect therapy for many years. L-DOPA remains the most efficient therapy to be used early in the development of the disease and was widely distributed for its easy oral administration. However, despite the

positive effects of this therapy, L-DOPA does not reduce the rate of neuron cell loss and the disease progression. Moreover, long term treatment induces dyskinesia (Heumann et al, 2014), a particular motor fluctuations associated with intermittent stimulation of dopamine receptors in association with a gradual decline of clinical efficiency (Davie, 2008). For these reasons, other classes of drugs have been developed: dopamine receptor agonists and inhibitors of enzymes responsible of dopamine-metabolism, such as monoamine oxidase-B (MAO-B) and catechol-O-methyltransferase (COMT) (Olanow and Schapira, 2013). These new drugs were introduced to attenuate symptoms in the later stage of the disease, but evidences highlight the development of both peripheral effects and psychiatric symptoms due to chronic use as secondary effects (Smith et al., 2012). Starting from these, novel therapies were developed to fight against the disease: surgical therapies based on deep brain stimulation (Coune et al., 2012) or less invasive treatments, such as gene and cell replacement, which are under investigation. Adeno-associated virus (AAV) or lentivirus vectors to improve DA synthesis and expression of L-DOPA-converting enzyme AADC offer a new potential therapy, against PD. However, clinical trials did not bring the expected results (Bartus et al, 2014). Cell replacement is also considered a great potential therapeutic strategy in PD (Loewenbruck and Storch, 2011; Badger et al., 2014), and intense research is directed toward the development of such therapies.

2. Leucine-rich repeat kinase 2 (LRRK2)

In 2004, two back-to-back studies identified that mutations in the *Lrrk2* (PARK8) gene cause a familial form of Parkinson's disease (PD) (Paisan-Ruiz et al., 2004; Zimprich et al., 2004). This gene encodes for a large multi-domain protein of about 286 kDa (2527 amino acids) with two enzymatic functions (Marín et al., 2008). LRRK2 belongs to a family of proteins called ROCO (Ras Of COmplex), characterized by two conserved domains (Gotthardt et al., 2008; Marín et al., 2006; Civiero et al., 2014): a Ras of complex (Roc) GTPase domain followed by a C-terminal of ROC (COR) domain. The Roc-COR domain is then followed by a serine/threonine kinase domain at the C-terminal. The GTPase/kinase enzymatic core is surrounded by protein-to-protein interaction domains both at N- and C-terminal of LRRK2 (Fig.2.1): the armadillo, ankyrin and leucine-rich repeat (LRR) domains at N-terminal (Marín et al., 2006), and the WD40 at the C-terminal, which seems to control LRRK2 function and kinase activity (Rudenko et al., 2012).

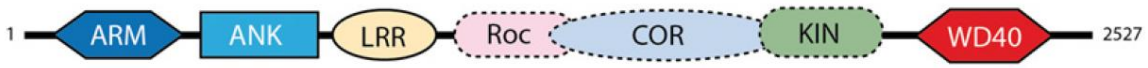

Fig.2.1 | Schematic representation of domain structure of LRRK2. LRRK2 has a multi-domain structure with an enzymatic core composed by a Roc-COR domain (GTPase activity) and Kinase domain (kinase activity), surrounded by protein-to-protein interaction domains. ARM (armadillo repeats), ANK (ankyrin-like repeats), LRR (leucine-rich repeats) and WD40 domains are shown (Adapted from: Civiero and Bubacco, 2012).

The kinase domain of LRRK2 is predicted to belong to the class of mitogen-activated protein kinase kinase kinase (MAPKKK), such as RAF (Gloeckner et al., 2009), and one feature of these kinases is the formation of dimers. A major challenge in the investigation of LRRK2 tertiary and quaternary structure is due to the technical hurdle of isolating sufficient high-quality/quantity LRRK2 full-length and/or domains. Therefore, structural information on full-length LRRK2 is still missing and clues on LRRK2 quaternary structure come from indirect evidence. It has been shown that highly purified full-length

LRRK2 proteins are capable of forming dimers in solution as revealed by immune-gold, looking at the distribution of distances among metal particles imaged by transmission electron microscopy (Civiero et al., 2012). Published in 2008, the first structure of the isolated human ROC domain (amino acids 1333-1516) in complex with GDP revealed a dimeric GTPase (Deng et al., 2008). Although the proposed model describes a canonical GTPase fold, the catalytic core of LRRK2-ROC adopts an unusual topology due to domain swapping, in which the N-terminal of one monomer interacts with the C-terminal of the second monomer, thereby forming a constitutive dimer. Two follow-up studies investigated the quaternary structure of isolated ROC in solution using size exclusion chromatography. Liu et al. showed that the ROC construct, which crystalizes as swapped dimer, purifies as a mixture of dimers and monomers and ROC phosphorylation by LRRK2 or Roco4 enhances the proportion of monomers (Liu et al., 2016). Of interest, the GTPase activity of monomers and dimers are nearly identical. A second study by Liao and collaborators (Liao et al., 2014) purified an extended ROC construct (amino acids 1329-1520) that resulted highly stable and exhibited two chromatographic peaks corresponding to the apparent size of a dimer and a monomer. The authors further demonstrated that the dimeric fraction can be converted into monomers by addition of guanine nucleotides (Liao et al., 2014). Therefore, the existence of both dimers and monomers in solution suggests that isolated ROC may not form a constitutive dimer and that the swapped 3D model might be a crystallographic artifact.

One important consideration to make is that the ROC domain always occurs in tandem with the C-terminal of ROC (COR) domain, and the ROC-COR module is conserved across species. Thus, it is likely that ROC-COR represents a single functional unit and structural and biophysical studies should be focused on this fragment rather than on isolated ROC. However, the difficulty of purifying sufficient amounts of stable recombinant human ROC-COR has hampered its structural investigation. Important structural information on the role of COR in ROC dimerization comes from studies with related ROCO proteins from bacteria. In 2008, a crystallographic study of the ROC-COR unit from the thermophilic green bacteria *Chlorobium tepidum* disclosed a dimeric organization of ROCO proteins. However, in contrast to the previously determined structure of human ROC domain, the structural analysis of bacterial ROC-COR revealed a canonical G protein

domain where dimerization is mediated by the C-terminal half of the COR domain and by highly conserved residues on the ROC-COR interface (Gotthardt et al., 2008). That COR is a stable dimerization device serving as a scaffold for the ROC domain was also confirmed by a more recent study in which site-direct spin labeling was used to evaluate by pulse EPR the distances defined by the constrains that govern dimerization (Rudi et al., 2015).

Notably, there are evidences that suggest the importance of the dimeric structure on both GTPase and kinase activity of LRRK2 (Sen et al., 2009; Berger et al., 2010).

2.1 GTPase And Kinase Activities Of LRRK2

A major feature of LRRK2 is the presence of a dual enzymatic core where the activity of one domain may influence the function of the other. The GTP-binding site of ROC possesses a region highly conserved among GTPases called P-loop (residues 1341–1348, GNTGSGKT) (Ito et al., 2007). This domain is responsible for nucleotide binding, while another important region, called Switch II motif (residues 1394–1398, DFAGR), contributes to LRRK2 capacity to hydrolyze GTP. Similar to other GTPases, the nucleotide binding changes the state of the protein that cycle from an active (GTP-bound) to an inactive state (GDP-bound). The presence of dual activities, kinase and GTPase, within the enzymatic core suggests that they may influence each other. There are some evidences that the GTPase activity of LRRK2 may regulate its kinase activity. In particular, addition of guanine nucleotide in the kinase reaction has been shown to increase LRRK2 autophosphoryaltion (Smith et al., 2006). Another study however was not able to replicate this result and proposed that GTP can increase LRRK2 kinase activity via an indirect mechanism (Taymans et al., 2011).

However, artificial mutations in the P-loop region (K1347A and T1348N) compromise the kinase activity possibly by altering the folding and produce a kinase dead form of the protein (Smith et al., 2006, West et al., 2007, Taymans et al., 2011). Altogether, these findings suggest that GTP binding to ROC may not directly affect kinase activity, but a correctly folded ROC (possibly in the dimeric conformation) is important for kinase

activity. The LRRK2 interactors ARHGEF7 and ArfGAP1 have been proposed as LRRK2 guanine nucleotide exchange factor (GEF) and GTPase Activating protein (GAP) protein, respectively (Haebig et al., 2010; Xiong et al., 2012). Of note, ArfGAP1 is also a substrate of LRRK2 kinase activity and this phosphorylation compromises its GAP activity, suggesting a reciprocal regulation of the two proteins with consequences on activity and cytotoxicity (Xiong et al., 2012). As discussed, LRRK2 is thought to function as a dimer and an alternative hypothesis is that LRRK2 may be activated by nucleotide-dependent dimerization thus functioning as a GAD (G proteins activated by nucleotide dependent dimerization). This mechanism of activation would eliminate the dependence on regulatory GAPs and GEFs proteins (Gasper et al., 2009).

Other studies reported that the cross-talk could be from the kinase to the GTPase domain. Supporting this notion, the majority of autophosphorylation sites within LRRK2 map in the Roc domain (Greggio et al., 2009; Gloeckner et al., 2010). Thus, the kinase domain may act intra-molecularly to regulate GTP binding and hydrolysis via phosphorylation of ROC. Of note, whilst several putative LRRK2 kinase substrates have been proposed (Yun et al., 2013; Martin et al., 2014), the most consistently reported and validated substrate of LRRK2 *in vivo* is LRRK2 itself (Sheng et al., 2012). Accordingly, a number of serine and threonine residues have been identified as autophosphorylation sites in vitro. Autophosphorylation of Ser1292 has been proven also in vivo (Sheng et al., 2012). The majority of the studies focused on kinase activity rather than GTPase activity as kinases are ideal pharmacological targets. An early study showed that pathological LRRK2 mutations (I1122V, R1441C or Y1699C) on a kinase-dead background resulted in a reduced formation of cytoplasmic inclusion bodies and cell death (Greggio et al., 2006). Moreover, LRRK2 pharmacological inhibition in vivo in rodent brains protects from neuronal cell death (Lee et al., 2010). To date, a number of selective and potent LRRK2 inhibitors have been developed and LRRK2 inhibition has been proven effective at reducing pathological phenotypes in the rodent brain (Daher et al., 2015). However, chronic administration of LRRK2 inhibitors in rodents and non-human primates results in lung toxicity (Tong et al., 2012; Baptista et al., 2013). Thus, more research is necessary to understand whether inhibition of LRRK2 can be translated in the clinics as a future cure for PD.

2.2 LRRK2 Localization

LRRK2 is expressed in different tissues and organs including kidneys, liver, lung, heart and, in the brain, within neurons, astrocytes and microglia (Miklossy et al., 2006). This ubiquitous pattern of expression suggests a role of this protein in different intracellular processes. In the cell, LRRK2 has been found associated with intracellular membranous structures including mitochondria (Hatano et al., 2007), the endo-lysosomal system (Alegre-Abarrategui et al., 2009), the endoplasmatic reticulum (ER) (Gloeckner et al., 2006) and the Golgi (Biskup et al., 2006). Postmortem human brain tissue from normal and PD patients shows LRRK2 localization in the cerebral cortex, striatum, cerebral cortex, hippocampus, cerebellum and, at low levels, in the substantia nigra (Higashi et al., 2007). In pathological conditions, LRRK2 was found associated with LBs (Zhu et al., 2006) and LNs (Giasson et al., 2006), although not as major component of this inclusions. Accumulating evidence indicates that impairment of autophagy-lysosomal pathways is as a major pathogenic event in neurodegenerative diseases, including PD (Dehay et al., 2013). Of interest, there is robust evidence that links LRRK2 with endolysosomal-autophagy processes (Rivero-Ríos et al., 2015). An increased lysosomal compartment was observed in primary cortical neurons (MacLeod et al., 2006) and SHSY-5Y cells expressing pathological LRRK2 mutations (Plowey et al., 2008). Moreover, in pathological brains LRRK2 was found colocalized with Rab7B, a late endosomal marker, and LAMP-2, a lysosomal marker (Higashi et al., 2009).

Multiple lines of evidence indicate that LRRK2 localization is controlled by 14-3-3 proteins. Specifically, 14-3-3s bind a cluster of serine residues at the N-terminal of LRRK2 (including S910 and S935) and this binding is thought to be important to maintain LRRK2 in the cytosol (Nichols et al., 2010; Dzamko et al., 2010). S910/S935 phosphorylation level is tuned by cellular activity, possibly through activation of PP1 phosphatases and/or inhibition of kinases such as CK1alpha and IKKs (Dzamko et al., 2012; Lobbestael et al., 2013; Chia et al., 2014). Dephosphorylation of S910/S935 results in LRRK2:14-3-3 complex dissociation (Nichols et al., 2010; Dzamko et al., 2010) with consequent relocalization of LRRK2 into defined cellular compartments including cytoskeletal elements and centrosomes (Nichols et al., 2010; Mamais et al., 2014). One striking feature of the majority of LRRK2 pathogenic mutations is that they all display moderate

to severe loss of S910/S935 phosphorylation in cell models, suggesting that LRRK2 cellular phosphorylation is an important biomarker for monitoring LRRK2 pathological state. An additional role of LRRK2:14-3-3 interaction could be the regulation of LRRK2 association with late endosomes and extracellular release via exosomes. The identification of LRRK2 within exosomes isolated from urine or cerebral spinal fluid (CSF) suggests a possible use of LRRK2 as a biomarker in clinical studies (Fraser et al., 2013). Interestingly 14-3-3 proteins have been linked to numerous neurological disorders including PD (Berg et al., 2003; Chen et al., 2005; Plotegher et al., 2014).

2.3 PD-Associated Mutations

Many of the pathological mutations of LRRK2 are located within the enzymatic core of the protein (Fig.2.3.1). Among all, the G2019S pathological mutation is the most frequent. For this reason is one of the most studied: it lies in the DXG motif (DYG in LRRK2) in the activation loop of the kinase domain, and is characterized by a "gain-of-function" effect on LRRK2 kinase activity that produce a hyperactive form of LRRK2 with 2-3 fold increased activity compared to the wild-type (Greggio and Cookson, 2009) and its overexpression in neurons is toxic (Greggio et al., 2006; Smith et al., 2006). Of interest, the fact that LRRK2 mutations cause familial PD and common variations in the *Lrrk2 locus* increase life-time risk (Dächsel and Farrer, 2010), suggest a link between sporadic and inherited PD with LRRK2 being a common player (Lee et al., 2012).

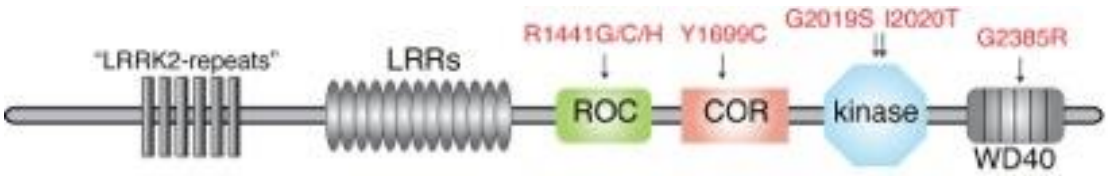

Fig.2.3.1 | LRRK2 pathological mutation. A focus on LRRK2 PD-related mutations and their localization inside LRRK2 different domains (Adapted from Greggio, 2012).

Mutations laying in the Roc (R1441C/G/H) and COR (Y1699C) domain have been shown to decrease GTP hydrolysis (Lewis et al., 2007; Li et al., 2009; Liao et al., 2014), suggesting a prolonged active state (GTP-bound) of LRRK2 and, hence, an abnormally

activated downstream signaling. The effect on kinase activity is variable, but integrating different studies there seems to be no consistent effect on this activity (Greggio and Cookson, 2009). One study addressed the effect of the Y1699C mutation within the COR domain on human ROC-COR dimerization (Daniëls et al., 2011). The authors found that the intra-molecular ROC:COR interaction is favoured over ROC:ROC dimerization. The pathogenic Y1699C mutation, situated at the ROC:COR interface, strengthens the intra-molecular ROC:COR interaction, weakening the dimerization of LRRK2 at the ROC-COR tandem domain and resulting in decreased GTPase activity (Daniëls et al., 2011). In *C. tepidum* ROC-COR, the Y804C PD mutation in the COR domain analogous to the Y1699C human mutation, and the two L487V and Y558A mutations in the ROC domain, analogous to the I1371V and R1441G/C PD mutations, have much lower GTPase activity but similar dimerization properties (Gotthardt et al., 2008). Taken together, the ROC-COR PD mutations seem to severely affect GTPase activity, whereas the effect on dimerization is unclear.

Only recently identified mutation in the Roc domain is the N1437H and its overexpression in cells enhances the phosphorylation on Ser1292 similar to what observed for R1441G/C, G2019S and I2020T (Sheng et al., 2012). As a consequence, LRRK2 associated cytotoxicity does not depend simply to an alteration on its kinase activity (Fig.2.3.2). The fact that the kinase domain phosphorylates ROC, it is possible that ROC is the important pathological site, with the G2019S mutation impacting GTPase activity via abonormal phosphorylation of ROC. Indeed, a decreased GTPase activity by 20% has been reported for the G2019S mutant (Herzig et al., 2011). Overall, LRRK2 PD mutations may promote decreased GTPase activity, which results in a prolonged active state of the protein.

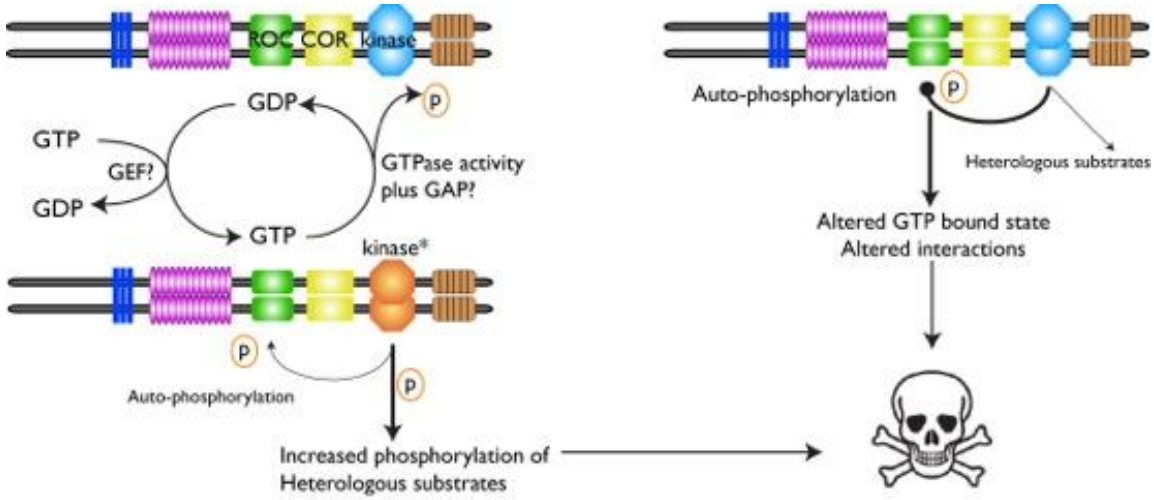

Fig.2.3.2 | Schematic representation of LRRK2 associated cytotoxicity. Increase in LRRK2 kinase activity enhances the phosphorylation on Ser1292, thus an increased phosphorylation of LRRK2 substrates (left). Moreover, the kinase domain may regulate GTP binding and hydrolysis *via* phosphorylation of ROC domain (right). These alterations in the normal function of LRRK2 lead to cytotoxicity inside neurons (image courtesy of Dr. Mark Cookson).

Using yeast as model organism, altered GTPase activity was suggested to promote impairment in the endocytic vesicular trafficking and autophagy (Xiong et al., 2010). Several animal models have been generated to understand how *Lrrk2* mutations affects the cellular processes *in vivo*. In particular, a number of LRRK2-mouse models have been generated, but only one of the LRRK2 transgenic mice models expressing G2019S mutation reproduces age-dependent loss of dopaminergic neuron (Ramonet et al., 2011). However, different mutant LRRK2 rodent models display neurotransmission defects (Tong et al., 2009; Melrose et al., 2010; Beccano-Kelly et al., 2014; Belluzzi et al., 2012), and, accordingly, several lines of evidence support a role of LRRK2 at the presynapse (Shin et al., 2008; Piccoli et al., 2011; Matta et al., 2012; Belluzzi et al., 2012; Migheli et al., 2013; Cirnaru et al., 2014; Beccano-Kelly et al., 2014). As discussed below, there are good molecular evidences linking LRRK2 kinase activity and regulation of synaptic vesicle trafficking, with pathogenic mutations impairing this process.

2.4 LRRK2 And Regulation Of Vesicles Dynamics

As described above, several studies showed an association between LRRK2 and vesicle structures in the mammalian brain suggesting a regulation in vesicles trafficking

(MacLeod et al., 2006; Stafa et al., 2012). Overexpression of wild-type or G2019S mutant leads to fragmentation of the Golgi complex (Lin et al., 2009). Furthermore, LRRK2 overexpression provokes an impairment of microtubule dynamics, Golgi organization, and the ubiquitin-proteasome pathway enhancing alpha-synuclein mediated cytotoxicity (Lin et al., 2009). In addition, an alteration in LRRK2 expression show an impairment in synaptic vesicle regulation This regulatory mechanism derived from the interaction between LRRK2 and small GTPases Rab protein, associated to all cellular compartments, regulating in the endosome maturation (Zerial and McBride, 2001). One example is Rab5, a regulator of vesicles transport from plasma membrane to EE compartment: Rab5 functional defects have been reported to compromise endocytosis (Wucherpfennig et al., 2003) and its over-expression can rescue the altered phenotype due to LRRK2 overexpression or knock-down (Shin et al., 2008). Recent studies demonstrate that Rab5b is a substrate of LRRK2 kinase activity *in vitro* and its GTPase activity is enhanced upon phosphorylation (Yun et al., 2015). Rab5 is not the only small GTPase found to interact with LRRK2: an interaction was also found with Rab7L1 (also called Rab29), which is associated with the TGN and mediate the retrograde trafficking (Wang et al., 2014). Recent studies showed how Rab7L1 interacts with LRRK2 to regulate retromer function and lysosomal pathways to modify intraneuronal protein sorting and PD risk (MacLeod et al., 2013). In addition, genome-wide association studies (GWAS) highlight a genetic interaction between Rab7L1 and LRRK2 (Beilina et al., 2014). Of interest, other studies show that LRRK2 phosphorylates EndophilinA (EndoA). EndoA is an evolutionary conserved protein known to drive vesicle formation through membrane interactions (Ringstad et al., 1997). EndoA “loss-of-function” causes defects in synaptic vesicle endocytosis and transmission (Milosevic et al., 2011). In *Drosophila*, LRRK2 was shown to phosphorylate EndoA at Ser-75 decreasing its affinity for the membranes (Matta et al., 2012).

From a screening of possible LRRK2-interacting proteins, LRRK2 has been also proposed to participate in the exo- and endo-cytic pathways by phosphorylating Snapin (Yun et al., 2013). Snapin is a SNAP-25-binding protein associated with the SNARE complex (Ilardi et al., 1999). Studies on Snapin knock-out mice show altered calcium exocytosis and impairment in SNAP-25:Synaptotagmin-1 binding (Tian et al., 2005), instead this

association is increased by protein kinase A (PKA) phosphorylation on Ser-50 (Thakur et al., 2004). LRRK2 was found to interact with and phosphorylates Snapin at Thr-117: phosphorylation rate is higher in the presence of LRRK2-G2019S pathological mutation and results in a decreased association of synaptotagmin-1 to the SNARE proteins (Yun et al., 2013). This suggests that the negative regulation of Snapin by LRRK2 may underlie the defects in synaptic transmission.

LRRK2 interacts with several presynaptic through its WD40 domain (Piccoli et al., 2014), which is important for both LRRK2 physiological and toxic role (Sheng et al., 2010). The PD-risk variant in the WD40 domain, G2385R, was found in Asian population (Funayama et al., 2007) and several presynaptic proteins, such as the N-ethylmaleimide Sensitive Fusion protein (NSF) later discussed, were shown to differentially interact with mutant-WD40 compared to wild-type-WD40 (Piccoli et al., 2014). In addition, LRRK2 kinase activity has been shown to be crucial for proper SV trafficking (Cirnaru et al., 2014).

2.5 LRRK2 And Cytoskeleton

Several studies support a role for LRRK2 in regulating cytoskeleton dynamics through differential protein-protein interactions. In particular, LRRK2 has been shown to interact with α/β tubulin heterodimers and microtubules (Gandhi et al., 2008; Law et al., 2014). Moreover, β-tubulin is a substrate of LRRK2 kinase activity *in vitro* and this is enhanced by 3-fold in presence of G2019S mutation (Gillardon, 2009). There are different hypotheses on the nature of LRRK2 interaction with microtubules: it may interact directly on microtubules, with microtubules-associated proteins or microtubules may localize LRRK2 within the cell by serving as scaffold for LRRK2 signaling. Interestingly, mutations in the Roc-COR domain (R1441C and Y1699C) cause impaired axonal transport and acetylation (Godena et al., 2014), as LRRK2 binding to tubulin is responsible of its stability (Law et al., 2014). Moreover, LRRK2 is able to phosphorylate tau protein only in the presence of tubulin altering its binding to microtubules (Kawakami et al., 2012). Since microtubule transport is critical for intracellular vesicle trafficking, the role LRRK2 in this mechanism may cause the trafficking deficits seen in PD and neurodegenerative

disorders. Taken together, these results suggest a possible mechanism compromised in PD that could serve as possible target against neurodegeneration.

2.6 LRRK2 And Autophagy

Deregulated neuronal autophagy can lead to Parkinson's disease phenotypes in rodent models (Komatsu et al., 2006; Hara et al., 2006; Zhu et al., 2007) and it may underlying the accumulation of ubiquitinated proteins that results in Lewy bodies. Knockdown of autophagy proteins attenuates the toxicity of LRRK2-G2019S in SH-SY5Y cells, accompanied by neurite shortening (Plowey et al., 2008). Moreover, the LRRK2-R1441C mutant causes an accumulation of abnormal Multivesicular bodies (MVBs) and autophagic vacuoles (AVs) and it is localized on autophagosomal and autolysosomal membranes (Alegre-Abarrategui et al., 2009). A link between LRRK2 and autophagy in vivo comes from a study where *Lrrk2* $^{-/-}$ mice display accumulation and aggregation of proteins, including a-syn, in the kidneys (Tong et al., 2010). In addition, kidneys from *Lrrk2* $^{-/-}$ mice display an altered level of lysosomal proteins and an accumulation of autolysosomes with an impairment of normal protein degradation pathways (Tong et al., 2012), suggesting a relationship between LRRK2 and protein degradation pathways in PD. However, the mechanism by which pathogenic LRRK2 alters autophagy is still an open question.

2.7 LRRK2 And Mitochondria

A number of studies described a role of LRRK2 in mitochondria. Over-expression of wild-type LRRK2 has been shown to induce mitochondrial fragmentation in SH-SY5Y cells and this effect was increased in the presence of pathogenic R1441C and G2019S mutations (Wang et al., 2012). In addition, co-expression of LRRK2 and DLP1, dynamin-like protein 1, caused DLP1 to translocate to mitochondrial membrane promoting mitochondrial clearance and induced oxidative stress (Niu et al., 2012). Another study proposed that wild-type LRRK2 can act as a neuroprotective agent against cell death caused by H_2O_2 in HEK293 and SH-SY5Y cells (Liou et al., 2008). On the other hand, G2019S-LRRK2 cells

were found to be more sensitive to ROS (Nguyen et al., 2011) and this could be due to the altered mitochondria morphology observed in fibroblasts from PD patients carrying this pathological mutation (Mortiboys et al., 2010). Over-expression of LRRK2-G2019S in SH-SY5Y cells causes mitochondrial uncoupling and a higher oxygen consumption (Papkovskaia et al., 2012). Mitochondrial damage has also been showed in transgenic mice carrying the G2019S mutation (Ramonet et al., 2011), whereas double transgenic mice with both G2019S-LRRK2 and A53T-aSyn mutations display impaired mitochondrial activity (Lin et al., 2009). Of note, inhibition of dynamin-related protein 1, DRP1, is able to rescue mitochondrial fragmentation due to G2019S-LRRK2 mutation in HEK293 and fibroblast (Su and Qi, 2013). All these evidences support a strong relationship between LRRK2 and mitochondrial damage, although it is still unclear if this represent an initial step in the development of the pathology, or if it is a secondary effect of LRRK2 toxicity. In fact, evidence supporting a direct role of LRRK2 in maintaining mitochondria homeostasis is currently missing.

2.8 LRRK2 As A Potential Therapeutic Target

At present, Parkinson's disease therapies can alleviate symptoms by administration of levodopa or dopamine receptors agonists, but cannot halt or slow the inexorable neurodegenerative process. Thus, disease-modifying approaches are urgently needed to cope with the high social and economic burden of the disease. Being LRRK2 a kinase, it has attracted much attention over the past ten years, since kinase inhibitors have been largely exploited in the clinic, especially for cancer therapies. Initial studies highlighted a central role of LRRK2 kinase activity in mediating the observed toxic phenotypes in cell models, providing the rationale to invest in the development of specific inhibitors. In particular, kinase dead mutants of LRRK2 exhibit reduced neuronal toxicity (Greggio et al., 2006; Smith et al., 2006), rescue of the neurite shortening phenotype observed with pathogenic mutations as well as reduced accumulation of tau-positive inclusions (MacLeod et al., 2006).

To date, over 100 hundred LRRK2 inhibitors have been described (reviewed in Taymans and Greggio, 2015). The early inhibitors (i.e. H1152 and sunitinib) had several unspecific

targets and the first molecule with good selectivity and potency was the LRRK2 inhibitor 1 (IN-1), which was capable of abrogating LRRK2 Ser910/Ser935 phosphorylation in cells (Dzamko 2010; Deng et al., 2011). However, the reduced blood brain barrier penetration limited its subsequent use *in vivo* (Kuss et al., 2014). Further studies identified the Glaxo-Smith-Kline inhibitor GSK2578215A as a better candidate for LRRK2 kinase inhibition (Reith et al., 2012).The recent Pfizer inhibitor PF06447475 is one of the most potent and selective molecules against LRRK2 kinase activity. Recent studies, however, have highlighted potential safety liabilities with LRRK2 inhibition. In particular, knock-out mice exhibit side pathologies on lung, liver and kidney (Baptista et al., 2013), whereas chronic treatment of non-human primates with the potent and selective MLi2 inhibitor results in lung pathology (Fuji et al., 2015). Thus, more research is needed to clearly understand whether LRRK2 inhibition can become a therapeutic strategy to combat PD. These observations also support the idea of investigating LRRK2 interactors and substrates to define the entire LRRK2 cellular pathways compromised during disease and, thus, identify alternative candidates rather than direct LRRK2 inhibition.

3. Synaptic Vesicle Trafficking

Accumulating evidence suggests that synaptic dysfunction and impaired neurotransmitter release may be one of the aspects that trigger neurodegeneration at early stages (Fernandez-Chacon et al., 2004; Burré et al., 2010), although the causes of this dysfunction remains unclear. Several studies focused on the presynaptic site to identify the mechanisms involved in synaptic vesicles (SV) recycling and neurotransmitter release and addressing how pathological mutations may affect the exo- and endocytic machinery.

3.1 Synaptic Vesicle Pools

SV are generally categorized in relation to their localization at the presynapse, their availability and stimulus needed for release. Different pools have been classified in relationship with their proximity to the Active Zone (AZ), a portion of the presynaptic membrane where fusion between vesicles and membrane occurs. SV are classified as the Ready Releasable Pool (RRP), the Recycling Pool (RP) and the Resting/Reserve Pool (RtP) (Südhof, 2004; Dittman and Ryan, 2009) as shown in Fig.3.2.1 A:

1. **RRP.** Vesicles belonging to this group are immediately available after a low stimulation and their highest fusion probability, in association with a fast recycling property, allow them to play the major role in neuronal transmission. Most of them are docked (“pre-primed”) or in close proximity to the AZ and represent 1-2% of the total number of vesicle (Hanse and Gustafsson, 2001; Schikorski and Stevens, 2001).
2. **RP**. Vesicles located here require a strong stimulation to be released and translocate into the RRP (Stevens and Wesseling, 1998). However, they display a high mobility necessary to replace SV in the RRP upon neurotransmitter release and they are continuously recycled and refilled from the RtP (Südhof, 2004). SV in the RP represents a higher fraction of vesicles, about 10-20% of the total number.

3. **RtP**. This pool is defined as a class of vesicles that substantially remains unreleased except after strong activity and stimulation (Richards et al., 2000; Denker et al 2009). This is considered as a stock pool of vesicles and represents 80-90% of total synaptic vesicles.

The number of vesicles that compose these three pools differs due to the type of junctions. Moreover, synaptic vesicle are located among the three different compartment to be prone for release and refilled at a specific rate. Neurotransmitter release is regulated by Ca^{2+} and the release probability depends on Ca^{2+} affinity of sensors, which denotes the recruitment of a specific pool (Wen et al., 2010). The peak depends on the duration of the action potential that modulates neurotransmitters release (Qian and Saggau, 1999), the open probability of Ca^{2+} channels and the Ca^{2+} concentration when they are opened since residual Ca^{2+} during repetitive action potentials causes short-term plasticity of release (Zucker and Regehr, 2002). However, the release probability per peak of Ca^{2+} concentration depends on the number of vesicles in the RRP and their responsiveness to the stimulus, pool size and kinetic: this feature differs from synapses (Xu-Friedmann et al., 2001) and changes in the long-term potentiation (LTP).

3.2 Synaptic Vesicle Composition

Vesicles have different forms of release during presynaptic activity and a different lipid-protein composition in association with their role and pathway inside the cell (Fig.3.2.1). SV are small vesicles with a diameter between 30-40 nm, are composed by a lipid bilayer and a 60% protein to lipid ratio (Takamori et al., 2006): over 400 different protein can be found both on the surface and inside the SV membrane (Grønborg et al., 2010). A different protein composition denotes the SV specialization (Poudel and Bai, 2014). All types of vesicles contain transport and trafficking proteins involved in neurotransmitters uptake and in the interactions with membranes in both exocytosis and endocytosis processes. The presence of additional proteins in addition to the basic components provides information on their different functional properties (Dittman and Ryan, 2009). Purified SV possess:

- **Proteins**. Among the hundreds of proteins described, few of them have been extensively characterized. The relative abundance of SV proteins differs and the stoichiometry between proteins is not well established across individual vesicles. Essential proteins that have a clear function on vesicles include synapsin I, a molecular marker for vesicles in the RP that theaters actin filaments with SV (Denker et al., 2011). When the RP needs to be mobilized, synapsin I is phosphorylated and loses affinity for SV (Verstegen et al., 2014). Moreover, the proton pump (vacuolar ATPase) whose functional role is necessary for neurotransmitter uptake through its transporter (Edwards, 2007), synaptotagmin I which acts as a calcium sensor essential for fast exocytosis (Chapman, 2008) and synaptobrevin2/VAMP2, later discussed, for the formation of the SNARE complex (Rizo and Rosenmund 2008);
- **Lipids**. SV were firstly described as composed by phosphatidylcoline, phosphatidylethanolamine, phosphatidylserine, phosphatidylinositol and cholesterol (Benfenati et al., 1989).

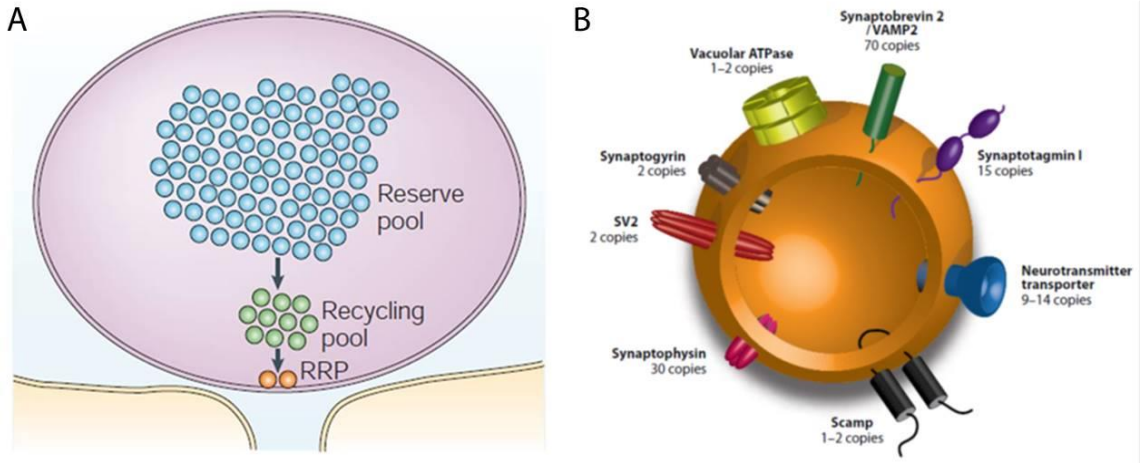

Fig.3.2.1 | The synaptic vesicle: (A) RRP is the more distant from the AZ, but is composed by 80-90% of the total vesicles, than the RP 10-20% and the RRP 1-2% (Rizzoli and Betz, 2005); (B) Proteins and their copy numbers identified through proteomic analysis on purified SV. (Dittman and Ryan, 2009).

Inclusion of distinct sensors and proteins to the SV membrane could characterize different presynaptic pathways with different release models and dynamics within the SV cycle.

3.3 Neurotransmitters Release And SV Cycle

Synaptic transmission begins when the action potential (AP)-mediated membrane depolarization reaches the axon terminal from the cell body. The change in membrane potential triggers neurotransmitters release from the presynaptic site into the synaptic cleft: AP stimulates the open of voltage Ca^{2+} channels increasing the amount of calcium inside the cell leading to fusion of SV to the membrane where exocytosis starts (Katz and Miledi, 1968). The membrane of the SV fuses with the cell membrane, aided by multiple membrane proteins. The fused area forms a pore and neurotransmitter diffuse across the gap into the synaptic cleft to bind with membrane receptors on the postsynaptic cell. When neurotransmitters bind to their receptors, the signal is transferred into the postsynaptic cell. After exocytosis, SV undergo endocytosis and are recycled inside the cell and refilled with neurotransmitters to be available for another fusion round.

Synaptic vesicles undergo a particular cycle in nerve terminal that can be divided into five steps:

1. Neurotransmitters are transported inside the synaptic vesicles;
2. SV cluster close to the active zone;
3. Vesicles in the RRP dock at the active zone;
4. Vesicles are pre-primed;
5. Ca^{2+} triggers the fusion-pore opening.

More than 40 years ago, different studies showed that after exocytosis, vesicles are rapidly refilled with neurotransmitters and that a number of vesicles recycled locally very fast. At the same time, data obtained from the neuromuscular junction highlight another fast way of vesicles recycling without a clathrin-coated intermediate (Ceccarelli et al.,1973), whereas an extensive stimulation produce a slow endocytosis of vesicles far from the synaptic terminal (Heuser and Reese, 1973). On the basis of these observations three vesicles pathways were proposed after neurotransmitters release in the synaptic cleft (Fig.3.3.1):

a) Vesicles are refilled with new neurotransmitters without undocking, thus remaining in the RRP (“kiss-and-stay”);

b) Vesicles undock, but remains in close to the active zone and recycle locally ("kiss-and-run");
c) Endocytic pathway through clathrin-coated pits, reacidify and refilled directly with neurotransmitters;
d) Instead of directly, neurotransmitters are refilled through an endosomal intermediate.

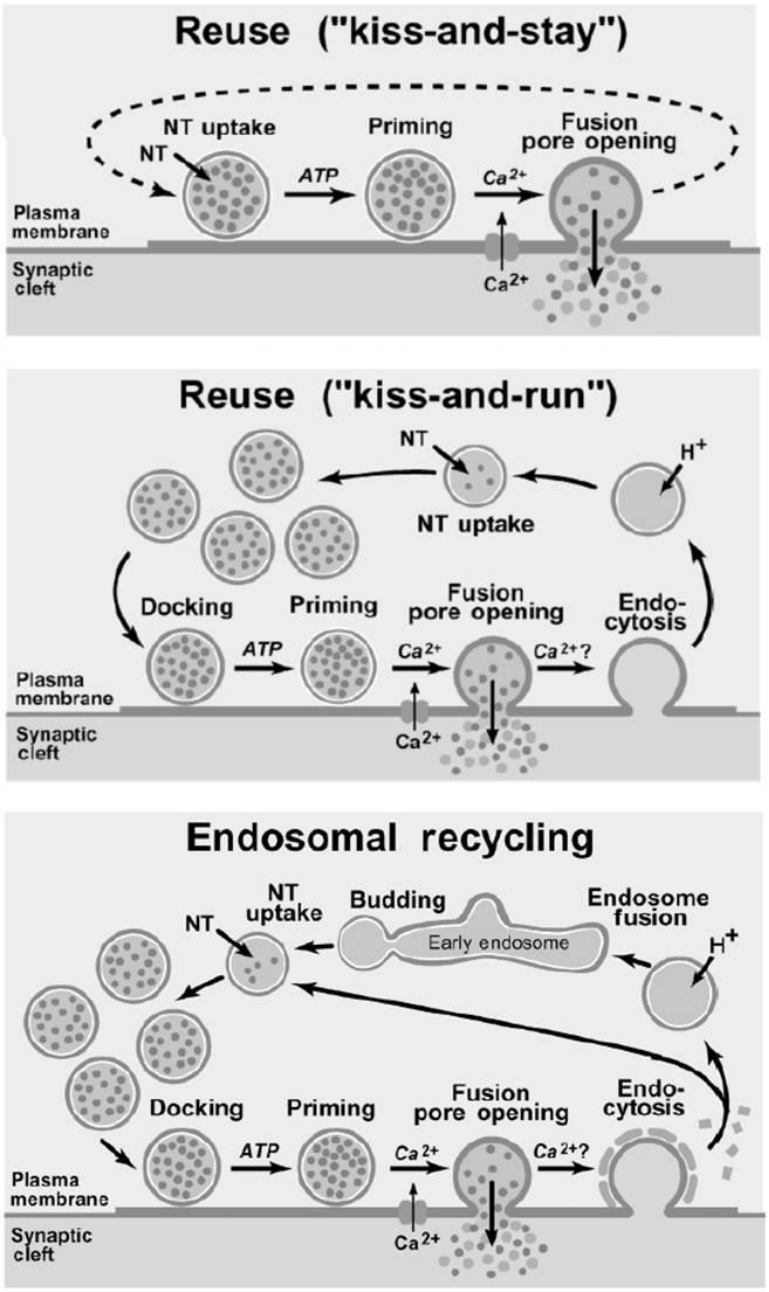

Fig.3.3.1 | Synaptic vesicle endocytic pathways: The three different pathway proposed in which vesicle remains in the RRP and refilled immediately with neurotransmitters ("kiss-and-stay"), a local recycling pathway within the RP ("kiss-and-run") and a clathrin-mediated endocytosis via endosomal recycling (Südhof, 2004).

These processes can be classified into "fast pathways" (a and b) or "slower pathway" (c and d) and a different fusion event can occurs: in the fast pathway vesicles probably utilize a transient fusion pore, whereas in the slow pathway the recycling involves a full fusion of the vesicle with the plasma membrane.

3.4 Trafficking Impairments In PD

As discussed previously, PD causes severe motor impairments due to a progressive degeneration of dopaminergic neurons in the substantia nigra pars compacta. A number of studies on familial forms of the disease revealed alterations in several cellular processes, but the link between mutations and neurodegeneration remains unclear. To this regard, growing evidence suggests that PD genes regulate presynaptic activity. Specifically, a study by Burré and co-workers reported that alpha-synuclein regulates the release of neurotrasmitters by promoting the assembly of the SNARE complex (Burré et al., 2010). Furthermore, alpha-synuclein knockout mouse exhibits an increase of evoked dopamine (DA) release, suggesting that alpha-synuclein is an activity-dependent negative regulator of DA neurotransmission (Abeliovich et al., 2000). Interestingly, also DJ-1 and PINK1 knockout mice exhibit reduced DA overflow and impaired striatal synaptic plasticity (Kitada et al., 2009). Finally, severe neurotransmission defects have been repeatedly observed in different LRRK2 rodent models (Belluzzi et al., 2012). Thus, defective neurotransmitter release could arise as a prodromal phase of the disease, contributing to the early stage symptoms of PD. Thus, one process that appears to be deregulated in different PD models is SV trafficking (Fig.3.4.1). However, genes implicated in PD are widely expressed and the main unanswered question is why the dopaminergic neurons are more prone to neurodegeneration (Zarow et al., 2003). One explanation seems to be that perturbation in SV trafficking causes an altered DA homeostasis, resulting in increased cytosolic levels of DA toxic which is toxic to the cell. This idea is supported by the finding that overexpression of aSyn leads to an higher cytoplasmatic DA level (Mosharov et al., 2006). Also other PD models, show a DA-dependent degeneration of DA neurons. Thus, the cellular impairments that affect SV trafficking may relate to deregulated DA storage/uptake, which in turn causes ROS increase leading to cytotoxicity and contributing to neurodegeneration (Bisaglia et al., 2013).

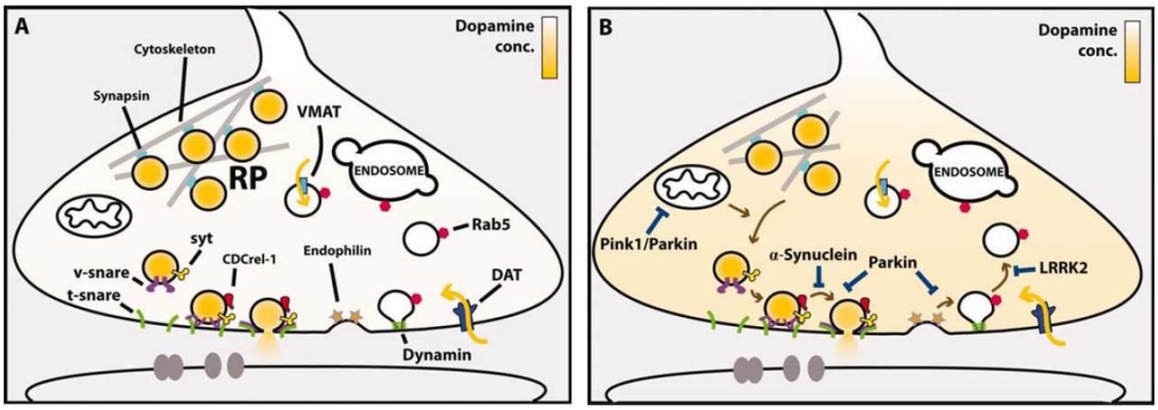

Fig.3.4.1 |Proteins associated to PD at the presynapse: (A) Schematic representation of vesicle trafficking at the presynaptic site. Vesicles filled with neurotransmitters move from the RP to the AZ. After docking and priming they are recycled inside the cell for another fusion event. (B) Effects of proteins related to PD at the presynaptic site in which an altered function produce a higher DA level allowing cytotoxicity. (Esposito et al., 2012).

4. Endocytic pathways

4.1 Organization And Function

Endocytosis is a cellular mechanism that allows internalization of extracellular components inside the cells and an important way of inter-cellular communication. Internalization of macromolecules and particles through an invagination of the plasma membrane is an essential step for maintenance of the intracellular framework and interaction with the environment (Mercer et al., 2010). In this scenario, endocytosis represents an important tuner of intra- and extra-cellular regulation and requires several elements necessary to reuse components or digest macromolecules through a recover or degradative system, respectively (Fig.4.1.1). The first step of the endocytic machinery is early endosomes (EEs) maturation, in which vesicles are directed to recycling, back to plasma membrane, or to late endosomes (LEs) maturation (Mayor and Pagano, 2007). EEs play a key role in determining the following sorting events such as recycling, degradation in LEs or lysosomes or delivery to the trans-Golgi network (TGN). In this regard, vesicles possess different morphology, localization, composition and function (van Meel and Klumperman, 2008). The maturation into LEs takes place from the EE compartment. During this maturation, vesicles communicate with the TGN (Bonifacino and Rojas, 2006) and this continuous vesicle sharing between these two compartments is a process extensively studied to unravel both vesicles destination and composition. LEs formed can fuse together and finally bind lysosomes to form bigger structures called endolysosomes (Luzio et al, 2007) that can be degraded through lysosomes. All those pathways provide a dynamic and continuous exchange mechanism and contribute in the maintenance of intracellular environment. The maturation process is characterized by changes in membrane components and the whole process is driven by regulating factors recruited at the surface of vesicle.

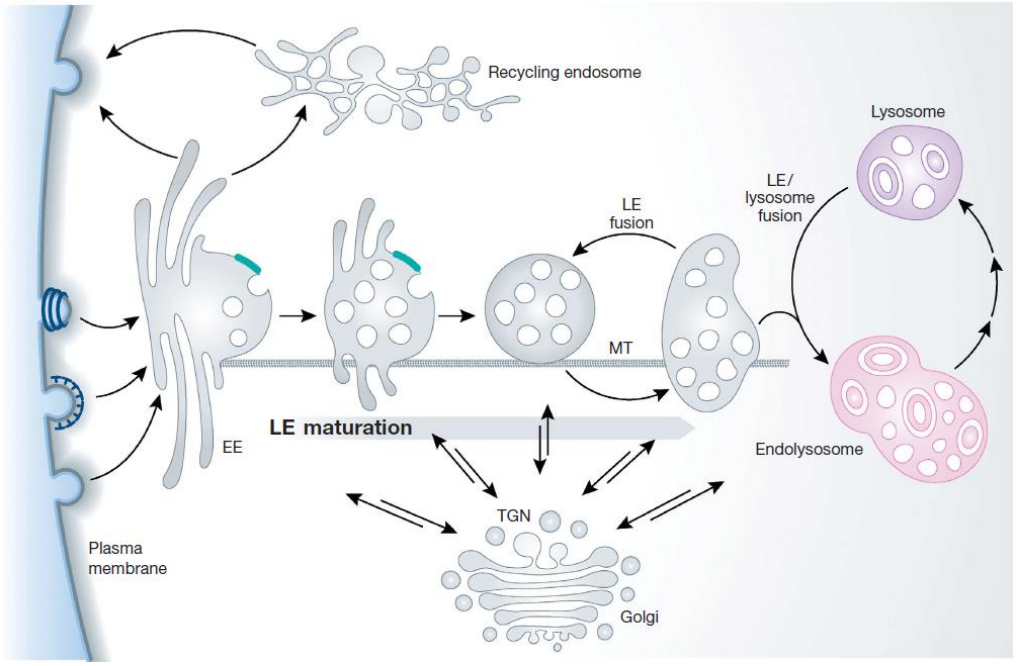

Fig.4.1.1 | The endocytic pathway: Endocytic vesicles move to the early endosome (EE) compartment, then can directly go back to the plasma membrane or moving towards to perinuclear space through microtubules (MT). Vesicles undergo several changes both on surface and in the lumen, acquiring more ILVs, and they deliver to lysosomes. At its final steps, vesicle fuses prior with a lysosome (endolysosome) in which components starts to be degradated, and then is converted into a lysosome (Huotari and Helenius, 2011)

4.2 Rab Proteins

Intracellular trafficking events are mediated by Rab proteins, a large family of monomeric small GTPases. Rabs are distributed in all cellular compartments (Fig.4.2.1) with multiple roles orchestrating organelles transport to regulate vesicle sorting inside the cell (Novick et al., 1997), therefore playing a major role in endocytic and vesicle trafficking also in neurons (Ng and Tang, 2008).

In humans, there are more than 60 Rab proteins localized on membranes (Schwartz et al., 2007; Pereira-Leal et al., 2001) and the regulatory principle is based on their GTP- and GDP- bound form: since they use GTP to explain their role, it is possible to distinguish between an active (GTP-bound state) or inactive (GDP-bound state) conformation of the protein. The interconversion between these two states is a label of their physiological function as molecular switches and it is characterized by conformational changes in specific regions: the structural basis of the Rab molecular switch can be defined as two portions of the proteins called Switch I and II regions, as for

Ras proteins (Pfeffer, 2005). The cycle between active and inactive state depends on the rates of nucleotide exchange and hydrolysis. Intrinsic GTPase activity of Rab proteins is low, but GTP hydrolysis is catalyzed by GAPs (Haas et al., 2007) and this function activates specific effectors involved in each transport step of vesicles maturation. At the same time, the GDP dissociation inhibitor (GDI) was identified as an important factor that prevent GDP-release from Rabs due to stabilize the inactive form (Matsui et al., 1990). To became active, they need to be recruited to membranes where GDI is removed and GDP replaced by GTP through GEF. An interesting feature is the different localization inside the cell of Rab proteins: this is mediated by the GDI displacement factors (GDFs) that plays a key role in Rab-GDP specific binding facilitating their specific association to membranes (Jovic et al., 2010). When they are in the active state, Rab proteins interact with a series of downstream effectors to modulate different pathways in vesicle maturation: Rab effector proteins control numerous steps providing a regulatory mechanisms complementary to SNARE proteins, further described. Each organelle has different Rabs on its surface that lend specificity on intracellular transport events, maintaining the specificity of interactions.. As mentioned before, the recycling vesicle through endocytosis is the main way to maintain the correct intracellular composition. During endosome maturation, EEs moved along microtubules (van Dam et al., 2002) acquiring components that manage their fate to specific compartments or vesicles could be immediately recycled back to the plasma membrane. At this point, Rab5 is the most important marker and a switch between it and other Rab proteins determines next events: Rab4 or Rab11 (Seaman et al., 2012) replaces Rab5 in the recycling endosome compartment (Schmidt and Haucke, 2007) for a fast or slow, through the perinuclear endosomal recycling compartment (ERC), vesicle fusion back to plasma membrane respectively (Stenmark, 2009).

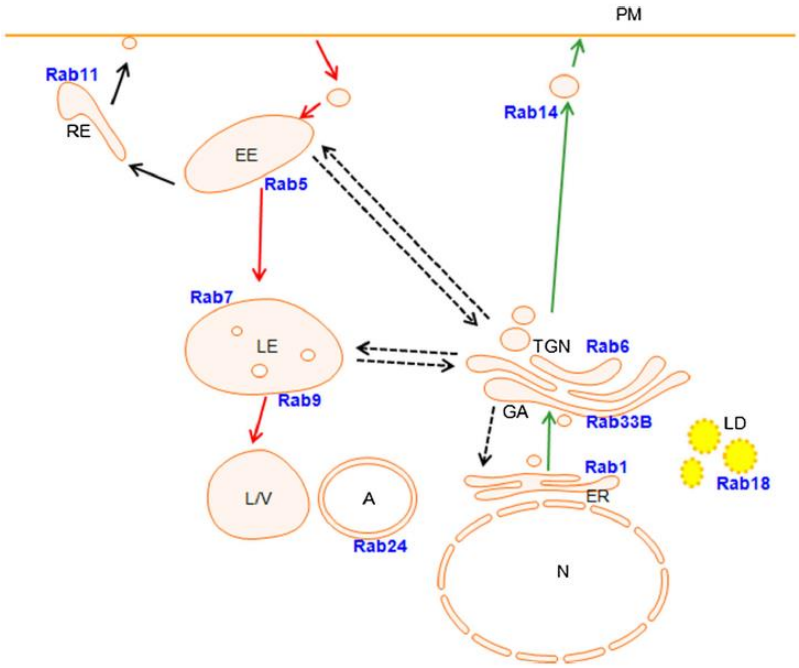

Fig.4.2.1 | Representative Rab proteins localization: The endocytic pathway (red arrows) from the plasma membrane (PM) involved several Rab proteins that acts in all different compartment through both for anterograde transport (green arrows) and EE recycled to PM and trans-Golgi Network (TGN, black arrows) (Adapted from Chua et al., 2015).

A number of studies showed how phosphorylation may regulate Rabs GTPase activity by direct phosphorylation or through phosphorylation of Rabs cofactors (Mattera et al., 2006; Chavez et al., 2008; Bailly et al., 1991). Previously in the introduction, LRRK2 has been described to associate with Rab5 proteins in the regulating synaptic vesicle endocytosis. Of interest, other studies identified also a relationship between PINK1-dependent phosphorylation and Rab proteins: PINK1 regulates Rab8A, 8B and 13 phosphorylation on Ser-111 and this phosphorylation impairs Rab:GEF interaction, in particular between Rab8A and Rabin8 (Lai et al., 2015).

All these findings highlight a potential novel regulatory mechanism altered in pathogenic conditions. An impairment of Rab GTPase-mediated signaling could alter the normal endocytic pathway and neurotransmitters release, thus representing an important mechanism compromised in PD.

4.3 Early Endosome (EE) Compartment

The first step of the internalization process requires maturation of vesicles to early endosomes (EEs), which is a crucial point that determines the fate of the proteins and lipids internalized. This maturation process begins with clathrin-dependent or -independent pathways. Molecules internalized could be either recycled back to the plasma membrane or undergo degradation in late endosome and then lysosome. The EE compartment receives vesicles directly from the plasma membrane and it is a structure with a high propensity to homotypic fusion (Gruenberg et al., 1989). It is characterized by the presence of regions with tubular extensions and multi-vesicular appearance (Gruenberg, 2001) that are important in vesicle sorting. It was demonstrated that the recycling pathway requires a step on the tubular membranes, whereas the multi-vesicular elements are responsible of addressing vesicle to the degradation pathway. In this scenario, most of the present ligands and molecules are degraded, conversely receptors are recycled back to the plasma membrane.

Intracellular fusion and trafficking events are mediated by specific soluble NSF-attachment receptors (SNAREs). These phenomena are specific and orchestrated by a class of proteins through the vesicular transport pathway. The regulation occurs at all the steps of vesicle maturation and a critical component is the small class of Rab GTPase proteins: these small enzymes bind GTP and became physiologically active. Upon activation, they can interact with other effector proteins with roles and functions that will be discussed later.

4.4 Late Endosomes (LEs)

The maturation process of EEs into late endosomes (LEs), which is in junction with the trans-Golgi network (TGN), requires several changes and transformations until endosomes fuse with lysosomes as a dead-end point. LEs formed move to the perinuclear region of the cell where they fuse with each other (Luzio et al., 2007). Through this process, different changes take place and only few components are rescued, such as receptors and SNARE proteins. The most important regulation step

from EE to LE allows the "Rab switch"(Carroll et al, 2001; Behnia and Munro, 2005): this process requires the exchange in membrane marker where Rab5, an essential factor for clathrin-mediated endocytosis, is converted to its GDP-bound form, dissociated from the vesicle and replaced by Rab7 (Rink et al., 2005, Poteryaev et al., 2010). The Rab5/Rab7 switch provides the most important regulation step from EE to LE maturation and organelles transport to lysosomes (Behnia and Munro, 2005; Carroll et al, 2001). Rab5 is on vesicle surface in its GTP-bound state, active, with its GEF Rabex-5; in this state Rabapitin-5, an effector of Rab5, binds the complex starting the dissociation of Rabex-5 from membrane (Lippé et al., 2001). Active Rabs can recruit additional effectors into these domains: this generates a loop resulting in Rab5 inactivation and dissociation through GAP inactivation in which Rab7 is recruited. At this point, Rab7 in the active state replaces Rab5 on vesicle (Grosshans et al., 2006). Apart from the "Rab switch", the lipid composition during vesicle maturation changes too: PtdIns(3)P on EE recruits the phosphatidylinositol 3-phosphate 5-kinase PIKfyve which converts it into PtdIns(3,5)P(2) on LE (Vicinanza et al., 2008). PIKfyve is also involved in the formation of intraluminal vesicles (ILVs), an important feature in the maturation process for further sorting events: the ESCRT complex (composed by ESCRT-0, -I, -II, -III) (Hurley and Hanson, 2010) and accessory proteins, such as VPS4 and Alix, are the main responsible of ILVs formation. The role of ESCRT machinery is to find the Ub-tags in the cytosolic domains of membrane proteins, which are subsequently removed. Their depletion results in a fewer ILVs formation, altered morphology and accumulation of cargo in endosomes (Razi and Futter, 2006). The acidification is another important aspect: EEs have a pH between 6.8 and 6.1 that decreases gradually down to 6.0-4.8 in LEs (Maxfield and Yamashiro, 1987). In addition, the lumen environment changes in Cl^-, Ca^{2+}, Na^+ and K^+ concentrations. Once LEs arrive in the perinuclear area they can fuse each other or with lysosomes (endolysosomes). The latter brings to a dead-end pathway since lysosomes are the degradative organelles in eukaryotic cells. Even if the LEs are mainly degraded in the lysosomal compartment, they can also be transferred to membrane diffusing their contents in the extracellular space through exosomes. Of interest, some components can be saved from degradation through the retromer complex (Bonifacino and Hurley, 2008; Seaman, 2012).

4.5 SNARE Proteins

In eukaryotic cells, exo- and endo-cytosis pathways and in general all intracellular fusion processes are mediated by specific interaction of proteins located on membrane surfaces. Vesicles are carried to the their destination moving to the target site that ends with docking and membranes fusion. Intracellular fusion events are mediated by a class of proteins called SNAREs (Soluble N-ethylmaleimide-sensitive factor Attachment protein REceptors) that guarantee the specificity of the interaction. The term SNAREs was firstly introduced in 1993 (Söllner et al., 1993) and since then more than a hundred different SNARE proteins have been discovered in several organisms, with 38 of them known to exist in humans (Malsam et al. 2008). The hallmark of all of them is the heptad repeat sequence: a conserved domain of about 70 amino acids (*SNARE motif*) with a propensities to form the coiled coils necessary for their interaction (Sudhof and Rothman, 2009). Monomeric SNAREs are unstructured, but their motif spontaneously form a stable four-bundle helical complex when they interact together (Fasshauer et al., 1997). The interaction is known as “zipper” model and starts from the N-terminal region to the membrane C-terminal of SNAREs and brings the two membranes in close proximity triggering membrane fusion (Hanson et al., 1997; Lin and Scheller, 1997). Due to this different localization inside the cells, SNARE proteins are divided into v-SNAREs (on vesicle) and t-SNAREs (target membrane) (Hong, 2005). Based on domain structure, all mammalian SNAREs have been classified as members of those three families. However from a structural point of view SNAREs can be classified also in R-SNAREs (arginine) or Q-SNAREs (glutamine) based on the key residue in the center of the SNAREs (Fasshauer et al., 1998). Generally, most R-SNAREs are members of the v-SNAREs and most of Q-SNAREs are t-SNAREs. The specificity of interaction leads to the formation of a coiled-helical bundle, highly stable and SDS-resistant (Poirier et al., 1998) complex with transmembrane domains (Chen and Scheller, 2001). This step is also characterized by a change in the SNARE structure that goes from a *trans*-SNARE complex to a *cis*-SNARE complex. In lipids fusion experiments it was demonstrated that two t-SNAREs and one v-SNAREs are required for membrane tethering and fusion (McNew et al., 2000).

4.6 The SNARE Complex

The crystal structure of the complex has been characterized and reveals a four-stranded coiled-coil assembly (Fig.4.6.1). In this conformation, the two membranes are in closed proximity and the binding among SNAREs triggers the membrane fusion (Zimmerberg et al., 1993). Biochemical studies reveal that the SNARE complex is high stable, up to 90°C (Hayashi et al., 1994), and SDS-resistant (Yang et al., 1999). Given this stability, the complex will not spontaneously disassemble, but this must be a mechanic process. However, the dissociation constant *in vivo* have not yet been described since the kinetic mechanism depends on SNARE concentration and membrane architecture, suggesting that additional protein are involved, such as SM (Sec1/Munc18-related) (Südhof and Rothman, 2009). In the nervous system, vesicle fusion to the pre-synaptic membrane, a calcium-dependent process (Heidelberger et al., 1994; Peters and Mayer, 1998), is an essential step in synaptic transmission. Neurotransmitters are released in the synaptic cleft: the neuronal SNAREs that mediate synaptic vesicle binding to the membrane are Synaptobrevin/VAMP (vesicle-associated membrane protein) protein and the plasma membrane SNAP-25 (synaptosomal-associated protein of 25 kDa) (Oyler et al., 1989) and Syntaxin-1 (STX-1) (Bennett et al., 1992) proteins. Therefore, neuronal SNARE core is composed by one coil of STX-1 and VAMP with two coils of SNAP-25 which constitutes the minimal functional unit of the SNARE complex *in vitro*. Regions that are not involved in the complex formation have also an important regulatory function: the C-terminal regions are involved in membrane interactions, and N-terminal regions might function as recruitment domains for SM-associated proteins (Jahn and Scheller, 2006). To date, a number of studies show that the N-terminal of STX-1 forms a “closed” conformation that competes with the others SNARE motifs for its binding in a negative regulation (Nicholson et al., 1998) and can recruit Munc-18, a chaperone that facilitates complex assembly (Hata et al., 1993). The loop region of SNAP-25 not involved in complex assembly is useful for membrane fusion, and thus crucial for synaptic transmission (Scales et al., 2000); the N-terminal region of VAMP probably is not involved in membrane fusion, but if depleted exocytosis is compromised (Scales et al., 2000)

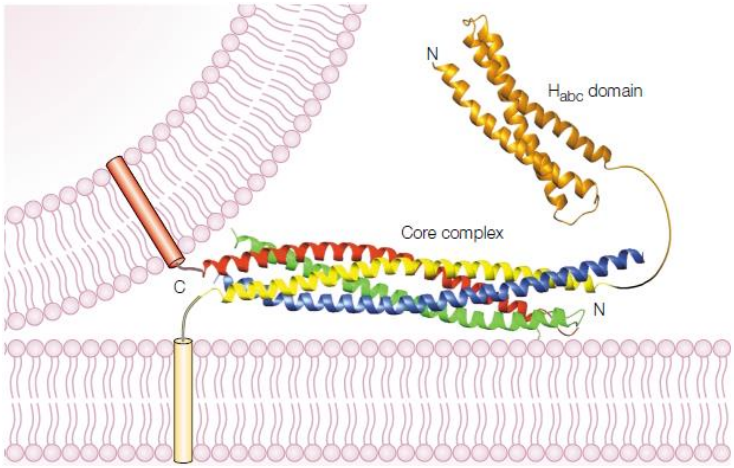

Fig.4.6.1 | The SNARE complex: Crystal structure of the SNARE complex composed by Synaptobrevin/VAMP (red), STX-1 (yellow) featuring its H_{abc} domain (orange) and both SNAP-25 N-terminal (blue) and C-terminal (green) (Rizo and Südhof, 2002).

After membrane fusion and neurotransmitters/molecules release, the complex could be disassembled to be reused inside the cells and synaptic vesicles undergo recycling through the endocytotic pathway. Since it is a high stable complex, ATP is needed to dissociate SNARE components: the disassembly process is carried out by the ATPase N-ethylmaleimide sensitive fusion (NSF) protein with its adaptor αSNAP (soluble NSF attachment protein).

4.7 The N-Ethylmaleimide Sensitive Fusion Protein (NSF)

In eukaryotic cells, intracellular trafficking requires SNARE proteins, therefore this complex needs to be disassembled after membranes fusion to make individual proteins available to be reused (Jahn et al., 2003). Spontaneous SNARE complex disassembly is slow, so this reaction is catalyzed by the N-ethylmaleimide Sensitive Fusion (NSF) protein that, with its adaptor protein αSNAP (Soluble NSF attachment protein) (Clary et al., 1990), binds the SNAREs and disassembles the four helix-bundle complex using the energy of ATP hydrolysis (Whiteheart et al., 2001).

NSF was firstly described in studies focused on TGN pathways (Block et al., 1988) as a regulatory factor in vesicle trafficking. NSF belongs to AAA+ (ATPases Associated with various cellular Activities), a wide family of ATPases found in all organisms. The hallmark of these proteins is the ATP binding domain of 200-250 amino acids characterized by

two conserved motifs: the Walker-A and Walker-B that mediate nucleotide binding (Ogura and Wilkinson, 2001; DeLaBarre and Brunger, 2003). AAA+ enzymes assemble into oligomers upon nucleotide binding and this is the biologically active conformation. In this state, they participate in several cellular processes by promoting conformational changes or remodeling of target proteins. The processes are proteolysis, protein disaggregation or protein-complex disassembly (Hanson and Whiteheart, 2005). This last function in eukaryotes is carried out by NSF itself to maintain intracellular network pathways, in which the disassembly of the SNARE complex is the main vesicle fusion regulation event. NSF is present in all tissues, but it is highly expressed in the nervous system, where it is responsible for synaptic transmission. Similar to other ATPases, NSF has two different ATP binding domain: one is necessary for conformational change from a monomeric structure to a homo-hexameric cylindrical quaternary structure; the second one is responsible for its ATPase activity. From a structural point of view, each subunit of NSF is composed by three different domains: the N-terminal domain (N, 1-205) necessary for interaction with αSNAP:SNAREs (Whiteheart et al., 2001), the D1 domain (206-477) with the ATP-binding domain necessary to disassemble the SNARE complex and the D2 (478-744) domain with the other ATP-binding domain necessary for hexamerization (Matveeva et al., 1997). The X-ray crystal structure of the N-terminal domain (May et al., 1999; PDB code: 1QDN) and D2 domain are well characterized (Lenzen et al., 1998; PDB code: 1NSF), but the structure of D1 domain lacks. Both D1 and D2 domains have the typical AAA+ structure for nucleotide binding with two subdomain called α and α/β motifs. When bound, αSNAP triggers the disassembly of the SNARE complex: prior to ATP hydrolysis the complex composed by SNAREs:αSNAP:NSF is called 20S, referred to its sedimentation constant, and the dissociation can start. Also this complex was well characterized by NMR and cryo-electron microscopy using all the structures of the single proteins available in the protein data bank (Chang et al., 2012; PDB code: 3J98).

4.7.1 NSF quaternary structure

Structural studies on NSF started when the protein was found in association with TGN trafficking (Balch et al., 1984). Further characterization demonstrated that the active state of NSF presents a homo-hexameric structure of 480 kDa (Hanson et al., 1996). Both the ATP- and ADP- bound state are organized into the three different layers one over the other referred to the three different domains of NSF described above (Fig.4.7.1.1): D2 domains at the bottom, D1 domains in the middle and N-terminal domains on top. This last mentioned domain has a different distribution between the two nucleotide-bound state and forms a layer of six or four domains for ATP- or ADP-bound state respectively (Zhao et al., 2015). To better describe the two different conformations, the chain with the closest distance between D1 and D2 domain is named Chain A in the D1 domain, then there are chains from B to F as distance increases. Active NSF is when the protein is in the D2 ATP-bound state.

The 3D reconstruction of NSF was obtained through cryo-EM density maps that well describe the distribution of the different domains. In the ATP-bound form, the D2 domain has a six-fold symmetry; however, D1 domain presents a chain stepping of 5 Å as showed by the position of the helix. In this conformation there is a step down from chain A to F and, being the F chain the one available at the lower structural resolution. This means that it is probably the more flexible part with a more open conformation of the D1 ring. In this state the diameter is about 112 Å for both D1 and D2 domains.

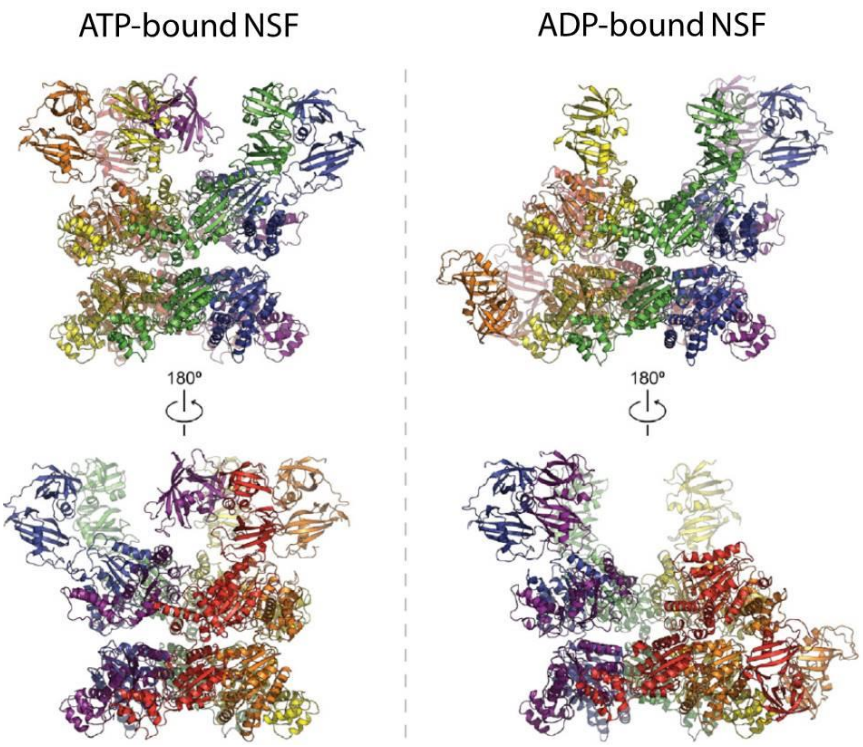

Fig.4.7.1.1 | Full-length NSF structures obtained with Cryo-EM: Side views of ATP- and ADP-bound state of NSF obtained from Cryo-EM density maps using cristal structures available from the Protein Data Bank (PDB) (Zhao and Brunger, 2015).

A difference between these two states is the α subdomain correlated to the different D1 conformation: D1 ring in ATP-state has a more compact structure, on the other hand in the ADP-bound has a more relaxed structure. On top there are the N-terminal domain (*up conformation*), and the lower density of this domain is probably due to its flexibility. This suggests a nucleotide-dependent movement of the flexible N-terminal domain and the different positions depend on NSF ATPase activity. The central hole has a dimeter of about 20 Å for D1 and near 24 Å on top to 7 Å at the bottom describing a more shaped structure of the D2 domain (Chang et al., 2012). For ADP-bound NSF, the D1 domain has a more expanded and planar conformation compared to its ATP-bound state, with a large opening between chain A and F that correspond to the gap in the D2 domain. The main difference is the position of the N-terminal domains that are allocated around the side (*down conformation*). Studies indicate the presence of four different N-terminal domains on top in this state (Zhao et al., 2015), despite previous data that placed all the six domains around the D1 (Chang et al., 2012). The D1 different conformation instead is related to a rotation of chains A and B and changes in their N domains.

Placing this structural information in the context of the 20S architecture (Fig.4.7.1.2), above NSF, there are the SNAREs and four different αSNAP that, with the N-terminal domains, surround the complex in a four-fold rotational symmetric arrangement. Moreover, αSNAP has a different twist compared to SNAREs: right and left-handed respectively. The SNARE proteins are in the center of the structure with a tighter conformation of D1 domain of NSF compared to the same domain alone in the ATP-state. The position of these proteins is located close to chains E and F near the small gap in D1 domain suggesting an interaction between these two parts. Previous findings indicate that *trans*-SNARE complex before membrane fusion is resistant to NSF activity (Weber et al., 2000) and the αSNAP-SNARE complex is not able to form until the "zipper" conformation has formed (Vivona et al., 2013). At this step NSF uses the energy derived from ATP hydrolysis to torque and pulling the SNAREs. Taken together, these forces disassembly the complex into individual proteins that are now available to reuse inside the cell.

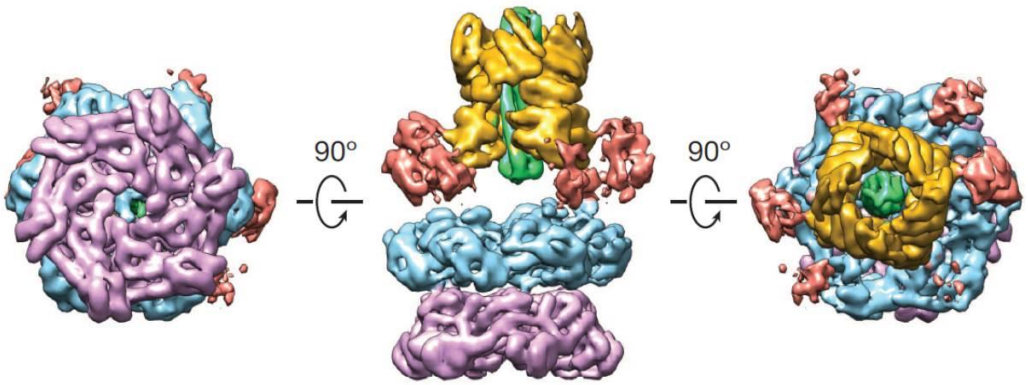

Fig.4.7.1.2 |3D density map of the 20S supercomplex: Schematic representation of the 20S supercomplex composed by NSF (N-ter, red, D1 domain, light blue, and D2 domain, pink), alpha-SNAP (yellow) and SNARE complex (green) (Zhao et al., 2015).

4.8 The SNARE Complex Disassembly

The working model of NSF-mediated SNARE complex disassembly is based on structures obtained with cryo-EM. Models are based on neuronal SNAREs, but in spite of the presence of different proteins in this class, it seems that only few SNAPs and NSF are required to disassemble them in eukaryotes (Jahn and Scheller, 2006; Clary et al., 1990). This process includes 4 different steps (Fig.4.8.1):

1. Up to four αSNAP binds the *cis*-SNARE complex anchored to the plasma membrane;
2. NSF binds the αSNAP:SNAREs generating the 20S complex where both D1 and D2 domain are tightened and N-terminal is immobilized due to its interaction with the complex; in the proposed model two N-terminal domains bind to one αSNAP.
3. The ATP hydrolysis is the key event where NSF starts to disassemble the SNAREs and a collection of four different events have been proposed as different molecular states in which the complex is twisted and stretched for the disassemble.
4. Multiple ATP hydrolysis events that produce a large conformational changes of NSF between ATP- and ADP-bound states. Here, a combination of movements through D1 changes, that turn to a more open conformation, and pulling forces by N-terminal domains towards the sides of NSF, result in the dissociation of SNARE complex into individual proteins. Two N-terminal domains go from top to side of the D1 ring.

The mechanism described above is the most recently proposed in the literature where cryo-EM was used to highlight the conformational changes between ATP- and ADP- state (Zhao et al., 2015). Even if it is well known that NSF can adopt those two different conformational states, intermediate species and the detailed ATP hydrolysis mechanism lack. Moreover, the number of subunits that must hydrolyze ATP remains unclear: studies suggest that the complex disassembly is induced by only one round of ATP hydrolysis (Ryu et al., 2015), as few as 10 (Shah et al., 2015) or at least 50 (Cipriano et al. 2013) molecules of ATP are needed per disassembly reaction. All these observation try

to clarify the process, but more detailed studies will be necessary shed light into the mechanism, which, at present, remains substantially unclear.

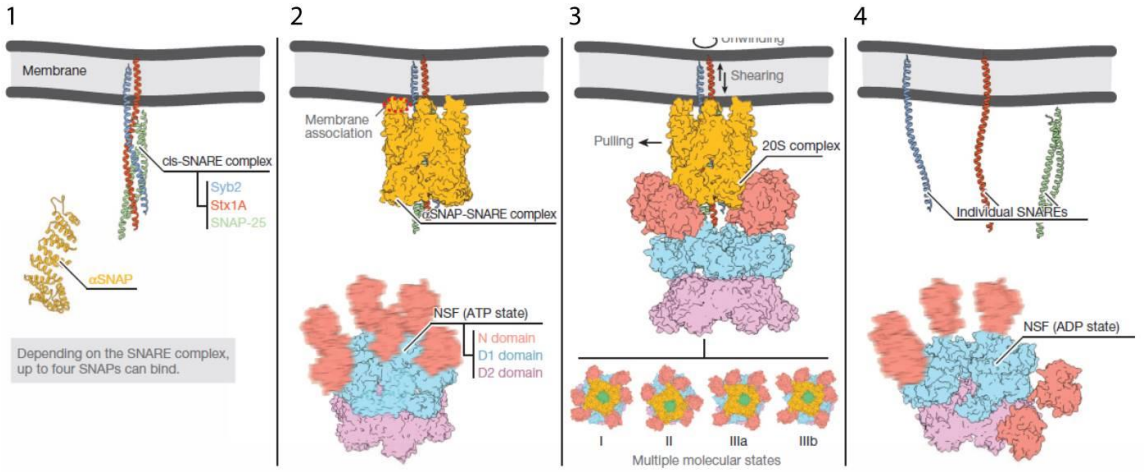

Fig.4.8.1 | Model of the SNARE complex disassembly: The model consists of four different steps in which alpha-SNAP binds the SNARE complex on the plasma membrane, then NSF is recruited and the complex is disassembled by pulling the complex. Colors are the same as above (Adapted from Zhao et al., 2015).

5. Aim of the Project

The research project of this thesis aims at identifying novel substrates of LRRK2 kinase activity. LRRK2 phosphorylation affects vesicle trafficking at the presynaptic site and its PD-related mutations lead to cytotoxicity and neurodegeneration (Greggio et al., 2006; Heo et al., 2010). Moreover, PD is characterized by an impairment of vesicle trafficking at early stages and a number of LRRK2 interactors are presynaptic proteins (Belluzzi et al., 2012).

Since alteration of vesicle recycling is likely to represent a crucial step in PD that triggers neurodegeneration, understanding whether LRRK2 can regulate vesicle-related processes through its kinase activity is a key aspect. N-ethylmaleimide Sensitive Fusion (NSF) protein has been found as a putative LRRK2 interactor (Piccoli et al., 2011). NSF is an ATPase responsible for SNARE complex disassembly, allowing correct vesicle recycling (Zhao and Brunger, 2015). After validating that recombinant human Flag-NSF is an active ATPase, we divided the project into three main objectives: i) to investigate the NSF:LRRK2 interaction; ii) to test whether NSF is a substrate of LRRK2 kinase activity by MS/MS analysis and iii) to study effects of phosphorylation on both NSF ATPase activity and SNARE complex disassembly.

Rab GTPases play a key role in vesicular sorting among all cellular compartments (Grosshans et al., 2006). Recent studies highlighted a possible interaction between *Rab7L1* and *Lrrk2* (Beilina et al., 2014). Indeed, *Rab7L1* overexpression suppressed the LRRK2 G2019S mutation-induced neurite length phenotype (MacLeod et al., 2013). Considering that neurotransmitter release is one frequently altered aspect in neurodegenerative diseases and *Rab7L1* was also found associated with a higher PD-risk, another aim of this work was to evaluate whether Rab7L1 is a substrate of LRRK2 kinase activity. In this scenario, an abnormal phosphorylation of Rab7L1 due to LRRK2 G2019S mutation could results in impaired vesicle sorting inside neurons.

The identification and validation of LRRK2 putative substrates is fundamental to shed light into LRRK2 physiological function, providing insights into the mechanisms that appear altered in PD. To date, LRRK2 kinase activity has been considered the most

tempting therapeutic target in PD (Kethiri and Bakthavatchalam, 2014). However, pharmacological compounds against LRRK2 kinase activity have been shown to produce severe side effects (Baptista et al., 2013; Luerman et al., 2014). Thus, identification of novel LRRK2 substrates might represent alternative targets to block the downstream effects of pathogenic LRRK2.

Chapter II
Materials and Methods

6. Materials and Methods

6.1 Plasmids And Constructs

NSF protein, conjugated with a Flag-tag, was cloned in pcDNA3 vector (Sigma-Aldrich, St. Louis, MO, USA) and the construct was already present in our laboratory. NSF N-terminal, D1 and D2 domains were cloned into p3XFLAG-CMV^{TM}-7.1 vector (Sigma-Aldrich, St. Louis, MO, USA) and amplified using forward primers with NotI overhang and reverse primers with KpnI overhang as following:

N-Domain (1–205aa): forward 5'-AAGCTTGCGGCCGCCTTCGCGGGCCGGAGC-3' and reverse 5'-TCGAC TGGTACCTTAGCGATTTTCCTTGGTTTT-3'

D1 domain (206-477aa): forward 5'-AAGCTTGCGGCCGCCCAATCAATTATCAATC-3' and reverse 5'-TCGACTGGTACCTTATCTCGTCACTTGCAGGC-3'

D2 domain (478-744aa): forward 5'-AAGCTTGCGGCCGCCGGAGACTTCCTTGCTTC-3'and reverse 5'-TCGACTGGTACCTCAATCAAAATCAAGGGG-3'.

NSF mutants were generated using the QuickChange mutagenesis kit (Agilent Technologies, CA, USA) according to the manufacturer's instructions. All plasmids were validated by restriction analysis and DNA sequencing.

pCHMWS 3xFlag-tagged LRRK2 wild-type, K1906M and G2019S have been previously described (Civiero et al., 2012). Rab proteins used (Rab7, Rab7L1, Rab9, Rab11 and Rab32) were cloned into p3XFLAG-CMV^{TM}-7.1 by our collaborators at the University of Granada (group of Dr. Sabine Hilfiker), that generated also all the site directed point mutants.

6.2 Cell Culture And Transfection

Human embryonic kidney cells (HEK293T) were cultured in Dulbecco's modified Eagle's medium (DMEM, Thermo Fisher, Waltham, MA USA) supplemented with 10% v/v fetal bovine serum (FBS, Thermo Fisher, Waltham, MA USA), penicillin (100 Units/ml) and

streptomycin (100 µg/ml) (Life Technologies) at 37°C and 5% CO_2. HEK293T were transiently transfected using linear polyethylenimine (PEI, Polysciences) with ratio DNA:PEI 1:2. 40 µg of DNA were dissolved in 1 ml of OPTI-MEM (Thermo Fisher, Waltham, MA USA) and 80 µl of PEI (40 µM) were added to 1 ml of OPTI-MEM. After 5 minutes of incubation, the two solutions were mixed together. After 20 minutes, to allow the formation of DNA/PEI complexes, the mix was added directly to the cells in 150 mm Petri dishes and used after 48-72 hours.

6.3 Protein Purification From Mammalian HEK293T Cells

6.3.1 Human Flag-tagged NSF

Human NSF, its mutants and single domains with an N-terminal Flag-tag, were purified from HEK293T cells after transient transfection as described above. Cells were resuspended in 1 ml of a Lysis buffer (20 mM Tris-HCl pH 7.5, 150 mM NaCl, 1 mM EDTA, 2.5 mM $Na_4P_2O_7$, 1 mM beta-glycerophosphate, 1mM Na_3VO_4, Protease Inhibitor Mixture (Sigma-Aldrich, St. Louis, MO, USA)) and then lysed with 5 cycles of freezing and thawing in liquid nitrogen. Cell lysate was collected after centrifugation at 18000xg for 40 minutes at 4°C. The supernatant was incubate overnight with 40 µl of Anti-Flag M2 Affinity gel (Sigma-Aldrich, St. Louis, MO, USA) at 4°C. After centrifugation, the supernatant was discarded and the beads with Flag-tagged proteins were washed with 1 ml of different buffers: WB1 (20 mM Tris-HCl pH 7.5, 500 mM NaCl) twice, WB2 (20 mM Tris-HCl pH 7.5, 350 mM NaCl) twice, WB3 (20 mM Tris-HCl pH 7.5, 150 mM NaCl) six times. The protein was then eluted by incubating the beads with 200 µl of WB5 or directly in the Kinase assay buffer (25 mM Tris-HCl pH 7.5, 5 mM beta-glycerophosphate, 2 mM DTT, 0,1 mM Na_3VO_4, 10 mM $MgCl_2$ supplemented with 0.007% Tween® 20) with 150 ng/µl 3xFlag peptide and mixing the sample for about 2 hours. The sample was centrifuged to pellet the resin and the supernatant was collected.

6.3.2 Human Flag-tagged LRRK2 wt/G2019S and Flag-tagged Rab proteins

1% Tween-20 was added to the Lysis buffer (composition described above) and samples were hold on ice for 30 minutes. Beads were washed with buffers with different concentration of Tween-20 added: WB1 (20 mM Tris-HCl pH 7.5, 500 mM NaCl, 1% Tween-20) twice, WB2 (20 mM Tris-HCl pH 7.5, 350 mM NaCl, 1% Tween-20) twice, WB3 (20 mM Tris-HCl pH 7.5, 150 mM NaCl, 1% Tween-20) twice, WB4 (20 mM Tris-HCl pH 7.5, 150 mM NaCl, 0.1% v/v Tween-20) twice, and WB5 (20 mM Tris-HCl pH 7.5, 150 mM NaCl, 0.02% v/v Tween-20) twice. Elution was done as described above.

6.4 Bacterial Cell Colture

For the experiments, two different bacterial *E. coli* cell lines were used: DH5α, to obtain DNA plasmids, and BL21 for protein's purification. Cells were grown in Luria-Bertani broth (LB), composed by: tryptone 1% w/v, yeast extract 0.1% w/v, NaCl 0.1% w/v and then deionazed H_2O to the final volume. For selection of positive clones, ampicillin (Sigma-Aldrich) was used between 50 and 100 μg/ml.

6.4.1 Recombinant alpha-SNAP production

Rat αSNAP cloned in pET28 plasmid in fusion with a His-tag was a kind gift of Dr. Reinhard Jahn (Max-Planck-Institute, Göttingen). αSNAP was subsequently expressed in *E. Coli* in BL21(DE3) strain. Bacteria were grown at 37°C to an OD at 600nm of 0.4-0.6, then induced with 0.25 mM isopropyl β-D-1-thiogalactopyranoside (IPTG) for 4 hours. Cells were then harvested by centrifugation and the pellet of 250 ml of culture was resuspended in 5-10 ml of Tris-HCl pH 8.0. Phenylmethylsulfonyl fluoride (PMSF) 100μM and a cocktail of protease inhibitors were added to the cells 1:100 (v/v) that were subsequently subjected to one French Press cycles (Constant Systems Ltd). The cell homogenate was centrifuged 30 minutes at 4°C and the supernatant loaded onto a Co^{2+} affinity column and eluted with a 0-500 mM linear gradient of imidazole at a flow rate of 0.5 ml/min. Protein solution was dialyzed in Tris-HCl 20 mM pH 7.5, NaCl 150 mM.

6.4.2 Recombinant SNARE complex production

Soluble SNARE complex was obtained by co-expression of wild type SNAP-25A, syntaxin-1A and His-tagged VAMP2(1-96) using the Duet expression system (Novagen) in *E. Coli* in BL21(DE3) strain. VAMP2(1-96)-His6-TEV pACYC-Duet and syntaxin-1A/SNAP-25A pET-Duet were a kind gift of Prof. A. Brunger (Stanford University, California) (Cipriano et al., 2013). Bacteria were grown at 37°C to an OD at 600nm of 0.6-0.8, then induced with 0.5 mM IPTG for 4 hours. Cell pellets of 250 ml of culture were suspended in 10 ml of 50 mM Tris-HCl, pH 8.0, 300 mM NaCl, 20 mM imidazole and 0.5 mM Tris(2-carboxyethyl)phosphine (TCEP) (SNARE buffer), supplemented with PMSF 100µM and protease inhibitors cocktail. Cell were lyses by two French Press cycles (Constant Systems Ltd) and the lysate was clarified by centrifugation for 1 hour at 15000g at 4°C. The supernatant was loaded onto a 1-ml Ni^{2+} affinity column, washed with 20 ml of SNARE buffer containing 7.5 M urea and then with 20 ml of SNARE buffer. The complex was then eluted with SNARE buffer containing 350 mM imidazole. After elution, SNARE complex was subjected to size exclusion chromatography using a Superdex 200 10/300 (GE Healthcare) that was equilibrated with 50 mM Tris-HCl, pH 7.5, 100 mM NaCl. The SNARE complex was checked and quantified by SDS-PAGE.

6.5 Sds-Page And Determination Of Protein Concentration

The desired amount of each sample was denatured by adding Sample Buffer, Laemmli, to a final 1X concentration (obtained by diluting 4X stock solution: 200 mM Tris-HCl pH 6.8, 8% w/v SDS, 400 mM DTT, 40% v/v glycerol and Bromophenol Blue to reach the desired colour intensity) and heated at 95°C for 10 minutes. Proteins were separated by Poly-Acrylamide Gel Electrophoresis (PAGE) in denaturing conditions, dependent on the presence of SDS. Gels were prepared with the opportune percentage of acrylamide (between 7.5 and 13%) according to the size of the proteins analyzed. For Flag-tagged NSF, NSF mutants and both LRRK2 wild type and G2019S, we used gels with 7.5% v/v acrylamide. For NSF N-terminal, D1 and D2 domains, Rab proteins, αSNAP and the SNARE complex with 13%. Protein were separated by electrophoresis in Tris-Glycine-SDS Running Buffer (25mM Tris Base, 250mM Glycine, 0.1% w/v SDS). The SHARPMASS™ V

PLUS Prestained Protein Ladder (EuroClone) was loaded in a separate lane of the gel to estimate the approximate molecular weight of proteins. After running, samples were stained in agitation with Coomassie Brilliant Blue (0.25% w/v Brilliant Blue R-250 Sigma-Aldrich, 40% v/v ethanol, 10% v/v acetic acid and water) for 45 minutes and destained in agitation with a Destaining Solution (10% v/v isopropanol, 10% v/v acetic acid and water) that was replaced several times. Gels were finally kept in a 10% v/v acetic acid solution in agitation to remove all the background staining. Proteins were quantified by comparison with different known concentrations of BSA (Bovine Serum Albumin) loaded on the same gel each time and the quantification was done with ImageJ software.

6.6 Western Blot Analysis

After SDS-PAGE gel electrophoresis, protein samples were transferred on a polyvinylidene fluoride (PVDF) membrane (Bio-Rad), previously activated in methanol, through the Trans-Blot® Turbo™ Transfer System (Bio-Rad) in semi-dry conditions, with the 1X Trans-Blot® Turbo™ Transfer Buffer (obtained diluting 5X Trans-Blot® Turbo™ Transfer Buffer, 20% v/v ethanol and deionized water), at 25V for 20 minutes. PVDF blots were then soaked for 40 minutes in 5% w/v skimmed milk dissolved in TBST buffer (20mM Tris-HCl pH 7.4; 150 mM NaCl; 0.1% v/v Tween-20) in order to saturate non-specific binding sites for proteins on the membranes. After, membranes were incubated with primary antibodies added to a 5% w/v skimmed milk dissolved in TBST solution for 1 hour at room temperature or over-night at 4°C. Membranes were subsequently washed with TBST (4x10 minutes) to remove the excess of antibody not bind to proteins or bound in a non-specific manner. Membrane was then incubated for 1 hour at room temperature with Horseradish-Peroxidase (HRP)-conjugated secondary antibodies, diluted in 5% w/v skimmed milk in TBST. Incubation with secondary antibody was followed by washes in TBST (4x10 minutes). Primary and secondary antibodies were used at the following dilutions:

Antibody	*Dilution*
Anti-Flag® M2-Peroxidase (Sigma-Aldrich)	1:40000
Mouse Anti-β-Tubulin (OriGene Technologies)	1:10000
Rabbit Anti-NSF (Cell Signaling, Danvers, MA, USA)	1:2000
Rabbit Anti-LRRK2 (C41-2, Abcam, Cambridge, UK)	1:1000
Rabbit Anti-LRRK2 phospho-T2483 (MJF-R8, Abcam, Cambridge, UK)	1:2000
Rabbit Anti-Mouse-Peroxidase (Sigma-Aldrich)	1:80000
Goat Anti-Rabbit-Peroxidase (Sigma-Aldrich)	1:16000

After washes, membranes were removed from TBST and incubated with Amersham™ ECL™ Western Blotting Detection Reagents (GE Healthcare) containing a substrate of HRP for Enhanced ChemiLuminescence (ECL). The visualization of the signal was detected employing the Amersham™ Hyperfilm ECL (GE Healthcare Waukesha, WI, USA), successively processed with developer and fixing solutions (Kodak® Developer and Replenisher and Kodak® Fixer and Replenisher, Sigma-Aldrich). Densitometric analysis was carried out using Image J software.

6.7 Primary Neuronal Cultures

Primary cortical neurons were obtained from E19 (embryonic days 19) mice with the Papain Dissociation System (Worthington Biochemical Corporation): brains were dissected from skull and olfactory bulbs, brainstems and meninges were removed. Cortices were then transferred to a separate dish containing cold Hank's BalancedSalt Solution (HBSS, Sigma-Aldrich), cut into smaller pieces and large fragments of tissue were broken up by pipetting. Dissociated tissue was transferred into Papain solution (one bottle of Papain, containing 199 Units -Worthington- was dissolved in 5ml of Earle's Balanced Salt Solution or EBSS, purchased from Sigma-Aldrich, and 250 µl of 0.1% w/v DNAse, Sigma-Aldrich, previously resuspended in 500 µl of EBSS, were added to this solution). The suspension was incubated for 40 minutes at 37°C and mixed by inversion every 10 minutes. After trituration, the mixture was centrifuged for 5 minutes at 1000 rpm. The supernatant was discarded and cells were resuspended in 3 ml of STOP

solution (250 µl of DNAse solution, 600 µl of 15.5mg/ml Papain Inhibitor, Worthington, and 5.4 ml of EBSS) and incubated at room temperature for 10 minutes. This permits the largest fragments precipitate by gravity. Later, the supernatant was slowly pipetted into 5 ml of 10/10 solution (0.1 g of Bovine Serum Albumin, BSA, and 0.1 g of Trypsin Inhibitor, both purchased from Sigma-Aldrich, in 10ml EBSS). After a 10 minutes spin at 800 rpm, the cell pellet was finally resuspended in warm Neurobasal medium (Life Technologies) supplemented with 5% v/v FBS, 2% v/v of B27 supplement (Invitrogen), 0.5 mM Glutamine (Life Technologies), penicillin and streptomycin and 2.5 µg/ml fungizone (Life Technologies). $1x10^6$ cells/coverslip were pleated in 2 ml of medium on 12 mm coverslip pre-treated with poly-D-lysine. After 10 days, neurons were washed with phosphate buffer saline (PBS) solution and fixed with paraformaldehyde (PFA) 4% for 30 minutes. PFA was removed and coverslip was washed three times with PBS. Cells were permeabilized using PBS with 0.1% Triton X-100 at room temperature and incubated in PBS with 5% fetal bovine serum (FBS) for 30 minutes both. Using the same buffer, neurons were then incubated with primary antibodies: a rabbit anti-NSF (1:100, D31C7Cell Signaling) and a mouse anti-LRRK2 (1:50, N231B/34 EMD Millipore (Davies P et al., 2013)) with overnight incubation. After three washes in PBS, cells were incubated with goat secondary antibodies linked to Alexa Fluor-488 and -568 (Life Technologies) at 1:200 dilution for 1 hour at room temperature. Coverslips were washed three times with PBS and mounted on a microscope slide (Thermo Scientific) with Mowiol (Calbiochem) supplemented with 1 µg/µl Hoechst33258 stain (Life Technologies). Images were acquired with Zeiss LSM 700 confocal microscope.

6.8 Pull-Down Assays

To perform pull-down assays, NSF domains and full length NSF were purified after transient transfection from HEK293T cells. Cells were harvested in 500 µl of Lysis buffer (50 mM Tris-HCl pH 7.5, 1 mM EDTA, 2.5 mM $Na_4P_2O_7$, 1 mM beta-glycerophosphate, 1 mM Na_3VO_4, 0.27 M Sucrose, 1% Triton X-100, Protease Inhibitor Mixture (Sigma-Aldrich, St. Louis, MO, USA)). The cell lysate was then centrifuged at 18000xg for 30 minutes at 4°C and further incubated overnight with 20 µl of Anti-Flag M2 Affinity gel

(Sigma-Aldrich, St. Louis, MO, USA) at 4°C. After centrifugation, the supernatant was discarded and the beads with NSF proteins were washed 3 times with 1 ml of a Washing buffer (50 mM Tris-HCl pH 7.5, 1 mM EDTA, 0.27 M Sucrose, 250 mM NaCl, 0.02% Triton X-100) and resuspended in 100 µl of the same buffer. An aliquot of suspension was collected and proteins were loaded on an SDS-PAGE gel. Concentration were quantified measuring the intensity of the band against known BSA standards with ImageJ software. Proteins were subsequently adjusted to the same concentration (2 µM). During the incubation time, we lysed the adult mouse brain with 5 ml of the same Lysis buffer. We quantified the protein content with BCA assay. After overnight incubation at 4°C between brain lysate (600 µl, ∼3 mg/ml concentrated) and resins, we removed the supernatant and wash the resin with 1 ml of Washing buffer used above. Resins were then boiled with sample buffer, loaded into a Mini-PROTEAN® TGX™ Precast Gels (Bio-Rad), run in Tris-Glycine-SDS running buffer and transferred onto PVDF membranes. Specific antibodies were used to detect the presence of the proteins.

6.9 Size Exclusion Chromatography (SEC) And Dot Blot Analysis

Flag-NSF was transfected into HEK293T cells, as described before, in a 100 mm Petri dish for 48h. Cells were resuspended in 500 µl of lysis buffer containing 1 % (v/v) Tween-20 and different ATP concentrations: 0, 0.09 and 1 mM were used. Cell lysates were centrifuged at 100000 g and supernatants were separated on a Superdex 200 column (Ge Healthcare, Waukesha, WI, USA) pre-equilibrated with TBS buffer supplemented with 1% v/v Tween-20. The flow rate used was 0.5 ml/min. Fractions of 0.5 ml were collected and spotted (1 µl) onto a nitrocellulose membrane and analysed by dot blot. The membrane was blocked with 10% w/v skimmed milk in TBST (composition described in Western blot analysis section) and incubated with mouse monoclonal anti-Flag M2-peroxidase (Sigma-Aldrich, St. Louis, MO, USA) dissolved in TBST with 10% milk. Immunoproteins were visualized using ECL (GE, Healthcare, Waukesha, WI, USA).

6.10 Transmission Electron Microscopy (TEM)

Purified flag-tagged NSF and its mutants proteins, at a concentration of 235 nM, were incubated with 1 mM ATP and 4 mM $MgCl_2$. A total of 0.5 ng of protein was adsorbed few minutes to a glow-discharged carbon-coated copper grid, washed with deionized water, and stained with 1% uranyl acetate. Images were collected using a Fei Tecnai T12 electron microscope equipped with a LaB6 filament and operated at an acceleration voltage of 100 kV.

6.11 In Vitro Kinase Assay

Purified NSF and all its domains were eluted in kinase assay buffer (0.007% v/v Tween-20). They were incubated with LRRK2 G2019S protein dissolved in the same buffer for 1 hour at 30 °C in the presence of ^{33}P-ATP (1 µCi) and 2.5 µM cold ATP. After SDS-PAGE, proteins were transferred on PVDF membrane and the incorporated ^{33}P-ATP was detected by autoradiography by Phospho-Imager system (Cyclone, Perkin-Elmer). The same membranes were probed with anti-Flag antibody for total protein loading and analysed using ImageJ software.

6.12 ATPase Enzymatic Assay

We employ Malachite Green enzyme assay to measure NSF ATPase activity. The amount of inorganic phosphate was quantified at a fixed time-point measuring the absorbance at 640 nm, through spectrophotometer. The assay was adapted from the method of Lanzetta et al., 1979. The Malachite Green Stock solution used for the assay was a mixture of two different solutions (one with 34 mg Malachite Green oxalate salt (Sigma-Aldrich. St. Louis, MO, USA) into 40 ml HCl 1M and the other with 1 g $(NH_4)_2MoO_4$ (Sigma-Aldrich, St. Louis, MO, USA) into 14 ml HCl 4M to a final volume of 100 ml with distilled water and then filtered through 0,45 nm. The concentration of human NSF used for the ATPase assay was 36 nM (hexamer) with different ATP concentration. Reactions were performed at 37°C and followed for 120 minutes. The time point aliquots collected (20 µl) were mixed with 150 µl of Malachite Green stock solution until the solution

became homogenous. Absorbance was measured at a wavelength of 640 nm using a corresponding Malachite Green solution as blank. Next, values were converted into µmol of free Pi in solution using a standard curve. The reported values for the kinetic constants (K_m, k_{cat} and V_{max}) were obtained by data fitting using the Michaelis-Menten kinetic model (Y = Vmax*S/(Km + [S])).

6.13 Reverse Phase Hplc (RP-HPLC) ATPase Assay

To determine the ATPase activity of NSF through RP-HPLC, ATP (500 or 700 µM) was added to 0.2 µM 3xFlag-NSF wt. Proteins were purified as previously described and incubated at 37°C in kinase buffer (composition described above). At the reported time-points, aliquots (20 µl) were collected up to final reaction time of 120 minutes. The samples were then heated for 3 minutes at 95°C with 0.1 M of EDTA to stop the reaction and then stored at -80°C. RP-HPLC was used to monitor the total amount of ATP and ADP present in any given sample. Nucleotides were separated on a Jupiter 5u C4 300A (Phenomenex) column using an Agilent HP 1100 HPLC, pre-equilibrated with 50 mM NaH_2PO_4 pH 6.5, 10 mM Tetra-n-butylammonium bromide and 4% ACN. The flow-rate used was 0.5 ml/min and the amount of the nucleotide was evaluated by measuring the area of the peak at 256 nm. To convert this value to the Pi generated by the reaction, a standard curve (in the ADP concentration range from … to …) was used. ADP concentrations detected in the assay were plotted as a function of time and interpolated with a linear regression using GraphPad Prism 5.

6.14 Flag-NSF HEK293 Stable Overexpressing Cell Line

HEK293 cells were plated on a 150 mm Petri dish. Transfection was performed with 40 µg DNA with ratio DNA:PEI 1:2, as described above. Therefore, cells were selected by culturing them in medium supplemented with the antibiotic geneticin (G418). After 24 hours, single clones of cells found positive to transfection, as reveled by the acquired resistance against G418, were transposed into 96-wells plate, 48-wells plate, 24-wells plate and 6-wells plate subsequently. Finally, positive clones able to growth through all

selective steps, were moved to T-75 flask. To confirm that Flag-NSF was stably expressed, cell lysates were analyzed by Western blot analysis and immunofluorescence with anti-Flag antibody, as described in paragraph 6.5 and 6.13.

6.15 Immunofluorescence

HEK293 cells stably expressing NSF were plated on 12 mm glass coverslips pre-treated with poly-D-lysine. Next, cells were washed with PBS solution and fixed for 30 min at room temperature (RT) with 4% paraformaldehyde (PFA). PFA was removed and coverslips were washed three times with PBS. Cells were permeabilized with 0.1% Triton X-100 in PBS for 30 min at RT and incubated in blocking solution (5% FBS in PBS) for 30 min. The cells were incubated for 1 hour at RT with a mouse anti-Flag M2 primary antibody (1:200, Sigma Aldrich). After three washes in PBS, cells were incubated with goat secondary antibodies linked to Alexa Fluor-568 (Life Technologies) at 1:200 dilution for 1 hour at room temperature. Coverslips were washed three times with PBS and mounted on a microscope slide (Thermoscientific) with Mowiol (Calbiochem) supplemented with 1 µg/µl Hoechst33258 stain (Life Technologies). Images were acquired with Leica 5000B microscope.

6.16 SNARE Disassembly Assay

The SNARE disassembly protocol used followed a method previously described (Cipriano et al., 2013). The assay buffer used was the Kinase buffer (composition described above). Subsequently 1.5 µM αSNAP, 480 nM SNAREs, 24 nM NSF (hexamer concentration) phosphorylated or not by LRRK2 G2019S (ratio NSF:LRRK2 20:1, 1 hour at 30°C) were added in presence of 2 mM ATP to start the reaction (final assay volume 240 µl). At defined time points, an aliquot (20 µl) was collected and loaded on SDS-PAGE gel without boiling the samples to preserve the SDS-resistant SNARE complex. The complex runs as a single band on SDS-PAGE and the intensity of the band was measured and normalized to the value at time zero. The experiments were performed in triplicate up to a reaction time of 150 minutes.

6.17 Circular Dichroism (Cd)

CD measurements were carried out on a JASCO J-810 spectropolarimeter. The CD spectra were acquired and processed using the J-700 software for Windows. All experiments were done at room temperature using an optical path length of 0.2 cm. The wavelength range of the measurements was 197–250 nm, using a bandwidth of 2 nm and a time constant of 8 s at a scan speed of 50 nm/min. The signal to noise ratio was improved by accumulating four scans for each sample. Spectra were acquired using purified proteins in 20 mM Tris-HCl pH 7.5, 150 mM NaCl and 0.007% Tween®20 (as collected from the last purification step) using the same buffer with 3xFlag peptide as a control. All the spectra are reported in terms of mean residue molar ellipticity (deg cm^2 $dmol^{-1}$). Protein concentrations in the samples were determined by SDS-PAGE and all the spectra were normalized for the measured protein concentration.

6.18 Intrinsic Fluorescence Measurements

The protein concentration of the sample used in the fluorescence experiment inside the sample was 0.9 µM in 20 mM Tris/HCl buffer (pH 7.5) with 150 mM NaCl buffer. Fluorescence emission spectra were recorded on a Cary Eclipse fluorescence spectrophotometer (Varian, Agilent Technologies, Santa Clara, CA) using the Cary Eclipse program. Sample measurements were carried out using optical path length of 10 mm. Fluorescence spectra were obtained using an excitation wavelength of 295 nm (Em = 330 nm), with an excitation bandwidth of 5 nm and slit width of 10 nm. Emission spectra were recorded between 300-400 nm at a scan rate of 30 nm/sec.

Chapter III
Results

7. LRRK2 phosphorylates NSF enhancing its ATPase activity and SNARE complex disassembly rate

7.1 LRRK2 Kinase Activity Influences Synaptic Vesicle Dynamics

As described in the introduction, LRRK2 is widely expressed in several cell types, but the majority of the studies focused on neurons, since mutations in *Lrrk2* gene are linked to both familial and sporadic forms of PD (Singleton et al., 2013). It has been previously demonstrated that LRRK2 inhibition impacts the presynaptic site leading to impaired SV trafficking and neurotransmitter release (Cirnaru et al., 2014). These findings suggest a possible role of LRRK2 catalytic activity in SV fusion cycle. In collaboration with Dr Giovanni Piccoli (University of Trento), we asked whether altered LRRK2 kinase activity leads to defects in SV dynamics (Belluzzi, Gonnelli et al., 2016; *Appendix*). To this aim, we used the sypHy (Synaptophysin-pHluorin) assay. This method of analysis is useful to monitor the behavior of SV cycle and it is based on a sensitive pH-fluorescent reporter. The reported is quenched in presence of an acid environment (vesicle lumen), but becomes fluorescent upon vesicle fusion, since it is exposed to a more basic pH (Granseth et al., 2006). We investigated the role of LRRK2 kinase activity in neurons in two complementary models using 1) primary cortical culture in presence or absence of a specific LRRK2 inhibitor (GSK2578215A), as a negative control, and 2) primary cortical neurons from BAC hG2019S transgenic mice, previously demonstrated to have LRRK2 G2019S overexpression and an increased LRRK2 kinase activity (Melrose et al., 2010). First, we confirmed that GSK2578215A was efficient at inhibiting LRRK2 kinase activity in our paradigm by Western blot analysis using an antibody against phosphor-Ser935, a well-known LRRK2 constitutively phosphorylated residue used as readout of LRRK2 kinase activity (Dzamko et al., 2010). Of interest, GSK2578215A did not provoke alterations in LRRK2 stability as showed in *Appendix* Fig.S1 a and b. To monitor the impact of LRRK2 inhibition or pathological mutation on SV trafficking, we used two different stimuli: 1) 40 AP (action potential) to mobilize SV of the ready releasable pool (RRP) and 2) 300 AP to mobilize the reserve pool. After the application of the stimulus,

we measured the time to return to the baseline and the decay in sypHy fluorescence corresponding to the exo- and endocytosis efficiency. Our results (*Appendix*, Fig.1) showed that the presence of GSK2578215A increased value of tau for both upstroke and decay, suggesting an impaired exo-endocytosis. In contrast, BAC hG2019S neurons exhibited a faster kinetic (decreased τ decay) at both two stimuli (ΔF40/F0 and ΔF300/F0) as show in *Appendix*, Fig.1 C. To better clarify the impact of LRRK2 G2019S pathological mutation and its role in synaptic vesicle dynamics we used a complementary approach. BAC hG2019S neurons were transduced at DIV4 (days in vitro) with viruses expressing GFP to track neuronal processes and assessed at DIV14., Briefly, cell medium was supplemented with antibodies directed against the intravesicular domain of synaptotagmin 1, which is internalized when vesicle fusion occurs. Afterwards, cells were fixed with PFA and exposed to an antibody against synaptophysin, used as counterstaining. A positive signal for both antibodies means that vesicle undergo to a correct exo-endocytic cycle. As shown in *Appendix* Fig.1 e, BAC hG2019S neurons are characterized by an increased number of positive clusters. However, the total number of SV pools was not altered in BAC hG2019S neurons (*Appendix* Fig. S1 d). Taken together, these results indicate that LRRK2 kinase activity plays a key role in SV dynamics and regulates SV fusion.

7.2 Expression And Purification Of Recombinant Human Flag-Tagged NSF

Given the observed effects of LRRK2 kinase activity on synaptic vesicle trafficking, we decided to explore potential LRRK2 presynaptic substrates. A number of putative presynaptic proteins have been previously identified to be able to interact with LRRK2 (Piccoli et al., 2014). We chose to explore the relationship between LRRK2 and NSF, an AAA+ ATPase, since LRRK2 kinase activity appears involved in the control of a step of the exo-endocytosis (paragraph 7.1) and NSF plays a pivotal role in SNARE complex disassembly and, hence, SV endocytosis (Zhao and Brunger, 2015). Moreover, NSF activity is tightly controlled by phosphorylation (Liu et al., 2006; Matveeva et al., 2001) and the ATPase has been found to accumulate in neuronal intranuclear inclusion bodies,

similar to Lewy Bodies, a pathological hallmark of PD (Pountney et al., 2008). Thus, to assess whether NSF is a LRRK2 substrate we first set out to find the optimal conditions to purify human recombinant NSF.

As reported in the introduction, NSF belongs to the AAA+ (ATPases Associated with various cellular Activities) superfamily of proteins and it is responsible of the SNARE complex disassembly during vesicle recycling. Until now structural studies have been focused on recombinant Chinese Hamster (*Cricetulus Griseus*) NSF purified from *E. coli* (Chang et al., 2012; Zhao et al., 2015), whilst no studies are available on human NSF. Our aim was to first purify human NSF from mammalian HEK293T cells and then characterize it biochemically. Although the sequence alignment of *C. Griseus* and Human NSF reveals an identity of 98% between the two proteins (Fig.7.2.1), we reasoned that expressing and purifying recombinant NSF from mammalian cells would be important in terms of post-translational modifications that *E. coli* cannot provide.

```
Hum_NSF    1 MAGRSMQAARCPTDELSLTNCAVVNEKDFQSGQHVIVRTSPNHRYTFTLKTHPSVVPGSI  60
             MAGRSMQAARCPTDELSL+NCAVV+EKD+QSGQHVIVRTSPNH+Y FTL+THPSVVPGS+
CrG_NSF    1 MAGRSMQAARCPTDELSLSNCAVVSEKDYQSGQHVIVRTSPNHKYIFTLRTHPSVVPGSV  60

Hum_NSF   61 AFSLPQRKWAGLSIGQEIEVSLYTFDKAKQCIGTMTIEIDFLQKKSIDSNPYDTDKMAAE  120
             AFSLPQRKWAGLSIGQEIEV+LY+FDKAKQCIGTMTIEIDFLQKK+IDSNPYDTDKMAAE
CrG_NSF   61 AFSLPQRKWAGLSIGQEIEVALYSFDKAKQCIGTMTIEIDFLQKKNIDSNPYDTDKMAAE  120

Hum_NSF  121 FIQQFNNQAFSVGQQLVFSFNEKLFGLLVKDIEAMDPSILKGEPATGKRQKIEVGLVVGN  180
             FIQQFNNQAFSVGQQLVFSFN+KLFGLLVKDIEAMDPSILKGEPA+GKRQKIEVGLVVGN
CrG_NSF  121 FIQQFNNQAFSVGQQLVFSFNDKLFGLLVKDIEAMDPSILKGEPASGKRQKIEVGLVVGN  180

Hum_NSF  181 SQVAFEKAENSSLNLIGKAKTKENRQSIINPDWNFEKMGIGGLDKEFSDIFRRAFASRVF  240
             SQVAFEKAENSSLNLIGKAKTKENRQSIINPDWNFEKMGIGGLDKEFSDIFRRAFASRVF
CrG_NSF  181 SQVAFEKAENSSLNLIGKAKTKENRQSIINPDWNFEKMGIGGLDKEFSDIFRRAFASRVF  240

Hum_NSF  241 PPEIVEQMGCKHVKGILLYGPPGCGKTLLARQIGKMLNAREPKVVNGPEILNKYVGESEA  300
             PPEIVEQMGCKHVKGILLYGPPGCGKTLLARQIGKMLNAREPKVVNGPEILNKYVGESEA
CrG_NSF  241 PPEIVEQMGCKHVKGILLYGPPGCGKTLLARQIGKMLNAREPKVVNGPEILNKYVGESEA  300

Hum_NSF  301 NIRKLFADAEEEQRRLGANSGLHIIIFDEIDAICKQRGSMAGSTGVHDTVVNQLLSKIDG  360
             NIRKLFADAEEEQRRLGANSGLHIIIFDEIDAICKQRGSMAGSTGVHDTVVNQLLSKIDG
CrG_NSF  301 NIRKLFADAEEEQRRLGANSGLHIIIFDEIDAICKQRGSMAGSTGVHDTVVNQLLSKIDG  360

Hum_NSF  361 VEQLNNILVIGMTNRPDLIDEALLRPGRLEVKMEIGLPDEKGRLQILHIHTARMRGHQLL  420
             VEQLNNILVIGMTNRPDLIDEALLRPGRLEVKMEIGLPDEKGRLQILHIHTARMRGHQLL
CrG_NSF  361 VEQLNNILVIGMTNRPDLIDEALLRPGRLEVKMEIGLPDEKGRLQILHIHTARMRGHQLL  420

Hum_NSF  421 SADVDIKELAVETKNFSGAELEGLVRAAQSTAMNRHIKASTKVEVDMEKAESLQVTRGDF  480
             SADVDIKELAVETKNFSGAELEGLVRAAQSTAMNRHIKASTKVEVDMEKAESLQVTRGDF
CrG_NSF  421 SADVDIKELAVETKNFSGAELEGLVRAAQSTAMNRHIKASTKVEVDMEKAESLQVTRGDF  480

Hum_NSF  481 LASLENDIKPAFGTNQEDYASYIMNGIIKWGDPVTRVLDDGELLVQQTKNSDRTPLVSVL  540
             LASLENDIKPAFGTNQEDYASYIMNGIIKWGDPVTRVLDDGELLVQQTKNSDRTPLVSVL
CrG_NSF  481 LASLENDIKPAFGTNQEDYASYIMNGIIKWGDPVTRVLDDGELLVQQTKNSDRTPLVSVL  540

Hum_NSF  541 LEGPPHSGKTALAAKIAEESNFPFIKICSPDKMIGFSETAKCQAMKKIFDDAYKSQLSCV  600
             LEGPPHSGKTALAAKIAEESNFPFIKICSPDKMIGFSETAKCQAMKKIFDDAYKSQLSCV
CrG_NSF  541 LEGPPHSGKTALAAKIAEESNFPFIKICSPDKMIGFSETAKCQAMKKIFDDAYKSQLSCV  600

Hum_NSF  601 VVDDIERLLDYVPIGPRFSNLVLQALLVLLKKAPPQGRKLLIIGTTSRKDVLQEMEMLNA  660
             VVDDIERLLDYVPIGPRFSNLVLQALLVLLKKAPPQGRKLLIIGTTSRKDVLQEMEMLNA
CrG_NSF  601 VVDDIERLLDYVPIGPRFSNLVLQALLVLLKKAPPQGRKLLIIGTTSRKDVLQEMEMLNA  660

Hum_NSF  661 FSTTIHVPNIATGEQLLEALELLGNFKDKERTTIAQQVKGKKVWIGIKKLLMLIEMSLQM  720
             FSTTIHVPNIATGEQLLEALELLGNFKDKERTTIAQQVKGKKVWIGIKKLLMLIEMSLQM
CrG_NSF  661 FSTTIHVPNIATGEQLLEALELLGNFKDKERTTIAQQVKGKKVWIGIKKLLMLIEMSLQM  720

Hum_NSF  721 DPEYRVRKFLALLREEGASPLDFD  744
             DPEYRVRKFLALLREEGASPLDFD
CrG_NSF  721 DPEYRVRKFLALLREEGASPLDFD  744
```

Fig.7.2.1 | Protein blast alignment: The result of full-length sequence alignment between Human NSF (*Hum_NSF*) and *Cricetulus Griseus* NSF (*CrG_NSF*) displays an identity on 732/744 residues (98%) among the three different domain (N-terminal 1-205, yellow; D1 206-487, red; D2 488-744, green).

We first validated recombinant human Flag-tagged NSF full-length, purified according to the procedures described in *materials and methods*. The flag tag is a short amino-acid peptide (DYKDDDDK), fused to human NSF at the N-terminal, widely used in a variety of cell types, including bacteria, yeast and mammalian cells. Furthermore, flag-tagged proteins have the advantage that can be purified by immunoprecipitation from the cell lysate using beads conjugated with antibodies and then eluted from the resin by competition with an excess of Flag peptides. Starting from $20x10^6$ cells, we obtained about 60 μg of highly pure monomeric human NSF at a concentration of 0.3 mg/ml (Fig.7.2.2 A). Since SDS-PAGE gel electrophoresis allows to detect only denatured NSF due to the presence of both sodium dodecyl sulfate (SDS) and dithiotreitol (DTT), we subsequently monitored the ability of purified proteins to assemble into hexamers. A common feature of all the AAA+ proteins is the *Walker A* motif, whose function is necessary for ATP binding and conformational changes (Hanson and Whiteheart, 2005). For this reason, to assess the capability of NSF to undergo from monomeric to homoexameric structure, we incubated the purified protein with 1 mM ATP and 4 mM $MgCl_2$. Based on the Cryo-EM structure of Chinese Hamster NSF recently published (Chang et al., 2012 e mechanicistic), we monitored the presence of hexamers in solution by Transmission Electron Microscopy (TEM). As shown in Fig.7.2.2 B, the presence of a structural transition into oligomeric state denotes the solubility of the protein and confirms that human flag-tagged NSF is able to form hexamers in the presence of ATP.

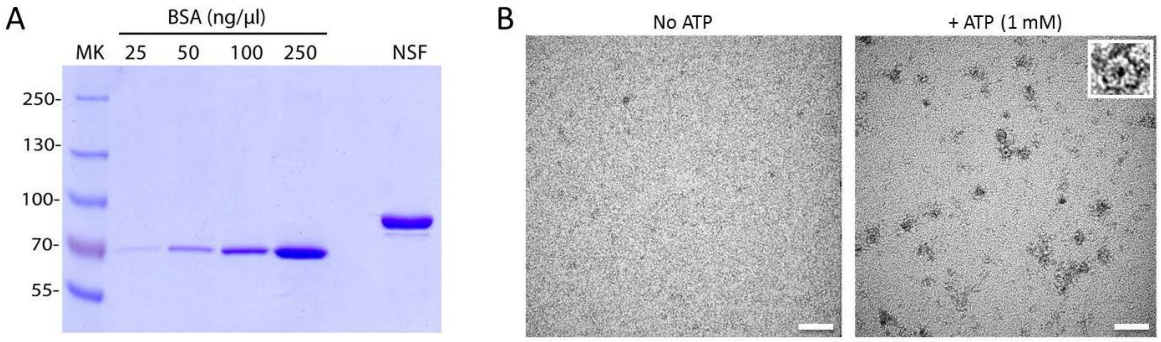

Fig.7.2.2 | Purification of recombinant human flag-NSF: (A) Purified human NSF separated on SDS-PAGE and quantified by comparison with different concentration of BSA (Bovine Serum Albumin); (B) (A) Purified human NSF separated on SDS-PAGE and quantified by comparison with different concentration of BSA (Bovine Serum Albumin); (B) Representative TEM micrograph of purified NSF with 1 mM ATP and 4 mM $MgCl_2$ reveals the presence of hexamers as highlighted in the large onset. (scale bar 50 nm).

In addition, we exploited size exclusion chromatography (SEC) to further monitor the ability of flag-tagged NSF to oligomerize upon ATP addition. To this aim, different amounts of ATP were added to the cell lysates and NSF-containing lysates were subsequently loaded into a Superdex200 gel filtration column (Fig.7.2.3). The elution profile of NSF was then monitored by a dot blot analysis collecting all the chromatographic fractions. As shown in Fig.7.2.3, the addition of the nucleotide causes a shift in the position of NSF elution peak toward shorter retention times, suggesting an increased hydrodynamic radius of the protein in presence of ATP. Moreover, the entity of the shift of the NSF chromatographic peak is different as a function the ATP concentration. The presence of an intermediate peak at 90 µM of ATP between 0 and 1 mM suggests that NSF may assemble into intermediate species before acquiring its hexameric conformation. Supporting this finding, early studies indicate that NSF can form trimers and that the two ATP binding sites (D1 and D2) possess different affinities for the nucleotide (Whiteheart et al., 1994; Matveeva et al., 1997).

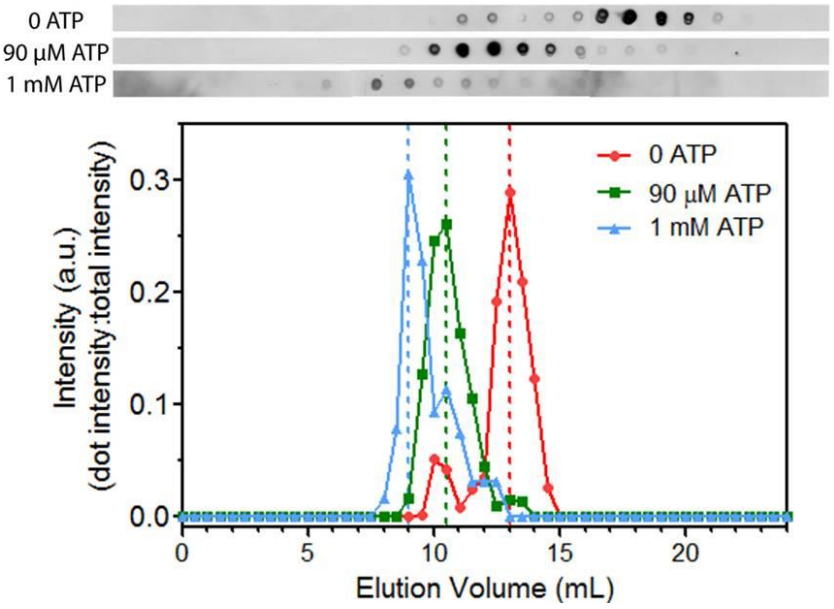

Fig.7.2.3 | SEC profile of cell lysates overexpressing flag-NSF adding different ATP concentration: Size exclusion chromatography fractions of HEK293T expressing flagged-NSF spotted onto nitrocellulose membrane and probed with anti-flag antibody; SEC profile of cell lysates adding different ATP concentrations in the Lysis buffer.

Interestingly, Flag-NSF purified with M2-Flag agarose beads binds endogenous NSF, as indicated by the presence of an extra band with an approximate molecular weight of the endogenous protein (82 kDa) and that is recognized by an antibody against NSF but not by the anti-flag antibody (Fig.7.2.4).

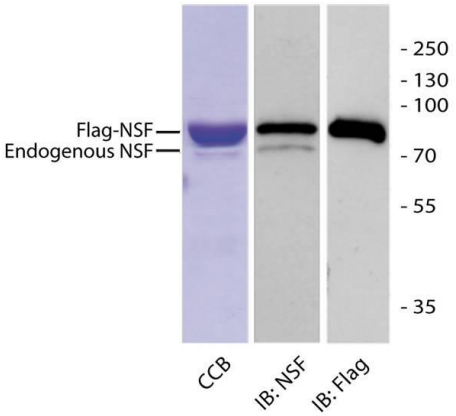

Fig.7.2.4 | Co-purification of endogenous NSF: western-blot analysis to validate the presence of endogenous NSF co-purification with recombinant human NSF using anti-flag and anti-NSF antibodies.

Taken together, these experiments support the notion that recombinant human flag-NSF purified from HEK293T cells is soluble and correctly folded.

7.3 Catalytic Properties Of Recombinant Human Flag-NSF

Having established that recombinant human NSF purified is correctly folded and able to form its functional hexameric structure, the next step was to evaluate NSF ATPase activity. We set up two complementary assays to monitor the catalytic activity of NSF: 1) a Malachite Green Enzyme assay and 2) an isocratic reversed-phase HPLC (RP-HPLC)-based assay. The latter, provides a direct measurements of ATP to ADP conversion by monitoring the areas of the peaks corresponding to the two nucleotides. The Malachite Green is a colorimetric assay that measures the inorganic phosphate (Pi) free in solution, released from ATP during the reaction (Lanzetta et al., 1979). Thus, it is an indirect measurement influenced by several aspects, such as Pi already present in the reaction buffer and/or produced by other sources (i.e. contaminating GTPases/ATPases). However, this assay has the advantage of being faster and scalable, since it measures the absorbance (at a wavelength of 640 nm) of the reaction at a given time (Fig.7.3.1).

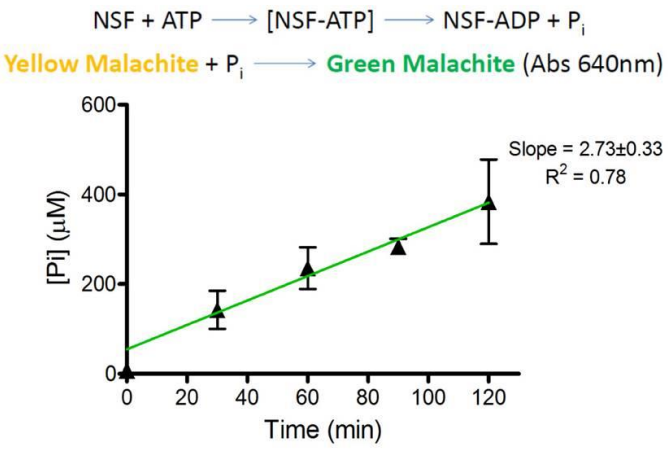

Fig.7.3.1 | Pi free in solution measured with Malachite Green assay: Schematic representation of the Malachite Green enzyme assay, on top, and the concentration of Pi free in solution as a function of time ([ATP] = 0.5 mM). Aliquots were collected as a function of time and subtracted by a control purification of untransfected cells. Velocities of the reactions (slopes) were calculated by linear regression using GraphPad Prism 5 software.

To validate the Malachite Green assay, we performed it in parallel with the HPLC-based assay, which provides a direct measurement of the ATP consumption and concomitant ADP formation, but has the limitation of requiring long running times and it cannot be implemented in a high-throughput fashion. For the Malachite Green assay, we collected aliquots of the reaction at different time points and evaluated the Pi formation by measuring the absorbance at 640 nm, as show in Fig.7.3.1. For the RP-HPLC assay, we detected the variation of ATP and ADP over time by injecting aliquots of the reaction collected at different time points (Fig.7.3.2). Both assays confirmed that human flag-tag NSF purified from mammalian cells is an active ATPase: as shown in Fig.7.3.2 B and 7.3.1, the amount of ADP and the concentration of Pi in solution increased as a function of the reaction time.

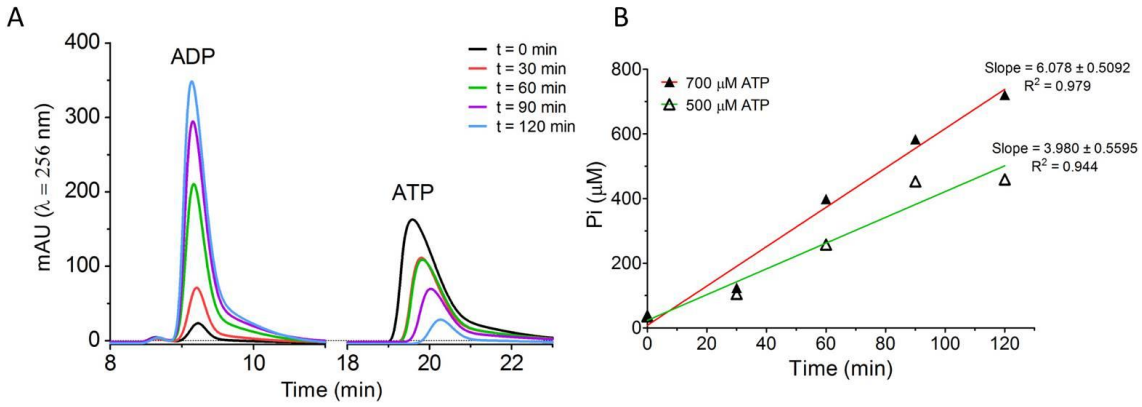

Fig.7.3.2 | Isocratic RP-HPLC assay: (A) Reaction profile of the two different nucleotide peaks over time ([ATP] = 0.7 mM). The ATPase activity of NSF was evaluated measuring the area under the peak of ADP (B). Aliquots were collected as a function of time and subtracted a control purification of untransfected cells. Velocities of the reactions (slopes) were calculated by linear regression using GraphPad Prism 5 software.

We then identified the best purification conditions to maximize the ATPase activity of NSF *in vitro*. Specifically, we tested if the presence Tween-20 has a negative effect on NSF catalytic activity. For this reason, we purified NSF in parallel with i) lysis buffer containing 1% of detergent, a purification protocol routinely used to purify LRRK2, and ii) with repeated freeze/thaw cycles. This new tested protocol was used because it is a gentle process of lysing cells and it can help maintaining the protein folding. After having validated, with a BCA assay, that 5 cycles are enough to disrupt plasma membranes, we

found that the ability of NSF to hydrolyze ATP is higher when purification is carried out using the freeze/thaw procedure. As shown in Fig.7.3.3 A, the rate of the reaction is higher and this suggest that the presence of the detergent may affect the correct protein folding which results in a lower rate of ATP to ADP hydrolysis as highlighted in Fig.7.3.3 B.

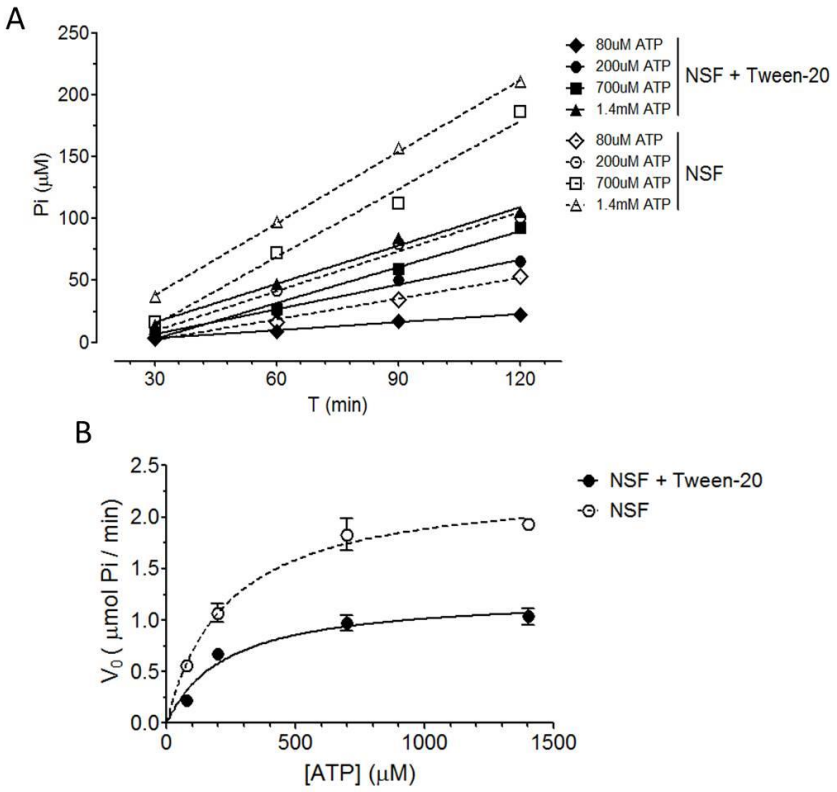

Fig.7.3.3 | Impact of Tween-20 on NSF ATPase activity: (A) Concentration of Pi free in solution with different amount of the substrate reveal that the rate of the reaction decrease in presence of the detergent, as highlight in (B) fitting slopes with Michaelis-Menten equation (NSF+Tween-20 Vmax=1.24 µmol/min; NSF Vmax=2.32 µmol/min).

Based on these observations, all the subsequent NSF purifications were carried out using a freeze/thaw protocol and the ATPase activity of NSF was measured using the Malachite Green assay.

Next, we determined the K_M of NSF using the Malachite Green enzyme assay. The K_M represents the concentration of substrate required to reach half of the reaction maximum velocity (Vmax) and provides an indication of the affinity of the substrate for

the enzyme. We monitored this value by comparing proteins at different days post-purification at 4°C. We found that the value of the Km did not change, however the Vmax substantially decreased (Fig.7.3.4 B). This phenomenon suggests that a fraction of the protein progressively becomes inactive, but the fraction of active NSF has unaltered affinity for the substrate (Fig.7.3.4 A). Collecting all the data obtained from independent experiments with different amount of ATP, we showed that human NSF possesses a Km of 180±10 µM.

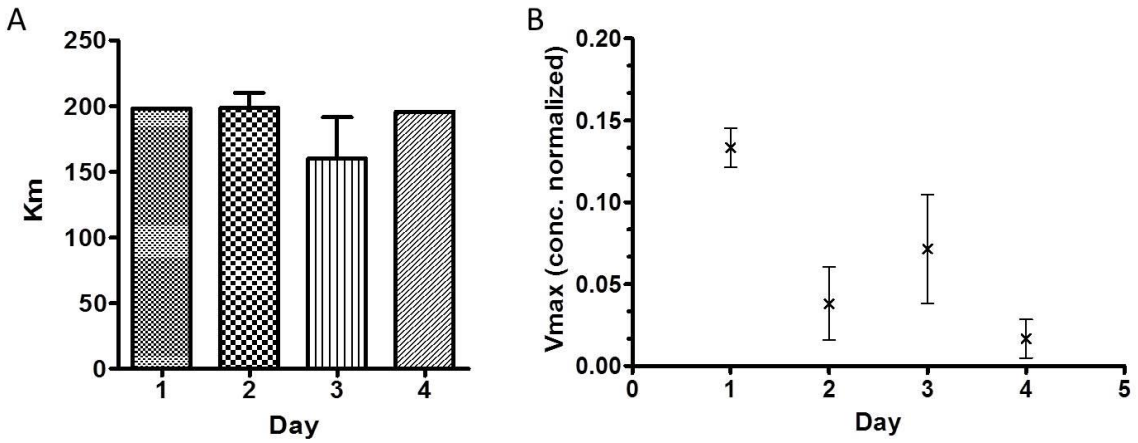

Fig.7.3.4 | Km of recombinant flag-NSF: The values of Km (A) and Vmax (B) calculated for NSF on different days after purification, keeping the protein at 4°C. Km value was equal to 180±10 µM and did not change in function of days, suggesting that this corresponds to its affinity for the substrate.

Taken together, these observations indicate that recombinant human Flag-NSF full length purified from mammalian HEK293T cells is an active ATPase.

7.4 Generation Of Stable Cell Line Expressing Human Flag-NSF

To optimize the purification procedure, we attempted to bypass transient transfection – which requires large amounts of transfection reagents - by generating HEK293T cell lines stably expressing human NSF. To this end, we took advantage of the presence within the NSF-coding plasmid of the Neomycin gene, which confers resistance to the antibiotic geneticin. After transfection, resistant cells were selected by culturing them in the selective medium containing geneticin (G418). We isolated three clones and tested them

for NSF expression. As indicated by western blot analysis in Fig.7.4.1 A, only one clone expressed Flag-NSF. Moreover, immunofluorescence analysis with confocal microscopy revealed that 100% of cells overexpressed Flag-NSF, indicating that the selection worked (Fig.7.4.1 B). We next compared the amount of the protein that we were able to purify from HEK cells either transiently transfected or stably expressing NSF.

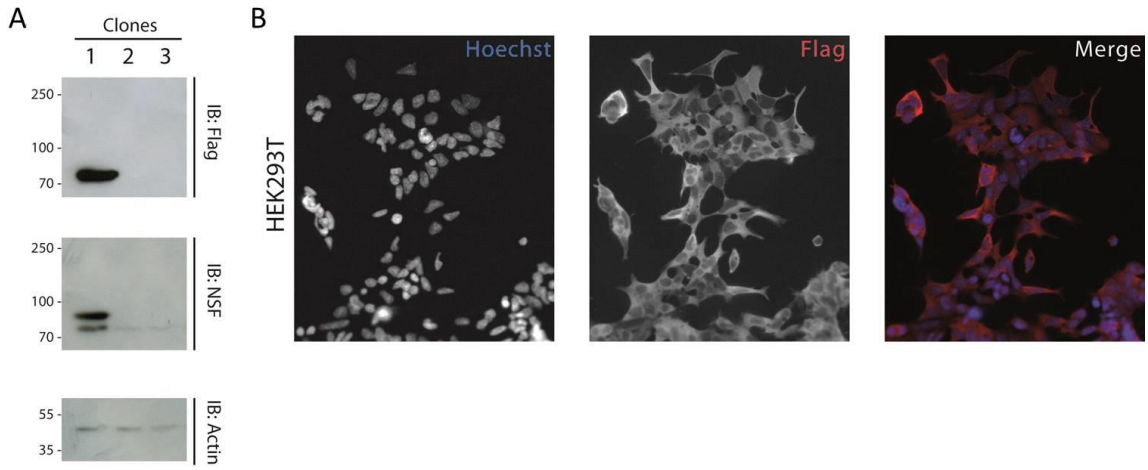

Fig.7.4.1 | NSF stable cell line: (A) Western-blot analysis on lysates from different clones of HEK293 cell line reveal the presence of flagged NSF stably expressed, on top, and its ability to interact with endogenous NSF. (B) Immunofluorescence microscopy. Red staining against Flag-tag show that human Flagged-NSF was ubiquity expressed in stably transfected HEK293 cells.

While we could purify NSF stably expressed in HEK293 cells, the total amount of protein recovered was about 75% lower compared to that obtained from cells transiently transfected (Fig.7.4.2). This result highlights that although these cells maybe useful to perform some cellular and biochemical evaluations, transient NSF expression is required to obtain a purification yield suitable for using the protein in enzymatic assays.

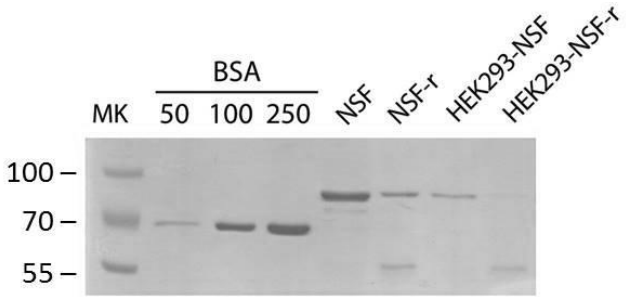

Fig.7.4.2 | Purification of flag-NSF from HEK293 cells: Comparison of purified human NSF derived from both transient transfection using HEK293T cells and stable HEK293 cells. Proteins were separated on SDS-PAGE and quantified by comparison with different concentration of BSA (Relative beads, named with "-r", were loaded as a control of correct elution on the gel).

7.5 LRRK2 Interacts With NSF *In Vitro*

Previous studies reported that LRRK2 can interact with proteins at the presynaptic site, modulating endosome maturation, microtubules formation and SNARE complex assembly with consequences on neurotransmitter release and vesicle recycling (Matta et al., 2012; Yun et al., 2013; Cho et al., 2014; Yun et al., 2015). A presynaptic protein that was demonstrated to interact with the WD40 domain of LRRK2 is NSF (Piccoli et al., 2011). Here, the aim was to confirm the interaction between these two proteins at the endogenous level and to map the domains involved in this interaction. In collaboration with Drs. Antonella Marte and Franco Onofri (University of Genova), we found that LRRK2 binds NSF in purified synaptosomes (Belluzzi, Gonnelli et al., 2016; *Appendix* Fig.2 a).

Next, we evaluated the interaction between LRRK2 and NSF in primary neurons using an antibody against LRRK2 already validated in the literature in hippocampal neurons (N231B/34; Davies et al., 2013). As show in Fig.7.5.1, LRRK2 and NSF largely co-localize, and co-localization is enriched within clusters along neurites.

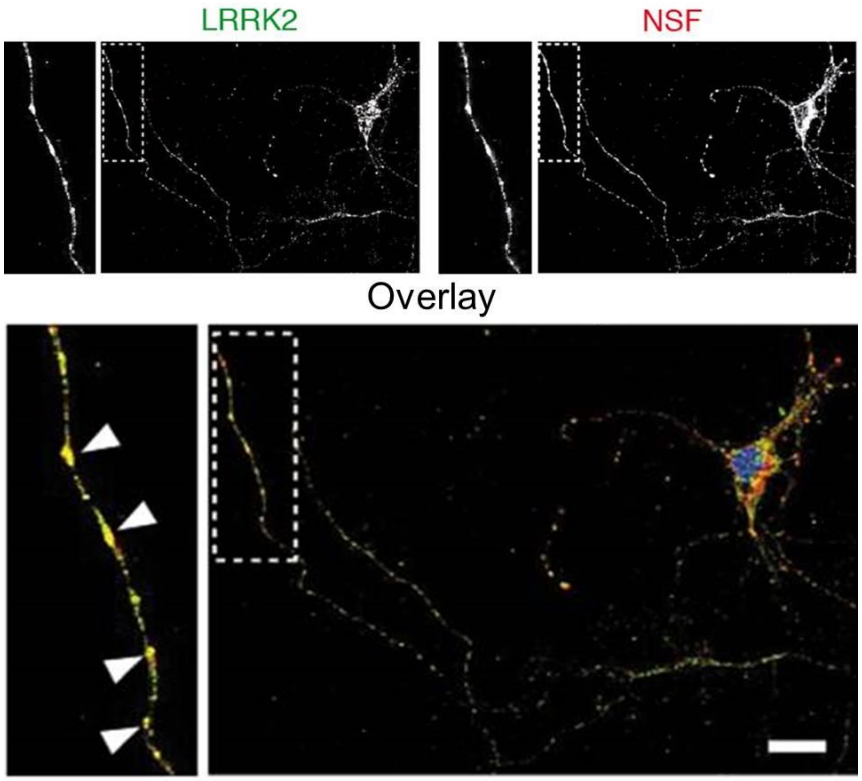

Fig.7.5.1 | LRRK2 interacts with NSF: Immunofluorescence of primary cortical neurons stained for endogenous LRRK2 (green) and endogenous NSF (red) (scale bar is 10 µm).

Next, we asked which domain(s) of NSF is responsible for the interaction. To this aim, we performed pulldown assays in presence of flag-tagged NSF full-length and all its three domains (N-ter 1-205, D1 206-487 and D2 488-744) also cloned with an N-terminal Flag-tag. Proteins were purified from HEK293T cells with Flag-conjugate beads and incubated at equimolar concentrations with a mouse brain lysate. As expected, full-length NSF pulls-down endogenous LRRK2, confirming the interaction. Moreover, we found that LRRK2 co-precipitates in presence of N-terminal and D2 domain, but not with the D1 domain (Fig.7.5.2). These data indicate that LRRK2 binds NSF at N-terminal and D2 domains.

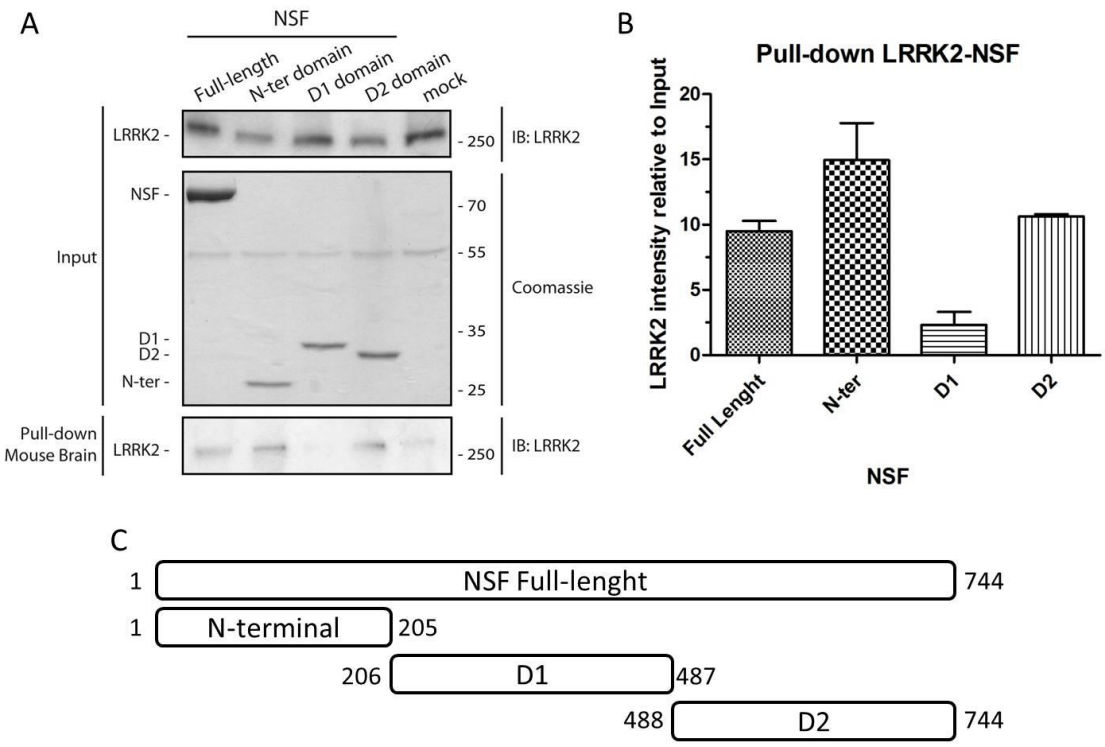

Fig.7.5.2 | LRRK2 pull-down assays: (A) Human flag-tagged NSF full-length or its domains purified from HEK293T and bound to M2 flag resin were incubated with a mouse brain lysate. (B) Pull-down reveals the interaction between LRRK2 and N and D2 domains (n=2). (C) Schematic representation of NSF full-length and the three different domains.

7.6 LRRK2 Phosphorylates NSF *In Vitro*

Having validated the interaction between LRRK2 and NSF, we next assessed whether NSF is also a substrate of LRRK2 kinase activity. To test this, full-length NSF was incubated with LRRK2 at a 1:10 ratio LRRK2:NSF with ^{33}P-ATP in kinase conditions. To evaluate if NSF is a specific substrate of LRRK2 kinase activity, the wild-type, the kinase dead mutant (K1906M) and the pathogenic G2019S form were used. The latter mutation is well known to increase LRRK2 kinase activity and this was also confirmed by enhanced its autophosphorylation compared to the wild-type (Fig.7.6.1). The M1906M is instead devoid of autophosphorylation as expected. Importantly, both LRRK2 wild-type and G2019S proteins were able to phosphorylate NSF (Fig.7.6.1). Moreover, NSF was not phosphorylated by the kinase dead mutant or in the presence of the LRRK2 inhibitor 1 (IN-1; Deng et al., 2011). The fact that we did not see any signal in presence of the kinase dead form of LRRK2 and upon IN-1 addition, supports the notion that NSF is a LRRK2

specific substrate *in vitro* and allows us to rule out that the observed phosphorylation is not due to the presence of other kinases co-purified with NSF, but depends on LRRK2. In addition, Fig.7.6.1 indicates also that ^{33}P incorporated by NSF in presence of the gain-of-function G2019S mutant is higher compared to the wild-type, as expected.

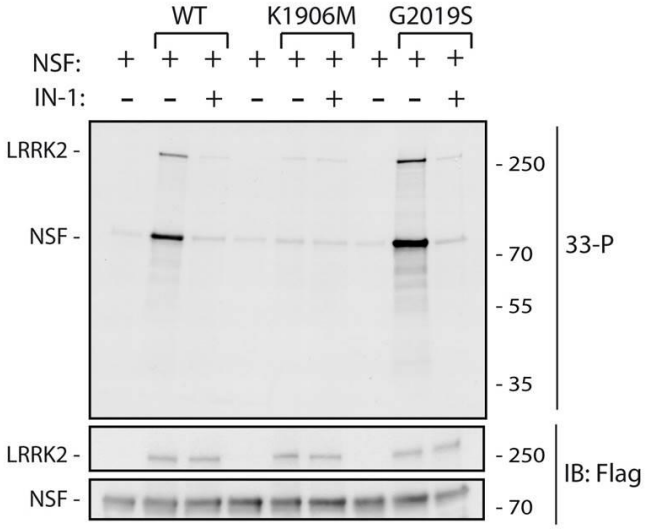

Fig.7.6.1 | NSF is a substrate of LRRK2 kinase activity: NSF is efficiently phosphorylated by full-lenght LRRK2 wild-type and to a greater extend by LRRK2 G2019S. Moreover, any signal was detected upon incubation with kinase dead mutant (K1906M) of LRRK2 and the presence of IN-1, supporting the notion that this NSF is a specific substrate of LRRK2 kinase activity.

To follow up these observations, we next calculated the stoichiometry of the reaction using different forms of LRRK2, including the N-terminal truncated LRRK2-G2019S (LRRK2-G2019S$^{970\text{-}2527}$), which has been previously shown to be hyperactive (Lewis, 2012). By measuring the phosphate incorporation, calculated with a calibration curve of known concentrations of ^{33}P-ATP (Fig.7.6.2 C), we found that the stoichiometry of phosphorylation was about 0.04, 0.1 and 0.4 moles of phosphate per mole of monomeric NSF in presence of LRRK2 wild-type, G2019S and LRRK2-G2019S$^{970\text{-}2527}$ respectively. Referring these stoichiometry values to hexameric NSF, 24% of NSF-hexamers possesses at least one phosphorylation in the presence of LRRK2 wild-type, 60% in the presence of LRRK2 G2019S and 240% (on average 2.4 monomers within each hexamer) in the presence of LRRK2-G2019S$^{970\text{-}2527}$. Percentages are reported in Fig.7.6.2 B. Thus, we concluded that LRRK2 phosphorylates NSF *in vitro* and the phosphorylation

stoichiometry in the presence of hyperactive LRRK2 is sufficient to imply the presence of at least one phosphorylated monomer per hexamer.

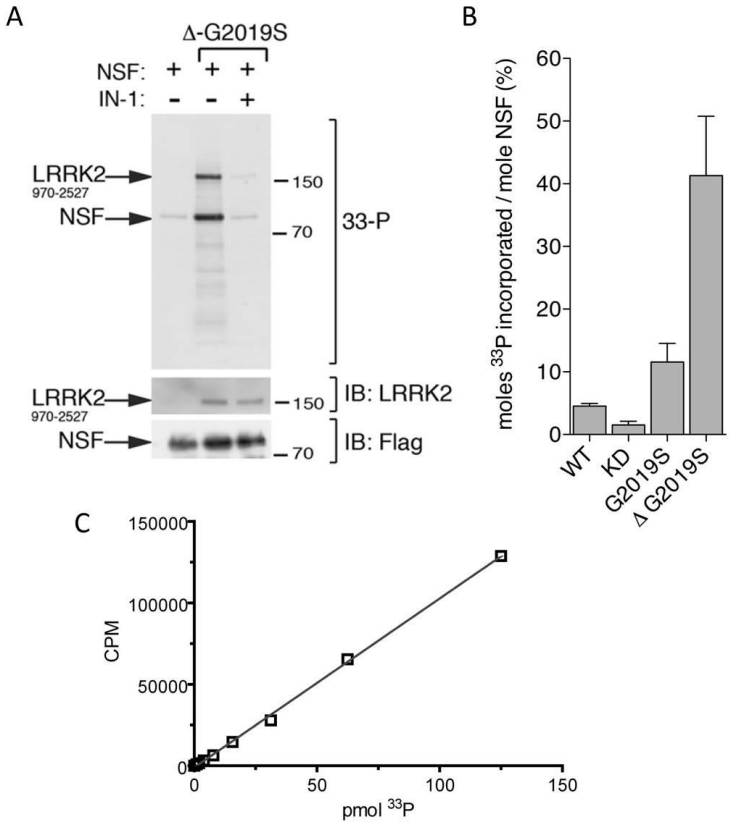

Fig.7.6.2 | Measurements of ^{33}P incorporated by NSF: (A) NSF in vitro phosphorylation by the hyperactive form of LRRK2 G2019S$^{970\text{-}2527}$ and (B) percentage of moles ^{33}P incorporated by NSF upon LRRK2 wild-type, kinase dead, G2019S (referred to Fig.7.6.1) and G2019S$^{970\text{-}2527}$ form using a (C) calibration curve with known ^{33}P-ATP concentrations (CPM=counts per million).

We next took advantage of NSF isolated domains to attempt mapping the domain(s) where this phosphorylation occurs. We therefore performed kinase assays in the presence of NSF full-length, N-terminal, D1 and D2 in the same conditions (1:10 ratio LRRK2:NSF/domains with ^{33}P-ATP). The assay revealed that, in addition to NSF full-length, only the D2 domain was phosphorylated, whilst no phosphorylation was observed for the other domains of NSF upon LRRK2-G2019S$^{970\text{-}2527}$ incubation (Fig.7.6.3).

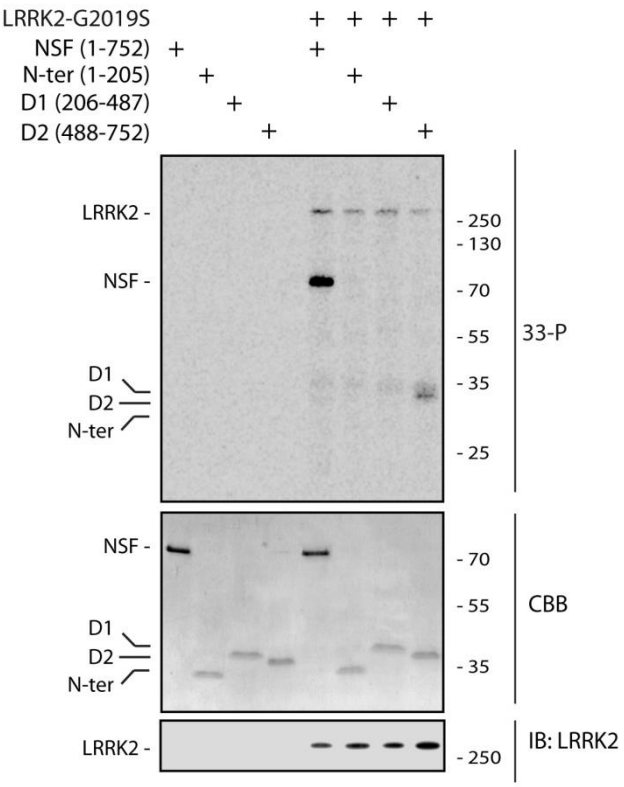

Fig.7.6.3 | LRRK2 phosphorylation occurs in the D2 domain: In vitro kinase assays using NSF full-length and all its domains incubated with LRRK2 GST-LRRK2$^{970\text{-}2527}$. The presence of a signal in the lane with D2 domain suggest phosphorylation preferentially occurs within this domain.

This result supports the hypothesis that the LRRK2 kinase activity-dependent regulation of synaptic vesicle dynamics might be mediated by NSF phosphorylation.

7.7 LRRK2 Phosphorylates NSF At Threonine-645

Starting from the results obtained with kinase assays, we next performed mass spectrometry analysis to identify possible LRRK2 phosphorylation sites within NSF. To this aim, in collaboration with Dr. Giorgio Arrigoni (Dept of Biomedical Science, University of Padova), we applied phosphopeptide enrichment coupled with liquid chromatography/tandem mass spectrometry (LCMS/MS) analysis. Specifically we incubated purified NSF, pretreated with alkaline phosphatase to eliminate possible cellular phosphorylation sites, with LRRK2-G2019S$^{970\text{-}2527}$ (to maximize the stoichiometry of phosphorylation). The sequence coverage before phosho-peptide enrichment was about 80% and three independent analyses consistently enriched the peptide

^{639}KLLIIGTTSR^{648}, indicating the presence of one phosphorylation event (Fig.7.7.1). To confirm this peptide as a candidate for bearing the LRRK2 phospho-site, we repeated the MS analysis in presence of both LRRK2 wild-type and G2019S and found that they were able to phosphorylates NSF within this peptide. Moreover, this phosphorylation did not occur in the presence of LRRK2 kinase dead form or IN-1. For these reasons, the ^{639}KLLIIGTTSR^{648} peptide appeared a very good candidate being within the D2 domain, although the exact residue phosphorylated - among Thr-645, Thr-646 and Ser-647 - could not be discriminated by the software.

A

Protein ID: Human N-ethylmaleimide sensitive fusion protein
Sequence coverage: 80.51%
Green: confidence >99%
Yellow: confidence >95%

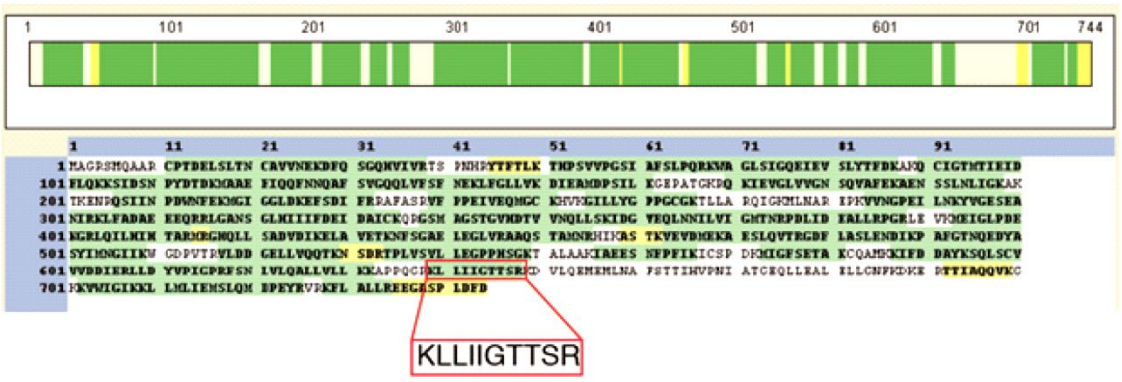

B

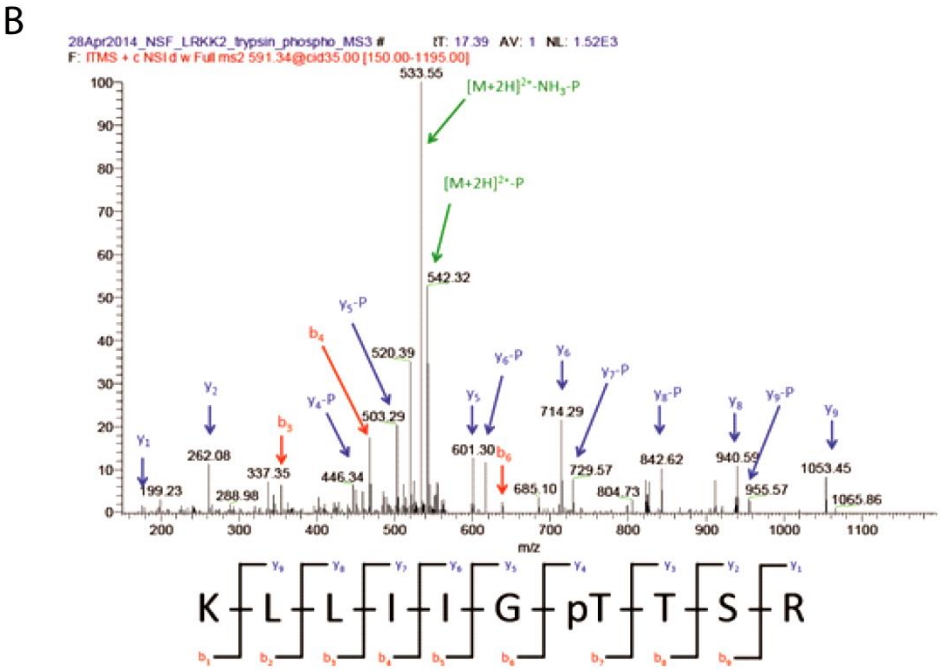

Fig.7.7.1 | LC-MS/MS analysis of NSF phosphorylated by LRRK2: (A) Sequence coverage of NSF phosphorylated by LRRK2. (B) Manually annotated MS/MS spectrum relative to the monophosphorylated peptide KLLIIGTTSR from NSF. Charge: +2, Monoisotopic m/z: 591.33636 Da (+0.03 mmu/+0.04 ppm respect to the theoretical m/z), MH+: 1181.66545 Da. Identified with Mascot with an IonScore of 60 (Exp Value of 2.5E-005). The presence of the fragment y2 suggests that the phosphorylation site is probably not located at the level of the serine residue. The fragmentation pattern is compatible with a phosphorylation at T645 or T646.

To confirm the MS result and map the phospho-site within the ^{639}KLLIIGTTSR^{648} peptide, we next generated phospho-deficient alanine mutants by site directed mutagenesis of all the possible residues that could be the substrate of the serine-threonine kinase

activity of LRRK2. Specifically, three different Flag-NSF mutants were generated by substituting the two threonine or the serine with an alanine (T645A, T646A and S647A). The mutated proteins were expressed and purified from HEK293T cells with the same protocol described above for the wild-type NSF (Fig.7.7.2).

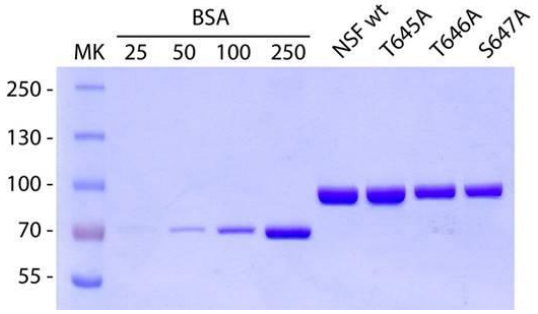

Fig.7.7.2 | **Purification of recombinant NSF and its mutants:** Purified human NSF wild-type, T645A, T646A and S647A mutants separated on SDS-PAGE and quantified by comparison with different concentration of BSA (Bovine Serum Albumine).

Kinase assays were then performed under the same conditions, incubating LRRK2-G2019S with NSF wild-type, T645A, T646A or S647A respectively. As evidenced in Fig.7.7.3, we found that the alanine substitution of Threonine-645 resulted in a 50% reduction of ^{33}P incorporation compared to wild-type, T646A and S647A mutants (Fig.7.7.3). Bands were quantified by densitometry and ^{33}P signal normalized by the total protein concentration (Coomassie blue staining on the PVDF membrane). Thus, phosphorylation occurs at T645 and this phosphorylation accounts for the 50% of the total LRRK2-mediated phosphorylation on NSF measured in kinase assays.

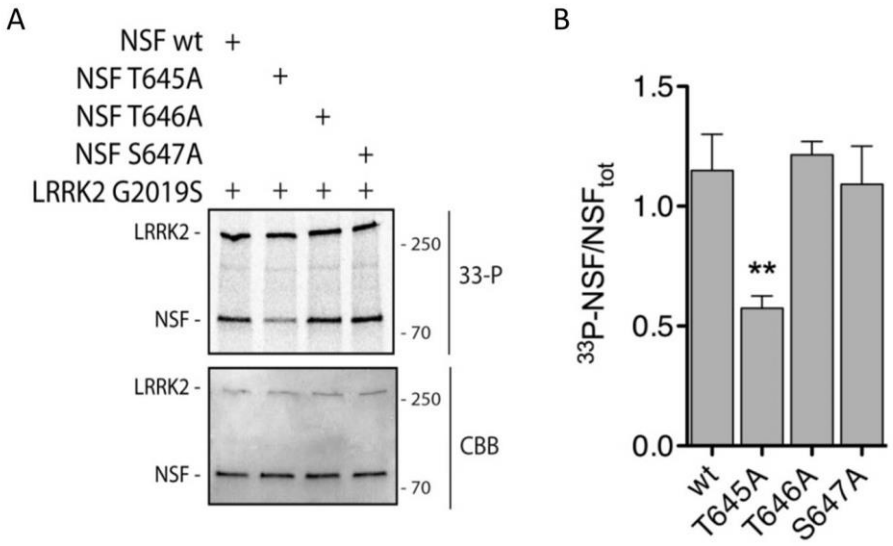

Fig.7.7.3 | Kinase assay on NSF mutants: (A) In vitro kinase assays with 3xFlag-LRRK2 G2019S and NSF wild-type or non-phosphorylable mutants T645A, T646A and S647A at 1:10 ratio LRRK2:NSF. (B) Quantification of ^{33}P incorporated by NSF (autoradiography in A upper panel) controlled for total NSF (NSF_{TOT}, Coomassie staining (CCB) in A lower panel) from n=4 independent experiments (bars represent the mean ± SEM). One way-ANOVA with Bonferroni's post-test (**p<0.01).

As discussed in the introduction, NSF is a substrate of Pctaire1 and Protein Kinase C (PKC) and phosphorylation by these kinases results in impairment on NSF hexamerization and alpha-SNAP binding respectively (Liu et al., 2006; Matveeva et al., 2001). To test whether phosphorylation on T645 is specific for LRRK2 or instead can be achieved by other kinases, both NSF wild-type and T645A were incubated with PKC, expressed and purified with Flag-affinity purification from HEK cells. As shown in Fig.7.7.4, PKC efficiently phosphorylates NSF, as expected, and ^{33}P incorporation was similar for wild-type and T645A, suggesting that T645A is a specific LRRK2 phosphorylation site.

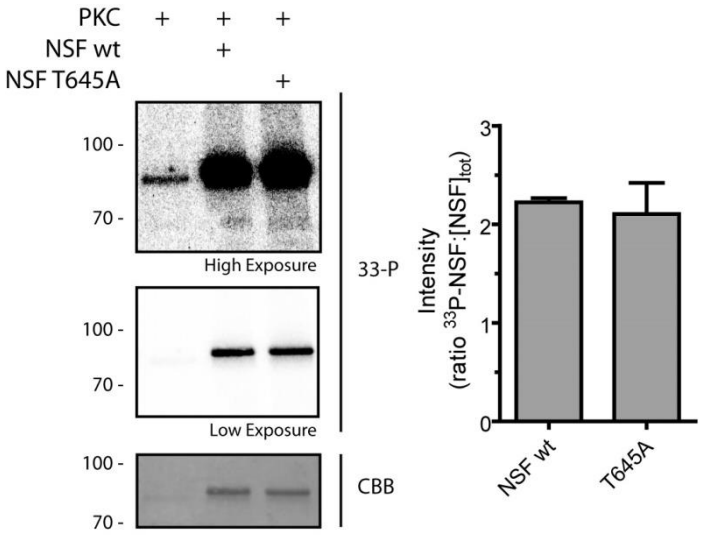

Fig.7.7.4 | NSF T645A mutation does not alter PKC phosphorylation: In vitro kinase assays with PKC and NSF (1:10, PKC:NSF). On the left, upper panel shows a high exposure image where autophosphorylation of PKC can be observed. Middle panel represent a low exposure phosphoscreen. Lower panel shows a coomassie of the same membrane to normalize for protein loading. On the right, quantification of radioactivity incorporated by NSF wild-type and T645A (n=3 independent experiments).

Taken together, these experiments indicate that NSF is a robust substrate of LRRK2 kinase activity *in vitro* and that phosphorylation occurs preferentially at T645. The fact that the phosphorylation signal was not completely abolished, suggest that there might be an additional site(s) phosphorylated by LRRK2.

7.8 LRRK2 Mediated Phosphorylation Increases NSF ATPase Activity

Once identified that NSF is a substrate of LRRK2 kinase activity, the next step was to investigate whether this phosphorylation has functional consequences on the ATPase activity of NSF. In contrast to NSF, purification of recombinant LRRK2 from HEK293T cells requires the presence of Tween-20 in the lysis buffer. One possibility is that LRRK2 is stabilized by the detergent, as it has been shown to interact with membranous structures inside the cell. We first identified the optimal reaction conditions at which both NSF and LRRK2 display their maximal activity, since we needed to pre-incubate NSF with LRRK2 (or only buffer) to allow phosphorylation, before proceeding with the ATPase assays. The activity of NSF was evaluated with the Malachite Green enzyme

assay adding different concentration of Tween-20 to the reaction buffer. LRRK2 activity was determined by monitoring the auto-phosphorylation of Thr-2483 using a specific antibody (Davies et al., 2013). As shown in Fig.7.8.1, the presence of the detergent is necessary for the activity of LRRK2 and the concentration of Tween-20 at which both proteins display maximum activity is 0.007%. This value corresponds to the detergent CMC (critical micelle concentration), suggesting that the presence of micelles in solution are required to maintain an enzymatically active LRRK2. Importantly, NSF ATPase activity is preserved at a low concentration of detergent, therefore the subsequent assays were performed with the presence of Tween-20 at its CMC concentration.

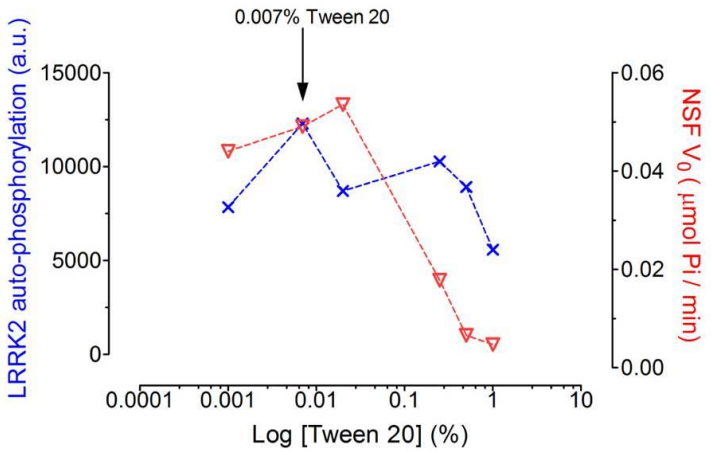

Fig.7.8.1 | Evaluation of the optimal detergent concentration: Optimal Tween-20 concentration for the reactions was evaluate within ability of LRRK2 to phosphorylate itself measuring the intensity of the band with an antibody against one of its auto-phosphorylation site (Thr-2483). At the same time, the activity of human NSF, using the same concentration of detergent, was evaluate measuring the V_0 of the reaction with the Malachite Green Enzyme assay.

NSF was treated with LRRK2-G2019S$^{970\text{-}2527}$ at a ratio NSF:LRRK2 = 20:1 or alone in the kinase buffer at 30°C for 1 hour and 30 minutes in the presence of 50 µM ATP which is sufficient to support LRRK2 phosphorylation and minimizes interference with the subsequent ATPase assay. We incubated 500 nM of NSF (monomer) and then performed ATPase assays at a final NSF concentration of 36 nM (hexameric) based on previous studies that employed this concentration to monitor NSF activity (Cipriano et al., 2013; Vivona et al., 2013). We used the Malachite Green enzyme assay, to measure the kinetic parameters of NSF and to evaluate if they change upon LRRK2 phosphorylation. Pi

release over time was measured in NSF-phosphorylated and NSF-unphosphorylated. As summarized in Fig.7.8.2, we found that the kinetic parameters of the reaction calculated for recombinant human flag-tagged NSF increased of about 2-fold upon LRRK2 phosphorylation.

A

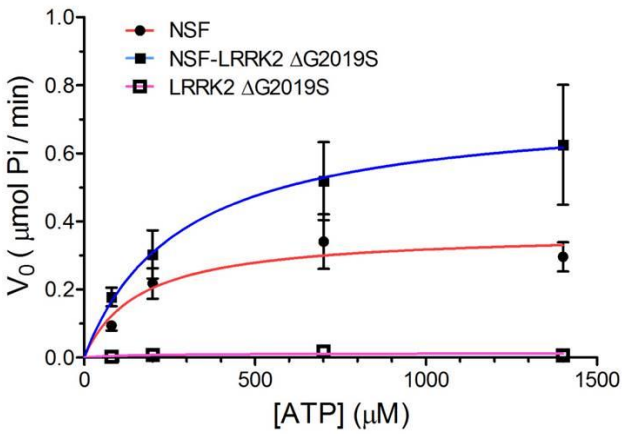

B

	NSF	NSF–LRRK2 G2019S$^{970-2527}$
Km (µM)	178 ± 12	355 ± 50
V_{max} (µmol/min)	0,37 ± 0,07	0,95 ± 0,22
k_{cat} (µmol Pi/min)	22 ± 4	40 ± 11

Fig.7.8.2 | LRRK2 phosphorylation increase the ATPase activity of NSF: (A)NSF ATPase activity was assessed with a Malachite green assays at 36 nM NSF (hexamer) at different ATP concentration to calculate the kinetic parameters of NSF (red, NSF) and NSF phosphorylated by LRRK2-G2019S$^{970-2527}$ (blue, NSF-LRRK2 ΔG2019S). Malachite Green assay was repeated for LRRK2-G2019S$^{970-2527}$ (pink, LRRK2 ΔG2019S) as a control. Data were fitted with the Michaelis-Menten kinetic model to determine kinetic constants (n=3). (B) Kinetic parameters obtained from the experiment show in A. Data reveal that NSF increases its activity within 2-fold upon LRRK2 ΔG2019S phosphorylation.

We then repeated the experiment in presence of the different NSF mutants and 1.4 mM ATP to evaluate whether the abolishment of the phosphorylation site would prevent the observed increased ATP activity observed upon LRRK2 phosphorylation. Interestingly we found that both T645A and T646A mutants display a low basal activity independently of phosphorylation, whereas S647A mutant has a similar ATPase activity compared to wild-type form (Fig.7.8.3). These results suggest that T645 and T646 residues may play a key role in NSF activity, since mutations into alanine provoke impairment of ATPase activity.

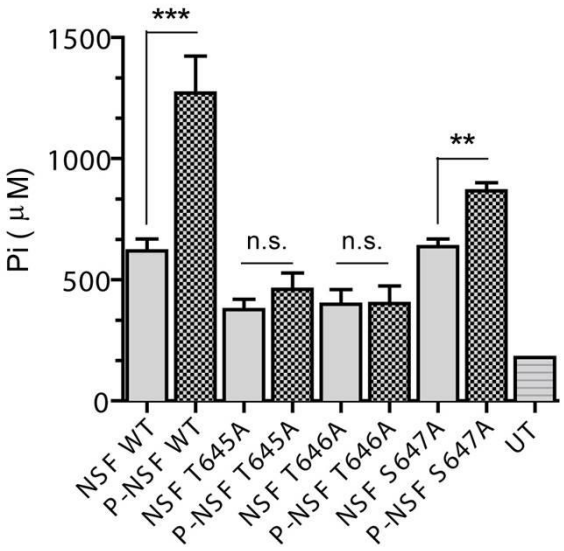

Fig.7.8.3 | ATPase activity of NSF wild-type and all mutants upon LRRK2 phosphorylation: Pi generated by ATP hydrolysis in the presence of NSF wild-type, NSF^{T645A} NSF^{T646A} NSF^{S647A} pre-phosphorylated or not by LRRK2 ΔG2019S (P-) was measured with the Malachite Green Assay at 120 min with an initial concentration of ATP of 1.4 mM (NSF^{WT} vs NSF^{T645A} **p<0.01; NSF^{WT} vs P-NSF^{WT} ***p<0.001; NSF^{T645A} vs P-NSF^{T645A} p>0.05, not significant, n.s.; NSF^{T646A} vs P-NSF^{T646A} p>0.05, n.s.; NSF^{S647A} vs P-NSF^{S647A} **p<0.01; one-way ANOVA, Bonferroni's post-test, n≥3). UT=untrasfected cells subjected to Flag-affinity purification to monitor background activity (n=1; excluded from the statistical analysis).

To rule out the possibility that these differences in the activity of NSF mutants may be due to an incorrect folding of the protein, we compared the circular dichroism (CD) and fluorescence properties of NSF wild-type, T645A, T646A and S647A mutants. As shown in Fig.7.8.4 B, all the proteins exhibit similar CD spectra showing a prevalent alpha-helix conformation. Moreover, intrinsic fluorescence values are also similar without differences in wavelength of the maximum emission value of the tryptophan peak (Fig.7.8.4 A).

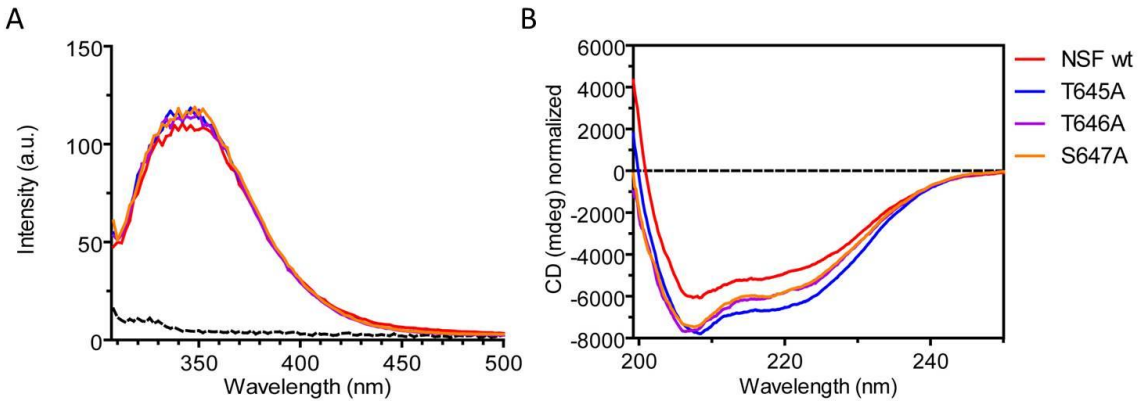

Fig.7.8.4 | Intrisic fluorescence and CD spectra of NSF wild-type and mutants: (A) Protein concentration used for Intrinsic Fluorescence measurements was 0.9 µM (Ec = 295 nm; Em = 330 nm). (B) CD spectra were normalized by protein concentration previously measured with an SDS-PAGE gel and reveal that all proteins are predominantly folded in alpha-helix conformation.

One final piece of evidence is that both T645A and T646A mutants are both able to form hexamers in solution as indicated by Transmission Electron Microscopy (TEM) in Fig.7.8.6. These results show that the alanine mutation in Thr-645 (as well as in the adjacent residue) does not alter the overall folding and the ability of NSF to goes from monomeric conformation.

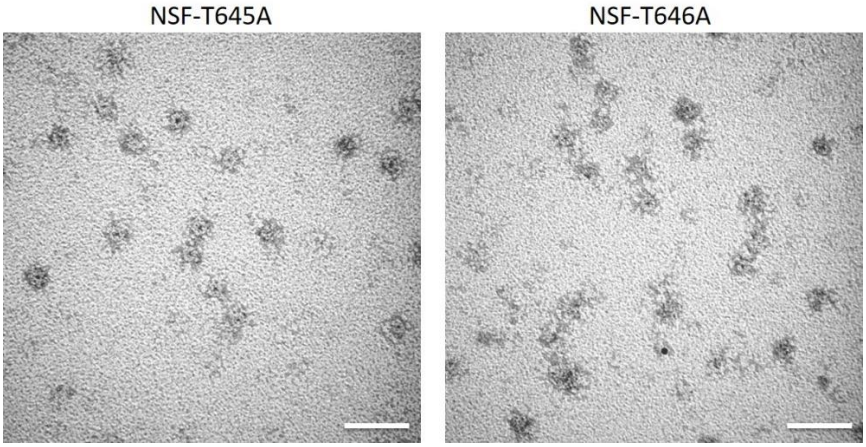

Fig.7.8.6 | NSF mutant form hexamers in solution: TEM micrograph of both NSF T645A and T646A mutant with 1 mM ATP and 4 mM $MgCl_2$. Images reveal the typical hexameric structures showed above for NSF wild-type in Fig.7.2.2 (scalebar 50 nm).

We then looked at the position of these sites within the *C. griseus* NSF structure, which presents a 98% amino acid identity with the human sequence and all the three residues are conserved among the two species (Fig.7.2.1). The peptide ^{639}KLLIIGTTSR^{648} is outside

the *Walker A* motif involved in nucleotide binding (^{543}GPPHSGKTA^{551}), and the PDB structure of the D2 domain highlights a possible role of these residues in mediating nucleotide binding (Fig.7.8.5), therefore mutations in these sites could compromise nucleotide binding, thus the ATPase activity of NSF.

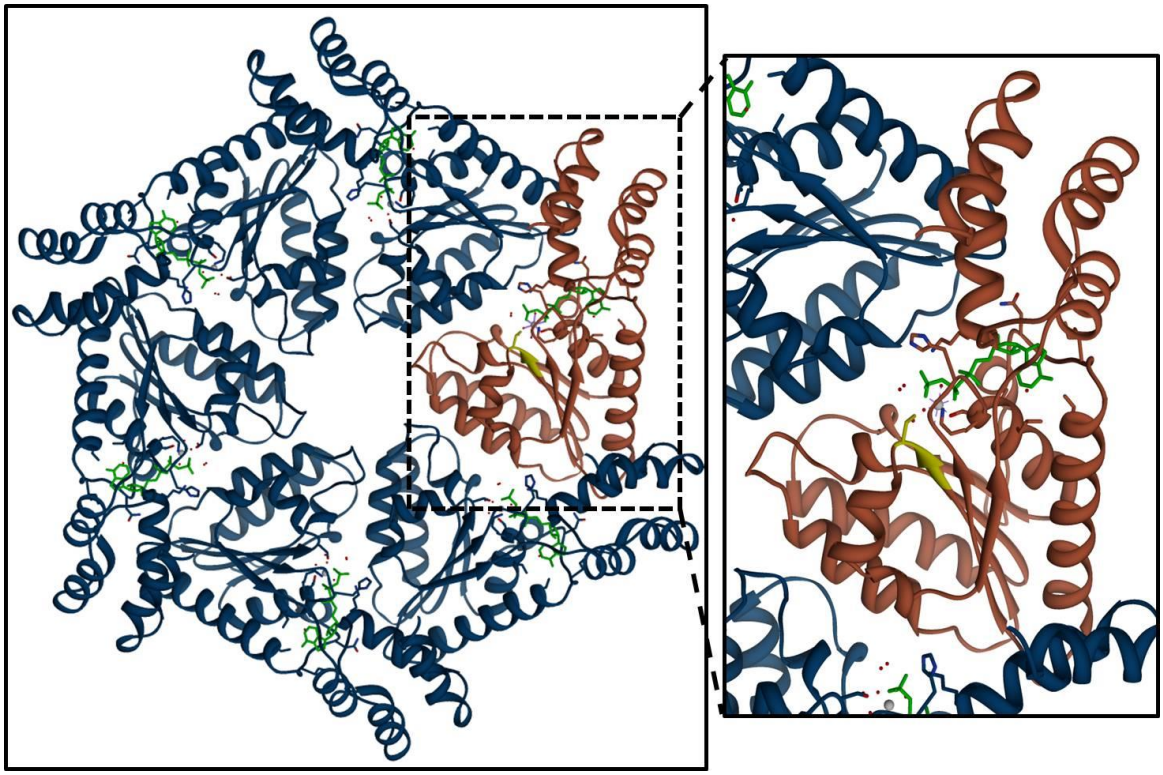

Fig.7.8.5 | 3D structure of NSF D2 domain complexed with ATP: ATP-dependent oligomerization D2 domain of NSF upon ATP (green) binding. D2 quaternary structure was solved using X-ray diffraction method with a resolution of 1.9 Å (PDB code: 1NSF). In figure residues T645-T646-S647 are yellow-labelled within the monomer (dark red).

Taken together, these data indicate that LRRK2 phosphorylation increase NSF ATPase activity and that T645 is a key site for the enzymatic activity of NSF.

7.9 Phosphorylation Increases Also The SNARE Complex Disassembly Rate

The physiological role of NSF inside neurons is to disassemble the SNARE complex and this phenomenon is an ATP-mediated process. Starting from the evidence collected so far, we next evaluated whether the altered ATPase activity measured in the presence of

NSF phosphorylated by LRRK2 would also reflect a different SNARE complex disassembly rate. Based on published methods, we co-expressed recombinant syntaxin, SNAP-25 and 6xHis-VAMP in *E. coli* (Vivona et al., 2013) and purified the SNARE-complex already assembled by IMAC affinity purification followed by size exclusion chromatography. The complex is SDS-resistant and eluted as a single band corresponding of its expected molecular weight (68 kDa). Upon heating, the three components of the complex dissociate as shown in Fig.7.9.1.

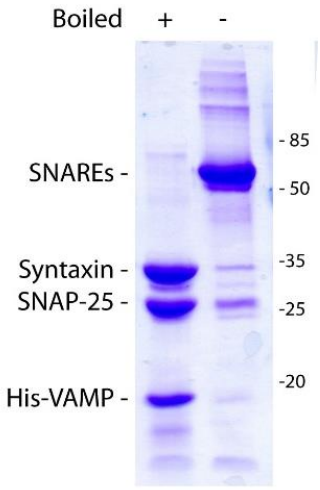

Fig.7.9.1 | SDS-PAGE gel of purified SNARE complex: the purified SDS-resistant SNARE complex (68 kDa) was obtained by co-expression of Syntaxin, SNAP-25 and 6xHis-VAMP in E. Coli BL21(DE3) strain, either boiled (+) and not (-) to disassemble the three single components.

To test the hypothesis that LRRK2 phosphorylation of NSF affects SNARE complex disassembly rate, we incubated the assembled SNARE complex (480 nM) together with alpha-SNAP (1.5 µM), the adaptor protein that permits NSF-SNARE binding, and NSF (24 nM) upon LRRK2 phosphorylation or not at 37°C. Reaction started when 2mM of ATP were added to the reaction mix. We then monitored the dissociation of the SNARE complex over time by measuring the intensity of the corresponding band at 68 kDa. As shown in Fig.7.9.2, we found that NSF phosphorylated by LRRK2 G2019S displayed a higher efficiency in disassembling the SNARE complex compared to unphosphorylated NSF.

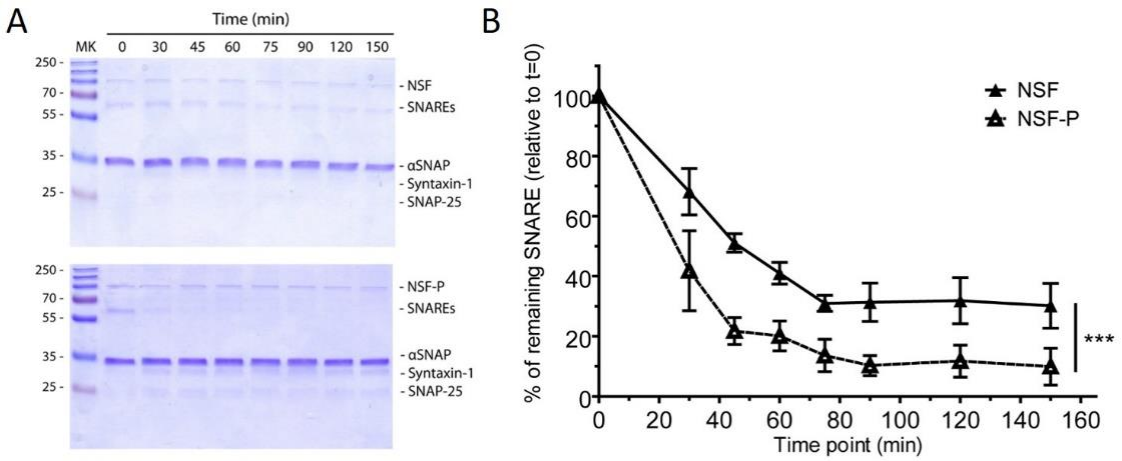

Fig.7.9.2 | SNARE complex disassembly rate is higher when NSF is phosphorylated: (A) Representative SDS-PAGE gels (CBB, coomassie brilliant blue) of SNARE complex incubated for increasing time with NSF phosphorylated or not by LRRK2-G2019S$^{970\text{-}2527}$ in the presence of the co-factor alpha-SNAP. (C) Quantification of n=3 independent experiments. Time points are relative to t=0 which was set at 100% (two-way ANOVA with Bonferroni's post-test, ***p<0.001).

These data support the notion that the altered catalytic activity of NSF due to LRRK2 phosphorylation has a downstream effect on SNARE complex disassembling.

8. Rab7L1 is a substrate of LRRK2 kinase activity

In the previous section, paragraph 7.1, we discussed the importance of LRRK2 kinase activity in synaptic vesicle trafficking. Among all the putative LRRK2 interactors at the presynaptic site, we focused on NSF, an AAA+ ATPase responsible for SNARE complex disassembly, and, thus vesicle endocytosis. We demonstrated that NSF co-localizes with LRRK2 inside primary cortical neurons (Fig.7.5.1) and pulls-down endogenous LRRK2 (Fig.7.5.2). Moreover, NSF is a substrate of LRRK2 kinase activity in vitro and, phosphorylation preferentially occurs at Thr-645 (Fig.7.7.3). We speculate that abnormal NSF phosphorylation due to LRRK2 mutation could represent one of the pathways compromised in LRRK2-linked PD, leading to neurodegeneration via impairments in the exo- and endocytic machinery. Thus, understanding how LRRK2 kinase activity regulates its presynaptic substrates is key to shed on into LRRK2 pathological function with potential impact in the development of novel therapeutic strategies against PD.

Several studies linked LRRK2 to vesicular trafficking events. In particular, there is growing evidence that LRRK2 interacts with Rab proteins (MacLeod et al., 2013; Gomez-Suaga et al., 2014; Dodson et al., 2014; Waschbusch et al., 2014). As discussed in the introduction, Rabs are a class of small monomeric GTPases localized in different cellular compartments that regulate a number of vesicle transport events.

Recently, genome-wide association studies (GWAS) highlighted a correlation between variants of the Rab7L1 gene, localized within the PARK16 locus, and PD-risk (Beilina et al., 2014). The authors also showed that overexpression of Rab7L1 is linked to a higher risk of PD in humans. Another group found instead that overexpression of Rab7L1 gene significantly rescued the LRRK2 G2019S PD-related neurite length phenotype, but did not alter neurite length in case of LRRK2 wt overexpression (MacLeod et al., 2013). It is possible that in the pathologic context, LRRK2 and Rab7L1 play adverse roles in vesicular trafficking. Rab7L1 has been shown to localize in association with the trans-Golgi apparatus and is implicated in vesicular sorting (Berger et al., 2009; Spanò et al., 2011), even though its precise function in neurons remains unknown. Furthermore, LRRK2 has

been shown to interact with Rab5B (Heo et al., 2010), Rab7 (Dodson et al., 2012) and functionally with Rab9, which promotes retromer-dependent recycling from late endosomes to the Golgi (Dodson et al., 2014).

We can make two hypotheses on the mechanism of LRRK2 regulation of Rabs activity: i) LRRK2 could directly regulate the GTPase activity of Rab proteins via phosphorylation or ii) it could alter the association between Rabs and their GEFs and/or GAPs, leading to impairment in vesicle sorting.

In this scenario, our aim was to test the first hypothesis, i.e. whether LRRK2 phosphorylates any relevant Rab protein.

8.1 LRRK2 Efficiently Phosphorylates Rab7L1

Over 60 Rab proteins (molecular weight about 26 kDa) are present in eukaryotic cells and some of them are known to be part of LRRK2 interactome. While pathological LRRK2 activity might compromise the endosome-lysosomal pathways, the molecular mechanism behind LRRK2-dependent Rab regulation is unknown. In collaboration with Dr. Sabine Hilfiker (Instituto de Parasitologia y Biomedicina "Lopez-Neyra", CSIC, Granada, Spain) who previously showed that LRRK2 delays degradative receptor trafficking by impeding late endosomal budding through decreasing Rab7 activity (Gomez-Suaga et al., 2014), we investigated whether LRRK2 acts on Rabs through phosphorylation. Thus, we focused on several Rab proteins, which are known to interact with LRRK2 or are related to neurodegeneration. As for NSF, impairment of vesicle sorting could be the consequence of an altered phosphorylation of these GTPases due to LRRK2 pathological mutations. We selected several Rab proteins from different subcellular compartments:

1. **Rab7**. It is implicated in late endosome (LE) to Lysosome trafficking and overexpression of a PD-related pathological mutation of LRRK2 results in a decreased level of active Rab7. This was observed in fibroblast from PD patients carrying G2019S LRRK2 mutation, important for LE trafficking (Gomez-Suaga et al., 2014);

2. **Rab7L1**. Rab7L1 gene lies within the PARK16 locus, a non-familial PD risk-associated locus, composed by five different genes: SLC45A3, NUCKS1, RAB7L1, SLC41A1, and PM20D1. As described before, previous studies show that overexpression of Rab7L1, but not other genes in this locus, is able to rescue LRRK2 G2019S pathological phenotype (MacLeod et al., 2013);
3. **Rab9**. It regulates trafficking between LE and both trans-Golgi network (TGN) and autophagosome in mammalian cells. Studies in Drosophila demonstrated that LRRK2 co-localize with Rab9 at the LE membrane suggesting a regulation in its membrane recruitment (Dodson et al., 2014);
4. **Rab11**. It was found associated with early endosomes (EE) regulating vesicular trafficking through recycling of EEs to the trans- Golgi network (TGN). Rab11 has been implicated in different neurodegenerative disorders, such as Alzheimer's disease and Huntington's disease (Bhuin and Roy, 2015), and therefore it might be also associated to PD, even though to date an interaction with LRRK2 has not been demonstrated;
5. **Rab32**. It is necessary for TGN organization with influences on endosomal trafficking and autophagy. Studies show that Rab32 and LRRK2 co-localize in recycling endosomes and an overexpression of Rab32 decreases the amount of LRRK2 in mitochondria and lysosome containing fractions (Waschbusch et al., 2014).

To test whether any of these Rabs are substrates of LRRK2 kinase activity, we purified all these proteins with a Flag-tag from mammalian HEK293T cells, following the same protocol previously optimized for LRRK2 (Fig.8.1.1).

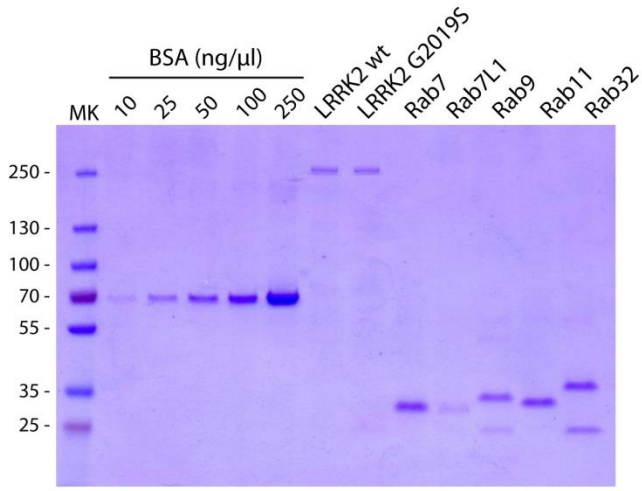

Fig.8.1.1 | Purification of recombinant Flag-Rab proteins from HEK293T cells. Purified human LRRK2 wt, G2019S mutant and Rab proteins separated on SDS-PAGE and quantified by comparison with different concentration of BSA (Bovine Serum Albumine).

Subsequently, we performed kinase assays in which proteins were incubated with both LRRK2 wild-type and G2019S form for 1 hour at 30°C at a 1:10 ratio of LRRK2:Rab(s) with ^{33}P-ATP. Incubation was performed with both LRRK2 wild-type and G2019S form to evaluate whether phosphorylation was enhanced in "pathological" conditions. Moreover, to verify that the phosphorylation signal detected was specifically due to LRRK2 activity and not to the presence of other kinases co-purified with Rabs, we added a LRRK2 spefic inhibitor, GSK2578215A (2 µM), as control. As shown in Fig.8.1.2, we found that only Rab7L1 is a clear substrate of LRRK2 kinase activity *in vitro*.

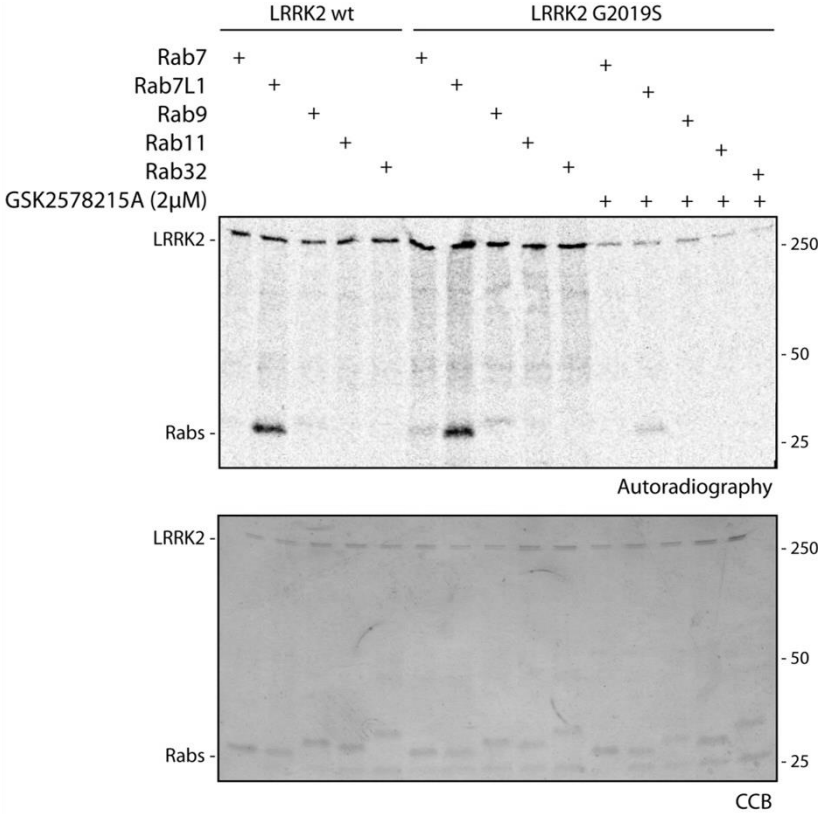

Fig.8.1.2 | LRRK2 phosphorylates Rab7L1. *In vitro* kinase assays between Flagged-Rab proteins and LRRK2 highlighted that only Rab7L1, among the tested Rabs, is efficiently phosphorylated by both LRRK2 wild-type and G2019S forms. The lower panel shows the same samples loaded on SDS-PAGE.

Thus, among the Rab proteins tested here, Rab7L1 is the only GTPase that appears to be phosphorylated by LRRK2. Given the previously reported genetic and functional interaction of LRRK2 and Rab7L1, this result appeared particularly interesting. Thus, an outstanding question is whether the Rab7L1 function(s) relevant for disease is regulated through phosphorylation by LRRK2. In this regard, the G2019S pathological mutation could abnormally phosphorylate Rab7L1 altering its GTPase activity, similar to what we observed for NSF, and, in turn, cause neurodegeneration.

To identify the residue within Rab7L1where this phosphorylation occurs, we performed MS analysis on purified Flag-tagged Rab7L1 protein after incubation with LRRK2 G2019S in the presence or absence of GSK2578215A as a control (in collaboration with Dr Giorgio Arrigoni, University of Padova).

8.2 Mass Spectrometry Analysis Identified A Phospho-Site In The P-Loop Region

As we previously did for NSF, we performed phosphopeptide enrichment coupled with liquid chromatography/tandem mass spectrometry (LCMS/MS) analysis on purified Rab7L1 upon LRRK2 G2019S phosphorylation. The incubation of Rab7L1 and LRRK2 was conducted with the same ratio and conditions of the kinase assay showed in Fig.8.1.2. Also in this case, GSK2578215A was added as a negative control. Interestingly, MS analysis identified the ^{10}VLVVGDAAVGKTSLVQR^{26} peptide as phosphorylated by LRRK2. Specifically, threonine-21 appeared the most likely to be phosphorylated (99-100% Post-Translational Modifications (PTM) Site probability) while phosphorylation on the adjacent residue, serine-22, resulted lower (45-75% PTM Site probability; Fig.8.2.1). Importantly, these sites were not found in the controls (reaction at t=0 and reaction conducted in the presence of inhibitor).

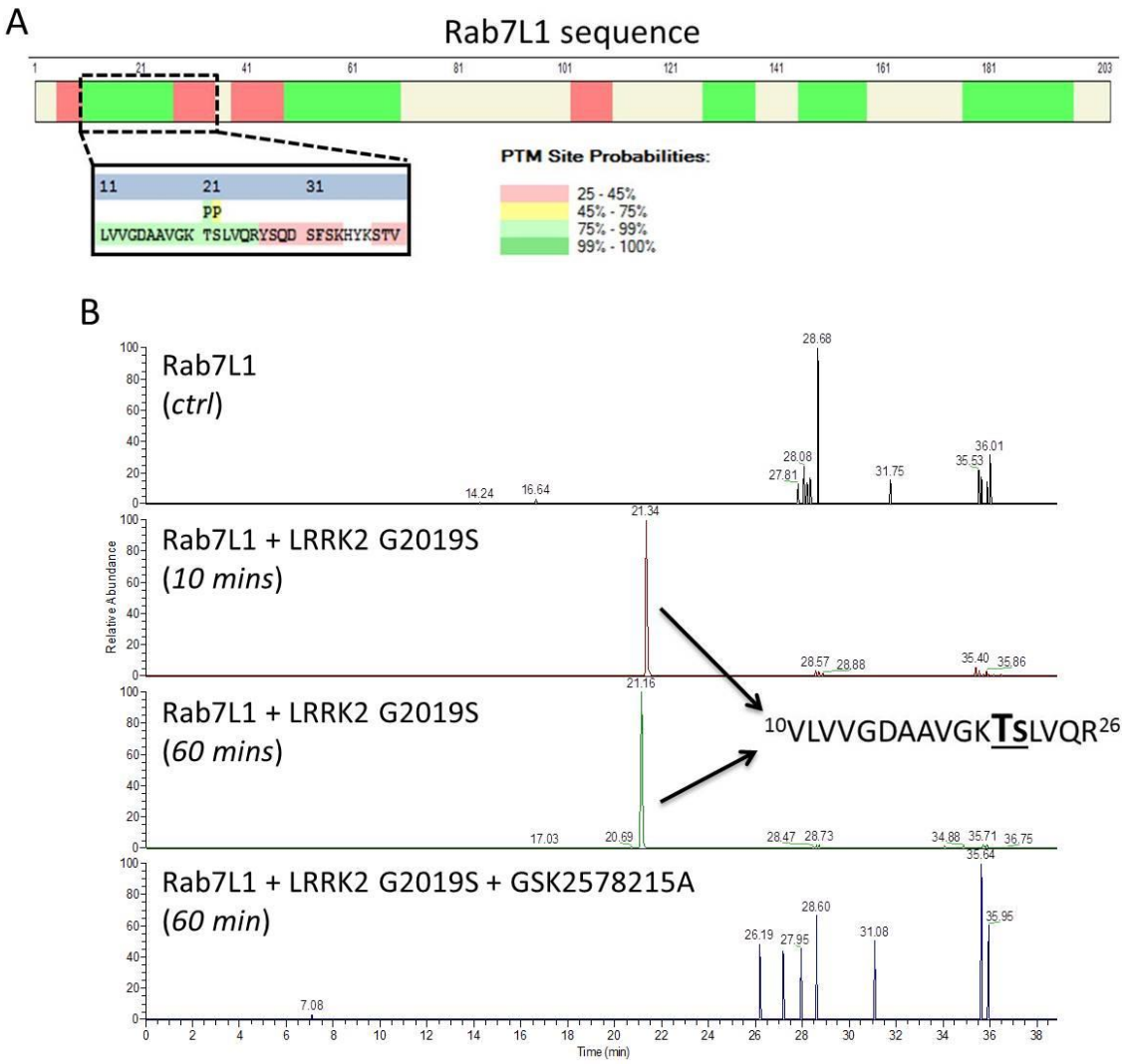

Fig.8.2.1 | LC-MS/MS analysis of Rab7L1 phosphorylated by LRRK2 G2019S: (A) Sequence coverage of Rab7L1 phosphorylated by LRRK2 G2019S (56.16%). In the large onset, the sequence with the peptide that was found phosphorylated. The signal highlight that LRRK2 G2019S phosphorylates Rab7L1 at T21 (75%-99% PTM Site Probabilities) and S22 (45%-75% PTM Site Probabilities). (B) Manually annotated MS/MS spectrum relative to the monophosphorylated peptide ^{10}VLVVGDAAVGKTSLVQR^{26} from Rab7L1. Charge: +2, Monoisotopic m/z: 896.4913 Da. Four different samples have been prepared to discriminate possible unspecific phospho-site. We stopped the reaction at different time points (after 10 minutes and 60 minutes), but there were no differences in the spectrum signal. In addition, the peptide ^{10}VLVVGDAAVGKTSLVQR^{26} was not detected as phosphorylated in the control and in presence of GSK2578215A inhibitor. This means that LRRK2 G2019S preferentially phosphorylates Rab7L1 at T21.

Noteworthy, Thr-21 is located in the P-loop region, near the K residue that mediates GTP binding. The nucleotide binding motif contains the consensus sequence ^{20}GXXXXGKTS^{27}, which is conserved among Rab proteins (Fig.8.2.2). This finding supports the hypothesis of a regulatory mechanism exerted by LRRK2, that, by modulating Rab7L1 GTP binding, might be able to influence its GTPase activity. Moreover, an altered phosphorylation

pattern of Rab7L1 in the neuron due to the presence of LRRK2 G2019S pathologic mutant could cause impairment in the trans-Golgi network activity.

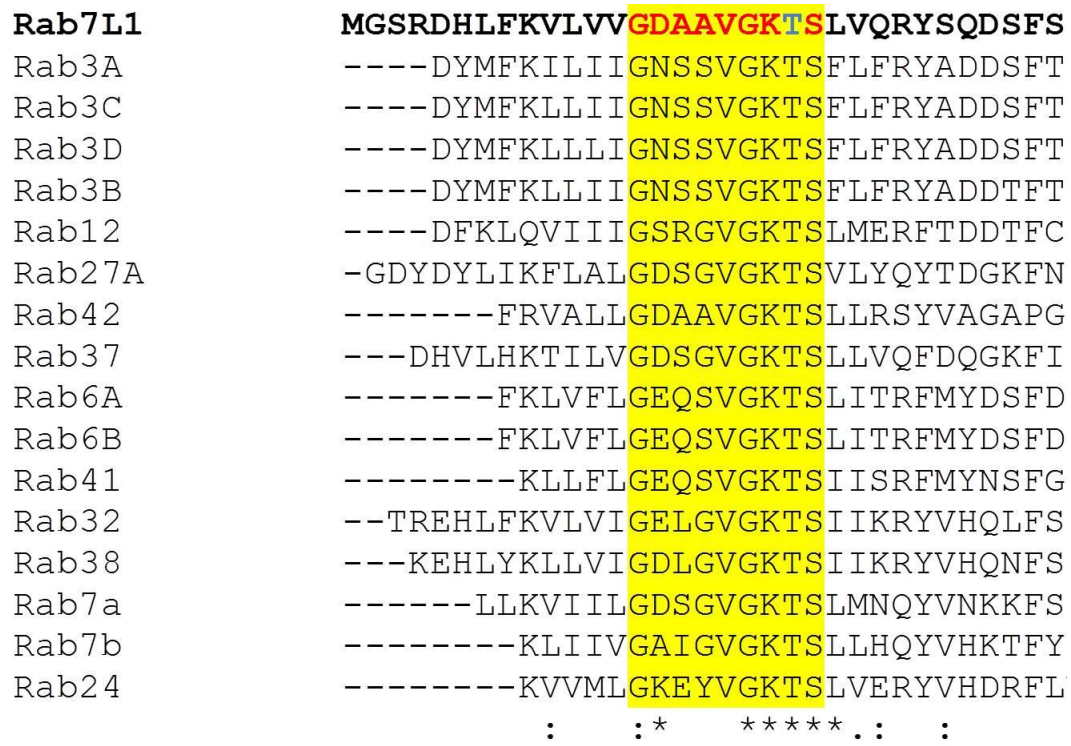

Fig.8.2.2 | Multiple sequence alignment. The P-loop region (yellow) involved in nucleotide binding, is a highly conserved motif among Rab proteins. In particular, the alignment highlights that Rab proteins carry a conserved ^{25}VGKTS^{28} sequence (red) and interestingly, the Thr-21 of Rab7L1 (blue), identified through phosphopeptide enrichment, is located inside this motif.

Next, to validate MS data, we generated by site-directed point mutation an unphosphorylable Rab7L1 mutant substituting Thr-21 with an alanine (Rab7L1-T21A) and phospho-mimetic mutants (Rab7L1-T21D and T21E). We also generated a second mutant by replacing Ser-22 with an alanine (Rab7L1-S22A) and the corresponding and phospho-mimetic mutants (Rab7L1-S22D and S22E).

8.3 Rab7L1 Possesses Possible Alternative Phosphosites

To validate the phospho-MS data, we purified Rab7L1 and its mutants (T21A, D and E and S22A, D and E) from mammalian HEK293T cells with the same protocol previously described. Fig.8.3.1 shows the result of protein purification. Of note, T21D, T21E and S22D mutants displayed the presence of bands at higher molecular weights, which possibly suggests the formation of aggregate(s). This hypothesis is also supported by the fact that the amount of all purified Rab7L1 mutants was lower than the wild-type form.

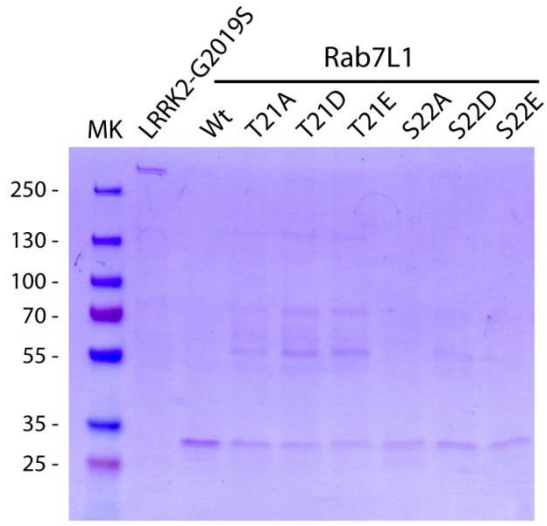

Fig.8.3.1 | Purification of Rab7L1 and all its mutants. Purified human LRRK2 G2019S mutant with Rab7L1 wild-type and all its mutants separated on SDS-PAGE. In presence of site directed mutations in Thr-21 and in S22D, there are bands corresponding to possible aggregates at 130, 70 and 55 kDa respectively. Of interest, this feature is highly present upon aminoacid substitution with aspartate (D).

Kinase assays were then performed with the different Rab7L1 mutants incubated for 1 hour at 30°C with ^{33}P-ATP at a 1:50 ratio of LRRK2:Rab(s) to maximize the signal of the substrate. Moreover, the large amount of substrate should result in a higher specificity for LRRK2 G2019S mediated phosphorylation.

As shown in Fig.8.3.2, the phosphorylation signals of Rab7L1 mutants were not abrogated in T21A or S22A mutants. This was completely unexpected since the MS analysis identified one single phospho-peptide which was enriched only upon incubation with LRRK2 G2019S (both after 10 and 60 minutes incubation with the kinase) but not

when the inhibitor was added to the reaction or when the reaction was analyzed at t=0. Phosphoscreen signals were quantified by densitometry and highlighted a non significant tendency towards a decrease in phosphorylation between wild-type and S22A, S22D and S22E. This may suggest that S22 has some degree of phosphorylated but that another site(s), within a different peptide not phosho-enriched, contributes for the majority of the signal observed. Of interest, the T21A, T21D, T21E and S22D mutants display additional bands at higher molecular weight that are also substrates of LRRK2 G2019S. These bands correspond to those previously detected in SDS-PAGE (Fig.8.3.1), suggesting they might be Rab7L1 aggregates. Of note, upon substitution of the two residues with aspartate (D) or glutamate (E), we observed a difference in the phosphorylation pattern of these bands by LRRK2 G2019S. As shown in Fig.8.3.2, the signal of incorporated ^{33}P in these bands is higher in Rab7L1-T21D, -T21E and -S22D than in the other forms.

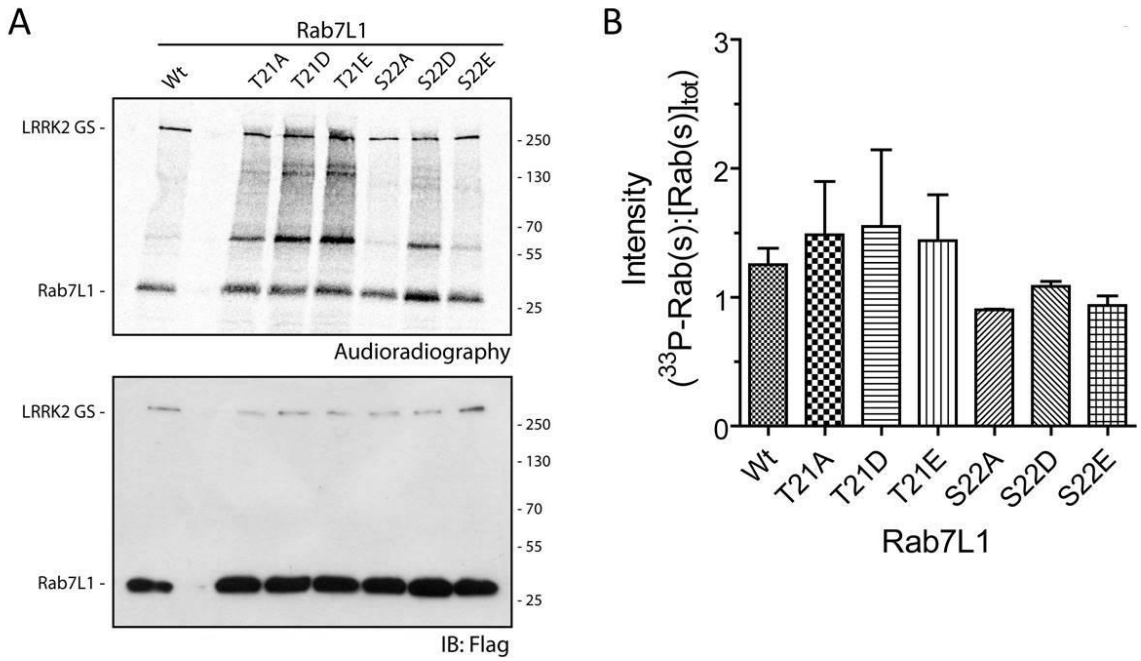

Fig.8.3.2 | Kinase assay on Rab7L1 mutants. (A) *In vitro* kinase assays with Flagged-Rab7L1 wt and all its mutants incubated with LRRK2-G2019S at 1:50 ratio LRRK2-G2019S:Rab(s). (B) Quantification of ^{33}P incorporated by Rab proteins (autoradiography) normalized by total amount of proteins ($[Rab(s)]_{tot}$, IB against Flag-tag) from n=2 independent experiments.

Taken together, while these results confirm that Rab7L1 is a substrate of LRRK2 kinase activity, we were not able to validate the MS results. One likely explanation could be that the phospho-peptide contributing to the majority of the observed phosphorylation was not processed (i.e. tryspin did not cut at the appropriate length for MS analysis). Thus, it is likely that additional LRRK2 phosphorylation site(s) are present within Rab7L1 sequence, that were not detected.

To try and overcome this pitfall, we next purified Rab7L1 with the freeze/thaw method. This should allow achieving a milder lysis, thus preserving Rab7L1 conformation to avoid possible unspecific phosphorylation due to partial misfolding. Since we previously demonstrated that the presence of Tween-20 impairs NSF ATPase activity, we decided to use the same protocol for Rab7L1, to see if there were differences on its phosphorylation signal. As shown in Fig.8.3.3, the amount of Rab7L1 purified without Tween-20 is slightly higher than in presence of the detergent, probably because this method is important to preserve a correct protein folding.

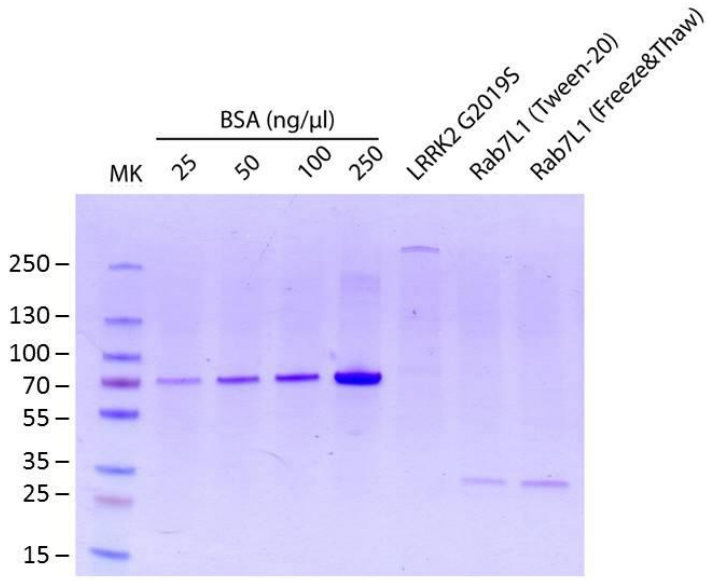

Fig.8.3.3 | Comparison between the different purification protocols. The amount of purified Rab7L1 is higher without adding Tween-20 in the Lysis buffer (Rab7L1 (Tween-20) = 1.7 µg; Rab7L1 (Freeze&Thaw) = 3.3 µg; starting from $20x10^6$ cells). Proteins were separated on SDS-PAGE and quantified by comparison with different concentrations of BSA (Bovine Serum Albumine).

Next, we incubated LRRK2 G2019S together with Rab7L1 obtained with the two methods of purification for 1 hour following the same conditions described for the previous experiments. Of interest, in absence of Tween-20, ^{33}P incorporation appeared lower (Fig.8.3.4). This might be the result of a more specific phosphorylation.

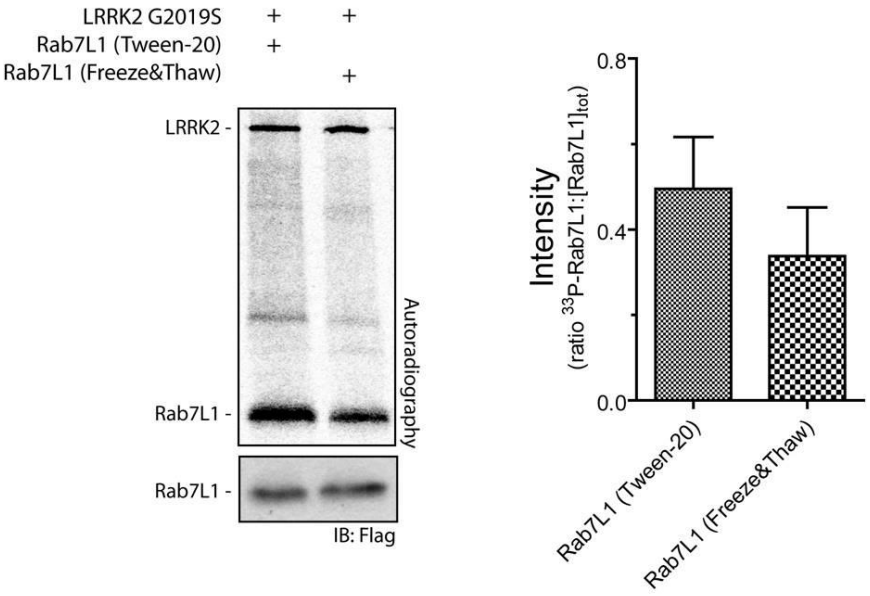

Fig.8.3.4 | Kinase assay on Rab7L1. *In vitro* kinase assay between LRRK2 G2019S and Rab7L1, purified with and without Tween-20, reveals that the absence of detergent decreases the amount of ^{33}P incorporation signal, suggesting a more specific phosphorylation (n=3).

This result is in accordance with data obtained from NSF experiments. Also in this case the phosphorylation could be more specific due to a proper folding of the protein.

Another set of samples was prepared for MS analysis in presence of GSK2578215A or not. The different purification protocol used (freeze/thaw), and, hopefully, a higher percentage of sequence coverage, will allow to clearly identify the major phospho-site(s) of Rab7L1 upon incubation with LRRK2 G2019S.

Once identified the site(s), the following aims will be to understand the impact of this phosphorylation on Rab7L1 GTPase activity and cellular function. If we can demonstrate that LRRK2-mediated phosphorylation of Rab7L1 is physiologically relevant, we will have in hand another cellular pathway that could be compromised in pathological condition and, in turn, lead to neurodegeneration.

Chapter IV
Discussions and Conclusions

9. Discussions and Conclusions

Neurodegenerative disorders result from the impairment of complex cellular processes that leads to loss of neuronal functionality and eventually to cell death. Among these, Parkinson's disease (PD) results from a specific neurodegeneration that mainly affects neurons in the midbrain region. In fact, the PD pathological hallmarks are the loss of dopaminergic neurons in the *substantia nigra pars compacta* (SNpc) and the presence of intracellular proteinaceous inclusions called "Lewy bodies" (LB) in surviving neurons (Damier et al., 1999; Frank et al., 2007). The etiology of PD remains unclear but it seems to be linked to a combination of factors, i.e. environment, genetics and aging (Dauer and Przedborski, 2013). Although PD is typically sporadic, several PD-related genes have been identified (Van Den Eeden et al., 2003). However, the molecular mechanisms underlying neurodegeneration in PD is still an open question. Accumulating evidence indicates that neuronal dysfunction through impairment of synaptic vesicle trafficking might represent an early event that triggers neurodegeneration. The molecular mechanisms that cause defects in synaptic vesicle dynamics remain however to be determined, being exo- and endocytosis highly regulated processes that require precise interactions among many proteins (Südhof, 2004).

In 2004, two studies identified mutations in the *Lrrk2* (PARK8) gene associated with familial forms of PD (Paisan-Ruiz et al., 2004; Zimprich et al., 2004) and, at present, autosomal dominant mutations in *Lrrk2* are the most common genetic cause of late-onset PD (Singleton et al., 2013). To date, both the physiological role and the neurotoxic properties of LRRK2 are poorly understood. A large variety of possible functions have been linked to LRRK2 and its pathological role during neurodegeneration (Zhu et al., 2006; Giasson et al., 2006; MacLeod et al., 2006; Plowey et al., 2008; Belluzzi et al., 2012; Greggio, 2012; Rivero-Ríos et al., 2015). The factors that have challenged the investigation of LRRK2 are i) its complex multi-domain structure, ii) the possible pleiotropic activity of LRRK2 and iii) the variety of models used that resulted in a large body of *in vitro* and *in vivo* studies present in the literature. Further complexity emerges in the evaluation of the function of LRRK2 in the context of the several pathological mutations identified. In this frame, the G2019S mutation induces a higher kinase activity

of LRRK2, which is likely to affect putative effector proteins (Gilks et al. 2005; Greggio and Cookson, 2009). Thus, the identification of a more specific role of LRRK2 at the presynaptic site is crucial to understand the early events in neurodegeneration, being that deregulation of synaptic vesicle trafficking seems to occur prior to the onset of motor symptoms (Fernandez-Chacon et al., 2004; Burre et al., 2010). Identification of substrates of LRRK2 kinase activity at the presynaptic site is the first step to unravel the molecular pathways in which LRRK2 is involved. This, in turn, will allow understanding which cellular pathways are deregulated by PD-related mutations of LRRK2. A large body of evidence supports a role of LRRK2 at the presynaptic compartment. Among these, LRRK2 has been found to interact with several proteins involved in vesicle recycling (Piccoli et al., 2011). Moreover, LRRK2 kinase activity has been described as regulating both synaptic vesicle exo- and endocytosis (Cirnaru et al., 2014) possibly *via* phosphorylation of presynaptic proteins, such as Snapin and EndophilinA (Yun et al., 2013; Matta et al., 2012). Furthermore, BAC hG2019S transgenic mice display a faster synaptic vesicle trafficking (Belluzzi, Gonnelli et al., 2016; *Appendix*). In my research project, I focused on the identification of two possible LRRK2 substrates at the presynaptic site. The first one is the N-ethylmaleimide Sensitive Fusion (NSF) protein, an ATPase responsible of the SNARE complex disassembling. The second substrate tested here is the small GTPase Rab7L1, which is encoded by *Rab7L1* gene within *PARK16*, a non-familial PD risk-associated locus. Rab7L1 was demonstrated to interact with LRRK2 to promote the clearance of Trans-Golgi derived vesicles (Beilina et al. 2014) and its overexpression suppresses the LRRK2-related phenotype (MacLeod et al., 2013).

As presented in the Results section, NSF and LRRK2 efficiently co-localize along neurites and we showed by pull-down assays that NSF is able to interact with endogenous LRRK2. Furthermore, we provided evidence that NSF is not only an interactor, but also a substrate of LRRK2 kinase activity *in vitro*. Previous studies showed that NSF is a target of other kinases and phosphorylation affects its activity. More in detail, Pctaire1 and PKC are both able to phosphorylate NSF modifying its oligomerization process and interaction with alpha-SNAP:SNAREs complex, respectively (Liu et al., 2006; Matveeva et al., 2001). In our study, we demonstrated that LRRK2 G2019S phosphorylation occurs at NSF-T645. Further analysis indicated that NSF has an increased ATPase activity upon

LRRK2 G2019S phosphorylation. This result is in agreement with previous studies, since phosphorylation appeared to be a critical modification for NSF activity. LRRK2-mediated phosphorylation on NSF could be an important process to tune its ATPase activity. Accordingly, we found that T645A is characterized by a reduced endogenous ATPase activity. The D2 domain of NSF is responsible for its structural changes (Matveeva et al., 1997). ATP binding occurs at the D2 domain within the *Walker A* motif, in which nucleotide binding is responsible for the NSF structural transition into hexamer. In this state, NSF is an active ATPase. Structural studies demonstrate that T645 is located in the beta-strand S4 (aa 639-646), which contributes to hexamer stability through interaction with alpha-helix H5 (Yu et al., 1998). For this reason, T645 might play a key role in mediating NSF oligomerization and consequently ATP hydrolysis, so the predicted key role of this residue for NSF activity supports the outcome of our results. We predict that the PD-related hyperactive form of LRRK2, G2019S mutant, might abnormally phosphorylate this residue resulting in an altered NSF ATPase activity, thus SNARE complex disassembly. Further investigation is necessary to better clarify how the impact of LRRK2 phosphorylation at T645 directly alters NSF hexamerization. To this end, we could monitor NSF hexameric conformation with Transmission Electron Microscopy (TEM) and evaluate whether oligomerization is altered in presence of a mutation that mimic phosphorylation (T645D/E). To cast these molecular data on isolated proteins in the contest of the living neuron,, we reasoned that the process regulated by LRRK2 may be the SNARE complex disassembly. An increased NSF phosphorylation would result in a higher ATPase activity and a faster SNARE complex disassembly rate, which may lead to impairment in the normal synaptic vesicle trafficking. Accordingly, our data support a faster SNARE complex dissociation when NSF is phosphorylated by LRRK2. Future studies should also be directed at understanding whether this enhanced disassembling kinetic occurs also in the cellular context in the presence of PD-related LRRK2 mutations.

An altered SV sorting at the presynaptic site could derive from impairment in vesicle recycling. Coherently, many intracellular trafficking events are mediated by Rab proteins, a large family of monomeric small GTPases, which regulate the endosome maturation (Novick et al., 1997; Ng and Tang, 2008). To date, there is growing evidence that LRRK2 interacts with Rab proteins (Wallings et al., 2015). In the second part of this

work, we investigated which among the several Rab proteins maybe substrates of LRRK2 kinase activity. Specifically, we selected Rabs from different cellular compartments, which are known to interact with LRRK2 and are related to neurodegeneration, i.e. Rab7 (Gomez-Suaga et al., 2014), Rab7L1 (MacLeod et al., 2013), Rab9 (Dodson et al., 2014), Rab11 (Bhuin and Roy, 2015) and Rab32 (Waschbusch et al., 2014). In our studies, kinase assays revealed that only Rab7L1 is a substrate of LRRK2 kinase activity. This feature is in agreement with recently published studies, which revealed a physical and functional interaction between Rab7L1 and LRRK2 (Beilina et al., 2014; MacLeod et al., 2013). *Rab7L1* gene lies within the *PARK16* locus, a non-familial PD risk-associated locus. In particular, an accumulation of the mannose phosphate receptor, a retromer component, is a typical consequence of LRRK2 G2019S mutations, which is efficiently recovered by Rab7L1 (MacLeod et al., 2013). Being LRRK2 a kinase, the first aspect in the regulatory mechanism that we investigated was phosphorylation. Therefore, we decided to run phospho-peptide enrichment and mass spectrometry analysis on Rab7L1 after incubation with LRRK2 G2019S. The MS results revealed that LRRK2 G2019S-mediated phosphorylation occurs preferentially on the residue T21 of Rab7L1. The region in which T21 lies is the highly conserved nucleotide binding region among GTPases (P-loop, ^{20}GXXXXGKTS^{27}). Thus, phosphorylation of T21 is predicted to alter GTP binding, with possible consequence on the activation of Rab7L1 downstream effectors. To validate the MS data, phosphorylation deficient mutants were generated at residues T21 and S22, which was also indicated as possible phosphorylation site, but with lower probability. Unexpectedly, we did not see significant differences in radioactivity incorporation between Rab7L1 witld-type and non-phosphorylatable mutants. This result could be explained by 1) the presence of additional phospho-site(s) not phospho-enriched with more favorable stoichiometry compared to P-T21; 2) the ability of Rab7L1 mutants to co-purify with kinases that can phosphorylate them (i.e. PKA or PKC, very active and poorly selective out of the tightly regulated cellular context); 3) the interchangeable phosphorylation between T21 and S22, in which case a double T21/S22 alanine mutant should rule out this possibility. We also aim to repeat MS analysis on proteins purified without detergent, since they display a lower, but possibly more specific phosphorylation.

Accumulating evidence supports a model where LRRK2 and Rab7L1 impairment leads to altered intracellular vesicle sorting at the level of the trans-Golgi network and retromer complex. Of interest, only Rab7L1 overexpression, among the gene within the *PARK16* locus, is able to rescue LRRK2 cellular defects, suggesting functional interaction between the two proteins (MacLeod et al., 2013). Rescue of mutant LRRK2 phenotypes can be achieved also with overexpression of VPS35, a retromer component. Mutations in VPS35 have been linked to familial inherited and idiopathic forms of PD (Follett et al., 2014). Dysfunction of VPS35 affects normal vesicle sorting between retrograde transport and Golgi that may end in the onset of PD. It is possible that PD-related defects in LRRK2 and RAB7L1 impact other aspects of vesicular trafficking besides retromer function.

Future studies are necessary to confirm these results in a cellular contest. Understanding whether NSF and Rab7L1 phosphorylation are relevant in the pathogenesis of PD might provide new targets against vesicle sorting impairment, biomarkers for early PD diagnosis and, in turn, more opportunities to find effective therapies to halt or slow PD progression.

References

References

Abeliovich A, Schmitz Y, Fariñas I, Choi-Lundberg D, Ho WH, Castillo PE, Shinsky N, Verdugo JM, Armanini M, Ryan A, Hynes M, Phillips H, Sulzer D, Rosenthal A, *Mice lacking alpha-synuclein display functional deficits in the nigrostriatal dopamine system*. Neuron. 2000 Jan;25(1):239-52.

Alegre-Abarrategui J, Christian H, Lufino MM, Mutihac R, Venda LL, Ansorge O, Wade-Martins R, *LRRK2 regulates autophagic activity and localizes to specific membrane microdomains in a novel human genomic reporter cellular model*. Hum Mol Genet. 2009 Nov 1;18(21):4022-34.

Andres-Mateos E, Perier C, Zhang L, Blanchard-Fillion B, Greco TM, Thomas B, Ko HS, Sasaki M, Ischiropoulos H, Przedborski S, Dawson TM, Dawson VL, *DJ-1 gene deletion reveals that DJ-1 is an atypical peroxiredoxin-like peroxidase*. Proc Natl Acad Sci U S A. 2007 Sep 11;104(37):14807-12.

Anglade P, Vyas S, Javoy-Agid F, Herrero MT, Michel PP, Marquez J, Mouatt-Prigent A, Ruberg M, Hirsch EC, Agid Y, *Apoptosis and autophagy in nigral neurons of patients with Parkinson's disease*. Histol Histopathol. 1997 Jan;12(1):25-31.

Avila J, *Tau protein, the main component of paired helical filaments*. J Alzheimers Dis. 2006;9(3 Suppl):171-5.

Babbey CM, Ahktar N, Wang E, Chen CC, Grant BD, Dunn KW, *Rab10 regulates membrane transport through early endosomes of polarized Madin-Darby canine kidney cells*. Mol Biol Cell. 2006 Jul;17(7):3156-75.

Badger JL, Cordero-Llana O, Hartfield EM, Wade-Martins R, *Parkinson's disease in a dish - Using stem cells as a molecular tool*. Neuropharmacology. 2014 Jan;76 Pt A:88-96.

Bailly E, McCaffrey M, Touchot N, Zahraoui A, Goud B, Bornens M, *Phosphorylation of two small GTP-binding proteins of the Rab family by p34cdc2*. Nature. 1991 Apr 25;350(6320):715-8.

Baptista MA, Dave KD, Frasier MA, Sherer TB, Greeley M, Beck MJ, Varsho JS, Parker GA, Moore C, Churchill MJ, Meshul CK, Fiske BK, *Loss of leucine-rich repeat kinase 2 (LRRK2) in rats leads to progressive abnormal phenotypes in peripheral organs*. PLoS One. 2013 Nov 14;8(11):e80705.

Bartus RT, Weinberg MS, Samulski RJ, *Parkinson's disease gene therapy: success by design meets failure by efficacy*. Mol Ther. 2014 Mar;22(3):487-97.

Beccano-Kelly DA, Kuhlmann N, Tatarnikov I, Volta M, Munsie LN, Chou P, Cao LP, Han H, Tapia L, Farrer MJ, Milnerwood AJ, *Synaptic function is modulated by LRRK2 and glutamate release is increased in cortical neurons of G2019S LRRK2 knock-in mice*. Front Cell Neurosci. 2014 Sep 26;8:301.

Behl C, Skutella T, Lezoualc'h F, Post A, Widmann M, Newton CJ, Holsboer F, *Neuroprotection against oxidative stress by estrogens: structure-activity relationship*. Mol Pharmacol. 1997 Apr;51(4):535-41.

Behnia R, Munro S, *Organelle identity and the signposts for membrane traffic*. Nature. 2005 Dec 1;438(7068):597-604.

Beilina A, Cookson MR, *Genes associated with Parkinson's disease: regulation of autophagy and beyond*. J Neurochem. 2015 Jul 30.

Beilina A, Rudenko IN, Kaganovich A, Civiero L, Chau H, Kalia SK, Kalia LV, Lobbestael E, Chia R, Ndukwe K, Ding J, Nalls MA; International Parkinson's Disease Genomics Consortium; North American Brain Expression Consortium, Olszewski M, Hauser DN, Kumaran R, Lozano AM, Baekelandt V, Greene LE, Taymans JM, Greggio E, Cookson MR, *Unbiased screen for interactors of leucine-rich repeat kinase 2 supports a common pathway for sporadic and familial Parkinson disease*. Proc Natl Acad Sci U S A. 2014 Feb 18;111(7):2626-31.

Beilina A, Van Der Brug M, Ahmad R, Kesavapany S, Miller DW, Petsko GA, Cookson MR, *Mutations in PTEN-induced putative kinase 1 associated with recessive parkinsonism have differential effects on protein stability*. Proc Natl Acad Sci U S A. 2005 Apr 19;102(16):5703-8.

Belluzzi E, Greggio E, Piccoli G, Presynaptic dysfunction in Parkinson's disease: a focus on LRRK2. Biochem Soc Trans. 2012 Oct;40(5):1111-6.

Benfenati F, Greengard P, Brunner J, Bähler M, *Electrostatic and hydrophobic interactions of synapsin I and synapsin I fragments with phospholipid bilayers*. J Cell Biol. 1989 May;108(5):1851-62.

Bennett MK, Calakos N, Scheller RH, *Syntaxin: a synaptic protein implicated in docking of synaptic vesicles at presynaptic active zones*. Science. 1992 Jul 10;257(5067):255-9.

Béraud D, Twomey M, Bloom B, Mittereder A, Ton V, Neitzke K, Chasovskikh S, Mhyre TR, Maguire-Zeiss KA, *α-Synuclein Alters Toll-Like Receptor Expression*. Front Neurosci. 2011 Jun 29;5:80.

Berg D, Holzmann C, Riess O, *14-3-3 proteins in the nervous system*. Nat Rev Neurosci. 2003 Sep;4(9):752-62.

Berger Z, Smith KA, Lavoie MJ. *Membrane localization of LRRK2 is associated with increased formation of the highly active LRRK2 dimer and changes in its phosphorylation*. Biochemistry. 2010 Jul 6;49(26):5511-23.

Berman SB, Hastings TG, *Dopamine oxidation alters mitochondrial respiration and induces permeability transition in brain mitochondria: implications for Parkinson's disease*. J Neurochem. 1999 Sep;73(3):1127-37.

Betarbet R, Sherer TB, MacKenzie G, Garcia-Osuna M, Panov AV, Greenamyre JT, *Chronic systemic pesticide exposure reproduces features of Parkinson's disease*. Nat Neurosci. 2000 Dec;3(12):1301-6.

Bisaglia M, Greggio E, Beltramini M, Bubacco L, *Dysfunction of dopamine homeostasis: clues in the hunt for novel Parkinson's disease therapies*. FASEB J. 2013 Jun;27(6):2101-10.

Bisaglia M, Tosatto L, Munari F, Tessari I, de Laureto PP, Mammi S, Bubacco L, *Dopamine quinones interact with alpha-synuclein to form unstructured adducts*. Biochem Biophys Res Commun. 2010 Apr 2;394(2):424-8.

Biskup S, Moore DJ, Celsi F, Higashi S, West AB, Andrabi SA, Kurkinen K, Yu SW, Savitt JM, Waldvogel HJ, Faull RL, Emson PC, Torp R, Ottersen OP, Dawson TM, Dawson VL, *Localization of LRRK2 to membranous and vesicular structures in mammalian brain*. Ann Neurol. 2006 Nov;60(5):557-69.

Block MR, Glick BS, Wilcox CA, Wieland FT, Rothman JE, *Purification of an N-ethylmaleimide-sensitive protein catalyzing vesicular transport*. Proc Natl Acad Sci U S A. 1988 Nov;85(21):7852-6.

Bombardier JP, Munson M, *Three steps forward, two steps back: mechanistic insights into the assembly and disassembly of the SNARE complex*. Curr Opin Chem Biol. 2015 Dec;29:66-71.

Bonifacino JS, Hurley JH, *Retromer*. Curr Opin Cell Biol. 2008 Aug;20(4):427-36.

Bonifacino JS, Rojas R, *Retrograde transport from endosomes to the trans-Golgi network*. Nat Rev Mol Cell Biol. 2006 Aug;7(8):568-79.

Bonifati V, Rizzu P, van Baren MJ, Schaap O, Breedveld GJ, Krieger E, Dekker MC, Squitieri F, Ibanez P, Joosse M, van Dongen JW, Vanacore N, van Swieten JC, Brice A, Meco G, van Duijn CM, Oostra BA, Heutink P, *Mutations in the DJ-1 gene associated with autosomal recessive early-onset parkinsonism*. Science. 2003 Jan 10;299(5604):256-9.

Breydo L, Wu JW, Uversky VN, *A-synuclein misfolding and Parkinson's disease*. Biochim Biophys Acta. 2012 Feb;1822(2):261-85.

Brunger AT, DeLaBarre B, *NSF and p97/VCP: similar at first, different at last*. FEBS Lett. 2003 Nov 27;555(1):126-33.

Burré J, Sharma M, Tsetsenis T, Buchman V, Etherton MR, Südhof TC, *Alpha-synuclein promotes SNARE-complex assembly in vivo and in vitro*. Science. 2010 Sep 24;329(5999):1663-7.

Burré J, Vivona S, Diao J, Sharma M, Brunger AT, Südhof TC, *Properties of native brain α-synuclein*. Nature. 2013 Jun 13;498(7453):E4-6; discussion E6-7.

Caesar M, Felk S, Aasly JO, Gillardon F, *Changes in actin dynamics and F-actin structure both in synaptoneurosomes of LRRK2(R1441G) mutant mice and in primary human fibroblasts of LRRK2(G2019S) mutation carriers*. Neuroscience. 2015 Jan 22;284:311-24.

Carroll KS, Hanna J, Simon I, Krise J, Barbero P, Pfeffer SR, *Role of Rab9 GTPase in facilitating receptor recruitment by TIP47*. Science. 2001 May 18;292(5520):1373-6.

Ceccarelli B, Hurlbut WP, Mauro A, *Turnover of transmitter and synaptic vesicles at the frog neuromuscular junction*. J Cell Biol. 1973 May;57(2):499-524.

Chang LF, Chen S, Liu CC, Pan X, Jiang J, Bai XC, Xie X, Wang HW, Sui SF, *Structural characterization of full-length NSF and 20S particles*. Nat Struct Mol Biol. 2012 Feb 5;19(3):268-75.

Chapman ER, *How does synaptotagmin trigger neurotransmitter release?* Annu Rev Biochem. 2008;77:615-41.

Chavez JA, Roach WG, Keller SR, Lane WS, Lienhard GE, *Inhibition of GLUT4 translocation by Tbc1d1, a Rab GTPase-activating protein abundant in skeletal muscle, is partially relieved by AMP-activated protein kinase activation*. J Biol Chem. 2008 Apr 4;283(14):9187-95. doi: 10.1074/jbc.M708934200. Epub 2008 Feb 7.

Chen HK, Fernandez-Funez P, Acevedo SF, Lam YC, Kaytor MD, Fernandez MH, Aitken A, Skoulakis EM, Orr HT, Botas J, Zoghbi HY, *Interaction of Akt-phosphorylated ataxin-1 with 14-3-3 mediates neurodegeneration in spinocerebellar ataxia type 1*. Cell. 2003 May 16;113(4):457-68.

Chen XQ, Liu S, Qin LY, Wang CR, Fung YW, Yu AC, *Selective regulation of 14-3-3eta in primary culture of cerebral cortical neurons and astrocytes during development*. J Neurosci Res. 2005 Jan 1-15;79(1-2):114-8.

Chen YA, Scales SJ, Scheller RH. *Sequential SNARE assembly underlies priming and triggering of exocytosis*. Neuron. 2001 Apr;30(1):161-70.

Chen YA, Scheller RH, *SNARE-mediated membrane fusion*. Nat Rev Mol Cell Biol. 2001 Feb;2(2):98-106.

Chia R, Haddock S, Beilina A, Rudenko IN, Mamais A, Kaganovich A, Li Y, Kumaran R, Nalls MA, Cookson MR*, Phosphorylation of LRRK2 by casein kinase 1α regulates trans-Golgi clustering via differential interaction with ARHGEF7*. Nat Commun. 2014 Dec 15;5:5827.

Chiariello M, Bruni CB, Bucci C, *The small GTPases Rab5a, Rab5b and Rab5c are differentially phosphorylated in vitro*. FEBS Lett. 1999 Jun 18;453(1-2):20-4.

Chua CE, Tang BL, *Role of Rab GTPases and their interacting proteins in mediating metabolic signalling and regulation*. Cell Mol Life Sci. 2015 Jun;72(12):2289-304.

Cipriano DJ, Jung J, Vivona S, Fenn TD, Brunger AT, Bryant Z, *Processive ATP-driven substrate disassembly by the N-ethylmaleimide-sensitive factor (NSF) molecular machine*. J Biol Chem. 2013 Aug 9; 288(32):23436-45.

Cirnaru MD, Marte A, Belluzzi E, Russo I, Gabrielli M, Longo F, Arcuri L, Murru L, Bubacco L, Matteoli M, Fedele E, Sala C, Passafaro M, Morari M, Greggio E, Onofri F, Piccoli G, *LRRK2 kinase activity regulates synaptic vesicle trafficking and neurotransmitter release through modulation of LRRK2 macro-molecular complex*. Front Mol Neurosci. 2014 May 27;7:49.

Civiero L, Bubacco L, *Human leucine-rich repeat kinase 1 and 2: intersecting or unrelated functions?* Biochem Soc Trans. 2012 Oct;40(5):1095-101.

Civiero L, Cirnaru MD, Beilina A, Rodella U, Russo I, Belluzzi E, Lobbestael E, Reyniers L, Hondhamuni G, Lewis PA, Van den Haute C, Baekelandt V, Bandopadhyay R, Bubacco L, Piccoli G, Cookson MR, Taymans JM, Greggio E, *Leucine-rich repeat kinase 2 interacts with p21-activated kinase 6 to control neurite complexity in mammalian brain*. J Neurochem. 2015 Dec;135(6):1242-56.

Civiero L, Dihanich S, Lewis PA, Greggio E, *Genetic, structural, and molecular insights into the function of ras of complex proteins domains*. Chem Biol. 2014 Jul 17;21(7):809-18.

Civiero L, Vancraenenbroeck R, Belluzzi E, Beilina A, Lobbestael E, Reyniers L, Gao F, Micetic I, De Maeyer M, Bubacco L, Baekelandt V, Cookson MR, Greggio E, Taymans JM, *Biochemical characterization of highly purified leucine-rich repeat kinases 1 and 2 demonstrates formation of homodimers*. PLoS One. 2012;7(8):e43472.

Clary DO, Griff IC, Rothman JE, *SNAPs, a family of NSF attachment proteins involved in intracellular membrane fusion in animals and yeast*. Cell. 1990 May 18;61(4):709-21.

Cohen G, *Oxy-radical toxicity in catecholamine neurons*. Neurotoxicology. 1984 Spring;5(1):77-82.

Cookson MR, *Parkinsonism due to mutations in PINK1, parkin, and DJ-1 and oxidative stress and mitochondrial pathways*. Cold Spring Harb Perspect Med. 2012 Sep 1;2(9):a009415.

Coune PG, Schneider BL, Aebischer P, *Parkinson's disease: gene therapies*. Cold Spring Harb Perspect Med. 2012 Apr;2(4):a009431.

Covy JP, Giasson BI, *Identification of compounds that inhibit the kinase activity of leucine-rich repeat kinase 2*. Biochem Biophys Res Commun. 2009 Jan 16;378(3):473-7.

Dächsel JC, Farrer MJ, *LRRK2 and Parkinson disease*. Arch Neurol. 2010 May;67(5):542-7.

Daher JP, Abdelmotilib HA, Hu X, Volpicelli-Daley LA, Moehle MS, Fraser KB, Needle E, Chen Y, Steyn SJ, Galatsis P, Hirst WD, West AB, *Leucine-rich Repeat Kinase 2 (LRRK2) Pharmacological Inhibition Abates α-Synuclein Gene-induced Neurodegeneration*. J Biol Chem. 2015 Aug 7;290(32):19433-44.

Damier P, Hirsch EC, Agid Y, Graybiel AM, *The substantia nigra of the human brain. II. Patterns of loss of dopamine-containing neurons in Parkinson's disease*. Brain. 1999 Aug;122 (Pt 8):1437-48.

Daniëls V, Vancraenenbroeck R, Law BM, Greggio E, Lobbestael E, Gao F, De Maeyer M, Cookson MR, Harvey K, Baekelandt V, Taymans JM, *Insight into the mode of action of the LRRK2 Y1699C pathogenic mutant*. J Neurochem. 2011 Jan;116(2):304-15.

Dauer W, Przedborski S, *Parkinson's disease: mechanisms and models*. Neuron. 2003 Sep 11;39(6):889-909.

Davidson WS, Jonas A, Clayton DF, George JM, *Stabilization of alpha-synuclein secondary structure upon binding to synthetic membranes*. J Biol Chem. 1998 Apr 17;273(16):9443-9.

Davie CA, *A review of Parkinson's disease*. Br Med Bull. 2008;86:109-27.

Davies P, Hinkle KM, Sukar NN, Sepulveda B, Mesias R, Serrano G, Alessi DR, Beach TG, Benson DL, White CL, Cowell RM, Das SS, West AB, Melrose HL, *Comprehensive characterization and optimization of anti-LRRK2 (leucine-rich repeat kinase 2) monoclonal antibodies*. Biochem J. 2013 Jul 1;453(1):101-13.

de Lau LM, Breteler MM, *Epidemiology of Parkinson's disease*. Lancet Neurol. 2006 Jun;5(6):525-35.

Dehay B, Martinez-Vicente M, Caldwell GA, Caldwell KA, Yue Z, Cookson MR, Klein C, Vila M, Bezard E, *Lysosomal impairment in Parkinson's disease*. Mov Disord. 2013 Jun;28(6):725-32.

DeLaBarre B, Brunger AT, *Complete structure of p97/valosin-containing protein reveals communication between nucleotide domains*. Nat Struct Biol. 2003 Oct;10(10):856-63.

Deng J, Lewis PA, Greggio E, Sluch E, Beilina A, Cookson MR, *Structure of the ROC domain from the Parkinson's disease-associated leucine-rich repeat kinase 2 reveals a dimeric GTPase*. Proc Natl Acad Sci U S A. 2008 Feb 5;105(5):1499-504.

Deng X, Dzamko N, Prescott A, Davies P, Liu Q, Yang Q, Lee JD, Patricelli MP, Nomanbhoy TK, Alessi DR, Gray NS, *Characterization of a selective inhibitor of the Parkinson's disease kinase LRRK2*. Nat Chem Biol. 2011 Apr;7(4):203-5.

Denker A, Bethani I, Kröhnert K, Körber C, Horstmann H, Wilhelm BG, Barysch SV, Kuner T, Neher E, Rizzoli SO, *A small pool of vesicles maintains synaptic activity in vivo*. Proc Natl Acad Sci U S A. 2011 Oct 11;108(41):17177-82.

Denker A, Kröhnert K, Rizzoli SO, Revisiting synaptic vesicle pool localization in the Drosophila neuromuscular junction. J Physiol. 2009 Jun 15;587(Pt 12):2919-26.

Dexter DT, Jenner P, *Parkinson disease: from pathology to molecular disease mechanisms*. Free Radic Biol Med. 2013 Sep;62:132-44.

Diao J, Burré J, Vivona S, Cipriano DJ, Sharma M, Kyoung M, Südhof TC, Brunger AT, *Native α-synuclein induces clustering of synaptic-vesicle mimics via binding to phospholipids and synaptobrevin-2/VAMP2*. Elife. 2013 Apr 30;2:e00592.

Dittman J, Ryan TA, *Molecular circuitry of endocytosis at nerve terminals*. Annu Rev Cell Dev Biol. 2009;25:133-60.

Dodson MW, Leung LK, Lone M, Lizzio MA, Guo M, *Novel ethyl methanesulfonate (EMS)-induced null alleles of the Drosophila homolog of LRRK2 reveal a crucial role in endolysosomal functions and autophagy in vivo*. Dis Model Mech. 2014 Dec;7(12):1351-63.

Dodson MW, Zhang T, Jiang C, Chen S, Guo M, *Roles of the Drosophila LRRK2 homolog in Rab7-dependent lysosomal positioning*. Hum Mol Genet. 2012 Mar 15;21(6):1350-63.

Doggett EA, Zhao J, Mork CN, Hu D, Nichols RJ, *Phosphorylation of LRRK2 serines 955 and 973 is disrupted by Parkinson's disease mutations and LRRK2 pharmacological inhibition*. J Neurochem. 2012 Jan;120(1):37-45.

Dzamko N, Deak M, Hentati F, Reith AD, Prescott AR, Alessi DR, Nichols RJ, *Inhibition of LRRK2 kinase activity leads to dephosphorylation of Ser(910)/Ser(935), disruption of 14-3-3 binding and altered cytoplasmic localization*. Biochem J. 2010 Sep 15;430(3):405-13.

Dzamko N, Inesta-Vaquera F, Zhang J, Xie C, Cai H, Arthur S, Tan L, Choi H, Gray N, Cohen P, Pedrioli P, Clark K, Alessi DR, *The IkappaB kinase family phosphorylates the Parkinson's disease kinase LRRK2 at Ser935 and Ser910 during Toll-like receptor signaling*. PLoS One. 2012;7(6):e39132.

Edwards RH, *The neurotransmitter cycle and quantal size*. Neuron. 2007 Sep 20;55(6):835-58.

el-Agnaf OM, Irvine GB, *Aggregation and neurotoxicity of alpha-synuclein and related peptides*. Biochem Soc Trans. 2002 Aug;30(4):559-65.

Esposito G, Ana Clara F, Verstreken P, *Synaptic vesicle trafficking and Parkinson's disease*. Dev Neurobiol. 2012 Jan;72(1):134-44.

Fahn S, *Description of Parkinson's disease as a clinical syndrome*. Ann N Y Acad Sci. 2003 Jun;991:1-14.

Farrer MJ, *Genetics of Parkinson disease: paradigm shifts and future prospects*. Nat Rev Genet. 2006 Apr;7(4):306-18.

Fasshauer D, Bruns D, Shen B, Jahn R, Brünger AT, *A structural change occurs upon binding of syntaxin to SNAP-25*. J Biol Chem. 1997 Feb 14;272(7):4582-90.

Fasshauer D, Sutton RB, Brunger AT, Jahn R, *Conserved structural features of the synaptic fusion complex: SNARE proteins reclassified as Q- and R-SNAREs*. Proc Natl Acad Sci U S A. 1998 Dec 22;95(26):15781-6.

Fernández-Chacón R, Wölfel M, Nishimune H, Tabares L, Schmitz F, Castellano-Muñoz M, Rosenmund C, Montesinos ML, Sanes JR, Schneggenburger R, Südhof TC, *The synaptic vesicle protein CSP alpha prevents presynaptic degeneration*. Neuron. 2004 Apr 22;42(2):237-51.

Fortin DL, Troyer MD, Nakamura K, Kubo S, Anthony MD, Edwards RH, *Lipid rafts mediate the synaptic localization of alpha-synuclein*. J Neurosci. 2004 Jul 28;24(30):6715-23.

Frank C, Pari G, Rossiter JP, *Approach to diagnosis of Parkinson disease*. Can Fam Physician. 2006 Jul;52:862-8.

Fraser KB, Moehle MS, Daher JP, Webber PJ, Williams JY, Stewart CA, Yacoubian TA, Cowell RM, Dokland T, Ye T, Chen D, Siegal GP, Galemmo RA, Tsika E, Moore DJ, Standaert DG, Kojima K, Mobley JA, West AB, *LRRK2 secretion in exosomes is regulated by 14-3-3*. Hum Mol Genet. 2013 Dec 15;22(24):4988-5000.

Fuji RN, Flagella M, Baca M, Baptista MA, Brodbeck J, Chan BK, Fiske BK, Honigberg L, Jubb AM, Katavolos P, Lee DW, Lewin-Koh SC, Lin T, Liu X, Liu S, Lyssikatos JP, O'Mahony J, Reichelt M, Roose-Girma M, Sheng Z, Sherer T, Smith A, Solon M, Sweeney ZK, Tarrant J, Urkowitz A, Warming S, Yaylaoglu M, Zhang S, Zhu H, Estrada AA, Watts RJ, *Effect of selective LRRK2 kinase inhibition on nonhuman primate lung*. Sci Transl Med. 2015 Feb 4;7(273):273ra15.

Funayama M, Li Y, Tomiyama H, Yoshino H, Imamichi Y, Yamamoto M, Murata M, Toda T, Mizuno Y, Hattori N, *Leucine-rich repeat kinase 2 G2385R variant is a risk factor for Parkinson disease in Asian population*. Neuroreport. 2007 Feb 12;18(3):273-5.

Gandhi PN, Wang X, Zhu X, Chen SG, Wilson-Delfosse AL, *The Roc domain of leucine-rich repeat kinase 2 is sufficient for interaction with microtubules*. J Neurosci Res. 2008 Jun;86(8):1711-20.

Gasper R, Meyer S, Gotthardt K, Sirajuddin M, Wittinghofer A, *It takes two to tango: regulation of G proteins by dimerization*. Nat Rev Mol Cell Biol. 2009 Jun;10(6):423-9.

Giasson BI, Covy JP, Bonini NM, Hurtig HI, Farrer MJ, Trojanowski JQ, Van Deerlin VM, *Biochemical and pathological characterization of Lrrk2*. Ann Neurol. 2006 Feb;59(2):315-22.

Gibb WR, Lees AJ, *The relevance of the Lewy body to the pathogenesis of idiopathic Parkinson's disease*. J Neurol Neurosurg Psychiatry. 1988 Jun;51(6):745-52.

Gilks WP, Abou-Sleiman PM, Gandhi S, Jain S, Singleton A, Lees AJ, Shaw K, Bhatia KP, Bonifati V, Quinn NP, Lynch J, Healy DG, Holton JL, Revesz T, Wood NW, *A common LRRK2 mutation in idiopathic Parkinson's disease*. Lancet. 2005 Jan 29-Feb 4;365(9457):415-6.

Gillardon F, *Leucine-rich repeat kinase 2 phosphorylates brain tubulin-beta isoforms and modulates microtubule stability--a point of convergence in parkinsonian neurodegeneration?* J Neurochem. 2009 Sep;110(5):1514-22.

Girotto S, Sturlese M, Bellanda M, Tessari I, Cappellini R, Bisaglia M, Bubacco L, Mammi S, *Dopamine-derived quinones affect the structure of the redox sensor DJ-1 through modifications at Cys-106 and Cys-53*. J Biol Chem. 2012 May 25;287(22):18738-49.

Gloeckner CJ, Boldt K, von Zweydorf F, Helm S, Wiesent L, Sarioglu H, Ueffing M, *Phosphopeptide analysis reveals two discrete clusters of phosphorylation in the N-terminus and the Roc domain of the Parkinson-disease associated protein kinase LRRK2*. J Proteome Res. 2010 Apr 5;9(4):1738-45.

Gloeckner CJ, Kinkl N, Schumacher A, Braun RJ, O'Neill E, Meitinger T, Kolch W, Prokisch H, Ueffing M, *The Parkinson disease causing LRRK2 mutation I2020T is associated with increased kinase activity*. Hum Mol Genet. 2006 Jan 15;15(2):223-32.

Gloeckner CJ, Schumacher A, Boldt K, Ueffing M, *The Parkinson disease-associated protein kinase LRRK2 exhibits MAPKKK activity and phosphorylates MKK3/6 and MKK4/7, in vitro*. J Neurochem. 2009 May;109(4):959-68.

Godena VK, Brookes-Hocking N, Moller A, Shaw G, Oswald M, Sancho RM, Miller CC, Whitworth AJ, De Vos KJ, *Increasing microtubule acetylation rescues axonal transport and locomotor deficits caused by LRRK2 Roc-COR domain mutations*. Nat Commun. 2014 Oct 15;5:5245.

Golub Y, Berg D, Calne DB, Pfeiffer RF, Uitti RJ, Stoessl AJ, Wszolek ZK, Farrer MJ, Mueller JC, Gasser T, Fuchs J, *Genetic factors influencing age at onset in LRRK2-linked Parkinson disease*. Parkinsonism Relat Disord. 2009 Aug;15(7):539-41.

Gotthardt K, Weyand M, Kortholt A, Van Haastert PJ, Wittinghofer A, *Structure of the Roc-COR domain tandem of C. tepidum, a prokaryotic homologue of the human LRRK2 Parkinson kinase*. EMBO J. 2008 Aug 20;27(16):2239-49.

Greggio E, Cookson MR, *Leucine-rich repeat kinase 2 mutations and Parkinson's disease: three questions*. ASN Neuro. 2009 Apr 14;1(1).

Greggio E, Jain S, Kingsbury A, Bandopadhyay R, Lewis P, Kaganovich A, van der Brug MP, Beilina A, Blackinton J, Thomas KJ, Ahmad R, Miller DW, Kesavapany S, Singleton A, Lees A, Harvey RJ, Harvey K, Cookson MR, *Kinase activity is required for the toxic effects of mutant LRRK2/dardarin*. Neurobiol Dis. 2006 Aug;23(2):329-41.

Greggio E, *Role of LRRK2 kinase activity in the pathogenesis of Parkinson's disease*. Biochem Soc Trans. 2012 Oct;40(5):1058-62.

Greggio E, Taymans JM, Zhen EY, Ryder J, Vancraenenbroeck R, Beilina A, Sun P, Deng J, Jaffe H, Baekelandt V, Merchant K, Cookson MR, *The Parkinson's disease kinase LRRK2 autophosphorylates its GTPase domain at multiple sites*. Biochem Biophys Res Commun. 2009 Nov 20;389(3):449-54.

Greggio E, Zambrano I, Kaganovich A, Beilina A, Taymans JM, Daniëls V, Lewis P, Jain S, Ding J, Syed A, Thomas KJ, Baekelandt V, Cookson MR, *The Parkinson disease-associated leucine-rich repeat kinase 2 (LRRK2) is a dimer that undergoes intramolecular autophosphorylation*. J Biol Chem. 2008 Jun 13;283(24):16906-14.

Greten-Harrison B, Polydoro M, Morimoto-Tomita M, Diao L, Williams AM, Nie EH, Makani S, Tian N, Castillo PE, Buchman VL, Chandra SS, *αβγ-Synuclein triple knockout mice reveal age-dependent neuronal dysfunction*. Proc Natl Acad Sci U S A. 2010 Nov 9;107(45):19573-8.

Grønborg M, Pavlos NJ, Brunk I, Chua JJ, Münster-Wandowski A, Riedel D, Ahnert-Hilger G, Urlaub H, Jahn R, *Quantitative comparison of glutamatergic and GABAergic synaptic vesicles unveils selectivity for few proteins including MAL2, a novel synaptic vesicle protein*. J Neurosci. 2010 Jan 6;30(1):2-12.

Grosshans BL, Ortiz D, Novick P, *Rabs and their effectors: achieving specificity in membrane traffic*. Proc Natl Acad Sci U S A. 2006 Aug 8;103(32):11821-7.

Gruenberg J, Griffiths G, Howell KE, *Characterization of the early endosome and putative endocytic carrier vesicles in vivo and with an assay of vesicle fusion in vitro*. J Cell Biol. 1989 Apr;108(4):1301-16.

Gruenberg J, *The endocytic pathway: a mosaic of domains*. Nat Rev Mol Cell Biol. 2001 Oct;2(10):721-30.

Haas AK, Yoshimura S, Stephens DJ, Preisinger C, Fuchs E, Barr FA, *Analysis of GTPase-activating proteins: Rab1 and Rab43 are key Rabs required to maintain a functional Golgi complex in human cells*. J Cell Sci. 2007 Sep 1;120(Pt 17):2997-3010.

Haebig K, Gloeckner CJ, Miralles MG, Gillardon F, Schulte C, Riess O, Ueffing M, Biskup S, Bonin M, *ARHGEF7 (Beta-PIX) acts as guanine nucleotide exchange factor for leucine-rich repeat kinase 2*. PLoS One. 2010 Oct 29;5(10):e13762.

Hanse E, Gustafsson B, *Vesicle release probability and pre-primed pool at glutamatergic synapses in area CA1 of the rat neonatal hippocampus*. J Physiol. 2001 Mar 1;531(Pt 2):481-93.

Hanson PI, Roth R, Morisaki H, Jahn R, Heuser JE, *Structure and conformational changes in NSF and its membrane receptor complexes visualized by quick-freeze/deep-etch electron microscopy*. Cell. 1997 Aug 8;90(3):523-35.

Hanson PI, Whiteheart SW, *AAA+ proteins: have engine, will work*. Nat Rev Mol Cell Biol. 2005 Jul;6(7):519-29.

Hara T, Nakamura K, Matsui M, Yamamoto A, Nakahara Y, Suzuki-Migishima R, Yokoyama M, Mishima K, Saito I, Okano H, Mizushima N, *Suppression of basal autophagy in neural cells causes neurodegenerative disease in mice*. Nature. 2006 Jun 15;441(7095):885-9.

Hardy J, Cai H, Cookson MR, Gwinn-Hardy K, Singleton A, *Genetics of Parkinson's disease and parkinsonism*. Ann Neurol. 2006 Oct;60(4):389-98.

Hardy J, Lewis P, Revesz T, Lees A, Paisan-Ruiz C, *The genetics of Parkinson's syndromes: a critical review*. Curr Opin Genet Dev. 2009 Jun;19(3):254-65.

Hata Y, Slaughter CA, Südhof TC, *Synaptic vesicle fusion complex contains unc-18 homologue bound to syntaxin*. Nature. 1993 Nov 25;366(6453):347-51.

Hatano T, Kubo S, Imai S, Maeda M, Ishikawa K, Mizuno Y, Hattori N, *Leucine-rich repeat kinase 2 associates with lipid rafts*. Hum Mol Genet. 2007 Mar 15;16(6):678-90.

Hayashi T, Yamasaki S, Nauenburg S, Binz T, Niemann H, *Disassembly of the reconstituted synaptic vesicle membrane fusion complex in vitro*. EMBO J. 1995 May 15;14(10):2317-25.

Heidelberger R, Heinemann C, Neher E, Matthews G, *Calcium dependence of the rate of exocytosis in a synaptic terminal*. Nature. 1994 Oct 6;371(6497):513-5.

Heo HY, Kim KS, Seol W, *Coordinate Regulation of Neurite Outgrowth by LRRK2 and Its Interactor, Rab5*. Exp Neurobiol. 2010 Sep;19(2):97-105.

Heo HY, Park JM, Kim CH, Han BS, Kim KS, Seol W, *LRRK2 enhances oxidative stress-induced neurotoxicity via its kinase activity*. Exp Cell Res. 2010 Feb 15;316(4):649-56.

Herzig MC, Kolly C, Persohn E, Theil D, Schweizer T, Hafner T, Stemmelen C, Troxler TJ, Schmid P, Danner S, Schnell CR, Mueller M, Kinzel B, Grevot A, Bolognani F, Stirn M, Kuhn RR, Kaupmann K, van der Putten PH, Rovelli G, Shimshek DR, *LRRK2 protein levels are determined by kinase function and are crucial for kidney and lung homeostasis in mice*. Hum Mol Genet. 2011 Nov 1;20(21):4209-23.

Heumann R, Moratalla R, Herrero MT, Chakrabarty K, Drucker-Colín R, Garcia-Montes JR, Simola N, Morelli M, *Dyskinesia in Parkinson's disease: mechanisms and current non-pharmacological interventions*. J Neurochem. 2014 Aug;130(4):472-89.

Heuser JE, Reese TS, *Evidence for recycling of synaptic vesicle membrane during transmitter release at the frog neuromuscular junction*. J Cell Biol. 1973 May;57(2):315-44.

Higashi S, Biskup S, West AB, Trinkaus D, Dawson VL, Faull RL, Waldvogel HJ, Arai H, Dawson TM, Moore DJ, Emson PC, *Localization of Parkinson's disease-associated LRRK2 in normal and pathological human brain*. Brain Res. 2007 Jun 25;1155:208-19.

Higashi S, Moore DJ, Yamamoto R, Minegishi M, Sato K, Togo T, Katsuse O, Uchikado H, Furukawa Y, Hino H, Kosaka K, Emson PC, Wada K, Dawson VL, Dawson TM, Arai H, Iseki E, *Abnormal localization of leucine-rich repeat kinase 2 to the endosomal-lysosomal compartment in lewy body disease*. J Neuropathol Exp Neurol. 2009 Sep;68(9):994-1005.

Hong W, *SNAREs and traffic*. Biochim Biophys Acta. 2005 Jul 10;1744(3):493-517.

Huotari J, Helenius A, *Endosome maturation*. EMBO J. 2011 Aug 31;30(17):3481-500.

Hurley JH, Hanson PI, *Membrane budding and scission by the ESCRT machinery: it's all in the neck*. Nat Rev Mol Cell Biol. 2010 Aug;11(8):556-66.

Ilardi JM, Mochida S, Sheng ZH, *Snapin: a SNARE-associated protein implicated in synaptic transmission*. Nat Neurosci. 1999 Feb;2(2):119-24.

Ito G, Okai T, Fujino G, Takeda K, Ichijo H, Katada T, Iwatsubo T, *GTP binding is essential to the protein kinase activity of LRRK2, a causative gene product for familial Parkinson's disease.* Biochemistry. 2007 Feb 6;46(5):1380-8.

Jahn R, Lang T, Südhof TC, *Membrane fusion*. Cell. 2003 Feb 21;112(4):519-33.

Jahn R, Scheller RH, *SNAREs--engines for membrane fusion*. Nat Rev Mol Cell Biol. 2006 Sep;7(9):631-43.

Jovic M, Sharma M, Rahajeng J, Caplan S, *The early endosome: a busy sorting station for proteins at the crossroads*. Histol Histopathol. 2010 Jan;25(1):99-112.

Kamikawaji S, Ito G, Iwatsubo T, *Identification of the autophosphorylation sites of LRRK2*. Biochemistry. 2009 Nov 24;48(46):10963-75.

Katz B, Miledi R, *The role of calcium in neuromuscular facilitation*. J Physiol. 1968 Mar;195(2):481-92.

Kauppi M, Simonsen A, Bremnes B, Vieira A, Callaghan J, Stenmark H, Olkkonen VM, *The small GTPase Rab22 interacts with EEA1 and controls endosomal membrane trafficking*. J Cell Sci. 2002 Mar 1;115(Pt 5):899-911.

Kawakami F, Yabata T, Ohta E, Maekawa T, Shimada N, Suzuki M, Maruyama H, Ichikawa T, Obata F, *LRRK2 phosphorylates tubulin-associated tau but not the free molecule: LRRK2-mediated regulation of the tau-tubulin association and neurite outgrowth*. PLoS One. 2012;7(1):e30834.

Kethiri RR, Bakthavatchalam R, *Leucine-rich repeat kinase 2 inhibitors: a review of recent patents (2011 - 2013)*. Expert Opin Ther Pat. 2014 Jul;24(7):745-57.

Kim RH, Smith PD, Aleyasin H, Hayley S, Mount MP, Pownall S, Wakeham A, You-Ten AJ, Kalia SK, Horne P, Westaway D, Lozano AM, Anisman H, Park DS, Mak TW, *Hypersensitivity of DJ-1-deficient mice to 1-methyl-4-phenyl-1,2,3,6-tetrahydropyrindine (MPTP) and oxidative stress*. Proc Natl Acad Sci U S A. 2005 Apr 5;102(14):5215-20.

Kitada T, Pisani A, Karouani M, Haburcak M, Martella G, Tscherter A, Platania P, Wu B, Pothos EN, Shen J, *Impaired dopamine release and synaptic plasticity in the striatum of parkin-/- mice*. J Neurochem. 2009 Jul;110(2):613-21.

Komatsu M, Waguri S, Chiba T, Murata S, Iwata J, Tanida I, Ueno T, Koike M, Uchiyama Y, Kominami E, Tanaka K, *Loss of autophagy in the central nervous system causes neurodegeneration in mice*. Nature. 2006 Jun 15;441(7095):880-4.

Kopin IJ, *MPTP: an industrial chemical and contaminant of illicit narcotics stimulates a new era in research on Parkinson's disease*. Environ Health Perspect. 1987 Nov;75:45-51.

Krebiehl G, Ruckerbauer S, Burbulla LF, Kieper N, Maurer B, Waak J, Wolburg H, Gizatullina Z, Gellerich FN, Woitalla D, Riess O, Kahle PJ, Proikas-Cezanne T, Krüger R, *Reduced basal autophagy and impaired mitochondrial dynamics due to loss of Parkinson's disease-associated protein DJ-1*. PLoS One. 2010 Feb 23;5(2):e9367.

Krüger R, Kuhn W, Müller T, Woitalla D, Graeber M, Kösel S, Przuntek H, Epplen JT, Schöls L, Riess O, *Ala30Pro mutation in the gene encoding alpha-synuclein in Parkinson's disease*. Nat Genet. 1998 Feb;18(2):106-8.

Kuang E, Qi J, Ronai Z, *Emerging roles of E3 ubiquitin ligases in autophagy*. Trends Biochem Sci. 2013 Sep;38(9):453-60.

Kuss M, Adamopoulou E, Kahle PJ. *Interferon-γ induces leucine-rich repeat kinase LRRK2 via extracellular signal-regulated kinase ERK5 in macrophages*. J Neurochem. 2014 Jun;129(6):980-7.

Lai YC, Kondapalli C, Lehneck R, Procter JB, Dill BD, Woodroof HI, Gourlay R, Peggie M, Macartney TJ, Corti O, Corvol JC, Campbell DG, Itzen A, Trost M, Muqit MM, *Phosphoproteomic screening identifies Rab GTPases as novel downstream targets of PINK1*. EMBO J. 2015 Nov 12;34(22):2840-61.

Lakshminarasimhan M, Maldonado MT, Zhou W, Fink AL, Wilson MA, *Structural impact of three Parkinsonism-associated missense mutations on human DJ-1*. Biochemistry. 2008 Feb 5;47(5):1381-92.

Langston JW, Ballard P, Tetrud JW, Irwin I, *Chronic Parkinsonism in humans due to a product of meperidine-analog synthesis*. Science. 1983 Feb 25;219(4587):979-80.

Lavara-Culebras E, Paricio N, *Drosophila DJ-1 mutants are sensitive to oxidative stress and show reduced lifespan and motor deficits*. Gene. 2007 Oct 1;400(1-2):158-65. Epub 2007 Jun 29.

Law BM, Spain VA, Leinster VH, Chia R, Beilina A, Cho HJ, Taymans JM, Urban MK, Sancho RM, Blanca Ramírez M, Biskup S, Baekelandt V, Cai H, Cookson MR, Berwick DC, Harvey K, *A direct interaction between leucine-rich repeat kinase 2 and specific β-tubulin isoforms regulates tubulin acetylation*. J Biol Chem. 2014 Jan 10;289(2):895-908.

Law BM, Spain VA, Leinster VH, Chia R, Beilina A, Cho HJ, Taymans JM, Urban MK, Sancho RM, Blanca Ramírez M, Biskup S, Baekelandt V, Cai H, Cookson MR, Berwick DC, Harvey K, *A direct interaction between leucine-rich repeat kinase 2 and specific β-tubulin isoforms regulates tubulin acetylation*. J Biol Chem. 2014 Jan 10;289(2):895-908.

Lee BD, Dawson VL, Dawson TM, *Leucine-rich repeat kinase 2 (LRRK2) as a potential therapeutic target in Parkinson's disease*. Trends Pharmacol Sci. 2012 Jul;33(7):365-73.

Lee BD, Shin JH, VanKampen J, Petrucelli L, West AB, Ko HS, Lee YI, Maguire-Zeiss KA, Bowers WJ, Federoff HJ, Dawson VL, Dawson TM, *Inhibitors of leucine-rich repeat kinase-2 protect against models of Parkinson's disease*. Nat Med. 2010 Sep;16(9):998-1000.

Lee S, Liu HP, Lin WY, Guo H, Lu B, *LRRK2 kinase regulates synaptic morphology through distinct substrates at the presynaptic and postsynaptic compartments of the Drosophila neuromuscular junction*. J Neurosci. 2010 Dec 15;30(50):16959-69.

Lee Y, Dawson VL, Dawson TM, *Animal models of Parkinson's disease: vertebrate genetics*. Cold Spring Harb Perspect Med. 2012 Oct 1;2(10).

Lees AJ, Hardy J, Revesz T, *Parkinson's disease*. Lancet. 2009 Jun 13;373(9680):2055-66.

Lenzen CU, Steinmann D, Whiteheart SW, Weis WI, *Crystal structure of the hexamerization domain of N-ethylmaleimide-sensitive fusion protein*. Cell. 1998 Aug 21;94(4):525-36.

Lesage S, Anheim M, Letournel F, Bousset L, Honoré A, Rozas N, Pieri L, Madiona K, Dürr A, Melki R, Verny C, Brice A; French Parkinson's Disease Genetics Study Group, *G51D α-synuclein mutation causes a novel parkinsonian-pyramidal syndrome*. Ann Neurol. 2013 Apr;73(4):459-71.

Lesage S, Brice A, *Role of mendelian genes in "sporadic" Parkinson's disease*. Parkinsonism Relat Disord. 2012 Jan;18 Suppl 1:S66-70.

Lev N, Barhum Y, Pilosof NS, Ickowicz D, Cohen HY, Melamed E, Offen D, *DJ-1 protects against dopamine toxicity: implications for Parkinson's disease and aging*. J Gerontol A Biol Sci Med Sci. 2013 Mar;68(3):215-25.

Lewis PA, *Assaying the kinase activity of LRRK2 in vitro*. J Vis Exp. 2012 Jan 18;(59).

Lewis PA, Greggio E, Beilina A, Jain S, Baker A, Cookson MR, *The R1441C mutation of LRRK2 disrupts GTP hydrolysis*. Biochem Biophys Res Commun. 2007 Jun 8;357(3):668-71.

Li Y, Dunn L, Greggio E, Krumm B, Jackson GS, Cookson MR, Lewis PA, Deng J, *The R1441C mutation alters the folding properties of the ROC domain of LRRK2*. Biochim Biophys Acta. 2009 Dec;1792(12):1194-7.

Liao J, Wu CX, Burlak C, Zhang S, Sahm H, Wang M, Zhang ZY, Vogel KW, Federici M, Riddle SM, Nichols RJ, Liu D, Cookson MR, Stone TA, Hoang QQ, *Parkinson disease-associated mutation R1441H in LRRK2 prolongs the "active state" of its GTPase domain*. Proc Natl Acad Sci U S A. 2014 Mar 18;111(11):4055-60.

Lin RC, Scheller RH, *Structural organization of the synaptic exocytosis core complex*. Neuron. 1997 Nov;19(5):1087-94.

Lin X, Parisiadou L, Gu XL, Wang L, Shim H, Sun L, Xie C, Long CX, Yang WJ, Ding J, Chen ZZ, Gallant PE, Tao-Cheng JH, Rudow G, Troncoso JC, Liu Z, Li Z, Cai H, *Leucine-rich repeat kinase 2 regulates the progression of neuropathology induced by Parkinson's-disease-related mutant alpha-synuclein*. Neuron. 2009 Dec 24;64(6):807-27.

Liou AK, Leak RK, Li L, Zigmond MJ, *Wild-type LRRK2 but not its mutant attenuates stress-induced cell death via ERK pathway*. Neurobiol Dis. 2008 Oct;32(1):116-24.

Lippé R, Horiuchi H, Runge A, Zerial M, *Expression, purification, and characterization of Rab5 effector complex, rabaptin-5/rabex-5*. Methods Enzymol. 2001;329:132-45.

Liu Z, Mobley JA, DeLucas LJ, Kahn RA, West AB, *LRRK2 autophosphorylation enhances its GTPase activity*. FASEB J. 2015 Sep 22.

Liu Z, Mobley JA, DeLucas LJ, Kahn RA, West AB, *LRRK2 autophosphorylation enhances its GTPase activity.* FASEB J. 2016 Jan;30(1):336-47.

Lobbestael E, Zhao J, Rudenko IN, Beylina A, Gao F, Wetter J, Beullens M, Bollen M, Cookson MR, Baekelandt V, Nichols RJ, Taymans JM, *Identification of protein phosphatase 1 as a regulator of the LRRK2 phosphorylation cycle*. Biochem J. 2013 Nov 15;456(1):119-28.

Loewenbrück K, Storch A, *Stem cell-based therapies in Parkinson's disease: future hope or current treatment option?*. J Neurol. 2011 May;258(Suppl 2):S346-53.

Luerman GC, Nguyen C, Samaroo H, Loos P, Xi H, Hurtado-Lorenzo A, Needle E, Stephen Noell G, Galatsis P, Dunlop J, Geoghegan KF, Hirst WD, *Phosphoproteomic evaluation of pharmacological inhibition of leucine-rich repeat kinase 2 reveals significant off-target effects of LRRK-2-IN-1*. J Neurochem. 2014 Feb;128(4):561-76.

Luzio JP, Pryor PR, Bright NA, *Lysosomes: fusion and function*. Nat Rev Mol Cell Biol. 2007 Aug;8(8):622-32.

MacLeod D, Dowman J, Hammond R, Leete T, Inoue K, Abeliovich A, *The familial Parkinsonism gene LRRK2 regulates neurite process morphology*. Neuron. 2006 Nov 22;52(4):587-93.

MacLeod DA, Rhinn H, Kuwahara T, Zolin A, Di Paolo G, McCabe BD, Marder KS, Honig LS, Clark LN, Small SA, Abeliovich A, *RAB7L1 interacts with LRRK2 to modify intraneuronal protein sorting and Parkinson's disease risk.* Neuron. 2013 Feb 6;77(3):425-39.

Magadán JG, Barbieri MA, Mesa R, Stahl PD, Mayorga LS, *Rab22a regulates the sorting of transferrin to recycling endosomes*. Mol Cell Biol. 2006 Apr;26(7):2595-614.

Malgieri G, Eliezer D, *Structural effects of Parkinson's disease linked DJ-1 mutations*. Protein Sci. 2008 May;17(5):855-68.

Malsam J, Kreye S, Söllner TH, *Membrane fusion: SNAREs and regulation*. Cell Mol Life Sci. 2008 Sep;65(18):2814-32.

Mamais A, Chia R, Beilina A, Hauser DN, Hall C, Lewis PA, Cookson MR, Bandopadhyay R, *Arsenite stress down-regulates phosphorylation and 14-3-3 binding of leucine-rich repeat kinase 2 (LRRK2), promoting self-association and cellular redistribution*. J Biol Chem. 2014 Aug 1;289(31):21386-400.

Manzoni C, Denny P, Lovering RC, Lewis PA, *Computational analysis of the LRRK2 interactome*. PeerJ. 2015 Feb 19;3:e778.

Marín I, *The Parkinson disease gene LRRK2: evolutionary and structural insights*. Mol Biol Evol. 2006 Dec;23(12):2423-33.

Marín I, van Egmond WN, van Haastert PJ, *The Roco protein family: a functional perspective*. FASEB J. 2008 Sep;22(9):3103-10.

Martin I, Kim JW, Lee BD, Kang HC, Xu JC, Jia H, Stankowski J, Kim MS, Zhong J, Kumar M, Andrabi SA, Xiong Y, Dickson DW, Wszolek ZK, Pandey A, Dawson TM, Dawson VL, *Ribosomal protein s15 phosphorylation mediates LRRK2 neurodegeneration in Parkinson's disease*. Cell. 2014 Apr 10;157(2):472-85.

Martinat C, Shendelman S, Jonason A, Leete T, Beal MF, Yang L, Floss T, Abeliovich A, *Sensitivity to oxidative stress in DJ-1-deficient dopamine neurons: an ES- derived cell model of primary Parkinsonism*. PLoS Biol. 2004 Nov;2(11):e327.

Matsui Y, Kikuchi A, Araki S, Hata Y, Kondo J, Teranishi Y, Takai Y, *Molecular cloning and characterization of a novel type of regulatory protein (GDI) for smg p25A, a ras p21-like GTP-binding protein*. Mol Cell Biol. 1990 Aug;10(8):4116-22.

Matta S, Van Kolen K, da Cunha R, van den Bogaart G, Mandemakers W, Miskiewicz K, De Bock PJ, Morais VA, Vilain S, Haddad D, Delbroek L, Swerts J, Chávez-Gutiérrez L, Esposito G, Daneels G, Karran E, Holt M, Gevaert K, Moechars DW, De Strooper B, Verstreken P, *LRRK2 controls an EndoA phosphorylation cycle in synaptic endocytosis*. Neuron. 2012 Sep 20;75(6):1008-21.

Mattera R, Tsai YC, Weissman AM, Bonifacino JS, *The Rab5 guanine nucleotide exchange factor Rabex-5 binds ubiquitin (Ub) and functions as a Ub ligase through an atypical Ub-interacting motif and a zinc finger domain*. J Biol Chem. 2006 Mar 10;281(10):6874-83.

Matveeva EA, He P, Whiteheart SW, *N-Ethylmaleimide-sensitive fusion protein contains high and low affinity ATP-binding sites that are functionally distinct*. J Biol Chem. 1997 Oct 17;272(42):26413-8.

Matveeva EA, He P, Whiteheart SW, *N-Ethylmaleimide-sensitive fusion protein contains high and low affinity ATP-binding sites that are functionally distinct*. J Biol Chem. 1997 Oct 17;272(42):26413-8.

Maxfield FR, Yamashiro DJ, *Endosome acidification and the pathways of receptor-mediated endocytosis*. Adv Exp Med Biol. 1987;225:189-98.

May AP, Misura KM, Whiteheart SW, Weis WI, *Crystal structure of the amino-terminal domain of N-ethylmaleimide-sensitive fusion protein*. Nat Cell Biol. 1999 Jul;1(3):175-82.

Mayor S, Pagano RE, *Pathways of clathrin-independent endocytosis*. Nat Rev Mol Cell Biol. 2007 Aug;8(8):603-12.

McNew JA, Weber T, Parlati F, Johnston RJ, Melia TJ, Söllner TH, Rothman JE, *Close is not enough: SNARE-dependent membrane fusion requires an active mechanism that transduces force to membrane anchors*. J Cell Biol. 2000 Jul 10;150(1):105-17.

Melrose HL, Dächsel JC, Behrouz B, Lincoln SJ, Yue M, Hinkle KM, Kent CB, Korvatska E, Taylor JP, Witten L, Liang YQ, Beevers JE, Boules M, Dugger BN, Serna VA, Gaukhman A, Yu X, Castanedes-Casey M, Braithwaite AT, Ogholikhan S, Yu N, Bass D, Tyndall G, Schellenberg GD, Dickson DW, Janus C, Farrer MJ, *Impaired dopaminergic neurotransmission and microtubule-associated protein tau alterations in human LRRK2 transgenic mice*. Neurobiol Dis. 2010 Dec;40(3):503-17.

Mercer J, Schelhaas M, Helenius A, *Virus entry by endocytosis*. Annu Rev Biochem. 2010; 79:803-33.

Meulener M, Whitworth AJ, Armstrong-Gold CE, Rizzu P, Heutink P, Wes PD, Pallanck LJ, Bonini NM, *Drosophila DJ-1 mutants are selectively sensitive to environmental toxins associated with Parkinson's disease*. Curr Biol. 2005 Sep 6;15(17):1572-7.

Migheli R, Del Giudice MG, Spissu Y, Sanna G, Xiong Y, Dawson TM, Dawson VL, Galioto M, Rocchitta G, Biosa A, Serra PA, Carri MT, Crosio C, Iaccarino C, *LRRK2 affects vesicle trafficking, neurotransmitter extracellular level and membrane receptor localization*. PLoS One. 2013 Oct 22;8(10):e77198.

Miklavc P, Ehinger K, Thompson KE, Hobi N, Shimshek DR, Frick M, *Surfactant secretion in LRRK2 knock-out rats: changes in lamellar body morphology and rate of exocytosis.* PLoS One. 2014 Jan 21;9(1):e84926.

Miklossy J, Arai T, Guo JP, Klegeris A, Yu S, McGeer EG, McGeer PL, *LRRK2 expression in normal and pathologic human brain and in human cell lines*. J Neuropathol Exp Neurol. 2006 Oct;65(10):953-63.

Milosevic I, Giovedi S, Lou X, Raimondi A, Collesi C, Shen H, Paradise S, O'Toole E, Ferguson S, Cremona O, De Camilli P, *Recruitment of endophilin to clathrin-coated pit necks is required for efficient vesicle uncoating after fission*. Neuron. 2011 Nov 17;72(4):587-601.

Mortiboys H, Johansen KK, Aasly JO, Bandmann O, *Mitochondrial impairment in patients with Parkinson disease with the G2019S mutation in LRRK2*. Neurology. 2010 Nov 30;75(22):2017-20.

Mosharov EV, Staal RG, Bové J, Prou D, Hananiya A, Markov D, Poulsen N, Larsen KE, Moore CM, Troyer MD, Edwards RH, Przedborski S, Sulzer D, *Alpha-synuclein overexpression increases cytosolic catecholamine concentration*. J Neurosci. 2006 Sep 6;26(36):9304-11.

Murray JW, Bananis E, Wolkoff AW, *Reconstitution of ATP-dependent movement of endocytic vesicles along microtubules in vitro: an oscillatory bidirectional process*. Mol Biol Cell. 2000 Feb;11(2):419-33.

Narendra D, Tanaka A, Suen DF, Youle RJ, *Parkin is recruited selectively to impaired mitochondria and promotes their autophagy*. J Cell Biol. 2008 Dec 1;183(5):795-803.

Narendra D, Tanaka A, Suen DF, Youle RJ, *Parkin is recruited selectively to impaired mitochondria and promotes their autophagy*. J Cell Biol. 2008 Dec 1;183(5):795-803.

Nemani VM, Lu W, Berge V, Nakamura K, Onoa B, Lee MK, Chaudhry FA, Nicoll RA, Edwards RH, *Increased expression of alpha-synuclein reduces neurotransmitter release by inhibiting synaptic vesicle reclustering after endocytosis*. Neuron. 2010 Jan 14;65(1):66-79.

Ness D, Ren Z, Gardai S, Sharpnack D, Johnson VJ, Brennan RJ, Brigham EF, Olaharski AJ, *Leucine-rich repeat kinase 2 (LRRK2)-deficient rats exhibit renal tubule injury and perturbations in metabolic and immunological homeostasis*. PLoS One. 2013 Jun 14;8(6):e66164.

Ng EL, Tang BL, *Rab GTPases and their roles in brain neurons and glia*. Brain Res Rev. 2008 Jun;58(1):236-46.

Nguyen HN, Byers B, Cord B, Shcheglovitov A, Byrne J, Gujar P, Kee K, Schüle B, Dolmetsch RE, Langston W, Palmer TD, Pera RR, *LRRK2 mutant iPSC-derived DA neurons demonstrate increased susceptibility to oxidative stress*. Cell Stem Cell. 2011 Mar 4;8(3):267-80.

Nichols RJ, Dzamko N, Morrice NA, Campbell DG, Deak M, Ordureau A, Macartney T, Tong Y, Shen J, Prescott AR, Alessi DR, *14-3-3 binding to LRRK2 is disrupted by multiple Parkinson's disease-associated mutations and regulates cytoplasmic localization*. Biochem J. 2010 Sep 15;430(3):393-404.

Nichols WC, Pankratz N, Hernandez D, Paisán-Ruíz C, Jain S, Halter CA, Michaels VE, Reed T, Rudolph A, Shults CW, Singleton A, Foroud T; Parkinson Study Group-PROGENI investigators, *Genetic screening for a single common LRRK2 mutation in familial Parkinson's disease*. Lancet. 2005 Jan 29-Feb 4;365(9457):410-2.

Nicholson KL, Munson M, Miller RB, Filip TJ, Fairman R, Hughson FM, *Regulation of SNARE complex assembly by an N-terminal domain of the t-SNARE Sso1p*. Nat Struct Biol. 1998 Sep;5(9):793-802.

Niu J, Yu M, Wang C, Xu Z, *Leucine-rich repeat kinase 2 disturbs mitochondrial dynamics via Dynamin-like protein*. J Neurochem. 2012 Aug;122(3):650-8.

Novick P, Zerial M, *The diversity of Rab proteins in vesicle transport*. Curr Opin Cell Biol. 1997 Aug;9(4):496-504.

Nuscher B, Kamp F, Mehnert T, Odoy S, Haass C, Kahle PJ, Beyer K, *Alpha-synuclein has a high affinity for packing defects in a bilayer membrane: a thermodynamics study*. J Biol Chem. 2004 May 21;279(21):21966-75.

Ogura T, Wilkinson AJ, *AAA+ superfamily ATPases: common structure--diverse function*. Genes Cells. 2001 Jul;6(7):575-97.

Olanow CW, Schapira AH, *Therapeutic prospects for Parkinson disease*. Ann Neurol. 2013 Sep;74(3):337-47.

Olzmann JA, Brown K, Wilkinson KD, Rees HD, Huai Q, Ke H, Levey AI, Li L, Chin LS, *Familial Parkinson's disease-associated L166P mutation disrupts DJ-1 protein folding and function*. J Biol Chem. 2004 Feb 27;279(9):8506-15.

Ooe H, Taira T, Iguchi-Ariga SM, Ariga H, *Induction of reactive oxygen species by bisphenol A and abrogation of bisphenol A-induced cell injury by DJ-1*. Toxicol Sci. 2005 Nov;88(1):114-26.

Oyler GA, Higgins GA, Hart RA, Battenberg E, Billingsley M, Bloom FE, Wilson MC, *The identification of a novel synaptosomal-associated protein, SNAP-25, differentially expressed by neuronal subpopulations*. J Cell Biol. 1989 Dec;109(6 Pt 1):3039-52.

Paisán-Ruíz C, Jain S, Evans EW, Gilks WP, Simón J, van der Brug M, López de Munain A, Aparicio S, Gil AM, Khan N, Johnson J, Martinez JR, Nicholl D, Carrera IM, Pena AS, de Silva R, Lees A, Martí-Massó JF, Pérez-Tur J, Wood NW, Singleton AB, *Cloning of the gene containing mutations that cause PARK8-linked Parkinson's disease*. Neuron. 2004 Nov 18;44(4):595-600.

Paisán-Ruíz C, Jain S, Evans EW, Gilks WP, Simón J, van der Brug M, López de Munain A, Aparicio S, Gil AM, Khan N, Johnson J, Martinez JR, Nicholl D, Carrera IM, Pena AS, de Silva R, Lees A, Martí-Massó JF, Pérez-Tur J, Wood NW, Singleton AB., *Cloning of the gene containing mutations that cause PARK8-linked Parkinson's disease*. Neuron. 2004 Nov 18;44(4):595-600.

Papkovskaia TD, Chau KY, Inesta-Vaquera F, Papkovsky DB, Healy DG, Nishio K, Staddon J, Duchen MR, Hardy J, Schapira AH, Cooper JM, *G2019S leucine-rich repeat kinase 2 causes uncoupling protein-mediated mitochondrial depolarization*. Hum Mol Genet. 2012 Oct 1;21(19):4201-13.

Pereira-Leal JB, Seabra MC, *Evolution of the Rab family of small GTP-binding proteins*. J Mol Biol. 2001 Nov 2;313(4):889-901.

Peters C, Mayer A, *Ca2+/calmodulin signals the completion of docking and triggers a late step of vacuole fusion*. Nature. 1998 Dec 10;396(6711):575-80.

Pfeffer SR, *Structural clues to Rab GTPase functional diversity*. J Biol Chem. 2005 Apr 22;280(16):15485-8.

Piccoli G, Condliffe SB, Bauer M, Giesert F, Boldt K, De Astis S, Meixner A, Sarioglu H, Vogt-Weisenhorn DM, Wurst W, Gloeckner CJ, Matteoli M, Sala C, Ueffing M, *LRRK2 controls synaptic vesicle storage and mobilization within the recycling pool.* J Neurosci. 2011 Feb 9;31(6):2225-37.

Piccoli G, Onofri F, Cirnaru MD, Kaiser CJ, Jagtap P, Kastenmüller A, Pischedda F, Marte A, von Zweydorf F, Vogt A, Giesert F, Pan L, Antonucci F, Kiel C, Zhang M, Weinkauf S, Sattler M, Sala C, Matteoli M, Ueffing M, Gloeckner CJ, *Leucine-rich repeat kinase 2 binds to neuronal vesicles through protein interactions mediated by its C-terminal WD40 domain*. Mol Cell Biol. 2014 Jun;34(12):2147-61.

Plotegher N, Kumar D, Tessari I, Brucale M, Munari F, Tosatto L, Belluzzi E, Greggio E, Bisaglia M, Capaldi S, Aioanei D, Mammi S, Monaco HL, Samo B, Bubacco L, *The chaperone-like protein 14-3-3η interacts with human α-synuclein aggregation intermediates rerouting the amyloidogenic pathway and reducing α-synuclein cellular toxicity*. Hum Mol Genet. 2014 Nov 1;23(21):5615-29.

Plowey ED, Cherra SJ 3rd, Liu YJ, Chu CT, *Role of autophagy in G2019S-LRRK2-associated neurite shortening in differentiated SH-SY5Y cells*. J Neurochem. 2008 May;105(3):1048-56.

Poirier MA, Xiao W, Macosko JC, Chan C, Shin YK, Bennett MK, *The synaptic SNARE complex is a parallel four-stranded helical bundle*. Nat Struct Biol. 1998 Sep;5(9):765-9.

Polymeropoulos MH, Lavedan C, Leroy E, Ide SE, Dehejia A, Dutra A, Pike B, Root H, Rubenstein J, Boyer R, Stenroos ES, Chandrasekharappa S, Athanassiadou A, Papapetropoulos T, Johnson WG, Lazzarini AM, Duvoisin RC, Di Iorio G, Golbe LI, Nussbaum RL, *Mutation in the alpha-synuclein gene identified in families with Parkinson's disease*. Science. 1997 Jun 27;276(5321):2045-7.

Poole AC, Thomas RE, Yu S, Vincow ES, Pallanck L, *The mitochondrial fusion-promoting factor mitofusin is a substrate of the PINK1/parkin pathway*. PLoS One. 2010 Apr 7;5(4):e10054.

Popat RA, Van Den Eeden SK, Tanner CM, McGuire V, Bernstein AL, Bloch DA, Leimpeter A, Nelson LM, *Effect of reproductive factors and postmenopausal hormone use on the risk of Parkinson disease*. Neurology. 2005 Aug 9;65(3):383-90.

Poteryaev D, Datta S, Ackema K, Zerial M, Spang A, *Identification of the switch in early-to-late endosome transition*. Cell. 2010 Apr 30;141(3):497-508.

Poudel KR, Bai J, *Synaptic vesicle morphology: a case of protein sorting?* Curr Opin Cell Biol. 2014 Feb;26:28-33.

Proikas-Cezanne T, Gaugel A, Frickey T, Nordheim A., *Rab14 is part of the early endosomal clathrin-coated TGN microdomain*. FEBS Lett. 2006 Oct 2;580(22):5241-6.

Proukakis C, Dudzik CG, Brier T, MacKay DS, Cooper JM, Millhauser GL, Houlden H, Schapira AH, *A novel α-synuclein missense mutation in Parkinson disease*. Neurology. 2013 Mar 12;80(11):1062-4.

Pungaliya PP, Bai Y, Lipinski K, Anand VS, Sen S, Brown EL, Bates B, Reinhart PH, West AB, Hirst WD, Braithwaite SP, *Identification and characterization of a leucine-rich repeat kinase 2 (LRRK2) consensus phosphorylation motif*. PLoS One. 2010 Oct 27;5(10):e13672.

Qian J, Saggau P, *Activity-dependent modulation of K+ currents at presynaptic terminals of mammalian central synapses*. J Physiol. 1999 Sep 1;519 Pt 2:427-37.

Qing H, Wong W, McGeer EG, McGeer PL, *Lrrk2 phosphorylates alpha synuclein at serine 129: Parkinson disease implications*. Biochem Biophys Res Commun. 2009 Sep 11;387(1):149-52.

Ramonet D, Daher JP, Lin BM, Stafa K, Kim J, Banerjee R, Westerlund M, Pletnikova O, Glauser L, Yang L, Liu Y, Swing DA, Beal MF, Troncoso JC, McCaffery JM, Jenkins NA, Copeland NG, Galter D, Thomas B, Lee MK, Dawson TM, Dawson VL, Moore DJ, *Dopaminergic neuronal loss, reduced neurite complexity and autophagic abnormalities in transgenic mice expressing G2019S mutant LRRK2*. PLoS One. 2011 Apr 6;6(4):e18568.

Ramsey CP, Giasson BI, *The E163K DJ-1 mutant shows specific antioxidant deficiency*. Brain Res. 2008 Nov 6;1239:1-11.

Reith AD, Bamborough P, Jandu K, Andreotti D, Mensah L, Dossang P, Choi HG, Deng X, Zhang J, Alessi DR, Gray NS, *GSK2578215A; a potent and highly selective 2-arylmethyloxy-5-substitutent-N-arylbenzamide LRRK2 kinase inhibitor*. Bioorg Med Chem Lett. 2012 Sep 1;22(17):5625-9.

Richards DA, Guatimosim C, Betz WJ, *Two endocytic recycling routes selectively fill two vesicle pools in frog motor nerve terminals*. Neuron. 2000 Sep;27(3):551-9.

Ringstad N, Nemoto Y, De Camilli P, *The SH3p4/Sh3p8/SH3p13 protein family: binding partners for synaptojanin and dynamin via a Grb2-like Src homology 3 domain*. Proc Natl Acad Sci U S A. 1997 Aug 5;94(16):8569-74.

Rink J, Ghigo E, Kalaidzidis Y, Zerial M, *Rab conversion as a mechanism of progression from early to late endosomes*. Cell. 2005 Sep 9;122(5):735-49.

Rivero-Ríos P, Gómez-Suaga P, Fernández B, Madero-Pérez J, Schwab AJ, Ebert AD, Hilfiker S, *Alterations in late endocytic trafficking related to the pathobiology of LRRK2-linked Parkinson's disease*. Biochem Soc Trans. 2015 Jun;43(3):390-5.

Rizo J, Rosenmund C, *Synaptic vesicle fusion*. Nat Struct Mol Biol. 2008 Jul;15(7):665-74.

Rizo J, Südhof TC, *Snares and Munc18 in synaptic vesicle fusion*. Nat Rev Neurosci. 2002 Aug;3(8):641-53.

Rizzoli SO, Betz WJ, *Synaptic vesicle pools*. Nat Rev Neurosci. 2005 Jan;6(1):57-69.

Rudenko IN, Kaganovich A, Hauser DN, Beylina A, Chia R, Ding J, Maric D, Jaffe H, Cookson MR, *The G2385R variant of leucine-rich repeat kinase 2 associated with Parkinson's disease is a partial loss-of-function mutation*. Biochem J. 2012 Aug 15;446(1):99-111.

Rudi K, Ho FY, Gilsbach BK, Pots H, Wittinghofer A, Kortholt A, Klare JP, *Conformational heterogeneity of the Roc domains in C. tepidum Roc-COR and implications for human LRRK2 Parkinson mutations*. Biosci Rep. 2015 Aug 26;35(5).

Ryu JK, Min D, Rah SH, Kim SJ, Park Y, Kim H, Hyeon C, Kim HM, Jahn R, Yoon TY, *Spring-loaded unraveling of a single SNARE complex by NSF in one round of ATP turnover*. Science. 2015 Mar 27;347(6229):1485-9.

Scales SJ, Chen YA, Yoo BY, Patel SM, Doung YC, Scheller RH, *SNAREs contribute to the specificity of membrane fusion*. Neuron. 2000 May;26(2):457-64.

Schikorski T, Stevens CF, *Morphological correlates of functionally defined synaptic vesicle populations*. Nat Neurosci. 2001 Apr;4(4):391-5.

Schmidt MR, Haucke V, *Recycling endosomes in neuronal membrane traffic*. Biol Cell. 2007 Jun;99(6):333-42.

Schwartz SL, Cao C, Pylypenko O, Rak A, Wandinger-Ness A, *Rab GTPases at a glance*. J Cell Sci. 2007 Nov 15;120(Pt 22):3905-10.

Seaman MN, *The retromer complex - endosomal protein recycling and beyond*. J Cell Sci. 2012 Oct 15;125(Pt 20):4693-702.

Sen S, Webber PJ, West AB, *Dependence of leucine-rich repeat kinase 2 (LRRK2) kinase activity on dimerization*. J Biol Chem. 2009 Dec 25;284(52):36346-56.

Shah N, Colbert KN, Enos MD, Herschlag D, Weis WI, *Three αSNAP and 10 ATP molecules are used in SNARE complex disassembly by N-ethylmaleimide-sensitive factor (NSF)*. J Biol Chem. 2015 Jan 23;290(4):2175-88.

Sheng D, Qu D, Kwok KH, Ng SS, Lim AY, Aw SS, Lee CW, Sung WK, Tan EK, Lufkin T, Jesuthasan S, Sinnakaruppan M, Liu J, *Deletion of the WD40 domain of LRRK2 in Zebrafish causes Parkinsonism-like loss of neurons and locomotive defect*. PLoS Genet. 2010 Apr 22;6(4):e1000914.

Sheng Z, Zhang S, Bustos D, Kleinheinz T, Le Pichon CE, Dominguez SL, Solanoy HO, Drummond J, Zhang X, Ding X, Cai F, Song Q, Li X, Yue Z, van der Brug MP, Burdick DJ, Gunzner-Toste J, Chen H, Liu X, Estrada AA, Sweeney ZK, Scearce-Levie K, Moffat JG, Kirkpatrick DS, Zhu H, *Ser1292 autophosphorylation is an indicator of LRRK2 kinase activity and contributes to the cellular effects of PD mutations*. Sci Transl Med. 2012 Dec 12;4(164):164ra161.

Sherer TB, Betarbet R, Greenamyre JT, *Environment, mitochondria, and Parkinson's disease*. Neuroscientist. 2002 Jun;8(3):192-7.

Shimura H, Hattori N, Kubo Si, Mizuno Y, Asakawa S, Minoshima S, Shimizu N, Iwai K, Chiba T, Tanaka K, Suzuki T, *Familial Parkinson disease gene product, parkin, is a ubiquitin-protein ligase*. Nat Genet. 2000 Jul;25(3):302-5.

Shin N, Jeong H, Kwon J, Heo HY, Kwon JJ, Yun HJ, Kim CH, Han BS, Tong Y, Shen J, Hatano T, Hattori N, Kim KS, Chang S, Seol W, *LRRK2 regulates synaptic vesicle endocytosis*. Exp Cell Res. 2008 Jun 10;314(10):2055-65.

Simpson JC, Griffiths G, Wessling-Resnick M, Fransen JA, Bennett H, Jones AT, *A role for the small GTPase Rab21 in the early endocytic pathway*. J Cell Sci. 2004 Dec 15;117(Pt 26):6297-311.

Singleton AB, Farrer MJ, Bonifati V, *The genetics of Parkinson's disease: progress and therapeutic implications*. Mov Disord. 2013 Jan;28(1):14-23.

Smith WW, Pei Z, Jiang H, Dawson VL, Dawson TM, Ross CA., *Kinase activity of mutant LRRK2 mediates neuronal toxicity*. Nat Neurosci. 2006 Oct;9(10):1231-3.

Smith Y, Wichmann T, Factor SA, DeLong MR, *Parkinson's disease therapeutics: new developments and challenges since the introduction of levodopa*. Neuropsychopharmacology. 2012 Jan;37(1):213-46.

Söllner T, Bennett MK, Whiteheart SW, Scheller RH, Rothman JE, *A protein assembly-disassembly pathway in vitro that may correspond to sequential steps of synaptic vesicle docking, activation, and fusion*. Cell. 1993 Nov 5;75(3):409-18.

Song S, Jang S, Park J, Bang S, Choi S, Kwon KY, Zhuang X, Kim E, Chung J, *Characterization of PINK1 (PTEN-induced putative kinase 1) mutations associated with Parkinson disease in mammalian cells and Drosophila*. J Biol Chem. 2013 Feb 22;288(8):5660-72.

Soppina V, Rai AK, Ramaiya AJ, Barak P, Mallik R, *Tug-of-war between dissimilar teams of microtubule motors regulates transport and fission of endosomes*. Proc Natl Acad Sci U S A. 2009 Nov 17;106(46):19381-6.

Spillantini MG, Crowther RA, Jakes R, Hasegawa M, Goedert M, *alpha-Synuclein in filamentous inclusions of Lewy bodies from Parkinson's disease and dementia with lewy bodies*. Proc Natl Acad Sci U S A. 1998 May 26;95(11):6469-73.

Stafa K, Trancikova A, Webber PJ, Glauser L, West AB, Moore DJ, *GTPase activity and neuronal toxicity of Parkinson's disease-associated LRRK2 is regulated by ArfGAP1*. PLoS Genet. 2012;8(2):e1002526.

Stevens CF, Wesseling JF, *Activity-dependent modulation of the rate at which synaptic vesicles become available to undergo exocytosis*. Neuron. 1998 Aug;21(2):415-24.

Su YC and Qi X, *Inhibition of excessive mitochondrial fission reduced aberrant autophagy and neuronal damage caused by LRRK2 G2019S mutation*. Hum Mol Genet. 2013 Nov 15;22(22):4545-61.

Südhof TC, Rothman JE, *Membrane fusion: grappling with SNARE and SM proteins*. Science. 2009 Jan 23;323(5913):474-7.

Südhof TC, *The synaptic vesicle cycle*. Annu Rev Neurosci. 2004;27:509-47.

Taira T, Saito Y, Niki T, Iguchi-Ariga SM, Takahashi K, Ariga H, *DJ-1 has a role in antioxidative stress to prevent cell death*. EMBO Rep. 2004 Feb;5(2):213-8.

Takamori S, Holt M, Stenius K, Lemke EA, Grønborg M, Riedel D, Urlaub H, Schenck S, Brügger B, Ringler P, Müller SA, Rammner B, Gräter F, Hub JS, De Groot BL, Mieskes G, Moriyama Y, Klingauf J, Grubmüller H, Heuser J, Wieland F, Jahn R, *Molecular anatomy of a trafficking organelle*. Cell. 2006 Nov 17;127(4):831-46.

Taymans JM, Greggio E, *LRRK2 Kinase Inhibition as a Therapeutic Strategy for Parkinson's Disease, Where Do We Stand?* Curr Neuropharmacol. 2015 Oct 29.

Taymans JM, Vancraenenbroeck R, Ollikainen P, Beilina A, Lobbestael E, De Maeyer M, Baekelandt V, Cookson MR, *LRRK2 kinase activity is dependent on LRRK2 GTP binding capacity but independent of LRRK2 GTP binding*. PLoS One. 2011;6(8):e23207.

Thakur P, Stevens DR, Sheng ZH, Rettig J, *Effects of PKA-mediated phosphorylation of Snapin on synaptic transmission in cultured hippocampal neurons*. J Neurosci. 2004 Jul 21;24(29):6476-81.

Tian JH, Wu ZX, Unzicker M, Lu L, Cai Q, Li C, Schirra C, Matti U, Stevens D, Deng C, Rettig J, Sheng ZH, *The role of Snapin in neurosecretion: snapin knock-out mice exhibit impaired calcium-dependent exocytosis of large dense-core vesicles in chromaffin cells*. J Neurosci. 2005 Nov 9;25(45):10546-55.

Tong Y, Giaime E, Yamaguchi H, Ichimura T, Liu Y, Si H, Cai H, Bonventre JV, Shen J, *Loss of leucine-rich repeat kinase 2 causes age-dependent bi-phasic alterations of the autophagy pathway*. Mol Neurodegener. 2012 Jan 9;7:2.

Tong Y, Pisani A, Martella G, Karouani M, Yamaguchi H, Pothos EN, Shen J, *R1441C mutation in LRRK2 impairs dopaminergic neurotransmission in mice*. Proc Natl Acad Sci U S A. 2009 Aug 25;106(34):14622-7.

Tong Y, Yamaguchi H, Giaime E, Boyle S, Kopan R, Kelleher RJ 3rd, Shen J, *Loss of leucine-rich repeat kinase 2 causes impairment of protein degradation pathways, accumulation of alpha-synuclein, and apoptotic cell death in aged mice*. Proc Natl Acad Sci U S A. 2010 May 25;107(21):9879-84.

Tsika E, Moore DJ, *Contribution of GTPase activity to LRRK2-associated Parkinson disease*. Small GTPases. 2013 Jul-Sep;4(3):164-70.

Ulmer TS, Bax A, *Comparison of structure and dynamics of micelle-bound human alpha-synuclein and Parkinson disease variants*. J Biol Chem. 2005 Dec 30;280(52):43179-87.

Valente EM, Abou-Sleiman PM, Caputo V, Muqit MM, Harvey K, Gispert S, Ali Z, Del Turco D, Bentivoglio AR, Healy DG, Albanese A, Nussbaum R, González-Maldonado R, Deller T, Salvi S, Cortelli P, Gilks WP, Latchman DS, Harvey RJ, Dallapiccola B, Auburger G, Wood NW, *Hereditary early-onset Parkinson's disease caused by mutations in PINK1*. Science. 2004 May 21;304(5674):1158-60.

van Dam EM, Ten Broeke T, Jansen K, Spijkers P, Stoorvogel W, *Endocytosed transferrin receptors recycle via distinct dynamin and phosphatidylinositol 3-kinase-dependent pathways*. J Biol Chem. 2002 Dec 13;277(50):48876-83.

Van Den Eeden SK, Tanner CM, Bernstein AL, Fross RD, Leimpeter A, Bloch DA, Nelson LM, *Incidence of Parkinson's disease: variation by age, gender, and race/ethnicity*. Am J Epidemiol. 2003 Jun 1;157(11):1015-22.

van der Sluijs P, Hull M, Huber LA, Mâle P, Goud B, Mellman I, *Reversible phosphorylation--dephosphorylation determines the localization of rab4 during the cell cycle*. EMBO J. 1992 Dec;11(12):4379-89.

van Meel E, Klumperman J, *Imaging and imagination: understanding the endo-lysosomal system*. Histochem Cell Biol. 2008 Mar;129(3):253-66.

Verstegen AM, Tagliatti E, Lignani G, Marte A, Stolero T, Atias M, Corradi A, Valtorta F, Gitler D, Onofri F, Fassio A, Benfenati F, *Phosphorylation of synapsin I by cyclin-dependent kinase-5 sets the ratio between the resting and recycling pools of synaptic vesicles at hippocampal synapses*. J Neurosci. 2014 May 21;34(21):7266-80.

Vicinanza M, D'Angelo G, Di Campli A, De Matteis MA, *Function and dysfunction of the PI system in membrane trafficking*. EMBO J. 2008 Oct 8;27(19):2457-70.

Vivona S, Cipriano DJ, O'Leary S, Li YH, Fenn TD, Brunger AT, *Disassembly of all SNARE complexes by N-ethylmaleimide-sensitive factor (NSF) is initiated by a conserved 1:1 interaction between α-soluble NSF attachment protein (SNAP) and SNARE complex*. J Biol Chem. 2013 Aug 23;288(34):24984-91.

Wallings R, Manzoni C, Bandopadhyay R, *Cellular processes associated with LRRK2 function and dysfunction*. FEBS J. 2015 Aug;282(15):2806-26.

Wang D, Qian L, Xiong H, Liu J, Neckameyer WS, Oldham S, Xia K, Wang J, Bodmer R, Zhang Z, *Antioxidants protect PINK1-dependent dopaminergic neurons in Drosophila*. Proc Natl Acad Sci U S A. 2006 Sep 5;103(36):13520-5.

Wang S, Ma Z, Xu X, Wang Z, Sun L, Zhou Y, Lin X, Hong W, Wang T, *A role of Rab29 in the integrity of the trans-Golgi network and retrograde trafficking of mannose-6-phosphate receptor*. PLoS One. 2014 May 2;9(5):e96242.

Wang X, Yan MH, Fujioka H, Liu J, Wilson-Delfosse A, Chen SG, Perry G, Casadesus G, Zhu X, *LRRK2 regulates mitochondrial dynamics and function through direct interaction with DLP1*. Hum Mol Genet. 2012 May 1;21(9):1931-44.

Webber PJ, Smith AD, Sen S, Renfrow MB, Mobley JA, West AB, *Autophosphorylation in the leucine-rich repeat kinase 2 (LRRK2) GTPase domain modifies kinase and GTP-binding activities*. J Mol Biol. 2011 Sep 9;412(1):94-110.

Weber T, Parlati F, McNew JA, Johnston RJ, Westermann B, Söllner TH, Rothman JE, *SNAREpins are functionally resistant to disruption by NSF and alphaSNAP*. J Cell Biol. 2000 May 29;149(5):1063-72.

Wen H, Linhoff MW, McGinley MJ, Li GL, Corson GM, Mandel G, Brehm P, *Distinct roles for two synaptotagmin isoforms in synchronous and asynchronous transmitter release at zebrafish neuromuscular junction*. Proc Natl Acad Sci U S A. 2010 Aug 3;107(31):13906-11.

West AB, Moore DJ, Choi C, Andrabi SA, Li X, Dikeman D, Biskup S, Zhang Z, Lim KL, Dawson VL, Dawson TM, *Parkinson's disease-associated mutations in LRRK2 link enhanced GTP-binding and kinase activities to neuronal toxicity*. Hum Mol Genet. 2007 Jan 15;16(2):223-32.

Whiteheart SW, Schraw T, Matveeva EA, *N-ethylmaleimide sensitive factor (NSF) structure and function*. Int Rev Cytol. 2001;207:71-112.

Winklhofer KF, *Parkin and mitochondrial quality control: toward assembling the puzzle*. Trends Cell Biol. 2014 Jun;24(6):332-41.

Wszolek ZK, Pfeiffer RF, Tsuboi Y, Uitti RJ, McComb RD, Stoessl AJ, Strongosky AJ, Zimprich A, Müller-Myhsok B, Farrer MJ, Gasser T, Calne DB, Dickson DW, *Autosomal dominant parkinsonism associated with variable synuclein and tau pathology*. Neurology. 2004 May 11;62(9):1619-22.

Wucherpfennig T, Wilsch-Bräuninger M, González-Gaitán M, *Role of Drosophila Rab5 during endosomal trafficking at the synapse and evoked neurotransmitter release*. J Cell Biol. 2003 May 12;161(3):609-24.

Xiong Y, Coombes CE, Kilaru A, Li X, Gitler AD, Bowers WJ, Dawson VL, Dawson TM, Moore DJ, *GTPase activity plays a key role in the pathobiology of LRRK2*. PLoS Genet. 2010 Apr 8;6(4):e1000902.

Xiong Y, Yuan C, Chen R, Dawson TM, Dawson VL, *ArfGAP1 is a GTPase activating protein for LRRK2: reciprocal regulation of ArfGAP1 by LRRK2*. J Neurosci. 2012 Mar 14;32(11):3877-86.

Xu-Friedman MA, Harris KM, Regehr WG, *Three-dimensional comparison of ultrastructural characteristics at depressing and facilitating synapses onto cerebellar Purkinje cells*. J Neurosci. 2001 Sep 1;21(17):6666-72.

Yang B, Gonzalez L Jr, Prekeris R, Steegmaier M, Advani RJ, Scheller RH, *SNARE interactions are not selective. Implications for membrane fusion specificity*. J Biol Chem. 1999 Feb 26;274(9):5649-53.

Yu RC, Hanson PI, Jahn R, Brünger AT, *Structure of the ATP-dependent oligomerization domain of N-ethylmaleimide sensitive factor complexed with ATP*. Nat Struct Biol. 1998 Sep;5(9):803-11.

Yun HJ, Kim H, Ga I, Oh H, Ho DH, Kim J, Seo H, Son I, Seol W, *An early endosome regulator, Rab5b, is an LRRK2 kinase substrate*. J Biochem. 2015 Jun;157(6):485-95.

Yun HJ, Park J, Ho DH, Kim H, Kim CH, Oh H, Ga I, Seo H, Chang S, Son I, Seol W, *LRRK2 phosphorylates Snapin and inhibits interaction of Snapin with SNAP-25*. Exp Mol Med. 2013 Aug 16;45:e36.

Zarow C, Lyness SA, Mortimer JA, Chui HC, *Neuronal loss is greater in the locus coeruleus than nucleus basalis and substantia nigra in Alzheimer and Parkinson diseases*. Arch Neurol. 2003 Mar;60(3):337-41.

Zarranz JJ, Alegre J, Gómez-Esteban JC, Lezcano E, Ros R, Ampuero I, Vidal L, Hoenicka J, Rodriguez O, Atarés B, Llorens V, Gomez Tortosa E, del Ser T, Muñoz DG, de Yebenes JG, *The new mutation, E46K, of alpha-synuclein causes Parkinson and Lewy body dementia*. Ann Neurol. 2004 Feb;55(2):164-73.

Zerial M, McBride H, *Rab proteins as membrane organizers*. Nat Rev Mol Cell Biol. 2001 Feb;2(2):107-17.

Zhao M, Brunger AT, *Recent Advances in Deciphering the Structure and Molecular Mechanism of the AAA+ ATPase N-Ethylmaleimide-Sensitive Factor (NSF)*. J Mol Biol. 2015 Nov 3. pii: S0022-2836(15)00619-1.

Zhao M, Wu S, Zhou Q, Vivona S, Cipriano DJ, Cheng Y, Brunger AT, *Mechanistic insights into the recycling machine of the SNARE complex*. Nature. 2015 Feb 5;518(7537):61-7.

Zhu JH, Horbinski C, Guo F, Watkins S, Uchiyama Y, Chu CT, *Regulation of autophagy by extracellular signal-regulated protein kinases during 1-methyl-4-phenylpyridinium-induced cell death*. Am J Pathol. 2007 Jan;170(1):75-86.

Zhu X, Siedlak SL, Smith MA, Perry G, Chen SG, *LRRK2 protein is a component of Lewy bodies*. Ann Neurol. 2006 Nov;60(5):617-8.

Zimmerberg J, Vogel SS, Chernomordik LV, *Mechanisms of membrane fusion*. Annu Rev Biophys Biomol Struct. 1993;22:433-66.

Zimprich A, Biskup S, Leitner P, Lichtner P, Farrer M, Lincoln S, Kachergus J, Hulihan M, Uitti RJ, Calne DB, Stoessl AJ, Pfeiffer RF, Patenge N, Carbajal IC, Vieregge P, Asmus F, Müller-Myhsok B, Dickson DW, Meitinger T, Strom TM, Wszolek ZK, Gasser T, *Mutations in LRRK2 cause autosomal-dominant parkinsonism with pleomorphic pathology*. Neuron. 2004 Nov 18;44(4):601-7.

Zucker RS, Regehr WG, *Short-term synaptic plasticity*. Annu Rev Physiol. 2002;64:355-405.

Abbreviations

AAA+: ATPase associated with various cellular activities

AADC: aromatic L-amino acid decarboxylase

AAV: adeno-associated virus

ADP:adenosine diphosphate

alpha-SNAP: Soluble NSF Associated Protein

AP: active potential

aSyn: alpha-synuclein

ATP: adenosine triphosphate

AV: autophagic vacuoles

AZ: active zone

AZ: Alzheimer’s disease

BAC: bacterial artificial chromosome

BBB: blood brain barrier

BSA: bovine serum albumin

CD: circular dichroism

COMT: catechol-O-methyltransferase

COR: C-ter of Roc

Cryo-EM: cryo-electron microscopy

DA: dopamine

DAQ: dopamine quinone

DMEM: Dulbecco's modified eagle medium

DTT: Dithiothreitol

EDTA: Ethylenediaminetetraacetic acid

EE: early endosome

ER: endoplasmatic reticulum

GAD: G proteins activated by nucleotide dependent dimerization

GAP: GTPase Activating protein

GDI: GDP dissociation inhibitor

GEF: guanine nucleotide exchange factor

GFP: Green Fluorescent Protein

GWAS: genome wide associated studies

ILV: intraluminal vesicle

LAMP2: Lysosomal-associated membrane protein 2

LB: Lewy bodies

L-DOPA:levodopa

LE: late endosome

LN: Lewy neurites

LRRK2: leucine-rich repeat kinase 2

MAO: monoamine oxidase

MAPKKK: mitogen-activated protein kinase kinase kinase

MPTP: 1-methyl-4-phenyl-1,2,3,6-tetrahydropyridine

MVB: multivesicular bodies

NSF: N-ethylmaleimide sensitive fusion protein

PBS: phosphate buffered saline

PD: Parkinson's disease

PKA: protein kinase A

PKC: Protein kinase C

RAF: rapidly accelerated fibrosarcoma

Roc: Ras of complex

ROS: reactive oxygen species

RP: recycling pool

RP-HPLC: reverse phase High Performance Liquid Chromatography

RRP: ready releasable pool

RtP: resting pool

SDS-PAGE: sodium dodecyl sulfate-polyacrylamide gel electrophoresis

SEC: size exclusion liquid chromatography

SM: Sec1/Munc18-related proteins

SNARE: Soluble N-ethylmaleimide Attachment protein REceptors

SNpc: substantia nigra pars compacta

SV: synaptic vesicle

TEM: transmission electron microscopy

TGN: trans-Golgi network

wt: wild-type

Appendix

Belluzzi et al. Molecular Neurodegeneration (2016) 11:1
DOI 10.1186/s13024-015-0066-z

Molecular Neurodegeneration

RESEARCH ARTICLE Open Access

LRRK2 phosphorylates pre-synaptic N-ethylmaleimide sensitive fusion (NSF) protein enhancing its ATPase activity and SNARE complex disassembling rate

Elisa Belluzzi[1,8†], Adriano Gonnelli[1†], Maria-Daniela Cirnaru[2], Antonella Marte[3], Nicoletta Plotegher[1,7], Isabella Russo[1], Laura Civiero[1], Susanna Cogo[1], Maria Perèz Carrion[2], Cinzia Franchin[4,5], Giorgio Arrigoni[4,5], Mariano Beltramini[1], Luigi Bubacco[1], Franco Onofri[3], Giovanni Piccoli[2,6] and Elisa Greggio[1*]

Abstract

Background: *Lrrk2*, a gene linked to Parkinson's disease, encodes a large scaffolding protein with kinase and GTPase activities implicated in vesicle and cytoskeletal-related processes. At the presynaptic site, LRRK2 associates with synaptic vesicles through interaction with a panel of presynaptic proteins.

Results: Here, we show that LRRK2 kinase activity influences the dynamics of synaptic vesicle fusion. We therefore investigated whether LRRK2 phosphorylates component(s) of the exo/endocytosis machinery. We have previously observed that LRRK2 interacts with NSF, a hexameric AAA+ ATPase that couples ATP hydrolysis to the disassembling of SNARE proteins allowing them to enter another fusion cycle during synaptic exocytosis. Here, we demonstrate that NSF is a substrate of LRRK2 kinase activity. LRRK2 phosphorylates full-length NSF at threonine 645 in the ATP binding pocket of D2 domain. Functionally, NSF phosphorylated by LRRK2 displays enhanced ATPase activity and increased rate of SNARE complex disassembling. Substitution of threonine 645 with alanine abrogates LRRK2-mediated increased ATPase activity.

Conclusions: Given that the most common Parkinson's disease LRRK2 G2019S mutation displays increased kinase activity, our results suggest that mutant LRRK2 may impair synaptic vesicle dynamics *via* aberrant phosphorylation of NSF.

Keywords: Parkinson's disease, Leucine-rich repeat kinase 2, N-ethylmaleimide sensitive fusion, Presynapse, Phosphorylation

Background

Leucine-rich repeat kinase 2 (LRRK2) is a large kinase with protein-to-protein interaction domains and dual enzymatic activities. The catalytic core includes a ROC (Ras Of Complex) domain with GTPase activity, followed by a COR (C-terminus Of ROC) domain likely involved in protein dimerization, and a serine-threonine kinase domain [1–3]. Mutations in *Lrrk2* cause late-onset autosomal dominant Parkinson's disease (PD) [4, 5], whereas more common variants around the *Lrrk2* locus act as risk factors for disease [6, 7]. As the most common G2019S mutation increases kinase activity in vitro and in vivo by ~3 fold, LRRK2 is being intensively explored as a pharmacological target for the treatment of PD [8]. Several substrates of LRRK2's kinase activity have been reported, however few of these have been extensively validated at a physiological level [9]. There is, therefore, an increasing interest in identifying LRRK2 substrates and cellular pathways compromised during pathological conditions that could serve as therapeutic alternatives to directly targeting LRRK2 kinase activity. LRRK2 has been found associated

* Correspondence: elisa.greggio@unipd.it
†Equal contributors
[1]Department of Biology, University of Padova, via Ugo Bassi 58/B, 35131 Padova, Italy
Full list of author information is available at the end of the article

with various membrane structures, including synaptic vesicles (SV) [10–15]. Multiple studies on different experimental models support a role for LRRK2 at the synapse. Mutant LRRK2 rodent models display defects in neurotransmission [16–19], and LRRK2 overexpression or knockdown results in impaired SV endocytosis/exocytosis [15, 20]. We recently showed that LRRK2 binds SV *via* interaction with a number of presynaptic proteins [21] and that its kinase activity modulates these interactions and impacts on SV dynamics [22]. Among the LRRK2 interactors identified, we found N-ethylmaleimide sensitive factor (NSF), which is involved in the fusion of SV orchestrated by SNARE (Soluble NSF-Attachment protein REceptor) proteins. During membrane fusion, vesicular and target SNAREs assemble into an alpha-helical trans-SNARE complex that juxtaposes the two membranes together to catalyze membrane fusion. NSF is the ATPase that catalyzes the release of SNARE complexes, thus allowing SV endocytosis and the next cycle of fusion [23]. Notably, NSF activity is tightly controlled by phosphorylation/dephosphorylation [24–26]. In the present study, using dynamic assays of SV cycling, we found that SV fusion is altered by LRRK2 kinase function, suggesting components of the exo/endocytic machinery may be a target of LRRK2 kinase activity. Given that LRRK2 interacts with NSF, we assessed whether NSF is a substrate for LRRK2 kinase activity. We found that LRRK2 can efficiently phosphorylate NSF in vitro, with phosphorylation primarily occurring at T645. Importantly, phosphorylated NSF displays enhanced ATPase activity and increased rate of SNARE complex disassembling in vitro. Our data implicate LRRK2 kinase activity in the regulation of SV exo/endocytosis by phospho-modulation of NSF activity and suggest that pathological LRRK2 may disturb SV dynamics *via* aberrant phosphorylation of NSF.

Results

LRRK2 kinase activity influences synaptic vesicle dynamics

We recently reported that inhibition of LRRK2 kinase activity causes impairment in synaptic vesicles (SV) dynamics, indicating a role for LRRK2 catalytic activity in SV fusion cycle [22]. To further determine the role of LRRK2 kinase activity at the presynapse, we performed dynamic assays of SV taking advantage of the sypHy assay in two complementary models: a) primary cortical cultures in the presence or absence of the LRRK2 inhibitor GSK2578215A (GSK in, 0.2 μM, 2 h), a brain penetrant, selective LRRK2 inhibitor (IC_{50} 10 nM) [27]; b) primary cortical neurons obtained from BAC hG2019S mice characterized by higher LRRK2 kinase activity [28]. GSK treatment induced LRRK2 dephosphorylation at Ser935, as predicted (Additional file 1: Figure S1-b), but did not cause protein destabilization (Additional file 1: Figure S1a–c), whereas BAC hG2019S neurons displayed increased LRRK2 expression due to the presence of the transgene (Additional file 1: Figure S1a-b-c). Synaptophysin-pHluorin (sypHy) is a pH-sensitive fluorescent reporter that, by analogy with the original synaptopHluorin (synaptobrevin-pHluorin), is quenched in the acidic intracellular space of the SV and will only become fluorescent upon SV fusion, when the contents of the SV is exposed to the more basic pH of the extracellular space [29]. As shown in Fig. 1, at the onset of the stimulus, exocytosis caused a rapid increase in sypHy fluorescence, which after cessation of the stimulus, slowly returned to baseline (Fig. 1a–b). The first stimulus, 40 AP, is predicted to mobilize SV belonging to the ready releasable pool, while 300 AP is sufficient to trigger the fusion of SV belonging to the total recycling pool [29]. Furthermore, the kinetics describing the on-set and the decay of the fluorescence are correlated to the efficiency of the exocytotic and endocytotic mechanism, respectively [29]. Interestingly, while we measured a significant impairment of SV fusion (decreased fluorescence) in the presence of GSK upon either 40 or 300 AP stimuli, BAC hG2019S neurons were characterized by a higher answer following the two stimulations (ΔF40/F0 and ΔF300/F0 respectively, Fig. 1c). Furthermore, while upon acute pharmacological inhibition the time taken for fluorescence decay was extended, τ decay was decreased in hG2019S cells (Tau decay, Fig. 1c). To further assess a role for LRRK2 in the SV cycle, we took advantage of the exo/endocytic assay previously reported [20, 21]. Using this approach, we previously demonstrated that acute pharmacological blockade of LRRK2 kinase activity impairs SV recycling [22]. Building upon these data, BAC hG2019S cortical cultures were transduced at DIV4 with control viruses co-expressing GFP to track neuronal processes and assayed at DIV14. Briefly, we exposed living cultures to rabbit polyclonal antibodies directed against the intravesicular domain of synaptotagmin1, which are internalized inside the vesicle lumen upon SV recycling [30]. Vesicles within GFP positive processes were then monitored *via* laser confocal microscopy. The vesicles appeared as clusters either synaptotagmin and synaptophysin positive (i.e. cycling vesicles) or only synaptophysin positive (Fig. 1d). The analysis showed that BAC hG2019S cultures are characterized by a significant increase in the number of synaptotagmin and synaptophysin positive clusters (Fig. 1e). The total number of synaptic contacts, however, remained unaltered despite any pharmacological treatments (Additional file 1: Figure S1d). Taken together, these results indicate that LRRK2 kinase activity is involved in the regulation of SV fusion.

LRRK2 interacts with NSF

Having found that LRRK2 kinase activity influences SV fusion, we next asked what the molecular mechanisms behind this phenotype might be. We had

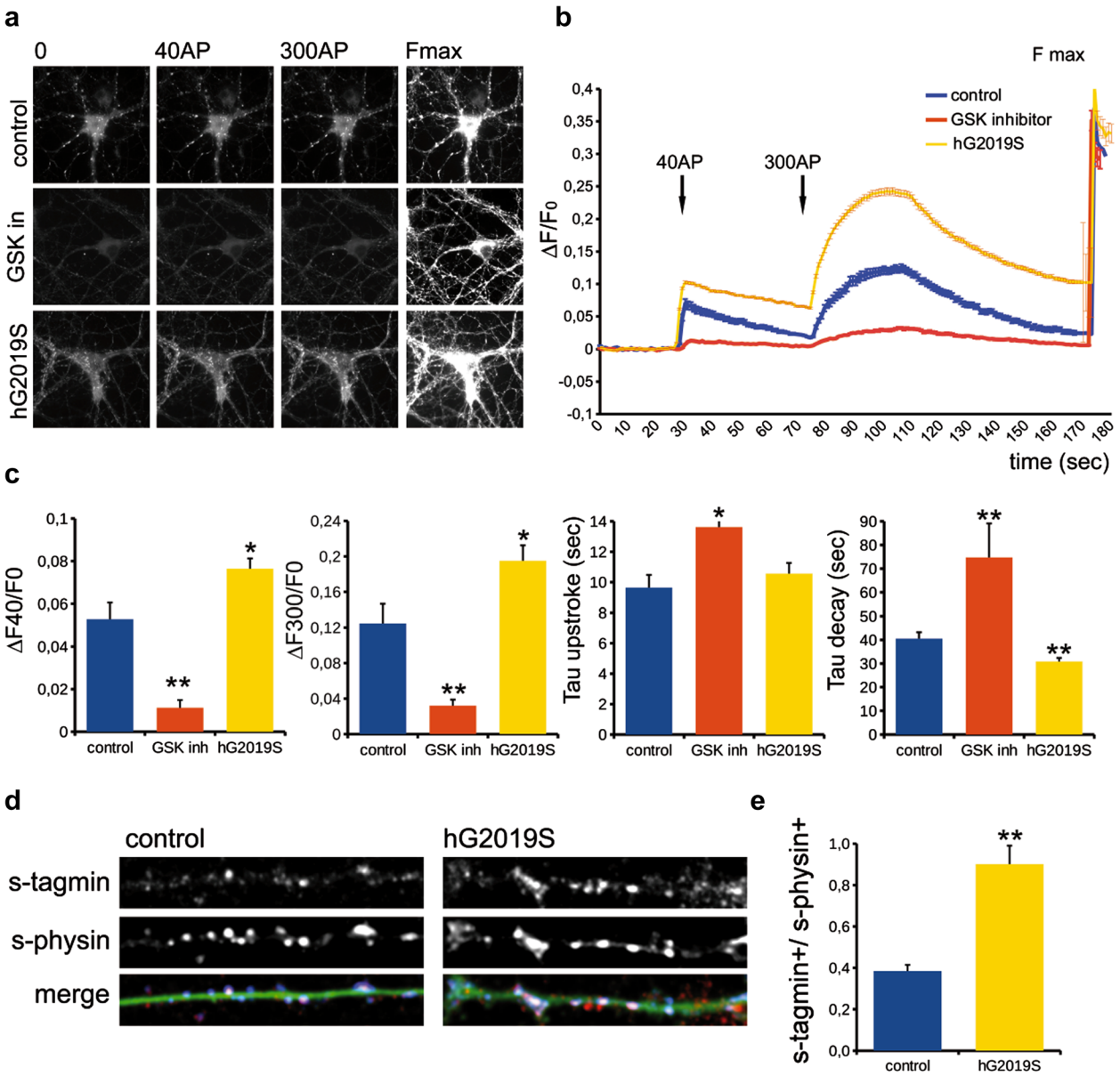

Fig. 1 LRRK2 kinase activity modulates synaptic vesicle fusion. **a** We recorded synaptophluorin fluorescence from DIV14 wild-type cortical neurons treated with DMSO (control) or treated with LRRK2 inhibitor GSK2578215A (GSK in, 0.2 μM, 2 h) and from cortical neurons obtained from BAC hG2019S mice (hG2019S). Representative snapshots were taken at DIV16 from 1 Hz recordings at rest (0), after 40 action potential stimulation (40AP), after 300 action potential stimulation (300AP) and upon neutralization with 50 mM NH_4Cl to reveal total fluorescence (Fmax). Panels size is 113 × 113 μm. **b** The graph shows representative pattern of fluorescence. Y-axis reports **Δ**F/F0 at the given time point (second). **c** The graphs report the increase in fluorescence after 40AP (**Δ**F40/F0) and 300AP (**Δ**F300/F0) and the kinetic of signal after 300AP expressed as time constant describing the increase (tau upstroke) and decay (tau decay) of fluorescence. Data are expressed as mean ± SEM, $n = 4$, at least 50 boutons from minimum five neurons were analyzed for experiment (* $p < 0.05$; ** $p < 0.01$ versus control, ANOVA). **d** The exo/endocytotic assay was performed at DIV14 on wild-type and BAC hG2019S cortical neurons infected at DIV4 with virus expressing GFP. Cycling SV appears as synaptotagmin (s-tagmin) positive clusters along neuron processes. Total SV pool was revealed by staining with anti-synaptophysin antibodies upon fixation and permeabilization. Images show signals acquired for synaptotagmin, synaptophysin and their superimposition plus GFP (merge). Panel size is 28 × 4 μm. (e) The percentage of s-tagmin and s-physin positive clusters within the totality of s-physin positive clusters reflects the pool of cycling vesicles. Data are expressed as mean ± SEM, $n = 4$, at least 7 neurons were analyzed for experiment (** $p < 0.01$ Student's *t*-test)

previously demonstrated that LRRK2 interacts with the vesicle fusing ATPase NSF through its WD40 domain [21].

We first confirmed LRRK2 and NSF interaction at the endogenous level in synaptosomal preparations. Using co-immunoprecipitation with endogenous proteins from

rat synaptosomes, we observed that LRRK2 efficiently co-precipitates NSF (Fig. 2a). Next, we dissected the domain(s) of NSF involved in binding LRRK2. To this aim, we cloned human full-length NSF (aa 1–744) and its different domains, namely N domain (aa 1–205), D1 domain (aa 206–487) and D2 domain (aa 488–744) in fusion with a N-terminal Flag-tag and purified the proteins from HEK293T cells. Proteins bounds to Flag-conjugated beads were adjusted to equal molar concentrations and subsequently incubated with a mouse brain lysate. As shown in Fig. 2b, full-length NSF pulls-down endogenous LRRK2. Interestingly, N and D2 domains, but not D1, also pull-down endogenous LRRK2 (Fig. 2b). To further confirm the interaction between LRRK2 and NSF, we used size exclusion chromatography (SEC) to fractionate HEK293T lysates expressing Flag-NSF or co-expressing Flag-NSF and 2xMyc-LRRK2, followed by dot blot analysis. As shown in Fig. 2c, NSF elutes between 11 and 17.5 mL. Interestingly, in the presence of LRRK2, NSF elution profile shifts toward shorter retention times (elution peak between 10 and 16.5 mL) suggesting the formation of a complex with higher molecular weight than NSF alone (Fig. 2c). We also evaluated the cellular localization of endogenous NSF and LRRK2 in primary neuronal cultures and found that the two proteins largely co-localize, and co-localization is enriched within clusters along the neurites (Fig. 2d). Collectively these data indicate that LRRK2 and NSF form a complex in the cell.

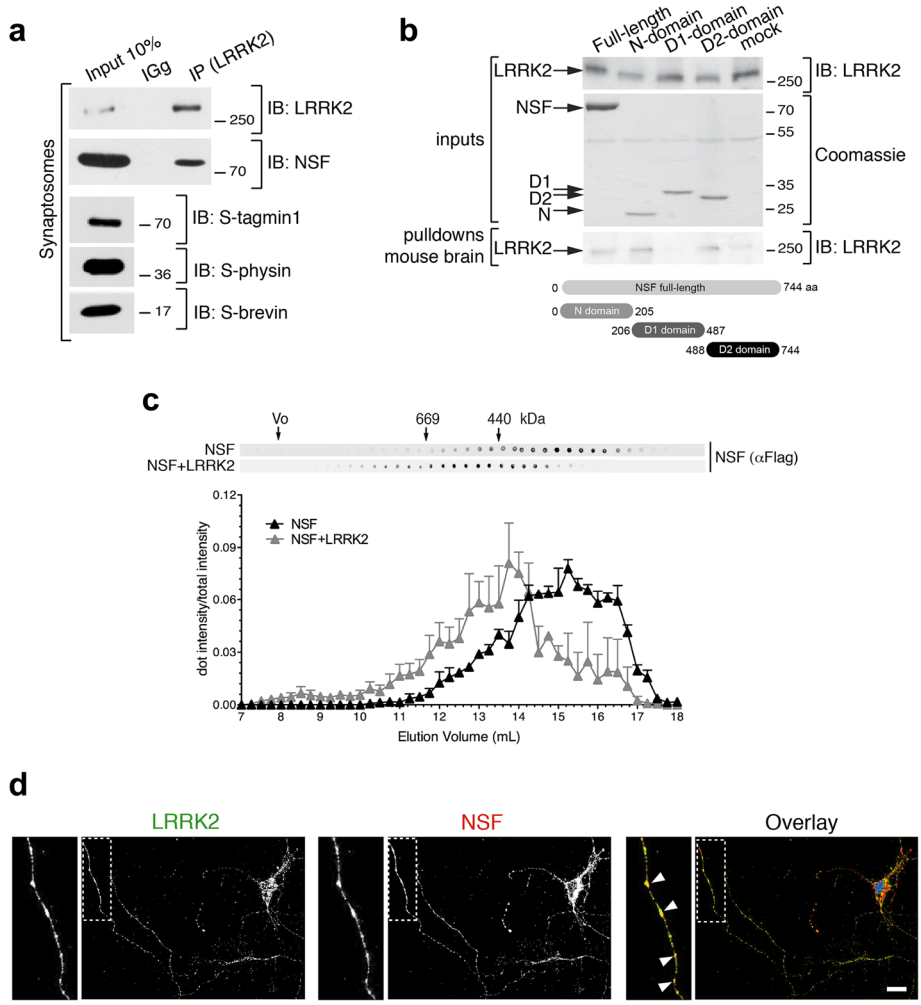

Fig. 2 LRRK2 interacts with NSF. **a** Extracts of purified cortical synaptosomes were incubated with anti-LRRK2 antibodies or rabbit IgG. The immunocomplexes were sedimented with protein G-Sepharose and the samples were resolved by SDS-PAGE and analyzed by immunoblotting with anti NSF and anti LRRK2 antibodies. Immunoblotting against synaptotagmin 1 (S-tagmin1), synaptophysin (S-physin) and synaptobrevin (S-brevin) were performed to confirm purity of synaptosomal preparation. **b** Flag-NSF full-length or domains (N, D1, D2) purified from HEK293T and bound to M2 flag resin were incubated with a mouse brain lysate. Samples were subjected to immunoblotting using anti-LRRK2 (MJFF2) or stained with Coomassie to show flag inputs. **c** Size exclusion chromatography fractions of HEK293T expressing ectopic flag-NSF alone or together with 2xMyc-LRRK2 spotted onto nitrocellulose membrane and probed with anti-flag antibody ($n = 3$ independent experiments). **d** Immunofluorescence of primary cortical neurons stained for endogenous LRRK2 and endogenous NSF (scale bar is 10 μm)

LRRK2 phosphorylates NSF in D2 domain

LRRK2 affects SV dynamics *via* its kinase activity (Fig. 1a–c) [22]. Therefore, we hypothesized that NSF could be a substrate of LRRK2 and, as such, be involved in the LRRK2 kinase dependent regulation of SV. To test this hypothesis, we performed in vitro kinase assays using recombinant LRRK2 and NSF purified from mammalian cells. We first validated recombinant human NSF biochemically. NSF purified as described in the methods section folds into hexamers when loaded with 1 mM ATP as evidenced by negative-stain transmission electron microscopy (TEM) (Additional file 1: Figure S2a). Of interest, Flag-tagged NSF purified with Flag affinity resin co-precipitates endogenous NSF as indicated by the presence of a band corresponding to endogenous NSF (Additional file 1: Figure S2b), further supporting the notion that Flag-NSF forms oligomers. To verify that purified NSF is functional, we measured ATP to ADP hydrolysis rate by isocratic reverse-phase HPLC (Additional file 1: Figure S2c-d) and malachite green colorimetric assay (Additional file 1: Figure S2e). NSF efficiently hydrolyzes ATP to ADP over time under these purification and assay conditions.

Having validated recombinant human full-length NSF, we next purified soluble 3xFlag-LRRK2 wild-type, the hyperactive clinical mutant G2019S and the kinase dead K1906M from HEK293T cells and subsequently incubated these purified proteins with full-length NSF in kinase assay conditions [31]. As shown in Fig. 3a, at a 1:10 ratio of LRRK2:NSF, we observe robust phosphorylation of NSF by LRRK2. Importantly, in the presence of LRRK2 K1906M or upon addition of 1 μM LRRK2 IN-1 inhibitor, NSF phosphorylation corresponds to the background levels observed for NSF alone, confirming that the incorporation of

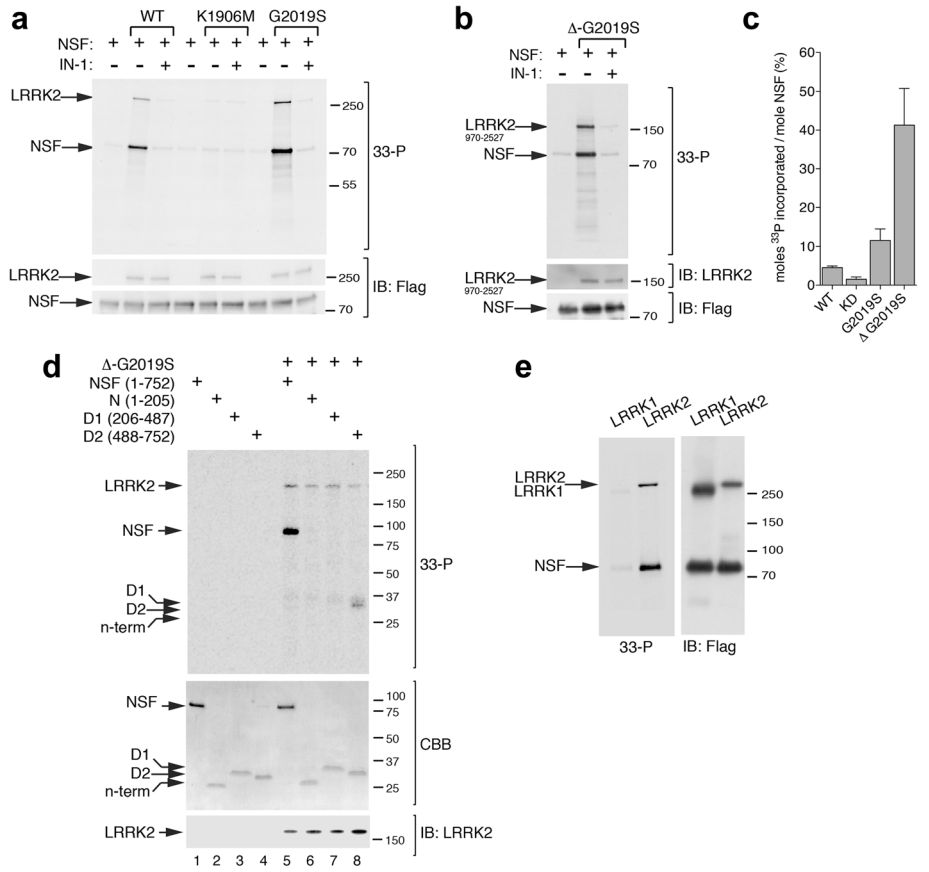

Fig. 3 LRRK2 phosphorylates NSF. **a** In vitro radioactive kinase assays of 3x-Flag LRRK2 wild-type, K1906M (kinase dead) and G2019S (hyperactive) and flag-NSF purified from HEK293T cells at 1:10 ratio. Radioactivity incorporated was revealed by autoradiography (*upper panel*) and total proteins loaded by flag immunoblotting (*lower panels*). LRRK2 inhibitor IN-1 was used at 1 μM concentration to confirm LRRK2 specific phosphorylation on NSF. **b** In vitro kinase assays as in (a) with the hyperactive GST-LRRK2$^{970–2527}$ fragment. **c** Quantification of moles of ^{33}P incorporated by NSF using a calibration curve with known concentration of ^{33}P-ATP. **d** In vitro kinase assays as in (a) using NSF full-length or domains as substrates of LRRK2 GST-LRRK2$^{970–2527}$ kinase activity at 1:10 ratio LRRK2:NSFs. Radioactivity incorporated was revealed by autoradiography (*upper panel*) and total proteins loaded by coomassie brilliant blue (CBB) staining for NSF (*middle panel*) or LRRK2 immunoblotting (*lower panel*). **e** In vitro radioactive kinase assays of 3xFlag-LRRK1 or 3xFlag-LRRK2 and Flag-NSF as substrate at 1:10 ratio. Left panel is an example of autoradiography and *right panel* represents the corresponding immunoblot of total loading

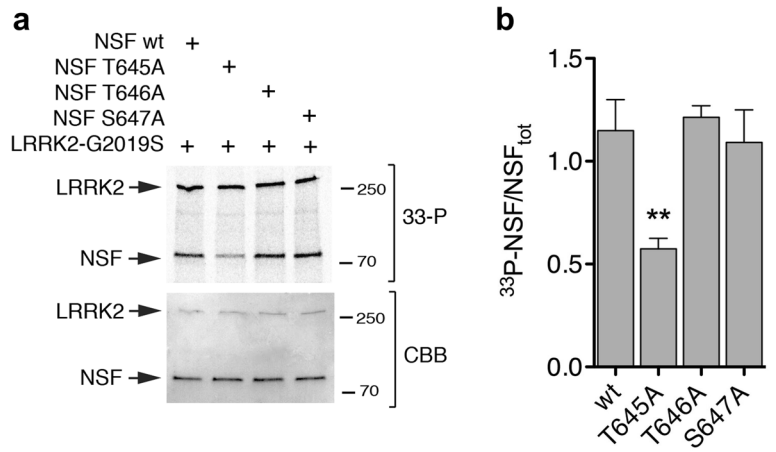

Fig. 4 LRRK2 phosphorylates NSF at T645. **a** In vitro kinase assays with 3xFlag-LRRK2 G2019S and NSF wild-type or non-phosphorylatable mutants T645A, T646A and S647A mutants at 1:10 ratio LRRK2:NSF. The G2019S hyperactive mutant was used to maximize ^{33}P incorporation. **b** Quantification of ^{33}P incorporated by NSF (autoradiography, *upper panel*) controlled for total NSF (NSF$_{TOT}$, coomassie staining, *lower panel*) from $n = 4$ independent experiments (bars represent the mean ± SEM). One way-ANOVA with Bonferroni's post-test (**$p < 0.01$)

radioactive phosphate is genuinely due to LRRK2 kinase activity (Fig. 3a). We confirmed LRRK2-mediated phosphorylation of NSF using the hyperactive G2019S-LRRK2$^{970–2527}$ fragment (Fig. 3b). The stoichiometry of phosphate incorporation, measured using a calibration curve with different concentrations of ^{33}P-ATP, is approximately 0.04 moles of phosphate per mole of monomeric NSF in the presence of LRRK2 wild-type, 0.1 in the presence of G2019S and 0.4 with an artificial truncated variant characterized by higher activity, G2019S-LRRK2$^{970–2527}$ (Fig. 3c). The low value for this stoichiometry, when taken in the context of a hexameric NSF complex, is sufficient to imply the presence of at least one phosphorylated monomer per hexamer. The reaction reached a plateau after 1-hour incubation (Additional file 1: Figure S3a-b), likely due to inactivation of LRRK2 under assay conditions as previously reported [32].

To define the region(s) of NSF phosphorylated by LRRK2, we performed kinase assays in the presence of NSF full-length or isolated domains. While we failed to detect any phosphorylation when N and D1 domains were incubated with G2019S-LRRK2$^{970–2527}$, we were able to measure phosphate incorporation in the D2 domain (Fig. 3d). Importantly, NSF is not a substrate of the cognate protein LRRK1 under these assay conditions (Fig. 3e), suggesting that this phosphorylation event is specific to LRRK2. *In toto*, these results indicate that LRRK2 likely phosphorylates the D2 domain of NSF.

LRRK2 phosphorylates NSF at threonine 645

We next set out to identify NSF phosphorylation site(s) targeted by LRRK2. To achieve this, we used phosphopeptide enrichment coupled with liquid chromatography/tandem mass spectrometry (LC-MS/MS) analysis on purified NSF pretreated with alkaline phosphatase to eliminate possible cellular phosphorylation sites, and subsequently phosphorylated by LRRK2 in vitro. Under the experimental conditions used, we were able to achieve ≈ 80 % NSF sequence coverage (Additional file 1: Figure S4a) and identified the peptide ^{639}KLLIIGTTSR^{648} as a *bona fide* phospho substrate. The MS analysis could not discriminate whether single/multiple phosphorylation occurred at T645, T646 or S647 or whether these sites may be multi-phosphorylated (Additional file 1: Figure S4b). This phosphopeptide was enriched following incubation with wild-type and G2019S LRRK2, but not in control samples (LRRK2 kinase dead or in the presence of 1 μM IN-1) indicating it contains specific LRRK2 phosphorylation site(s). We next validated the MS data by site-direct mutagenesis and in vitro kinase assays. Wild-type and phospho-deficient NSF mutants T645A, T646A and S647A were expressed and purified in HEK293T cells and subsequently incubated in vitro with catalytically active LRRK2 under phosphorylation permissive conditions. T645A displayed ~50 % reduction of ^{33}P incorporation compared to NSF wild-type, T646A and S647A (**$p < 0.01$, One-Way ANOVA with Bonferroni's post-test) (Fig. 4). Since NSF is also phosphorylated by PKC but within a different residue (S237) [26], we next assessed whether PKC is able to phosphorylate NSF at T645 to rule out any promiscuous effect. As shown in Additional file 1: Figure S5, we confirm that PKC efficiently phosphorylates NSF in vitro, but NSF^{T645A} exhibits similar ^{33}P incorporation as NSF wild-type, suggesting that T645 is a LRRK2 specific phospho-site. Overall, our data indicate that T645 is a LRRK2 phosphorylation site within NSF.

LRRK2-mediated phosphorylation increases NSF ATPase activity

We next investigated whether LRRK2 mediated phosphorylation of NSF has a functional consequence on its ATPase activity. We first identified the optimal detergent concentrations at which both LRRK2 and NSF display maximal catalytic activity (0.007 % of polysorbate 20, the critical micelle concentration of the detergent; Additional file 1: Figure S6). Subsequently, full-length NSF was exposed to LRRK2-G2019S$^{970–2527}$ or buffer in kinase assays conditions (with 50 μM ATP to minimize interference with the subsequent ATPase assay) for 30 min. As shown in Fig. 5a, NSF phosphorylated by LRRK2 exhibits increased ATPase activity ($K_m = 355 \pm 50$ μM; $k_{cat} = 40 \pm 11$ min^{-1}; $V_{max} = 0.95 \pm 0.22$ μmol/min, from $n = 4$ independent purifications) compared to unphosphorylated NSF ($K_m = 178 \pm 12$ μM; $k_{cat} = 19 \pm 4$ min^{-1}; $V_{max} = 0.37 \pm 0.07$ μmol/min, from $n = 4$ independent purifications). Given that we identified threonine 645 as a *bona fide* LRRK2 target, we next assessed the ATPase activity of NSF^{T645A}, along with NSF wild-type, NSF^{T646A} and NSF^{S647A}, pre-treated with LRRK2-G2019S$^{970–2527}$ or buffer control in kinase assay conditions. As shown in Fig. 5b, NSF^{T645A} displays impaired ability to hydrolyze ATP and, importantly, activity could not be restored when NSF^{T645A} is pre-phosphorylated by LRRK2. Interestingly, the neighboring T646 mutated to alanine also exhibits impaired ATPase activity that cannot be recovered by LRRK2 phosphorylation, whereas NSF^{S647A}, two residues apart from T645, displays ATPase activity similar to wild-type, and this activity is enhanced by LRRK2 phosphorylation. These results strongly indicate that T645 and T646 are critical for NSF catalytic activity. To rule out that NSF^{T645A} impaired activity was due to partial unfolding, we used circular dichroism (CD) and fluorescence spectroscopy to compare the secondary structures of NSF wild-type and NSF^{T645A}. Tryptophan fluorescence is similar among wild-type and NSF^{T645A} (Additional file 1: Figure S7a). CD spectra also confirm that the overall folding is maintained (Additional file 1: Figure S7b). In addition, TEM imaging confirms that NSF^{T645A} retains the ability to form hexamers (Additional file 1: Figure S7c). Taken together, these data indicate that NSF phosphorylated by LRRK2 possesses enhanced ATPase activity and T645 is a crucial site for enzymatic catalysis.

LRRK2-mediated phosphorylation of NSF increases the rate of SNARE complex disassembling

NSF-mediated ATP hydrolysis promotes disassembly of the SNARE complex [33]. Given that NSF phosphorylation by LRRK2 increases its ATPase activity (Fig. 5), we next postulated that this also impacts upon the rate of SNARE complex dissociation. To test this, we monitored the kinetic of SNARE complex disassembling in vitro as previously described [34, 35]. We co-expressed in *E. coli* recombinant soluble syntaxin, SNAP-25 and 6xHis-VAMP and purified the assembled complex by IMAC affinity purification followed by size exclusion chromatography [35]. As shown in Additional file 1: Figure S8, the complex elutes as single band corresponding to the expected molecular weight for the soluble SNARE complex (68 kDa), which is dissociated into the three SNARE components upon heating. To assess whether LRRK2 phosphorylation on NSF impacts the rate of SNARE complex disassembling in vitro, we incubated SNARE complex (480 nM) with 1.5 μM of alpha-SNAP, an essential co-factor, and 24 nM of NSF (phosphorylated or not by LRRK2) in the presence of 2 mM of ATP, and

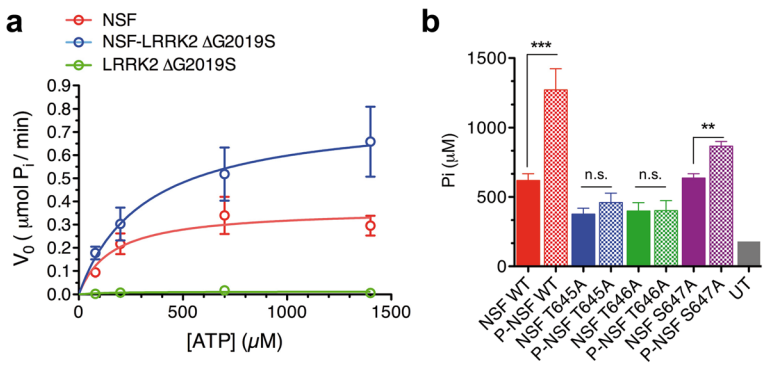

Fig. 5 Phosphorylated NSF exhibits enhanced ATPase activity. **a** NSF ATPase activity was assessed with a Malachite green assays at 36nM NSF and increasing concentrations of ATP substrate (up to 1.4 mM) in the presence of NSF alone, NSF pre-phosphorylated by LRRK2-G2019S$^{970–2527}$ (ΔG2019S) or LRRK2-G2019S$^{970–2527}$ (ΔG2019S) alone (NSF:LRRK2 20:1). Data were fitted with the Michaelis-Menten kinetic model to determine kinetic constants. **b** Phosphate generated by ATP hydrolysis in the presence of NSF wild-type, NSF^{T645A} NSF^{T646A} NSF^{S647A} pre-phosphorylated or not by ΔG2019S was measured with the Malachite Green Assay at 120 min with an initial concentration of ATP of 1.4 mM (NSF^{WT} vs NSF^{T645A} $^{**}p < 0.01$; NSF^{WT} vs P-NSF^{WT} $^{***}p < 0.001$; NSF^{T645A} vs P-NSF^{T645A} $p > 0.05$, non significant, n.s.; NSF^{T646A} vs P-NSF^{T646A} $p > 0.05$, n.s.; NSF^{S647A} vs P-NSF^{S647A} $^{**}p < 0.01$; one-way ANOVA, Bonferroni's post-test, $n \geq 3$). UT = untrasfected cells subjected to Flag-affinity purification to monitor background activity ($n = 1$; excluded from the statistical analysis)

subsequently analyzed the kinetic of SNARE complex disappearance over 150 min. Under these assay conditions, NSF phosphorylated by LRRK2 displayed a markedly increased efficiency in disassembling SNARE complex compared to non-phosphorylated NSF (Fig. 6a–b). These data further support the notion that LRRK2-mediated phosphorylation increases NSF catalytic activity with consequent acceleration of the disassembly of SNARE complexes in vitro.

Discussion

Identification of heterologous substrates of LRRK2 kinase activity is essential for understanding the cellular pathways deregulated in PD caused by mutations in this gene [3]. Here we provided evidence that the presynaptic ATPase NSF is a substrate of LRRK2 kinase activity, and that phosphorylated NSF displays enhanced ATP hydrolysis and SNARE complex dissociation activity in vitro.

Multiple lines of evidence support a role of LRRK2 at the presynaptic compartment. We previously found that LRRK2 controls SV storage and mobilization within the recycling pool [20] and that this process is dependent on LRRK2 kinase activity [22]. Synaptosomes treated with LRRK2 inhibitors exhibit decreased evoked glutamate release [22] whereas elevated glutamate release and synaptic transmission were observed in LRRK2 G2019S knock-in mice [16]. Altogether, these data indicate that LRRK2 kinase may play an important role in modulating a step of the exo-endocytic pathway. LRRK2 is a complex kinase with several protein interaction domains, which was shown to assemble multiprotein complexes during signal transduction [11]. At the presynapse, LRRK2 interacts with several proteins [21]. Moreover, accumulating literature suggests that LRRK2 regulates SV dynamics *via* phosphorylation of presynaptic proteins, such as Snapin, and EndophilinA [36–38]. The present work provides evidence that NSF is not only an interactor but also a substrate of LRRK2 in vitro. Recently, another LRRK2 interactor, the ribosomal protein s15, has been shown to serve as LRRK2 substrate [39], further emphasizing the value of examining LRRK2 interacting proteins as potential kinase substrates.

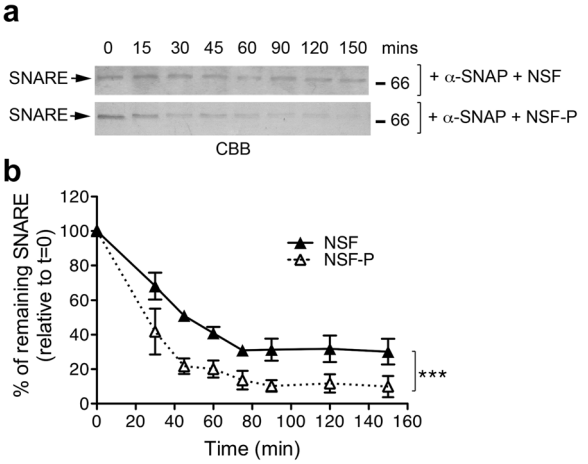

Fig. 6 Phosphorylated NSF exhibits increased rate of SNARE complex disassembling in vitro. **a** Representative coomassie gels (CBB, coomassie brilliant blue) of SNARE complex incubated for increasing time with NSF phosphorylated or not by LRRK2-G2019S$^{970–2527}$ in the presence of the co-factor alpha-SNAP. **b** Quantification of $n = 3$ independent experiments. Time points are relative to t = 0 which was set at 100 % (two-way ANOVA with Bonferroni's post-test, ***$p < 0.001$)

Here, we demonstrated that LRRK2 phosphorylates NSF at T645. The functional consequence of this is that NSF hydrolyses ATP faster when phosphorylated by LRRK2 at this residue. The physiological relevance of this finding is further supported by the observed increased rate of SNARE complex disassembling in the presence of phosphorylated NSF. Indeed, we found T645A is characterized by a reduced endogenous ATPase activity. Given that T645 is located within the D2 domain of NSF, which is thought to be important for NSF oligomerization *via* ATP binding [40], these results are consistent with our current understanding of NSF function. Specifically, T645 is part of the beta strand S4 (aa 639–646), which stabilizes the hexamer through interaction with the neighboring alpha-helix H5 [41]. Therefore, T645 is predicted to be a key residue for protein oligomerization, which impacts the ability of the D1 domain to hydrolyze ATP. Clearly, further investigation is merited to determine whether LRRK2 phosphorylation at T645 directly alters NSF oligomerization.

Translating these findings into the neuronal context, these data imply that LRRK2 may play a role in tuning the kinetics of SV fusion by accelerating SNARE complex dissociation *via* NSF phosphorylation. Previous studies reported NSF as substrate of other serine-threonine kinases: NSF is phosphorylated by Pctaire1 at S569 in the D2 domain, and this phosphorylation reduces NSF oligomerization [25]; NSF is also phosphorylated by PKC in vitro at Ser-237 of the catalytic D1 domain which negatively regulate NSF binding to alpha-SNAP-SNARE complexes (Additional file 1: Figure S5) [26]. Therefore, both Pctaire1 and PKC appear to switch off NSF activity. In our current study, we report multiple strands of evidence that suggest that NSF phosphorylated by LRRK2 is more active in vitro, however it is still unknown whether this is replicated in vivo. Wild-type LRRK2 is characterized by a low basal activity that may become pathologically relevant in the presence of gain of function mutations. We predict that in the presence of pathological hyperactive LRRK2 variant, SV endocytosis may be abnormally fast. Such alteration could result in 1) increased neurotransmitter release or 2) impaired

neurotransmitter release by accelerating SV endocytosis. While the second hypothesis would fit with the reduced dopamine release observed in mice expressing LRRK2 G2019S selectively in midbrain dopaminergic neurons [42], increased glutamate release has been reported in G2019S knock-in neurons [16] – consistent with the first hypothesis. Thus, additional research is needed to clearly identify the best representative model of LRRK2 function and dysfunction in the neuron.

We also provide robust evidence that the kinase activity of LRRK2 affects SV dynamics using two complementary models: LRRK2 inhibition and hyperactive LRRK2 (BAC hG2019S) in primary cortical neurons. The strong impairment of SV exo-endocytosis observed in the presence of pharmacological inhibition (Fig. 1, [22]) suggests that a consequence of therapeutic LRRK2 kinase inhibition might be alterations in the biology of the presynaptic compartment, likely impairing neurotransmitter release and synaptic function. These observations, together with the reported side effects in peripheral organs [43] suggest that additional strategies should be considered to target pathological LRRK2 function.

Conclusions

In the present study, we report LRRK2 kinase as a positive regulator of NSF activity and SNARE complex disassembling in vitro. Future studies should also be directed at understanding whether this phosphorylation is relevant in the pathogenesis of PD.

Methods

Animals, neuron cultures and drugs

Housing and handling of mice were carried out in compliance with the guidelines established by the European Community Council (Directive 2010/63/EU of March 4th, 2014) and approved by the Italian Ministry of Health (IACUC 625). Non-transgenic wild-type and LRRK2 BAC hG2019S mice, back-crossed on a C57BL/6J strain, were obtained from Mayo Clinic (Jacksonville, FL, USA) through a collaboration with Dr. Heather Melrose [28]. Animals were kept following guidelines of Ministry of Education, Universities and Research (MIUR). Neuron cultures were prepared from either mouse cortexes or hippocampi obtained from embryonic day 15.5–16.5 mice (C57BL/6 J). High-density (750–1000 cells/mm^2) and medium-density (150–200 cells/mm^2) neuron cultures were plated and grown as described on 12-well plastic tissue culture plates (Iwaki; Bibby Sterilin Staffordshire, UK) or on 12 mm diameter coverslips put into 24-well plastic tissue culture plates (Iwaki) [44]. GSK-2578215A compound (Tocris Bioscience, Bristol, UK) or DMSO were added to culture media at the concentrations indicated through the text. For immunocytochemistry, primary cultured neurons were fixed with 4 % paraformaldehyde and probed with primary rabbit anti-NSF (1:200, D31C7, Cell Signaling, Danvers, MA, USA) and mouse anti-LRRK2 (1:200 N231B/34, NeuroMab, Davis, CA, USA) and secondary anti-mouse Alexa Fluor 488 and anti-rabbit Alexa Fluor 568 (Thermo Fisher, Waltham, MA USA).

Plasmids and constructs

pCHMWS 3xFlag-tagged LRRK2 wild-type, K1906M and G2019S, 2x-Myc LRRK2 constructs have been previously described [31]. NSF constructs (full-length and domains) were cloned into p3XFLAG-CMV-7.1 vector (Sigma-Aldrich, St. Louis, MO, USA). NSF domains were amplified using forward primers with NotI overhang and reverse primers with KpnI overhang as following:

N-Domain (1–205): forward 5′ -AAGCTTGCGGCCGC CTTCGCGGGCCGGAGC-3′ and reverse 5′ -TCGAC TGGTACCTTAGCGATTTTCCTTGGTTTT-3′
D1 domain (206-477aa): forward 5′ -AAGCTTGCGGC CGCCCAATCAATTATCAATC-3′ and reverse 5′ -TC GACTGGTACCTTATCTCGTCACTTGCAGGC-3′
D2 domain (478-744aa): forward 5′ -AAGCTTGCGGC CGCCGGAGACTTCCTTGCTTC-3′ and reverse 5′ -TCGACTGGTACCTCAATCAAAATCAAGGGG-3′ .

NSF mutants were generated using the QuickChange mutagenesis kit (Agilent Technologies, CA, USA) according to the manufacturer's instructions. All plasmids were validated by restriction analysis and DNA sequencing.

Cell culture and transfection

Human embryonic kidney cells (HEK293T) were cultured in Dulbecco's modified Eagle's medium (DMEM, Thermo Fisher, Waltham, MA USA) supplemented with 10 % fetal bovine serum (FBS, Thermo Fisher, Waltham, MA USA) at 37 °C and 5 % CO_2. HEK293T were transiently transfected using linear polyethylenimine (PEI, Polysciences) with ratio DNA:PEI 1:2. 40 μg of DNA were dissolved in 1 ml of OPTI-MEM (Thermo Fisher, Waltham, MA USA) and 80 μl of PEI (40 μM) were added to 1 ml of OPTI-MEM. After 5 min of incubation the two solutions were mixed together and incubated for 20 min to allow the formation of DNA/PEI complexes. Then, the mix was added directly to the cells in Petri dishes of 15 cm^2 and used after 48–72 h.

Antibodies, SDS-PAGE and western blot analysis

Antibodies used for western blotting were as follows: anti-Flag M2 (1:10000, Sigma-Aldrich, St. Louis, MO, USA); anti-NSF (1:500, Cell Signaling, Danvers, MA, USA); anti-LRRK2 (1:1000, C41-2, Abcam, Cambridge, UK); anti-Synaptobrevin, anti-synaptophysin and anti-

Synaptotagmin 1 (1:1000, Synaptic System, Göttingen, Germany).

Between 10 and 20 μg of protein samples were dissolved in 4–20 % Tris-glycine polyacrylamide gels (Biorad) in SDS/Tris-glycine running buffer. Precision Plus molecular weight markers (Biorad) were used for size estimation. Solubilized proteins were then transferred to polyvinylidenedifluoride (PVDF) membranes in transfer buffer containing 10 % methanol. The PVDF sheets were blocked in Tris-buffered saline plus 0.1 % Triton (TBS-T) plus 5 % nonfat dry milk for 1 h at 4 °C and then incubated overnight at 4 °C with primary antibody in TBS-T plus 5 % non-fat dry milk. The PVDF membranes were washed in TBS-T (3 × 10 min) at room temperature (RT) followed by incubation for 1 h at RT with horseradish peroxidase-conjugated anti-mouse IgG. Blots were then washed in TBS-T (4 × 10 min) at RT and rinsed in TBS, and immunoreactive proteins were visualized using enhanced chemiluminescence plus (ECL +, GE Healthcare, Waukesha, WI, USA). Densitometric analysis was carried out using Image J software.

Protein purification

Human NSF with a N-terminal Flag tag or NSF domains were purified from HEK293T cells after transient transfection as described above. Cells were resuspended in 1 ml of a lysis buffer (20 mM Tris–HCl pH 7.5, 150 mM NaCl, 1 mM EDTA, 2.5 mM $Na_4P_2O_7$, 1 mM beta-glycerophosphate, 1 mM Na_3VO_4, Protease Inhibitor Mixture (Sigma-Aldrich, St. Louis, MO, USA)) and then lysed with 5 cycles of freezing and thawing in liquid nitrogen. The cell lysate was collected after centrifugation at 18000xg for 40 min at 4 °C. The supernatant was incubate overnight with 40 μl of Anti-Flag M2 Affinity gel (Sigma-Aldrich, St. Louis, MO, USA) at 4 °C. After centrifugation, the supernatant was discarded and the beads with human NSF were washed with 1 ml of different buffers: WB1 (20 mM Tris–HCl pH 7.5, 500 mM NaCl) twice, WB2 (20 mM Tris–HCl pH 7.5, 350 mM NaCl) twice, WB3 (20 mM Tris–HCl pH 7.5, 150 mM NaCl) six times. The protein was then eluted by incubating the beads with 200 μl of 20 mM Tris–HCl pH 7.5, 150 mM NaCl or directly in the kinase assay buffer (25 mM Tris–HCl pH 7.5, 5 mM beta-glycerophosphate, 2 mM DTT, 0,1 mM Na_3VO_4, 10 mM $MgCl_2$) with 150 ng/μl 3xFlag peptide and mixing the sample for about 2 h. The sample was centrifuged to pellet the resin and the supernatant was collected. Note that all the purification steps were carried out in the absence of detergent, a condition that resulted essential to maintain NSF folding and to detect specific phosphorylation by LRRK2. Purified human NSF was separated on SDS-PAGE and quantified by comparison with different concentrations of BSA (Bovine Serum Albumin). Proteins were electrophoretically resolved on 4–20 % Tris-glycine polyacrylamide gels (Biorad) using SDS/Tris-glycine running buffer. To estimate the molecular weight of proteins Precision Plus molecular weight marker (Biorad) was used. After the run, proteins were stained with Coomassie Brillant blue to enable the quantification with ImageJ software.

Synaptosomes preparation and immunoprecipitation

Brains from adult rats were quickly removed and the cerebral cortex dissected out at 4 °C. Purified synaptosomes were prepared on Percoll gradients (Sigma-Aldrich, St Louis, MO, USA) essentially according to Nakamura et al. with minor modifications [45]. Briefly, the tissue was homogenized in 14 volumes of 0.32 M sucrose, Tris–HCl pH 7.4, using a glass-teflon tissue grinder (clearance 0.25 mm, 12 up–down strokes in about 1 min). The homogenate was centrifuged (5 min, 1000 g at 4 °C) to remove nuclei and debris and the supernatant was gently stratified on a discontinuous Percoll gradient (2, 6, 10, and 20 % v/v in Tris-buffered sucrose) and centrifuged at 33,500 g for 5 min at 4 °C.

The layer between 10 and 20 % Percoll (synaptosomal fraction) was collected, washed by centrifugation and resuspended in RIPA buffer (NaCl 150 mM, Tris 50 mM (pH 7.4), NP40 (1%v/v), SDS (0.1%v/v) and protease inhibitors). To precipitate the immunocomplexes the extract was incubated for 2 h at RT with anti-LRRK2 antibodies (10 μg/sample; MJFF C41-2, Abcam, Cambridge, UK) or a control rabbit IgG (10 μg/sample; Sigma-Aldrich, St. Louis, MO, USA) conjugated with 25 μl of settled prewashed protein G-Sepharose beads (GE-Healthcare, Waukesha, WI, USA). The eluted proteins were separated by SDS-PAGE, transferred onto nitrocellulose membrane (GE-Healthcare, Waukesha, WI, USA) and analyzed by western-blotting with anti-LRRK2 and anti-NSF (Cell Signaling, Danvers, MA, USA) antibodies. Western-blotting with anti-synaptotagmin 1, anti-synaptophysin and anti-synaptobrevin were performed to confirm purity of synaptosomal preparation.

Pull-down assays

NSF domains and full length NSF were purified after transient transfection from HEK293T cells. Cells were harvested in 500 μl of Lysis buffer (50 mM Tris–HCl pH 7.5, 1 mM EDTA, 2.5 mM $Na_4P_2O_7$, 1 mM beta-glycerophosphate, 1 mM Na_3VO_4, 0.27 M Sucrose, 1 % Triton X-100, Protease Inhibitor Mixture (Sigma-Aldrich, St. Louis, MO, USA)). The cell lysate was then centrifuged at 18000xg for 30 min at 4 °C. Subsequently, the lysate was incubated overnight with 20 μl of Anti-Flag M2 Affinity gel (Sigma-Aldrich, St. Louis, MO, USA) at 4 °C. After centrifugation, the supernatant was discarded and the beads with NSF proteins were washed three times with 1 ml of a Washing buffer (50 mM

Tris–HCl pH 7.5, 1 mM EDTA, 0.27 M Sucrose, 250 mM NaCl, 0.02 % Triton X-100) and resuspended in 100 μl of the same buffer. Proteins were loaded on an SDS-PAGE gel and their concentration was quantified measuring the intensity of the band against known BSA standards with ImageJ software.

Proteins were subsequently adjusted to the same concentration (2 μM) and incubated with 600 μl mouse brain lysate (2.5 mg/ml concentrated) overnight at 4 °C. The day after, resins were boiled with sample buffer, loaded into a SDS-PAGE gel and transferred onto PVDF membranes.

Size Exclusion Chromatography (SEC) and dot blot analysis

Flag-NSF alone or Flag-NSF and 2xmyc-LRRK2 transfected HEK293T cells were lysed in 500 μl of lysis buffer containing 0.06 % (v/v) Triton X-100 and centrifuged. Cell lysates clarified were separated on a Superose 6 10/300 column (Ge Healthcare, Waukesha, WI, USA) pre-equilibrated with 20 mM Tris–HCl pH 7.5, 150 mM NaCl and 0.06 % (v/v) Triton X-100. The flow rate used was 0.5 ml/min. A calibration curve was produced using the following proteins and relative elution volumes: 7.5 ml for Blue Dextran (void volume), 11.5 ml for hemocyanin from *Carcinus aestuarii* (900 kDa), 12 ml for thyroglobulin (669 kDa), 14 ml for ferritin (440 kDa) and 12.5 ml for catalase (232 kDa). Fractions of 0.25 ml were collected and spotted onto a nitrocellulose membrane and analyzed by dot blot. The membrane was blocked with 10 % milk in TTBS and incubated with mouse monoclonal anti-Flag M2-peroxidase (Sigma-Aldrich, St. Louis, MO, USA) or anti-myc (Roche) in TTBS with 10 % milk. A secondary rabbit antibody (Sigma-Aldrich, St. Louis, MO, USA) was used to stain the anti-myc. Immunoproteins were visualized using ECL (GE, Healthcare, Waukesha, WI, USA).

Electron microscopy

Purified NSF proteins were incubated with 1 mM ATP and 2 mM $MgCl_2$. A total of 15 ng of protein was adsorbed few minutes to a glow-discharged carbon-coated copper grid, washed with deionized water, and stained with 1 % uranyl acetate. Images were collected using a Fei Tecnai T12 electron microscope equipped with a LaB6 filament and operated at an acceleration voltage of 100 kV.

In vitro kinase assay

Purified NSFs eluted in kinase assay buffer were incubated with LRRK2 proteins dissolved in kinase buffer for 1 h at 30 °C in the presence of ^{33}P-ATP (1 μCi) and 10 μM cold ATP as previously described [31].

Incorporated ^{33}P-ATP was detected by autoradiography or by Phospho-Imager system (Cyclone, Perkin-Elmer). The same membranes were probed with anti-Flag antibody for total protein loading and analyzed using ImageJ software.

SypHy assay

We infected DIV4 primary neurons with viruses expressing sypHy, a fusion construct of synaptophysin and super ecliptic pHluorin [29]. At DIV14 neurons were treated with DMSO (control) or GSK2578215A (0.2 μM, 2 h). Syphy positive boutons were assayed in a stimulation chamber on the stage of a Zeiss Axiovert 200 M equipped with a mono-chromator (Poly V) and a cooled CCD camera (PCO, Imago QE), both from TILL photonics (Gräfelfing, Germany). The assay was carried out as described previously [46]. Briefly, cells were submerged in 500 μl of KRH buffer (125 mM NaCl, 5 mM KCl, 1.8 mM $CaCl_2$ 2.6 mM $MgSO_4$ 5 mM Hepes, pH 7.2) in presence of APV (2 μM, Sigma-Aldrich, St. Louis, MO, USA) and CNQX (2 μM, Sigma-Aldrich, St. Louis, MO, USA). SypHy was excited at 475 nm and its fluorescence emission collected at 525 nm using a 60X, 1.1 NA water immersion objective. Images were acquired every second for 200 s using TillVision software (TILL Photonics). At frame 30, cells were stimulated with 40 action potential (AP, 20Hz) then at frame 70 with 300 AP (20 Hz). Total fluorescence was measured upon incubation with 50 mM NH_4Cl. Quantitative measurements of the fluorescence intensity at individual boutons were obtained by averaging a selected area of pixel intensities using ImageJ. Net fluorescence changes (ΔF) were obtained by subtracting the average intensity of the first 15 frames (F0) from the intensity of each frame (Ft) for individual boutons and normalized F0 (ΔF/F0). The fluorescence increase and decay, reflect exo- and endocytosis, respectively [29]. Both the fluorescence upstroke and decay were fitted with a single exponential τ ($\tau_{upstroke}$ and τ_{decay} respectively). Data are expressed as mean ± SEM and statistical significance was assessed by unpaired two-tailed Student's *t* test (GraphPad Prism).

Exo/endocytotic assay

The endocytosis assay to monitor SV recycling was performed using rabbit polyclonal antibodies directed against the intravesicular domain of synaptotagmin1 (Synaptic System), applied for 5 min at RT on the cultures, as described previously [30]. Incubations with the antibody (1:400) were performed in Tyrode solution containing 124 mM NaCl, 5 mM KCl, 2 mM $MgCl_2$, 30 mM glucose, 25 mM HEPES, pH 7.4 and 2 mM $CaCl_2$. After fixation and permeabilization, a synaptophysin counter staining with mouse anti synaptophysin,

1:400 (Sigma-Aldrich) visualized the totality of synaptic vesicles. Acquired images were processed and quantitatively analyzed with ImageJ software as previously described [47]. Briefly, cultures were infected at DIV4 with GPF expressing viruses and assayed at DIV14 as in [22]. GFP positive processes were manually tracked and the number of synaptotagmin and synaptophysin positive clusters and synaptophysin positive clusters present in the region of interest were automatically counted.

Proteins digestion

Approximately 2 μg of purified NSF pre-dephosphorylated with alkaline phosphatase (Promega) and subsequently phosphorylated or not with LRRK2 in the presence of 100 μM ATP were loaded into a SDS-precasted gel (Biorad). Gel slices corresponding to purified NSF were excised, cut in smaller pieces, dehydrated with 100 μl of acetonitrile (ACN) for 10 min, then dried under vacuum. A protein reduction step was performed with 100 μl of freshly prepared 10 mM Dithiothreitol (DTT, Fluka) in 50 mM NH_4HCO_3, at 56 °C. After 1 h DTT solution was discarded and 100 μl of a freshly prepared solution of 55 mM iodoacetamide (Sigma-Aldrich, St. Louis, MO, USA) in 50 mM NH_4HCO_3 was added to the gel pieces for 45 min at room temperature and in the dark. Gel pieces were washed 4 times (10 min each) alternating 100 μl of 25 mM NH_4HCO_3 and 100 μl of ACN, dried under vacuum, and suspended in 20 μl of a sequencing grade modified trypsin solution (Promega, 12.5 ng/mL in 25 mM NH_4HCO_3). Digestion was performed overnight at 37 °C. Peptides were extracted with three changes (50 μl each) of 50 % ACN/0.1 % formic acid (FA, Fluka). Samples were dried under vacuum and stored at −20 °C till the phosphopeptide enrichment procedure was performed.

Enrichment of phosphopeptides

Phosphopeptides were enriched with home made micro-columns of TiO_2 as previously described [48]. TiO_2 micro-columns were conditioned twice with 50 μl of ACN and twice with loading buffer (80 % ACN/6 % trifluoroacetic acid (TFA, Riedel-de Haën)). Samples were suspended in 50 μl of loading buffer and slowly loaded into the columns, which were then washed twice with 50 μl of loading buffer and twice with washing buffer (0.1 % TFA). Phosphopeptides bound to TiO_2 were eluted with 50 μl of freshly prepared 5 % NH_4OH and subsequently with 50 μl of 50 % ACN/0.1 % FA. Samples were immediately acidified by adding 5 μl of 100 % FA and dried under vacuum.

Mass spectrometry analysis

Mass spectrometry analysis of phosphopeptides was performed with a LTQ-Orbitrap XL mass spectrometer (Thermo Fisher Scientific) coupled online with a nano-HPLC Ultimate 3000 (Dionex-Thermo Fisher Scientific). Samples were dissolved in 30 μl of 3 % ACN/0.1 % FA and for every analysis 8 μl of sample were loaded at a flow rate of 8 μl/min into a trap column (300 mm I.D., 300 Å, C18, 3 mm; SGE Analytical Science). Samples were injected into a home-made 10 cm pico-frit capillary column (75 μm I.D., 15 μm tip; New Objective) packed with C18 material (Aeris Peptide 3.6 um XB-C18, Phenomenex). Peptides were separated using a linear gradient from 3 to 40 % of ACN/0.1 FA in 20 min at a flow rate of 250 nl/min.

To increase the confidence in the identification of phosphopeptides, the MS analysis of each sample was performed with three different acquisition methods, as reported in [49]. A MS^2 data dependent acquisition (1 full-MS scan in the range 300–1700 Da on the Orbitrap with a resolution of 60,000, followed by MS/MS spectra acquired in the linear ion trap for the ten most abundant ions); a MS^3 neutral loss-triggered dependent acquisition (one full-MS scan on the Orbitrap, followed by MS/MS scans on the three most intense ions and by MS^3 upon detection of neutral loss of phosphoric acid in MS^2 spectra); a Multi Stage Acquisition (MSA) (1 full-MS scan at a resolution of 60,000 followed by MS/MS scans on the three most abundant ions with the activation of neutral loss product without an additional isolation cycle).

Raw data files were analyzed with Proteome Discoverer software (version 1.4, Thermo Fisher Scientific) connected to a Mascot Server version 2.2.4 (Matrix Science, UK) and a SequestHT search engine version 28.0 (Thermo Fisher Scientific) against the Uniprot Human Database (version 2013.11.13 used by SequestHT, version 2014.04.16 used by Mascot). Trypsin was set as digesting enzyme with up to two missed-cleavages. Carbamidomethyl cysteine was set as fixed modification, while phosphorylation of Ser/Thr/Tyr and methionine oxidation were set as variable modifications. Peptide and fragment tolerance were 10 ppm and 0.6 Da respectively. Percolator was used to calculate False Discovery Rate (FDR) based on the search against the corresponding randomized database. MS/MS spectra of phosphopeptides were manually inspected for confirmation and assignment of phosphorylation sites.

ATPase enzymatic assay

NSF ATPase activity was quantified using the Malachite Green Assay by measuring the release of inorganic phosphate (Pi) due to the ATP hydrolysis with spectrophotometer. The assay was adapted from the method of Lanzetta et al. [50]. The Malachite Green Stock solution used for the assay was a mixture of two different solutions (one with 34 mg Malachite Green oxalate salt (Sigma-Aldrich. St. Louis, MO, USA) into 40 ml HCl 1 M and the other with 1 g $(NH_4)_2MoO_4$ (Sigma-

Aldrich, St. Louis, MO, USA) into 14 ml HCl 4 M to a final volume of 100 ml with distilled water and then filtered through 0,45 nm. The concentration of human NSF used for the ATPase assay was 216 nM (36 nM hexameric concentration) with different ATP concentration. Reaction was performed at 37 °C and followed for 120 min. The time point aliquots collected (20 μl) were mixed with 150 μl of Malachite Green stock solution until the solution became homogenous and the absorbance measured at 640 nm using a corresponding Malachite Green solution as blank. The values of absorbance were then converted into μmol of free Pi in solution using a standard curve. To reported values for the kinetic constants (K_m, k_{cat} and V_{max}) were obtained by data fitting with the Michaelis-Menten kinetic model (Y = Vmax*S/(Km + [S])).

Reverse-phase HPLC ATPase assay

To determine the ATPase activity of NSF, 500 or 700 μM ATP was added to 0.2 μM 3xFlag-NSF wt. Proteins were purified as previously described and incubated at 37 °C for 1 h in the same kinase buffers and conditions of the Malachite Green Assay. At the reported time-points, aliquots (20 μl) were taken up to 120 min and heated for 3 min at 95 °C with 0.1 M of EDTA to stop the reaction. Samples were stored at −80 °C. Reverse Phase High-Performance Liquid Chromatography (RP-HPLC) was used to monitor the amount of ATP and ADP present in the sample. Nucleotides were separated on a Jupiter 5u C4 300A (Phenomenex) column using an Agilent HP 1100 HPLC, pre-equilibrated with 50 mM NaH_2PO_4 pH 6.5, 10 mM Tetra-n-butylammonium bromide and 4 % ACN. The flow-rate used was 0.5 ml/min and the amount of the nucleotides was monitored measuring the increase in area of the peak corresponding to ADP measured at 256 nm with a total run time of 35 min. To convert this value to the Pi released by the reaction, a standard curve generated with different ADP concentration was used. ADP concentrations detected in the assay were plotted as a function of time and an equation was obtained through linear regression with GraphPad Prism 5.

Recombinant alpha SNAP and SNARE proteins production

Rat alpha-SNAP cloned in pET28 plasmid in fusion with a His-tag was a kind gift of Dr. Reinhard Jahn, Max-Planck-Institute, Göttingen). Alpha-SNAP was subsequently expressed in *E. Coli* in BL21(DE3) strain. Bacteria were grown at 37 °C to an OD at 600 nm of 0.4–0.6, then induced with 0.25 mM isopropyl β-D-1-thiogalactopyranoside (IPTG) for 4 h. Cells were then harvested by centrifugation and the pellet of 250 ml of culture was resuspended in 5–10 ml of Tris–HCl pH 8.0. Phenylmethylsulfonyl fluoride (PMSF) 100 μM and a cocktail of protease inhibitors were added to the cells 1:100 (v/v) that were subsequently subjected to one French Press cycles (Constant Systems Ltd). The cell homogenate was centrifuged and the supernatant loaded onto a Co^{2+} affinity column and eluted with a 0–500 mM linear gradient of imidazole at 0.5 ml/min. Protein solution was dialyzed versus Tris–HCl 20 mM pH 7.5, NaCl 150 mM.

Soluble SNARE complex was obtained by co-expression of wild type SNAP-25A, of syntaxin-1A and of His-tagged VAMP2(1–96) using the Duet expression system (Novagen) in *E. Coli* in BL21(DE3) strain. VAMP2(1–96)-His6-TEV pACYC-Duet and syntaxin-1A/SNAP-25A pET-Duet were a kind gift of Prof. A. Brunger (Stanford University, California) [34]. Bacteria were grown at 37 °C to an OD at 600 nm of 0.6–0.8, then induced with 0.5 mM IPTG for 4 h. Cell pellets of 250 ml of culture were suspended in 10 ml of 50 mM NaPi, pH 8.0, 300 mM NaCl, 20 mM imidazole and 0.5 mM Tris(2-carboxyethyl)phosphine (TCEP) (SNARE buffer), supplemented with PMSF 100 μM and protease inhibitors cocktail. Cell were lyses by two French Press cycles (Constant Systems Ltd) and the lysate was clarified by centrifugation for 1 h at 15,000 g at 4 °C. The supernatant was loaded onto a 1-ml Ni^{2+} affinity column, washed with 20 ml of SNARE buffer containing 7.5 M urea and then with 20 ml of SNARE buffer. The complex was then eluted with SNARE buffer containing 350 mM imidazole. After elution, SNARE complex was subjected to size exclusion chromatography using a Superdex 200 10/300 (GE Helthcare) that was equilibrated with 50 mM Tris–HCl, pH 7.5, 100 mM NaCl. The SNARE complex was checked and quantified by SDS-PAGE.

SNARE dissociation assay

As previously described [34] the SNARE dissociation assays were performed at 37 °C in 240 μl in a 1.5 ml micro-tube. The assay buffer was composed of 25 mM Tris–HCl pH 7.5, 5 mM β–glycerophosphate, 2 mM dithiotreitol (DTT), 0.1 mM Na_3VO_4, 10 mM $MgCl_2$ and 0.007 % polysorbate 20. Subsequently 1.5 μM αSNAP, 480 nM SNAREs, 24 nM NSF (hexameric concentration) phosphorylated or not by LRRK2 (ratio NSF:LRRK2 20:1) were added in the presence of 2 mM ATP to start the reaction. At defined time points, an aliquot (20 μl) was collected and loaded into an SDS-PAGE gel without boiling the samples: being the SNARE complex is SDS-resistant, it runs as a single band on SDS-PAGE gel. The intensity of each SNARE complex band was calculated and normalized to its time zero. The experiments were performed in triplicate up to 150 min of reaction.

Circular Dichroism (CD)

CD measurements were carried out on a JASCO J-810 spectropolarimeter interfaced with a personal computer. The CD spectra were acquired and processed using the J-700 software for Windows. All experiments were done at room temperature using an optical path length of 0.2 cm. The wavelength range of the measurements was 197–250 nm, using a bandwidth of 2 nm and a time constant of 8 s at a scan speed of 50 nm/min. The signal to noise ratio was improved by accumulating four scans. Spectra were acquired using purified proteins in the elution buffer (20 mM Tris–HCl pH 7.5, 150 mM NaCl and 0.007 % polysorbate-20) using the same buffer with 3xFlag peptide as a control. All the spectra are reported in terms of mean residue molar ellipticity (deg cm^2 $dmol^{-1}$). Protein concentrations in the samples were determined by SDS-PAGE and all the spectra were normalized for the measured protein concentration.

Intrinsic fluorescence

Fluorescence emission spectra were recorded on a Cary Eclipse fluorescence spectrophotometer (Varian, Agilent Technologies, Santa Clara, CA) using the Cary Eclipse program. Sample measurements were carried out using optical path length of 10 mm. Fluorescence spectra were obtained using an excitation wavelength of 288 nm, with an excitation bandwidth of 5 nm and slit width of 10 nm. Emission spectra were recorded between 300 and 400 nm at a scan rate of 30 nm/sec. Spectra were acquired using 80 nM proteins in 20 mM Tris/HCl buffer (pH 7.5), 150 mM NaCl and 0.02 % Tween 20.

Statistical analysis

All quantitative data are expressed as mean ± SEM and represent at least three independent sets of experiments. Significance of differences between two groups was assessed by two-tailed unpaired *t*-test or one-way or two-way ANOVA with Bonferroni's post-test when more than two groups were compared. Significance was set at $p < 0.05$.

Additional file

Additional file 1: Figure S1. Expression and phosphorylation of LRRK2 in primary cortical neurons subjected to SypHy assays. **Figure S2.** Biochemical validation of recombinant human NSF. **Figure S3.** LRRK2 phosphorylation of NSF occurs within the first 30 minutes. **Figure S4.** LC-MS/MS analysis of NSF phosphorylated by LRRK2. **Figure S5.** PKC does not phosphorylate NSF at T645. **Figure S6.** Evaluation of optimal detergent concentration for LRRK2 and NSF activities. **Figure S7.** NSF wild-type and T645A have similar overall folding and T645A forms hexamers. **Figure S8.** Expression and purification of SDS-resistant SNARE complex. (DOCX 2062 kb)

Abbreviations

NSF: n-ethylmaleimide sensitive fusion; LRRK2: leucine-rich repeat kinase 2; SNARE: soluble NSF-attachment protein receptor; PD: Parkinson's disease; ANOVA: analysis of variance; TBS: tris-buffered saline; SV: synaptic vesicles; sypHy: synaptophysin-pHluorin; CD: circular dichroism; MS: mass spectrometry; TEM: transmission electron microscopy; DIV: days in vitro.

Competing interests

The authors declare that they have no competing interests.

Authors' contributions

EB and AG performed and analyzed the kinase, ATPase and SNARE disassembling assays. MDC performed and analyzed the sypHy assay. AM performed the co-immunoprecipitation from synaptosomes. NP expressed and purified the SNARE complex. IR and LC helped with the in vitro experiments. SC cloned the NSF constructs. MPC measured LRRK2 steady state levels in primary neurons. CF and GA performed the LC-MS/MS. MB, LB, FO, GP and EG conceived the study, designed the experiments and analyzed the data. EG wrote the paper with contribution from all authors. All authors read and approved the final manuscript.

Funding

We would like to thank Dr. Patrick Lewis for proofreading the manuscript. This study was supported by the Michael J Fox Foundation (to EG, FO and GP). We also thank the financial support of Telethon - Italy (Grant no. GGP12237 to EG, FO and GP) and the University of Padova (Progetto di Ateneo CPDA 124045/12 to MB), Regione Lombardia (Projects MbMM-Convenzione No. 18099/RCC to GP) and Fondazione Grigioni per il morbo di Parkinson (GP). We gratefully thank Prof. Axel T. Brunger and Dr. Sandro Vivona for the kind gift of the soluble SNARE constructs. The authors wish to thank the "Cassa di Risparmio di Padova e Rovigo" (Cariparo) for funding the acquisition of the LTQ-Orbitrap XL mass spectrometer.

Author details

[1]Department of Biology, University of Padova, via Ugo Bassi 58/B, 35131 Padova, Italy. [2]San Raffaele Scientific Park & University Vita-Salute San Raffaele, Milan, Italy. [3]Department of Experimental Medicine, University of Genova, Genova, Italy. [4]Department of Biomedical Sciences, University of Padova, Padova, Italy. [5]Proteomics Center of Padova University, Padova, Italy. [6]IN-CNR Milano, Milano, Italy. [7]Present Address: Department of Cell and Developmental Biology, University College London, London WC1E 6BT, UK. [8]Present Address: Rheumatology Unit, Department of Medicine – DIMED, University Hospital of Padova, Padova, Italy.

Received: 24 July 2015 Accepted: 22 December 2015
Published online: 13 January 2016

References

1. Gasper R, Meyer S, Gotthardt K, Sirajuddin M, Wittinghofer A. It takes two to tango: regulation of G proteins by dimerization. Nat Rev Mol Cell Biol. 2009; 10(6):423–9. doi:10.1038/nrm2689.
2. Taymans JM. The GTPase function of LRRK2. Biochem Soc Trans. 2012;40(5): 1063–9. doi:10.1042/BST20120133.
3. Greggio E. Role of LRRK2 kinase activity in the pathogenesis of Parkinson's disease. Biochem Soc Trans. 2012;40(5):1058–62. doi:10.1042/BST20120054.
4. Paisan-Ruiz C, Jain S, Evans EW, Gilks WP, Simon J, van der Brug M, et al. Cloning of the gene containing mutations that cause PARK8-linked Parkinson's disease. Neuron. 2004;44(4):595–600. doi:10.1016/j.neuron.2004.10.023.
5. Zimprich A, Biskup S, Leitner P, Lichtner P, Farrer M, Lincoln S, et al. Mutations in LRRK2 cause autosomal-dominant parkinsonism with pleomorphic pathology. Neuron. 2004;44(4):601–7. doi:10.1016/j.neuron.2004.11.005.
6. Satake W, Nakabayashi Y, Mizuta I, Hirota Y, Ito C, Kubo M, et al. Genome-wide association study identifies common variants at four loci as genetic risk factors for Parkinson's disease. Nat Genet. 2009;41(12):1303–7. doi:10.1038/ng.485.
7. Simon-Sanchez J, Schulte C, Bras JM, Sharma M, Gibbs JR, Berg D, et al. Genome-wide association study reveals genetic risk underlying Parkinson's disease. Nat Genet. 2009;41(12):1308–12. doi:10.1038/ng.487.
8. Rudenko IN, Cookson MR. Heterogeneity of leucine-rich repeat kinase 2 mutations: genetics, mechanisms and therapeutic implications. Neurotherapeutics. 2014;11(4):738–50. doi:10.1007/s13311-014-0284-z.
9. Reynolds A, Doggett EA, Riddle SM, Lebakken CS, Nichols RJ. LRRK2 kinase activity and biology are not uniformly predicted by its autophosphorylation and cellular phosphorylation site status. Front Mol Neurosci. 2014;7:54. doi:10.3389/fnmol.2014.00054.

10. Alegre-Abarrategui J, Christian H, Lufino MM, Mutihac R, Venda LL, Ansorge O, et al. LRRK2 regulates autophagic activity and localizes to specific membrane microdomains in a novel human genomic reporter cellular model. Hum Mol Genet. 2009;18(21):4022–34. doi:10.1093/hmg/ddp346.
11. Beilina A, Rudenko IN, Kaganovich A, Civiero L, Chau H, Kalia SK, et al. Unbiased screen for interactors of leucine-rich repeat kinase 2 supports a common pathway for sporadic and familial Parkinson disease. Proc Natl Acad Sci. 2014;111(7):2626–31. doi:10.1073/pnas.1318306111.
12. Berger Z, Smith KA, Lavoie MJ. Membrane localization of LRRK2 is associated with increased formation of the highly active LRRK2 dimer and changes in its phosphorylation. Biochemistry. 2010;49(26):5511–23. doi:10.1021/bi100157u.
13. Biskup S, Moore DJ, Celsi F, Higashi S, West AB, Andrabi SA, et al. Localization of LRRK2 to membranous and vesicular structures in mammalian brain. Ann Neurol. 2006;60(5):557–69. doi:10.1002/ana.21019.
14. Hatano T, S-i K, Imai S, Maeda M, Ishikawa K, Mizuno Y, et al. Leucine-rich repeat kinase 2 associates with lipid rafts. Hum Mol Genet. 2007;16(6):678–90. doi:10.1093/hmg/ddm013.
15. Shin N, Jeong H, Kwon J, Heo HY, Kwon JJ, Yun HJ, et al. LRRK2 regulates synaptic vesicle endocytosis. Exp Cell Res. 2008;314(10):2055–65. doi:10.1016/j.yexcr.2008.02.015.
16. Beccano-Kelly DA, Kuhlmann N, Tatarnikov I, Volta M, Munsie LN, Chou P, et al. Synaptic function is modulated by LRRK2 and glutamate release is increased in cortical neurons of G2019S LRRK2 knock-in mice. Front Cell Neurosci. 2014;8:301. doi:10.3389/fncel.2014.00301.
17. Li X, Patel JC, Wang J, Avshalumov MV, Nicholson C, Buxbaum JD, et al. Enhanced striatal dopamine transmission and motor performance with LRRK2 overexpression in mice is eliminated by familial Parkinson's disease mutation G2019S. J Neurosci. 2010;30(5):1788–97. doi:10.1523/JNEUROSCI.5604-09.2010.
18. Li Y, Liu W, Oo TF, Wang L, Tang Y, Jackson-Lewis V, et al. Mutant LRRK2(R1441G) BAC transgenic mice recapitulate cardinal features of Parkinson's disease. Nat Neurosci. 2009;12(7):826–8. doi:10.1038/nn.2349.
19. Tong Y, Pisani A, Martella G, Karouani M, Yamaguchi H, Pothos EN, et al. R1441C mutation in LRRK2 impairs dopaminergic neurotransmission in mice. Proc Natl Acad Sci U S A. 2009;106(34):14622–7. doi:10.1073/pnas.0906334106.
20. Piccoli G, Condliffe SB, Bauer M, Giesert F, Boldt K, De Astis S, et al. LRRK2 controls synaptic vesicle storage and mobilization within the recycling pool. J Neurosci. 2011;31(6):2225–37. doi:10.1523/JNEUROSCI.3730-10.2011.
21. Piccoli G, Onofri F, Cirnaru MD, Kaiser CJ, Jagtap P, Kastenmuller A, et al. LRRK2 binds to neuronal vesicles through protein interactions mediated by its C-terminal WD40 domain. Mol Cell Biol. 2014;34:2147–61. doi:10.1128/MCB.00914-13.
22. Cirnaru MD, Marte A, Belluzzi E, Russo I, Gabrielli M, Longo F, et al. LRRK2 kinase activity regulates synaptic vesicle trafficking and neurotransmitter release through modulation of LRRK2 macro-molecular complex. Front Mol Neurosci. 2014;7:49. doi:10.3389/fnmol.2014.00049.
23. Sudhof TC, Rizo J (2011) Synaptic vesicle exocytosis. Cold Spring Harb Perspect Biol 3 (12). doi: 10.1101/cshperspect.a005637
24. Huynh H, Bottini N, Williams S, Cherepanov V, Musumeci L, Saito K, et al. Control of vesicle fusion by a tyrosine phosphatase. Nat Cell Biol. 2004;6(9):831–9. doi:10.1038/ncb1164.
25. Liu Y, Cheng K, Gong K, Fu AK, Ip NY. Pctaire1 phosphorylates N-ethylmaleimide-sensitive fusion protein: implications in the regulation of its hexamerization and exocytosis. J Biol Chem. 2006;281(15):9852–8. doi:10.1074/jbc.M513496200.
26. Matveeva EA, Whiteheart SW, Vanaman TC, Slevin JT. Phosphorylation of the N-ethylmaleimide-sensitive factor is associated with depolarization-dependent neurotransmitter release from synaptosomes. J Biol Chem. 2001;276(15):12174–81. doi:10.1074/jbc.M007394200.
27. Reith AD, Bamborough P, Jandu K, Andreotti D, Mensah L, Dossang P, et al. GSK2578215A; a potent and highly selective 2-arylmethyloxy-5-substitutent-N-arylbenzamide LRRK2 kinase inhibitor. Bioorg Med Chem Lett. 2012;22(17):5625–9. doi:10.1016/j.bmcl.2012.06.104.
28. Melrose HL, Dachsel JC, Behrouz B, Lincoln SJ, Yue M, Hinkle KM, et al. Impaired dopaminergic neurotransmission and microtubule-associated protein tau alterations in human LRRK2 transgenic mice. Neurobiol Dis. 2010;40(3):503–17. doi:10.1016/j.nbd.2010.07.010.
29. Granseth B, Odermatt B, Royle SJ, Lagnado L. Clathrin-mediated endocytosis is the dominant mechanism of vesicle retrieval at hippocampal synapses. Neuron. 2006;51(6):773–86. doi:10.1016/j.neuron.2006.08.029.
30. Matteoli M, Takei K, Perin MS, Sudhof TC, De Camilli P. Exo-endocytotic recycling of synaptic vesicles in developing processes of cultured hippocampal neurons. J Cell Biol. 1992;117(4):849–61.
31. Civiero L, Vancraenenbroeck R, Belluzzi E, Beilina A, Lobbestael E, Reyniers L, et al. Biochemical characterization of highly purified leucine-rich repeat kinases 1 and 2 demonstrates formation of homodimers. PLoS One. 2012;7(8):e43472. doi:10.1371/journal.pone.0043472.
32. Webber PJ, Smith AD, Sen S, Renfrow MB, Mobley JA, West AB. Autophosphorylation in the leucine-rich repeat kinase 2 (LRRK2) GTPase domain modifies kinase and GTP-binding activities. J Mol Biol. 2011;412(1):94–110. doi:10.1016/j.jmb.2011.07.033.
33. Zhao C, Slevin JT, Whiteheart SW. Cellular functions of NSF: not just SNAPs and SNAREs. FEBS Lett. 2007;581(11):2140–9. doi:10.1016/j.febslet.2007.03.032.
34. Cipriano DJ, Jung J, Vivona S, Fenn TD, Brunger AT, Bryant Z. Processive ATP-driven Substrate Disassembly by the N-Ethylmaleimide-sensitive Factor (NSF) Molecular Machine. J Biol Chem. 2013;288(32):23436–45. doi:10.1074/jbc.M113.476705.
35. Vivona S, Cipriano DJ, O'Leary S, Li YH, Fenn TD, Brunger AT. Disassembly of all SNARE complexes by N-ethylmaleimide-sensitive factor (NSF) is initiated by a conserved 1:1 interaction between alpha-soluble NSF attachment protein (SNAP) and SNARE complex. J Biol Chem. 2013;288(34):24984–91. doi:10.1074/jbc.M113.489807.
36. Yun HJ, Park J, Ho DH, Kim H, Kim C-H, Oh H, et al. LRRK2 phosphorylates Snapin and inhibits interaction of Snapin with SNAP-25. Exp Mol Med. 2013;45:e36. doi:10.1038/emm.2013.68.
37. Arranz AM, Delbroek L, Van Kolen K, Guimaraes MR, Mandemakers W, Daneels G, et al. LRRK2 functions in synaptic vesicle endocytosis through a kinase-dependent mechanism. J Cell Sci. 2015;128(3):541–52. doi:10.1242/jcs.158196.
38. Matta S, Van Kolen K, da Cunha R, van den Bogaart G, Mandemakers W, Miskiewicz K, et al. LRRK2 Controls an EndoA Phosphorylation Cycle in Synaptic Endocytosis. Neuron. 2012;75(6):1008–21. http://dx.doi.org/10.1016/j.neuron.2012.08.022.
39. Martin I, Kim JW, Lee BD, Kang HC, Xu JC, Jia H, et al. Ribosomal protein s15 phosphorylation mediates LRRK2 neurodegeneration in Parkinson's disease. Cell. 2014;157(2):472–85. doi:10.1016/j.cell.2014.01.064.
40. Matveeva EA, He P, Whiteheart SW. N-Ethylmaleimide-sensitive fusion protein contains high and low affinity ATP-binding sites that are functionally distinct. J Biol Chem. 1997;272(42):26413–8.
41. Yu RC, Hanson PI, Jahn R, Brunger AT. Structure of the ATP-dependent oligomerization domain of N-ethylmaleimide sensitive factor complexed with ATP. Nat Struct Biol. 1998;5(9):803–11. doi:10.1038/1843.
42. Liu G, Sgobio C, Gu X, Sun L, Lin X, Yu J, Parisiadou L, Xie C, Sastry N, Ding J, Lohr KM, Miller GW, Mateo Y, Lovinger DM, Cai H (2015) Selective Expression of Parkinson's disease-related Leucine-rich Repeat Kinase 2 G2019S Missense Mutation in Midbrain Dopaminergic Neurons Impairs Dopamine Release and Dopaminergic Gene Expression. Hum Mol Genet. doi: 10.1093/hmg/ddv249
43. Fuji RN, Flagella M, Baca M, Baptista MA, Brodbeck J, Chan BK, et al. Effect of selective LRRK2 kinase inhibition on nonhuman primate lung. Sci Transl Med. 2015;7(273):273ra215. doi:10.1126/scitranslmed.aaa3634.
44. Piccoli G, Verpelli C, Tonna N, Romorini S, Alessio M, Nairn AC, et al. Proteomic analysis of activity-dependent synaptic plasticity in hippocampal neurons. J Proteome Res. 2007;6(8):3203–15. doi:10.1021/pr0701308.
45. Nakamura Y, Iga K, Shibata T, Shudo M, Kataoka K. Glial plasmalemmal vesicles: a subcellular fraction from rat hippocampal homogenate distinct from synaptosomes. Glia. 1993;9(1):48–56. doi:10.1002/glia.440090107.
46. Sankaranarayanan S, Ryan TA. Real-time measurements of vesicle-SNARE recycling in synapses of the central nervous system. Nat Cell Biol. 2000;2(4):197–204. doi:10.1038/35008615.
47. Verderio C, Coco S, Bacci A, Rossetto O, De Camilli P, Montecucco C, et al. Tetanus toxin blocks the exocytosis of synaptic vesicles clustered at synapses but not of synaptic vesicles in isolated axons. J Neurosci. 1999;19(16):6723–32.
48. Salvi M, Trashi E, Cozza G, Franchin C, Arrigoni G, Pinna LA. Investigation on PLK2 and PLK3 substrate recognition. Biochim Biophys Acta. 2012;1824(12):1366–73. doi:10.1016/j.bbapap.2012.07.003.

49. Venerando A, Franchin C, Cant N, Cozza G, Pagano MA, Tosoni K, et al. Detection of phospho-sites generated by protein kinase CK2 in CFTR: mechanistic aspects of Thr1471 phosphorylation. PLoS One. 2013;8(9): e74232. doi:10.1371/journal.pone.0074232.
50. Lanzetta PA, Alvarez LJ, Reinach PS, Candia OA. An improved assay for nanomole amounts of inorganic phosphate. Anal Biochem. 1979;100(1):95–7.

Additional file 1

LRRK2 phosphorylates pre-synaptic N-ethylmaleimide sensitive fusion (NSF) protein enhancing its ATPase activity and SNARE complex disassembling rate

Elisa Belluzzi, Adriano Gonnelli, Maria-Daniela Cirnaru, Antonella Marte, Nicoletta Plotegher, Isabella Russo, Laura Civiero, Susanna Cogo, Maria Perèz Carrion, Cinzia Franchin, Giorgio Arrigoni, Mariano Beltramini, Luigi Bubacco, Franco Onofri, Giovanni Piccoli, Elisa Greggio

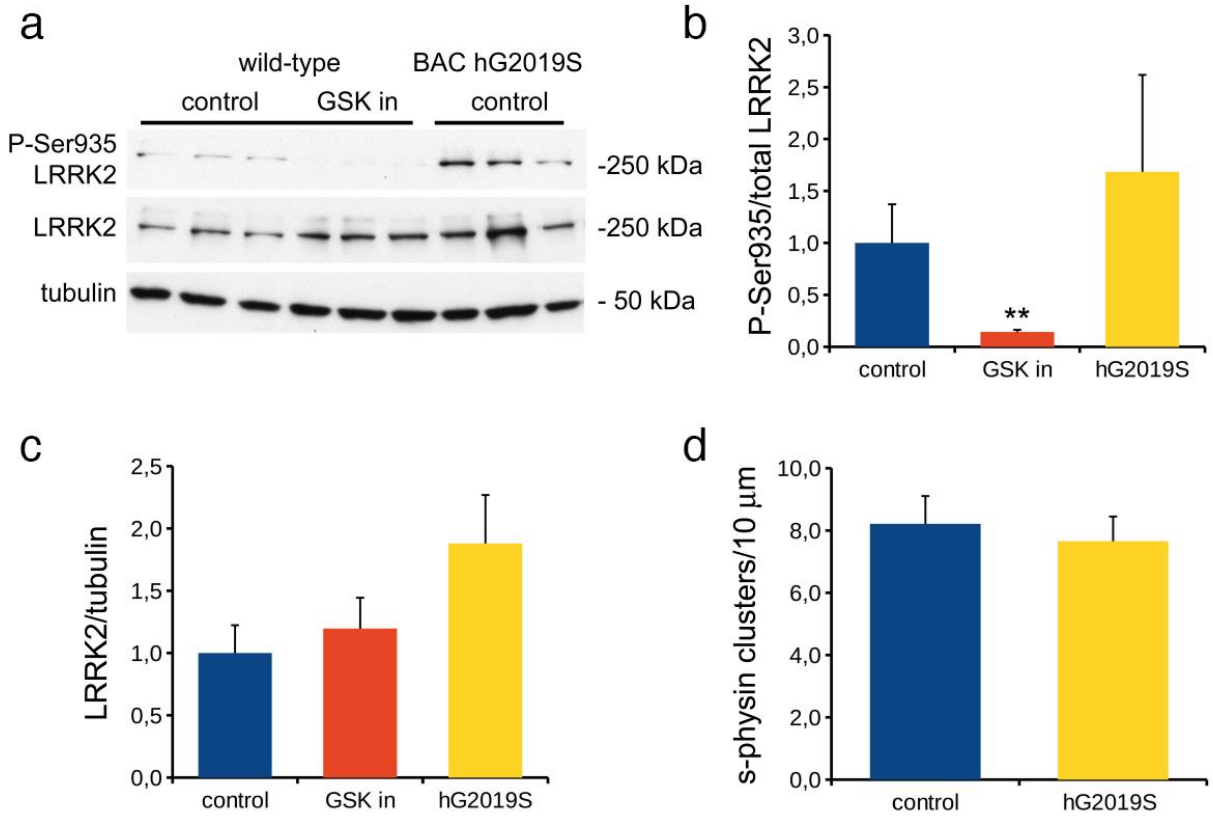

Figure S1. Expression and phosphorylation of LRRK2 in primary cortical neurons subjected to SypHy assays. (a) Cortical neurons from wild-type and BAC hG2019S mice were kept in culture until DIV14, treated or not with LRRK2 inhibitor GSK2578215A (GSK in, 0.2 µM, 2h) and assayed for western blotting. Samples were processed to measure LRRK2 phosphorylation at Ser935, total LRRK2 and tubulin level. Graphs report P-Ser935 level normalized on total LRRK2 level (b), total LRRK2 level normalized on tubulin amount (c). Data are expressed as mean ± SEM, n=3 (** $p<0.01$ versus control, ANOVA). (d) Total number of SV pools was not altered in BAC hG2019S neurons. The graph reports number of synaptophysin-positive clusters per 10 µm of GFP-positive process.

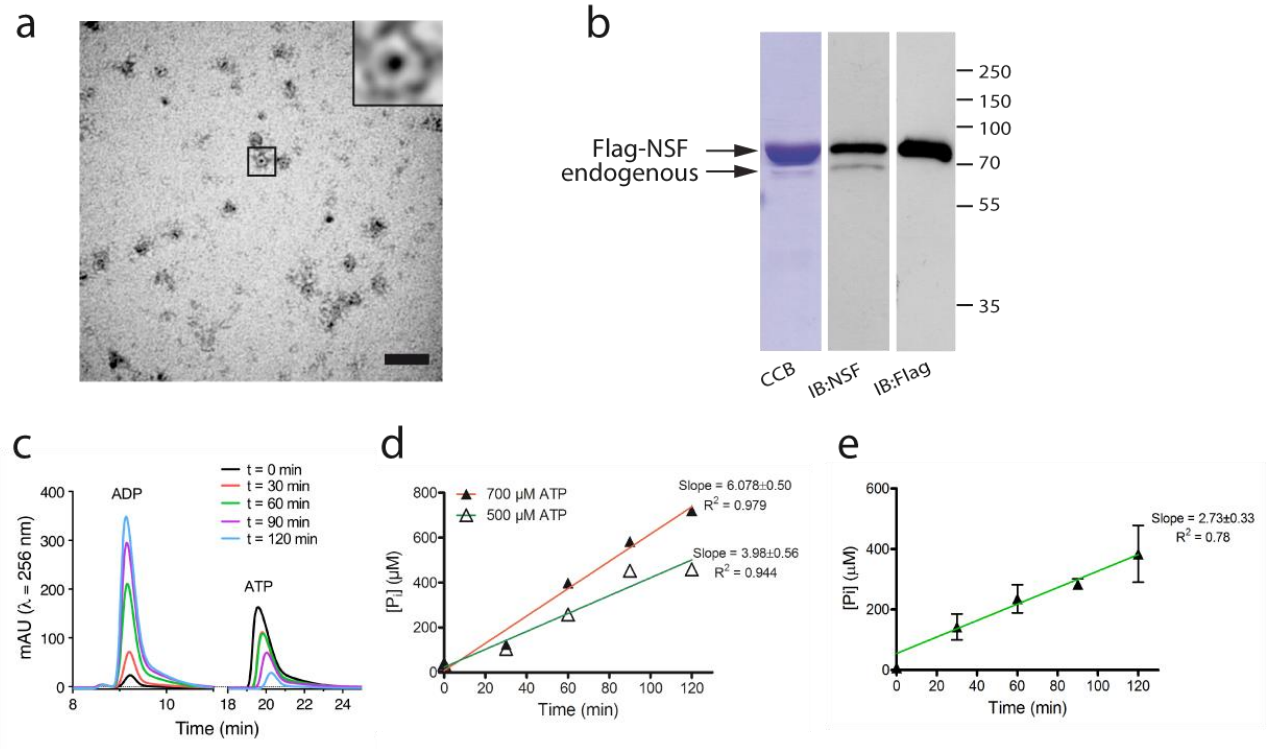

Figure S2. Biochemical validation of recombinant human NSF. (a) Representative TEM micrograph of purified Flag NSF wild type (20 ng/µl) with 1 mM ATP and 4 mM $MgCl_2$ showed the typical hexameric structure (scale bar 50 nm). (b) Recombinant human NSF co-purifies with endogenous NSF as confirmed by western blot analysis with anti-flag and anti-NSF antibodies. (c) Isocratic RP-HPLC profile of the two different nucleotide peaks over time ([ATP] = 0.7 mM). The ATPase activity of NSF was evaluated also with the rate of inorganic phosphate (P_i) released measuring the area under the peak of ADP with RP-HPLC (d) and with the Malachite Green Enzyme Assay ([ATP] = 0.5 mM) collecting aliquots as a function of time (n = 5) and subtracting a control purification of untransfected cells (e). Velocities of the reactions (slopes) were calculated by linear regression using GraphPad Prism 5 software.

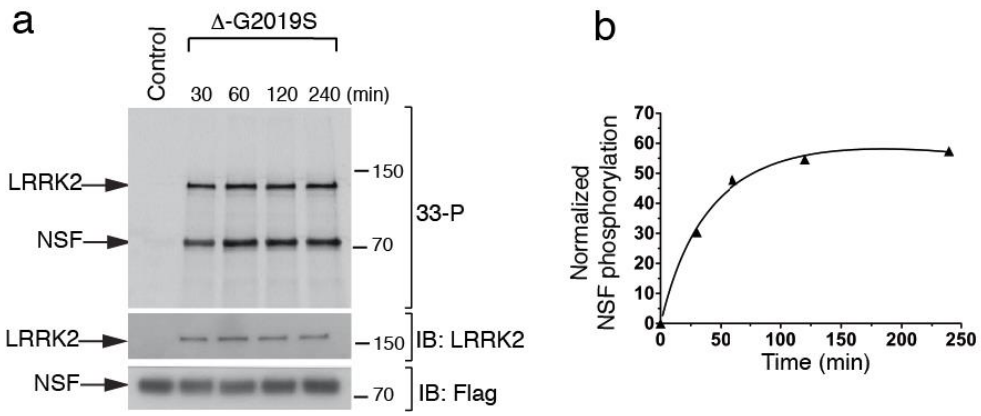

Figure S3. LRRK2 phosphorylation of NSF occurs within the first 30 minutes.
(a) In vitro kinase assays with LRRK2-G2019S$^{970\text{-}2527}$ and NSF up to 240 minute reaction time. (b) Quantification of radioactivity incorporated by NSF over time.

a

Protein ID: Human N-ethylmaleimide sensitive fusion protein
Sequence coverage: 80.51%
Green: confidence >99%
Yellow: confidence >95%

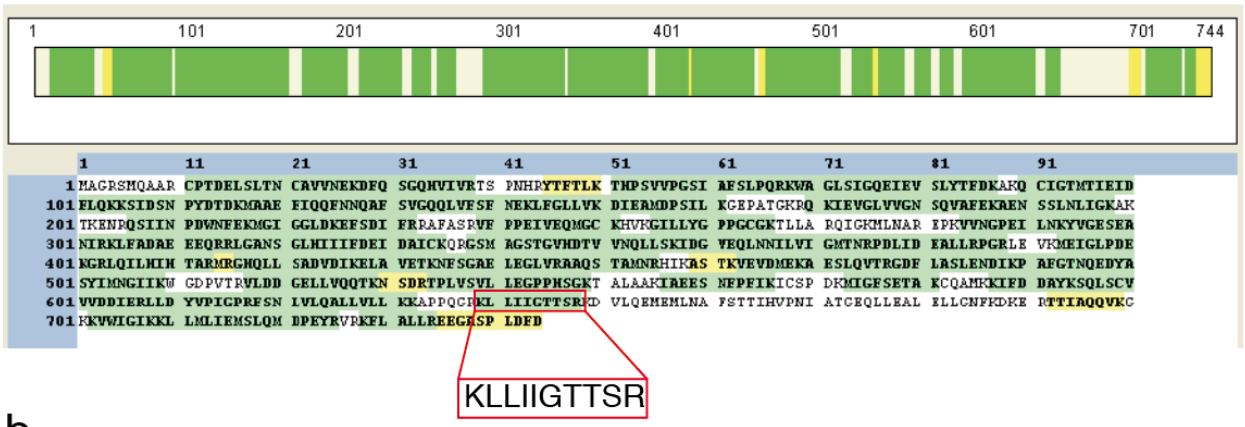

b

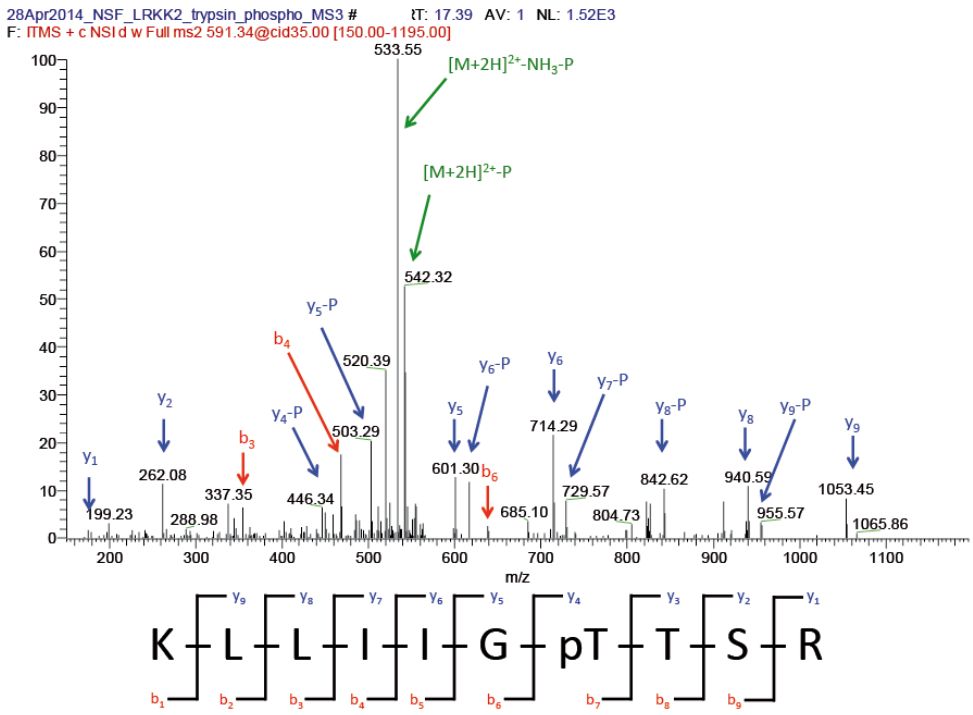

Figure S4. LC-MS/MS analysis of NSF phosphorylated by LRRK2.
(a) Sequence coverage of NSF phosphorylated by LRRK2. (b) Manually annotated MS/MS spectrum relative to the monophosphorylated peptide KLLIIGTTSR from NSF. Charge: +2, Monoisotopic m/z: 591.33636 Da (+0.03 mmu/+0.04 ppm respect to the theoretical m/z), MH+: 1181.66545 Da. Identified with Mascot with an IonScore of 60 (Exp Value of 2.5E-005). The presence of the fragment y2 suggests that the phosphorylation site is probably not located at the level of the serine residue. The fragmentation pattern is compatible with a phosphorylation at T645 or T646.

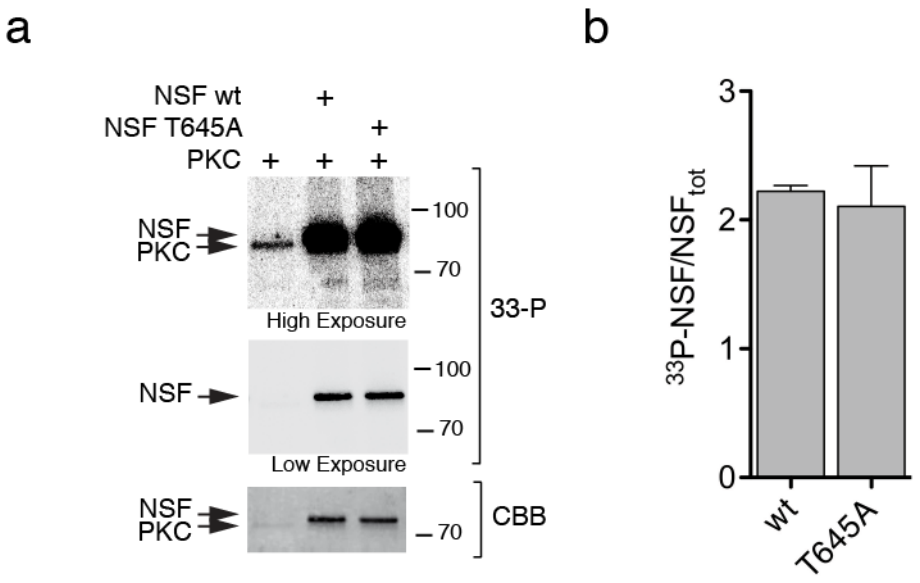

Figure S5. PKC does not phosphorylate NSF at T645.
(a) In vitro kinase assays with PKC and NSF (1:10, PKC:NSF). Upper panel shows a high exposure image where autophosphorylation of PKC can be observed. Middle panel represent a low exposure phosphoscreen. Lower panel shows a coomassie of the same membrane to normalize for protein loading. (b) Quantification of radioactivity incorporated by NSF wild-type and T645A (n=3 independent experiments).

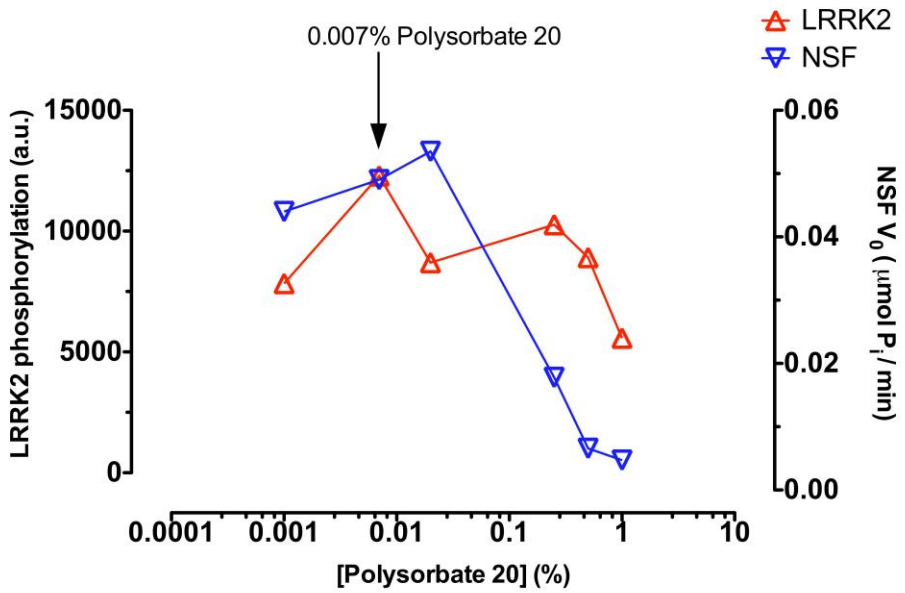

Figure S6. Evaluation of optimal detergent concentration for LRRK2 and NSF activities.

Optimal polysorbate 20 concentration for the reactions was evaluate within ability of LRRK2 to phosphorylate itself measuring the intensity of the band with an antibody against one of its auto-phosphorylation site (T2483). At the same time, the activity of human NSF, using the same concentration of detergent, was evaluate measuring the V_0 of the reaction with the Malachite Green Enzyme assay.

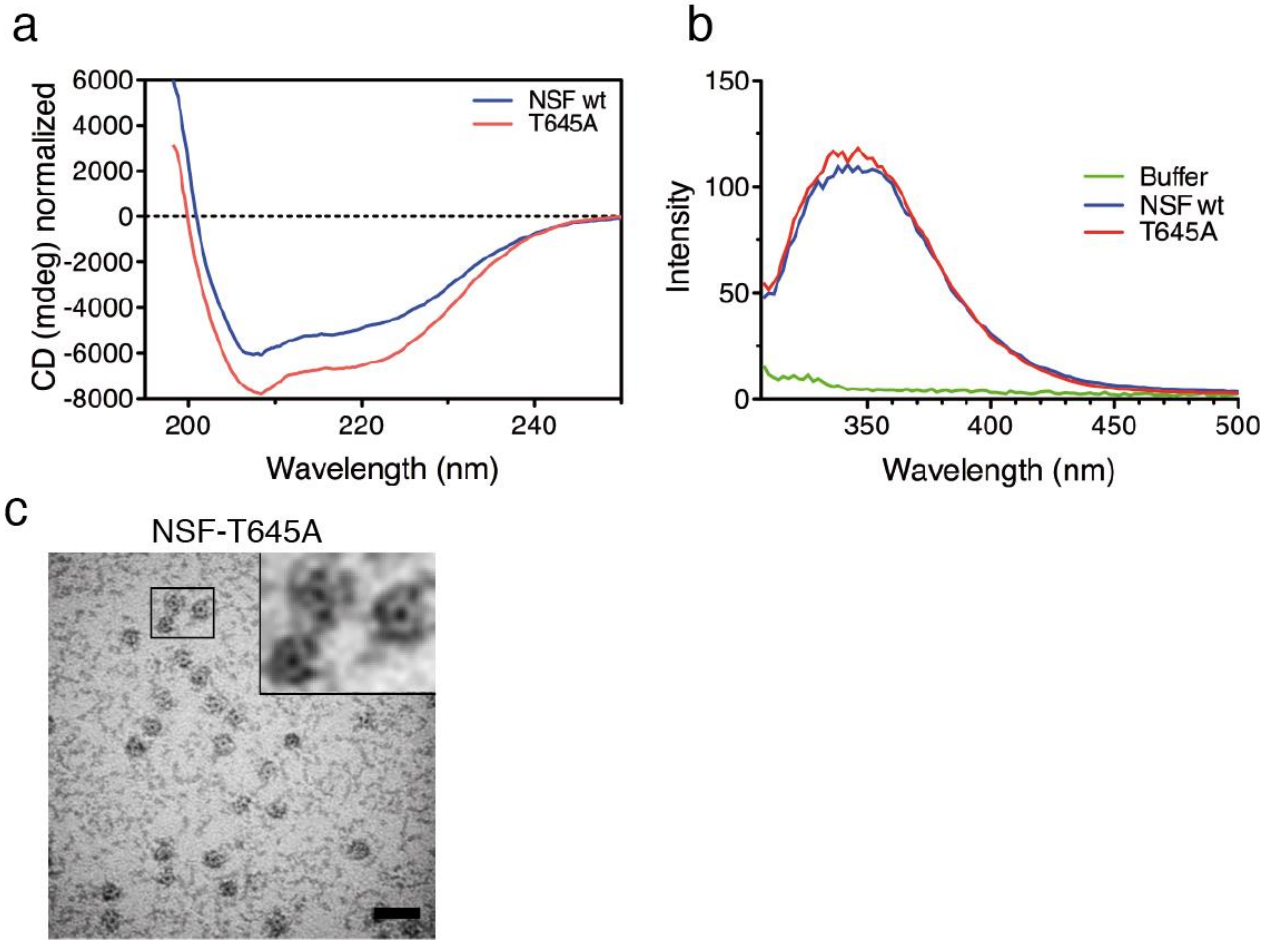

Figure S7. NSF wild-type and T645A have similar overall folding and T645A forms hexamers.

Recombinant human NSF wild type and NSF^{T645A} were analyzed measuring the CD and Intrinsic Fluorescence Spectra. (a) CD spectra were normalized by protein concentration previously measured with an SDS-PAGE gel. (b) The protein concentration used for Intrinsic Fluorescence measurements was 0.9 µM. (c) Representative TEM micrograph of purified Flag NSF-T645A (20 ng/µl) with 1 mM ATP and 4 mM $MgCl_2$ (scale bar 50 nm).

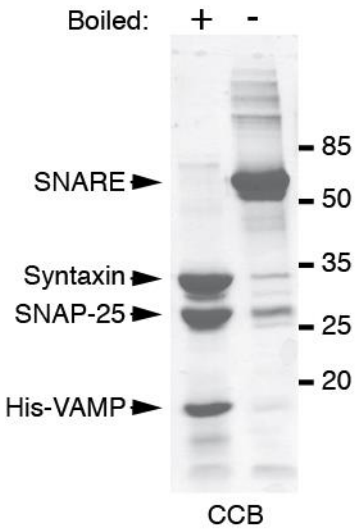

Figure S8. Expression and purification of SDS-resistant SNARE complex.
SDS-PAGE gel of the purified SDS-resistant SNARE complex (68 kDa) obtained by co-expression of Syntaxin, SNAP-25 and 6xHis-VAMP in *E. Coli* BL21(DE3) strain, either boiled (+) and not (-) to disassemble the three single components.